Università Degli Studi di Parma

Dottorato in Produzioni Animali, Biotecnologie Veterinarie, Qualità e Sicurezza degli Alimenti
XXII Ciclo

"Biophysical characterization of Vertebrates Odorant Binding Proteins and Their Biotechnological Applications"

Supervisor:

Ch.mo Prof. Roberto Ramoni

Candidate:

Dr.ssa Roberta Crescenzo

Tutor:

Dr. Sabato D'Auria

Academic Year 2008-2009

Università Degli Studi di Parma

Dottorato in Produzioni Animali, Biotecnologie Veterinarie, Qualità e Sicurezza degli Alimenti XXII Ciclo

"Caratterizzazione Biofisica di Odorant Binding Proteins da Vertebrato e Possibili Applicazioni Biotecnologiche"

Relatore :

Ch.mo Prof. Roberto Ramoni

Candidato:

Dr.ssa Roberta Crescenzo

Tutor:

Dr. Sabato D'Auria

Anno Accademico 2008-2009

SUMMARY

The Binding Protein family is a class of proteins characterized of a ligand binding site able to bind different probes of biological nature. For this reason it appears that these biomolecules are currently studied in several labs around the world since they also represent excellent candidates in designing of specific optical biosensors for detection of small analytes.

Odorant Binding Proteins (OBPs), a sub-class of lipocalins, are defined by their property of reversibly binding volatile chemicals called "odorants".

Odorants and pheromones are important signals conditioning the behaviour of animals. These soluble proteins of low molecular mass, synthesized in the lateral nasal glands and secreted into the nasal mucosa, seem to play important roles in chemical communication [Pelosi P., *Ann. N. Y.Acad. Sci.*, 1998]. They are present at high concentrations in biological fluids, involved in the perception and in the delivery of chemical messages of pheromonal significance.

This class of proteins have been isolated from such as cow, rabbit, pig and mouse. Vertebrates' OBPs share a typical β-barrel folding and an hydrophobic binding pocket for ligands [Bianchet M.A., et al., *Nat. Struct. Biol.* 1996; Tegoni M., et al., *Nat Struct Biol*, 1996].

The subject of this PhD project is the structural and functional characterization of the *eukaryotic* Odorant Binding Proteins (OBPs) originally characterized from bovine and pig nasal mucosa.

The work was based on recombinant OBPs obtained upon gene cloning in *E. coli* and protein expression and purification procedures.

The main aim of the work was to perform a structural characterization of the OBPs by optical spectroscopy in order to investigate the stability and the conformational dynamics of these biomolecules.

OBPs also represent an interesting and simple model for studying the phenomena of protein aggregation and how the formation of protein dimers and/or protein oligomers is depending upon single amino acid mutations in protein primary structure.

In addition, the project is aimed at acquiring basic knowledge on the structure and stability of proteins and at developing biotechnological applications such as the design of innovative optical OBP-based biosensors for the detection of small molecules. As a consequence, it is of interest to study the factors regulating the stability of these proteins, and to establish general guidelines that allow to address a large variety of different questions in biosensing applications.

To this end, fluorescence correlation spectroscopy (FCS), fluorescence anisotropy measurements and ultracentrifugation (AUC) experiments were carried out to gain information on the thermodynamic parameters related to OBPs stability.

The obtained results show that OBPs are good candidates as probe for specific optical biosensors for sensing small analytes. They also suggest their potential use as a biological scaffold for a variety of biotechnological applications.

In fact, in the frame of this thesis project two different biosensor prototypes were realized: a) fluorescence-based biosensor; b) surface acoustic wave-based biosensor. In particular the fluorescence biosensors was realized by immobilizing the OBP onto carbon nano-tubes. The binding of the ligand, 1-octen-3-ol (OCT) to the immobilized OBP was detected following the efficiency of the process resonance energy transfer (RET) between intrinsic tryptophan residues of OBP and an energy acceptor 1-amino-anthracene (AMA) that fits in the OBP funnel.

As regard the SAW-based biosensor, OBP were immobilized onto a wafer realized by deposition of 5 nm gold film on a 100 nm aluminum film and mounted on a TO39 package.

Both, fluorescence biosensors and surface acoustic wave (SAW) biosensors are currently being used in medicine, environment monitoring, biotechnology, food industry and security applications.

1. INTRODUCTION

1.1. Lipocalin as binding proteins for small hydrophobic molecules with potentials for applications in biosensor technology

Lipocalins are a family of binding proteins for small hydrophobic compounds of different chemical classes and biological functions characterized by a common structure. Based on their binding properties and structural stability, lipocalins are good candidates for the design of biological recognizing elements to be employed in biosensors specific for low molecular weight analytes. These proteins, which are devoted to the recognition of small hydrophobic molecules (MW 150-300 Da) have the potential of complementing the existing portfolio of protein affinity reagents, and in particular antibodies, that usually bind compounds of higher dimensions and structural complexity.

1.2. Lipocalin's family

Lipocalins form part of a larger structural superfamily: "The Calycins" which also includes fatty acids binding proteins (involved in lipid metabolism), avidins (which exhibit high affinity for biotin), metalloproteinase inhibitors and triabin (proteinase inhibitors) [Flower D.R., et al. *Biochim. Biophys. Acta* 2000].

Mammalian lipocalins are soluble, extracellular proteins, monomeric, with molecular weights between 16 and 20 kDa.

Despite of a low sequence similarity these proteins are characterized, at the structural level, by a common structural frame named 'Lipocalin folding'.

They bind a large number of hydrophobic molecules of different chemical classes including pheromones, odorants, retinol.

Mammalian lipocalins are usually secretory proteins found in large amounts in biological fluids, such as nasal mucus, lachrymal fluid, urine, saliva or vaginal secretions and milk, know to be carriers of pheromonal cues. [Tegoni M., et al. *Biochim. Biophys. Acta* 2000]

Some of the lipocalins, such as Retinol Binding Proteins or Aphrodisine bind a limited number of molecules and are generally purified in complex with their natural ligands. [Godovac-Zimmermann J. *Trends Biochem Sci.* 1988].

Others lipocalins, like the Odorant Binding Proteins from nasal mucus which, have a broader ligand specificity, (OBPs), are generally purified devoid of ligands.

The lipocalin folding is invariably constituted by two domains: a β-barrel domain, that includes the ligand binding site (it includes about 80% of the aminoacid residues), and a carboxy-terminal α-helix domain of still unknown function. The two domains are joined by a short hinge region and their reciprocal position is stabilized by a disulphide bridge established between two highly conserved cysteine residues present in the OBP primary structure.

Lipocalins of known three-dimensional structure include retinol-binding protein (RBP), [Bartsch, S. and Tschesche, H. *FEBS* 1995], β-lactoglobulin (Blg), [Ganfornia, M.D., et al. *Development* 1995], insecticyanin [Arruda, L.K. et al., *J. Biol. Chem.* 1995], bilin-binding protein (BBP), the major urinary protein, α_{2u}-globulin [Zagalsky, P. F., et al. *Comp. Biochem. Physiol* 1995 ; Bishop, R. E. et al., *J. Biol. Chem.* 1995], the epididymal retinoic acid-binding protein and neutrophil lipocalin odorant binding protein.

The common structure of the lipocalin protein fold is a highly symmetrical "up and down β-barrel" that encloses an internal cavity designing the ligand-binding site and an external loop scaffold.

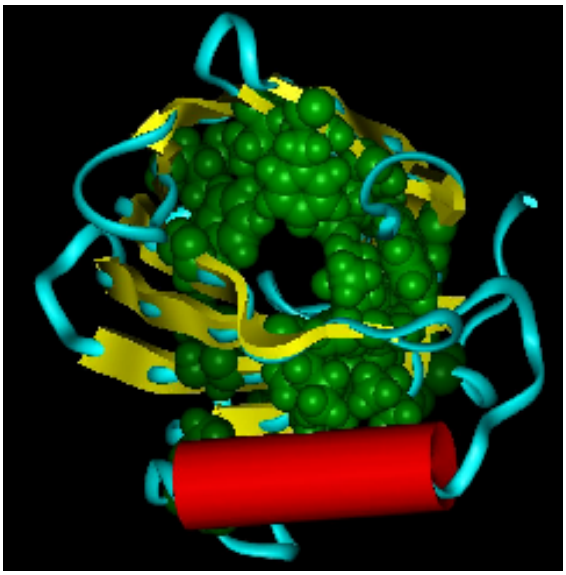

Lipocalin scaffold

The disulfide bridge, with the exception of homo-dimeric bovine odorant binding protein (bOBP), is conserved in all the lipocalins identified so far, bOBP, in fact, is a peculiar lipocalin characterized by a reciprocal exchange, within the dimer molecule, of the two domains that form each protein subunit. These particular protein structural feature, named domain swapping, in bOBP is due on one side to the linearity and rigidity of the hinge region, and on the other side to the absence of a disulfide bond that in monomeric lipocalins stabilizes the reciprocal position of the two protein domains within the three dimensional organization of the protein.

In the past lipocalins were simply classified as protein carriers for small hydrophobic molecules. Today it is clear that members of this protein class are responsible for specific biological functions such as retinol transport, cryptic coloration of crustaceans, olfaction, pheromone transport and the enzymatic synthesis of prostaglandins.

Some of lipocalins have also been found to be implicated in the regulation of immune response and the modulation of cellular homoeostasis. [Flower, D. R. *Biochem J.* 1996]

In most cases, their physiological role lies in the storage or transport of hydrophobic and/or chemically sensitive organic compounds.

At the open end of the conical structure the β-strands are connected in a pair-wise fashion by four loops, which form the entrance to the ligand-binding pocket. In contrast with the highly conserved β-barrel topology, this loop region differs considerably among individual lipocalins, both in conformation and length of the corresponding polypeptide segments. Hence, there is some natural resemblance with the antigen-binding region of immunoglobulins.

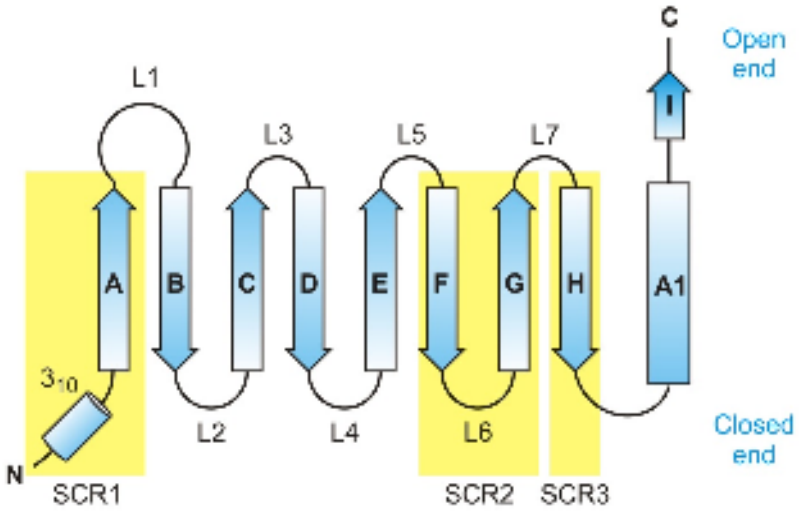

Scheme of the common core that Lipocalin fold

The figure above shows that the common core, of lipocalin fold, is dominated by the presence of three large structurally conserved regions (SCRs): named SCR1 (strand A and the 3_{10}-like helix preceding it), SCR2 (strand F and G, and loop L6 linking them), and SCR3 (strand H and the adjoining residues). Each of these SRC regions contains a sequence motif that is wholly, or partly, invariant. Together with two other distinct protein families, the fatty-acid-binding proteins (FABPs) and the avidins metalloproteinase inhibitors, the lipocalin family forms part of a larger structural super-family: the calycins. [Flower,D.R. et al., *Biochem. Biophys. Res. Commun.*, 1991; Flower D.R. *FEBS* Lett. 1993]. The

"structural super-family" is composed of proteins with closely related three-dimensional structures with limited similarity at the sequence level.

1.3. Odorant Binding Proteins

The term odorant binding protein, OBP, designates two major classes of soluble proteins of small size abundantly present at the periphery of the olfactory system, those highly expressed in the nasal mucus of vertebrates and those in the sensillary lymph of insects where odorant molecules come in contact with the olfactory epithelium; they are completely different in structure, but, probably, similar in function. In fact, despite their common name, vertebrate and insect OBPs belong to different structural families of proteins. Vertebrates' OBPs belong to the superfamily of lipocalins [Flower D.R., *J. Mol. Recognit.*,1995], that shares a typical β-barrel folding and a hydrophobic binding pocket for organic molecules [Bianchet M.A., et al., *Nat. Struct. Biol.* 1996; Tegoni M., et al., *Nat Struct Biol*, 1996]. Those OBPs from insects are mainly folded in α-helical domains that again define a ligand-binding cavity [Tegoni M., et al, *Trends Biochem. Sci.*, 2004].

The first member of this family was found, in nasal mucus and epithelium of cows, where it is expressed at millimolar concentrations. Other vertebrate OBPs were later found in other animal species including rat, rabbit and pig as well as in humans. Now several sequences of OBPs are available (either from protein or DNA sequencing, including that of the two human forms).

OBPs are synthesized by glands located in the sub-mucosal layers of nasal epithelium and vomeronasal organ and secreted in the mucus that layers these tissues. In poly-acrilamide gel electrophoresis under denaturing conditions, the molecular weights of vertebrate OBPs can be estimated between 17 kDa an 20 kDa.

In the latest years some investigations have been carried out to elucidate the mechanism of unfolding/refolding of porcine and bovine odorant binding protein (bOBP) in the presence of chemical denaturants such as guanidine

hydrochloride. These studies have shown the reversibility of the denaturation process even starting from the denatured monomeric forms [Parisi et al., *Biochim. Biophys. Acta*, 2003].

Odorant binding proteins can be present with different isoforms in the same animal species. Sequence similarity investigations have shown that, even within the same species, the homology of OBP primary structures can be as low as 30%. This led to hypothesize that in some cases, non allelic OBP genes could encode for different protein forms with different binding properties for alternative categories of odorant molecules.

Odorant binding proteins show a broad binding specificity towards hydrophobic compounds of different chemical classes: good ligands, which bind reversibly with dissociation constants in the micromolar range, include aromatic molecules, pyrazines (like 2-isobuthyl-3-methoxypyrazine (PYR)), thymol and terpenoids of the menthol series. Other odorant molecules, which are structurally related to the former, such as 2-methyl-3-methoxypyrazine, 2-phenyl-ethanol (PHE) and round-shaped terpenoids, do not show appreciable binding to OBPs up to 0.1 mM concentration.

In addition to OBPs (porcine, bovine, rat1 and rat2) other lipocalins were found to have significant similarity (more than 10% identity) with this category of proteins : these are VEGs, with a topological localization (Von Ebmer Glands, also called gustatory glands) close to OBPs, or mammalian pheromone binding proteins (boar salivary lipocalin-SAL, major urinary protein- MUP and aphrodisin). [Guiraudie, G. et al., *Chem. Senses*, 2003]

Other lipocalins, like serum retinol binding protein-SRBP (7%), are far below 10% sequence identity (7% with serum retinol binding protein, SRBP). [Bartsch, S. et al. , *FEBS Lett.*, 1985].

As already mentioned, the OBPs share the conserved folding pattern of lipocalins that is constituted of an eight-stranded β-barrel flanked by an α-helix structure at the protein C-terminal region. The β-barrel creates a central non-polar cavity whose role is the binding and transport of hydrophobic molecules.

These proteins reversibly bind their ligands with dissociation constants ranging from nanomolar to micromolar values range.

1.4. Physiological roles of OBPs

In spite of the considerable ability of OBPs to bind odorant molecules, their physiological role in olfactory perception is still unclear.

The olfactory receptors are separated from the air by a protective layer of hydrophilic secretion, named nasal mucus and sensillary lymph in mammals and in insects, respectively. The odorant molecules, which are hydrophobic and volatile compounds, to reach the receptors, have to cross this hydrophilic barrier. Proteins with the role of transporters of odorants across secretions covering olfactory epithelia, probably might have appeared during the adaptation of living organisms to terrestrial life, and such function has been formulated for the OBPs.

In fact it has been hypothesized that both in vertebrates and in insects, OBPs mediate the olfactory and pheromon perception by reversibly binding with odours and pheromones and transferring the ligands to receptors expressed by the olfactory neurons. The activation of the receptors, finally, leads (by the activation of specific G-proteins) to the generation of a potential action that is propagated to the brain by the way of the olfactory bulb.

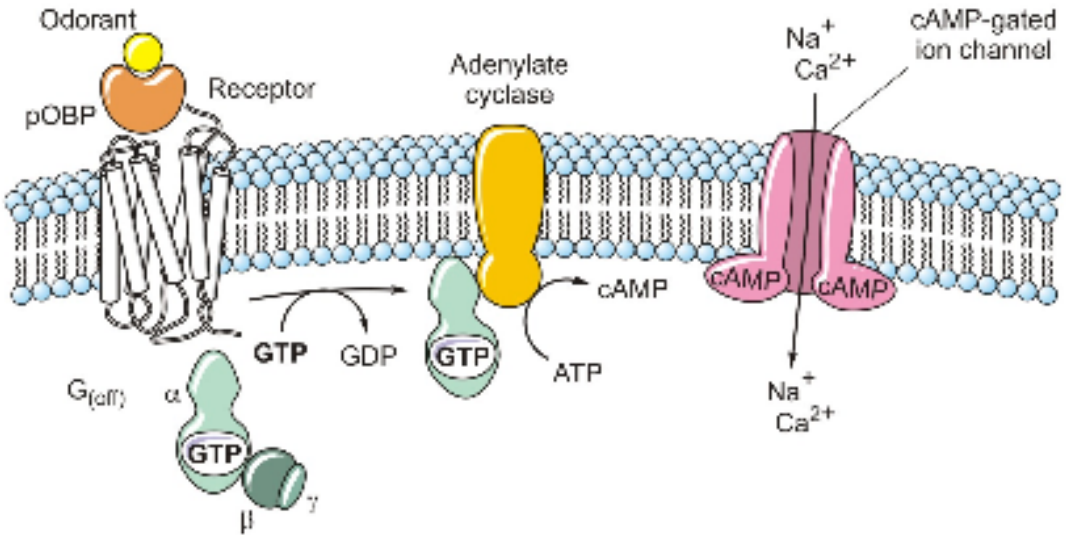

Pathway for olfactory signal transduction

In addition to this function, several different physiological roles have been proposed for the OBPs. In particular, with regard to mammalian OBPs, it has been hypothesized that they might represent protein scavengers for regeneration of olfactory receptors which have been previously activated by odorants [Tegoni, M. et al., *Biochim Biophys Acta*, 2000]. In fact, the broad binding specificity found in mammalian OBPs, makes plausible a scavenger function that allows, to prevent the saturation of olfactory receptors when odours are present at high concentration. Alternatively, and in a way reminiscent of bacterial chemotaxis, where sugars are perceived only when coupled to binding proteins, OBPs might be mandatory for the transduction process, if the complex OBPs/odorant is recognized by the receptor. Finally, it was suggested that OBP, which bind with high affinity cytotoxic and genotoxic alkylic aldehydes (6-11 carbon atoms) generated from peroxidation of membrane polyunsaturated fatty acids, might play a role of protection of nasal mucosa, against injuries caused by oxidative agents eventually inhaled.

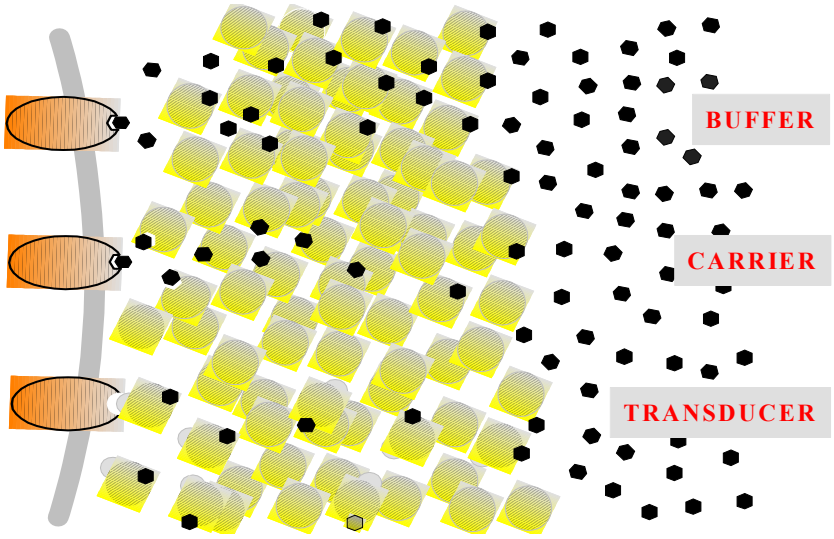

Some of possible roles of odorant binding protein

1.5. Porcine Odorant Binding Protein (pOBP)

Porcine OBP (pOBP) is a monomer composed of 157 aa, with an isoelectric point of 4.2. It is noteworthy that the estimation of pOBP molecular weight is dependent protein concentration. In fact, the evaluation of MW ranges from 18 to 28 kDa depending the techniques used for it. Formation of pOBP aggregates have been detected when high concentration protein samples were prepared for FT-IR measurements.

pOBP structure resembles that of a monomeric lipocalin showing the typical folding of this family of proteins whose characteristics have been described earlier.

The pOBP internal cavity inside the β-barrel is layered by R groups belonging to hydrophobic and aromatic amino acid residues which are responsible of the interactions with the ligands.

The cavity designed by the β-barrel of pOBP is devoid of any significant electron density. The cavity does not communicate directly with the external solvent, and a few amino acid side chains blocking the access to the outside would have to move to make the binding of odours possible. The naturally occurring ligand found in bovine OBP (see below) could fit the pOBP cavity without any major constraints, except for making clashes with Val-80 (Ala in OBPb) and Phe-88 (Phe-89 in bOBP, conserved). The position of Phe-88 side

chain in pOBP corresponds to that observed in bOBP complexed with cyclic compound and resulting from a 120° rotation from the position observed in the natural complex.

Sequence comparison with other lipocalins revealed a good similarity (42%) with bovine odorant-binding protein, the only member of this class which does not contain disulphide bonds and of which the three-dimensional structure recently has been resolved (see below). Nine out of the 16 residues lining the binding pocket in bovine OBP are conserved in pOBP, suggesting the presence structural similarities in this region of the molecule. Several compounds were able to bind the protein as revealed by competitive binding experiments. [Paolini, S. et al., *Chem Senses.*, 1998].

It was shown that the pOBP is able to reversibly bind several odorants with an affinity spectrum similar to that of the bovine OBP. The contacts between pOBP and the different ligands, as shown by X-ray crystallography of several binding complexes, is based on Van der Waals interactions.

The orientation of the ligands inside the cavity appeared to be opportunistic, with no specific target patches for aromatic groups and no correlation between the number of contacts and the affinity measured in solution. In particular, no special characteristic could be ascribed to the nature of good binders, and upon interaction with all odorants, all the amino-acid residue side-chains lining the cavity kept the conformation observed in the native protein.

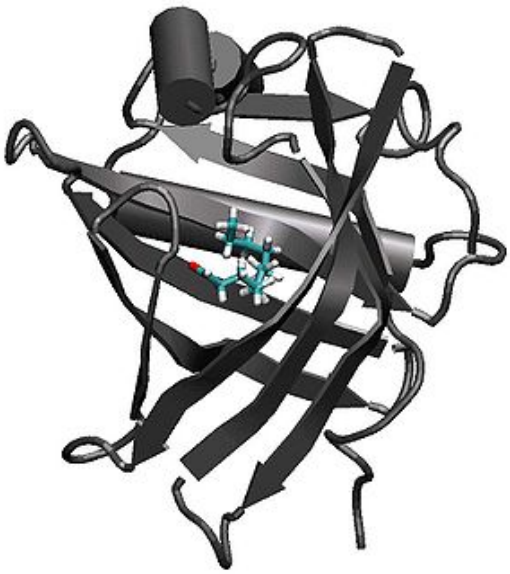

Structure of pOBP in complex with a ligand . [Vincent, F. at al. *J Mol Biol.* **300(1):** 127-39, 2000**]**

1.6. Bovine Odorant Binding Protein (bOBP) and Mutant Odorant Binding Protein (GCCbOBP)

Bovine odorant binding protein, bOBP is a soluble protein composed of 159 amino acid residues, with an isoelectric point of 4.2, and a molecular weight of 19 KDa. At neutral pH, bOBP is a dimer with an elongated shape, where, according to domain swapping, each subunits exchanges the α-elices and the β-barrell between each other. Each monomer is composed of a nine-stranded β-barrell, representing the ligand binding site, connected by an extended stretch of residues to the α-helix that crosses the dimer interface. Besides the contact surface of the two subunits designs a central pocket in communication with the solvent that might interact with additional ligands. As already mentioned before, the structural reasons for bOBP dimerization must be found on one end in the absence of the disulphide bridge that stabilizes the reciprocal positions of the α-elices and β-barrel in monomeric lipocalins (bOBP lacks Cys63 and Cys155) and on the other side in the lack of a conserved glycine residue in position 121, keeping the hinge region rigid and straight by preventing the flanking of the two domains.

The experimental evidence of the role of Cys63, Cys155 and of Gly 121 in bOBP domain swapping was given by two subsequent sets of site directed mutagenesis experiments.

In fact, it has been shown first that a mutant bOBP, in where a glycine residue was inserted in position 121 (mutant M3), appeared as a deswapped form with a monomeric structure. A second mutant was then produced by introducing two cysteine residues in position 64 and 156 of M3. This form, named GCC-bOBP or also MB1 mutant, is a triple mutant of bOBP: G122+, W64C, H156C with the structure typical of monomeric lipocalins presenting the disulfide bridge that stabilizes the contact between the β-barrel and α-helix. In particular, MB1 shows a structure very similar to that of monomeric porcine OBP. [Ramoni, R. at al. *Biochem. J.*, 2002]

A natural ligand, co-purified with the protein, was found in the β-barrel cavity of bOBP. This molecule was unambiguously identified as the kariomone 1-octen-3-ol (OCT), a compound produced by bovine rumination, that attracts insects by stimulating their olfactory receptors. This finding suggested a role of bOBP in the ecological relationships between bovine and several insect species [Ramoni, R. et al., *J. Biol. Chem.*, 2001].

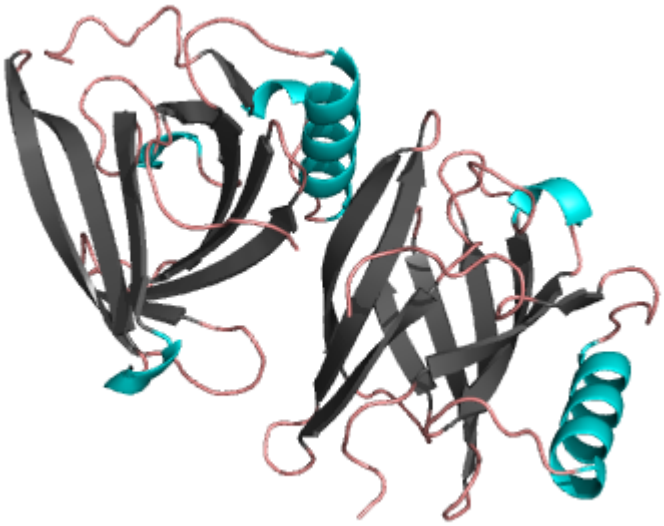

Bovine Odorant Binding Protein

2. AIM OF THE WORK

2.1. Aim of the work

The subject of this PhD project is the structural and functional characterization of the Odorant Binding Protein (OBP) from porcine and bovine species. The work was based on recombinant wild-type and mutants forms expressed in *E. coli.*

The initial scope of this study was the production of an alloprotein (a protein that contains amino acids which are not natural) where the unique Trp residue in the primary structure of porcine OBP is replaced with a Trp analog showing absorbance and fluorescence properties distinguishable from that of the native residue.

The goal was that of obtaining an alloprotein whose spectroscopic properties could be evaluated in solutions containing different other proteins presenting natural Trp residues.

As a consequence, a part of the thesis work had to be dedicated to the functional characterization of this new form though optical spectroscopy, in order to establish its intrinsic emission fluorescence response upon binding of non fluorescent ligands.

The longer-term goal of this project would be the production of OBP forms to be employed as recognizing elements for the specific detection of target odours in biosensors. With regard to this, the work of the thesis will include a characterization of the stability of these proteins, to establish the general guidelines that could enable, their use in biosensor applications.

2.2. Biosensors

Biosensors are analytical instruments (devices) characterized by the presence of biological recognition elements (such as nucleic acids, enzymes and antibodies) immobilized on a solid support. The interaction between the recognition

element and a specific analyte gives rise to a signal (spectroscopic, potentiometric etc.), that is amplified, transduced and finally quantified.

On these basis, the use of proteins like enzymes and antibodies as recognition elements is due to the binding specificity and affinity that these proteins show for their ligands.

Other advantages of the use of proteins in biosensor technology are there solubility in water, the relatively low costs of production and, taking advantage of the progresses of molecular genetics, the possibility of improving/changing some of properties of the proteins by genetic manipulation.

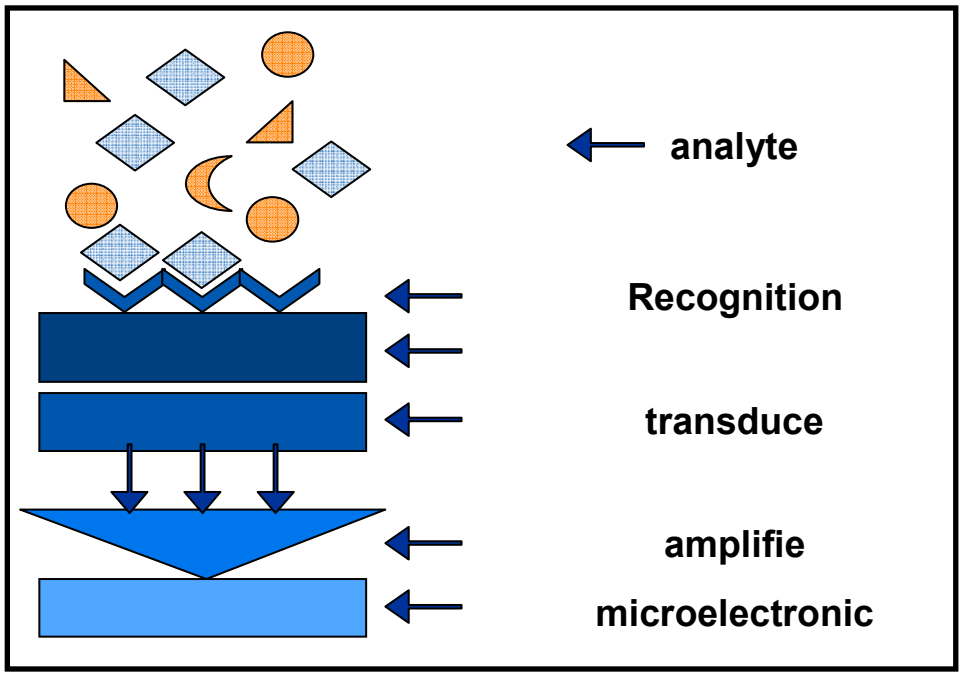

Example of biosensor

2.3. Amino acid Analogs and Alloproteins

Amino acid analogs are synthetic molecules with similar chemical structures that can be incorporated in proteins sequences to give rise to ALLOPROTEINS that can be employed for different type of investigations, included spectroscopy studies. To this aim, are of relevant interest the tryptophan analogues 5-

hydroxytryptophan (5HW) and 7-azatryptophan (7AW). They have spectral properties different from those of tryptophan, in fact their peaks of absorbance and fluorescence emission are red shifted of 10 and 50 nm respectively. When these analogs are incorporated in the polypeptide chains, it is possible to do a selective excitation and monitoring the emission fluorescence of the alloprotein, discriminating it among the others.

The amino acid 5HW has a quantum yield similar to that of tryptophan and has a small and solvent-insensitive Stokes shift (i.e., its emission maximum is about 339 nm in water). In contrast, 7AW has a low quantum yield and a large Stokes shift in water.

The yield and Stokes shift of 7AW depend on the protic nature of the solvent and is related to the existence of different tautomeric species in solution. [Avouris, P. et al., *Photochem. Photobiol.*, 1976; Chapman & Marconcelli, *J. Phys. Chem.*, 1992; Y. Chen et al., *J. Phys. Chem.*, 1993]. Although weakly fluorescent in water, the 7-azaindole ring shows much stronger fluorescence in aprotic solvents such as acetonitrile, suggesting that 7AW might be very sensitive to its microenvironment in a protein.

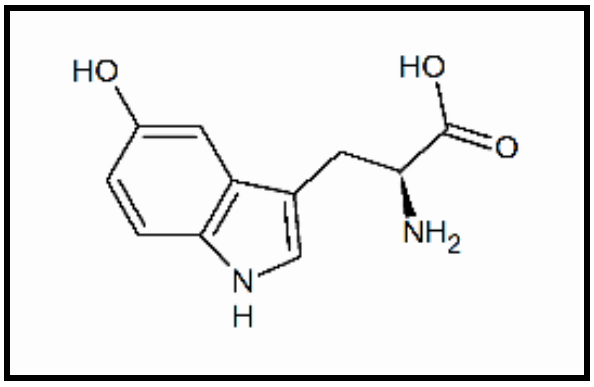

5-Hydroxy-L-Tryptophan

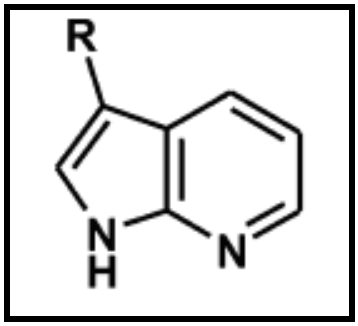

7-Aza-Tryptophan

2.4. Biotechnological applications

Biotechnology means "the study and application of living tools" in human activities such as agriculture, food processing, industrial production, environmental cleanup and medicine.

Defined broadly, biotechnology is the use of a living organism to make a product or run a process. Narrower definitions often limit biotechnology to genetic engineering and recombinant DNA technology but Biotechnology includes a wide range of diverse technologies and they may be applied in each of the different sectors.

For example one of the applications could be the realization of Microarrays, biosensors which consist of large numbers of parallel hybrid receptors (DNA, proteins, oligonucleotides). Microarrays are also referred to as biochip, DNA chip, DNA microarray or Proteins arrays and offer unprecedented opportunities and approaches to diagnostic and detection methods. They can be used for the detection of pathogens, pesticides, toxins and environmental pollutants and offer considerable potential for facilitating process control.

My PhD studies investigated the possibility of using natural and specifically modified Odorant Binding Proteins for biotechnological applications. In particular we investigated their use like biosensing elements. Such applications require stable proteins and since OBPs are endowed with such characteristics, so we expect they will perform well in such applicative uses.

Finally we realized two prototypes of biosensors: (1) an advanced nano-biosensor onto carbon nanotubes based on a competitive resonance energy transfer (RET) assay between the protein tryptophan residues located at the

positions 17 and 133 (W17 and W133) of bOBP and the 1-amino-anthracene (AMA), a molecule that fits in the binding site of bOBP; (2) a SAW biosensor system, based on the chemical interaction between the bOBP and its natural ligand, potentially useful to detect a wide range of analytes.

3. MATERIALS AND METHODS

3.1. Materials

Standard chemicals, solvents, and buffers were purchased from Sigma-Aldrich. All solutions were prepared using deionised water, further purified by means of a Milli-Q Millipore system. Oregon Green 488 succinimidyl ester (6-isomer 488-X Mr = 622.5) was from Molecular Probes, Invitrogen (Eugene, OR). 5-OHTrp analog was purchased from Sigma-Aldrich.

Carbon nanotubes were from Sigma.

All other chemicals were commercial samples of the best available quality.

3.2. Bacterial strains, plasmids and growth condition

BL21(DE3) (Novagen) was the *E. coli* strain used in this study for the expression of pOBP, bOBP and GCC-bOBP.

A coding sequence for a 6×His affinity at the N-terminal of all the OBP forms was palced in the different cDNAs by polymerase chain reaction (PCR) using specific primers. The fused cDNAs were subcloned in the expression vectors.

The plasmids used for cloning were pGEX2TK (GE Healthcare Life Sciences) for pOBP and pT7-7 (USB) for bOBP and GCC-bOBP [Ramoni, R. et al., *Biochem. J.*, 2002].

The transformants were selected on LB ampicillin agar plates (100µg/ml). Recombinant *E. coli* strains were cultured at 37°C in Luria-Bertani broth supplemented with ampicillin.

3.3. Growth of bacterial cells, bOBP and GCC-bOBP expression and purification.

250 ml of Luria-Bertani medium containing 100 µg/ml Ampicillin were inoculated with 2,5 ml of an overnight *E. coli* culture in the same medium and grown at 37°C. Protein expression was induced, when the at A_{600} was 0.6 A.U., with 0.8 mM isopropyl thio-β-D-galactoside. After 5 h Bacterial cells were

harvested by centrifugation at 5000 rpm for 20 min at 4°C and resuspended, for the following affinity chromatography purification, in 1X Ni-NTA Binding Buffer (5 ml per gram wet bacteria). The buffer was composed of 50 mM sodium phosphate, pH 8; 300 mM NaCl, and 10 mM imidazole. The suspension of *E. coli* cells was finally supplemented with 1 mg/ml lysozyme, 0.05 mg/ml DNAase and 5 mM $MgCl_2$ after a 1 h incubation at 37°C the cells were disrupted by French Press and the soluble fraction was separated from cell debris by centrifugation at 10000 g for 30 min.

For purification of His-tagged OBPs, the supernatant was loaded onto a Ni-nitrilotriacetic acid agarose column equilibrated with 50 mM sodium phosphate, pH 8.0, 300 mM NaCl and 10 mM imidazole. After loading with the protein extract, the column was washed with several volumes of the same buffer and affinity bound OBP forms were eluted as a single peak by increasing the imidazole concentration to 250 mM. Fractions of 1 ml were collected and the determination of protein concentration was monitored by measuring the absorbance values at 280 nm using an extinction coefficient of 48,000 M^{-1} cm^{-1} for dimeric bOBP and 19,400 M^{-1} cm^{-1} for the monomeric GCC-bOBP mutant.

The OBP containing A_{280}, fractions were then pooled and dialyzed in 10 mM Tris/HCl, pH 7.5.

Gels electrophoresis (12.5%) in denaturing condition according to Laemmly were performed ~~to~~ check the protein~~s~~ purity.

This purification procedure yielded on average of 15 mg of purified bOBP from a growth cell suspension of 500 ml.

3.4. Cloning, expression and purification of pOBP

The cDNA of pOBP that was first cloned in the plasmidic vector pET3a. But, due to the low yield of expression, the same cDNA was finally cloned in the vector pGEX2TK.

The pOBP cDNA was PCR-amplified from plasmid pET3a with the primers BamHIpOBPFw 5'-(ACGGGATCCCGTATGCAAGAGCCTCAACC), which anneals to the 5'-end of the coding region and introduces a unique BamHI restriction site (underlined), and EcoRIpOBPRv 5'-(AAGCGAATTCTCATCACTTGGCAGGACAG) which anneals near the stop codon.

The PCR product was digested by EcoRI/BamHI and purified by agarose gel electrophoresis followed by extraction with a QIAEXII kit (Qiagen). The pOBP cDNA was inserted in pGEX-2TK expression vector via BamHI/EcoRI yielding the plasmid pGEX-2TK-pOBP. This plasmid encodes for a fusion protein with glutathione S-transferase (GST). The expression constructs were transformed into E. coli BL21. The entire BamHI/EcoRI fragment, including the whole coding region, was verified by DNA sequencing.

For the expression of protein, 250 ml of Luria-Bertani medium containing 100 µg/ml Ampicillin was inoculated with 2,5 ml of an overnight culture and grown at 37°C. The induction of recombinant pOBP expression was carried out in a culture with an optical density at 600nm of 0.9 by adding 0.5 mM isopropyl β-D-thiogalactoside (` IPTG'); the incubation time after induction was of other 3 h at 37°C.

Cells were harvested by centrifugation at 3500 rpm for 30 min at 4°C and resuspended in PBS (140 mM NaCl, 2.7 mM KCl, 10 mM Na_2HPO_4 , 1.8 mM KH_2PO_4 pH 7.4) at a ratio of 3 ml of buffer per gram wet bacteria.

The suspension, after addition of 1 mg/ml lysozyme, 0.05 mg/ml DNAse and 5 mM $MgCl_2$, was incubated at 37°C for 1 h. The cells were disrupted by French Press and the soluble material was separated from cell debris by centrifugation at 10000 g for 30 min. The supernatant was collected and used for affinity chromatography. The protein extract was loaded onto as Glutathione Sepharose column equilibrated with PBS pH 7.4, incubated with resin at 4°C for about 1h, and washed extensively.

pOBP was finally obtained throughout a proteolitic cut of the fusion protein obtained by the addition of Trombin Protease (1unit/µL dissolved in 1X PBS). Cleavage of GST fusion protein bound to the column eliminated the extra step of separating the released protein from GST, since the GST moiety remained attached on the column. The purified proteins were analysed by SDS-PAGE as described by Laemmli [Laemmli U.K., *Nature*, 1970], yielding a single band at ~ 22 kDa and the protein concentration was determined using an extinction coefficient of 13,000 M^{-1} cm^{-1} at 280 nm.

3.5. Competent cells and transformation with pGEX-2TK plasmid for E. coli strain CY15077

The E. coli tryptophan auxotroph strain CY15077 (W3110ΔtrpEA2) with mutation in the tra gene (transfer gene) and deletion of the Trp operon, was a generous gifts from Alexander Ross (University of Montana but is from Dr. Charles Yanofsky, Stanford University).

Cells were made competent by the $CaCl_2$ method [Silhavy, T.J. at al., *New York: Cold Spring Harbor* , 1984].

The strain was transformed with pGEX-2TK/pOBP and the presence of the fragment was verified by BamHI/EcoRI Digestion.

3.6. Expression and Purification of ALLO-pOBP

An overnight culture of bacteria, grown in LB-rich medium, was diluted 1:10 into M9 medium [Maniatis T. at al., Cold Spring Harbor, NY, 1982] supplemented with 0.5% glucose, 1% Casamino acids, 0.1% thiamine, glycerol 80% and 0.25 mM L-tryptophan. The culture was grown with shaking at 37°C to an OD_{550} of 1.0. The cells were then harvested by centrifugation at 3500 rpm for 20′ and resuspended in an equal volume of the same medium, centrifuged and resuspended a second time in the same medium except that 5-OHTrp was

substituted for L-tryptophan. After the culture was grown for an additional 30 min to an OD_{550} of 1.3, the expression of repressor was induced by addition of solid isopropyl β-D-thiogalactopyranoside (final concentration, 1.0 mM). After overnight shaking at 37°C, the cells were centrifuged at 10000 rpm for 30', and resuspended in PBS. After the addition of 1 mg/ml lysozyme, 0.05 mg/ml DNAsi and 5 mM $MgCl_2$ and an incubation at 37°C for 1 h, cells were lysed by two passes through a French press [Ross, J.B.A. at al., Biochem., 1992] .

After centrifugation the supernatant was collected and used for affinity chromatography. The bacterial protein extract was loaded onto as Glutathione Sepharose column equilibrated with PBS, that, after an incubation at 4°C for about 1h, was washed extensively. ALLO-pOBP was finally obtained throughout a proteolitic cut of the fusion protein obtained by the addition of Trombin Protease (1unit/µL dissolved in 1X PBS). Cleavage of GST fusion protein bound to the column eliminated the extra step of separating the released protein from GST, since the GST moiety remained attached on the column. The purified proteins , that was analysed by SDS-PAGE as described by Laemmli [Laemmli U.K., *Nature*, 1970], gave a single band at ~ 22 kDa. ALLO-pOBP concentration was determined using an extinction coefficient of 13,000 M^{-1} cm^{-1} at 280 nm.

3.7. Immobilization of proteins onto carbon nanotubes

The OBPs were immobilized onto carbon nanotubes (CTs) by simple incubation of the CTs-bOBP at room temperature for 10 min in aqueous buffers (PBS, pH 6.5).

3.8. Production and check of OBP-1AMA complex

1 ml samples of 1 µM OBP, in2 0mM Tris-HCl buffer pH 7.8, were incubated overnight at 4°C in the presence of increasing concentrations of AMA (0.156–10

µM). Fluorescence emission spectra between 450 and 550 nm were recorded with a Perkin-Elmer LS 50 luminescence spectrometer (excitation and emission slits of 5 nm) at a fixed excitation wavelength of 380 nm and the formation of the AMA–OBP complex was followed as an increase of the fluorescence emission intensity at 480 nm. The dissociation constants of the AMA–OBP complexes were determined from the hyperbolic titration curves using the nonlinear fitting program of Sigma Plot 5.0 (Cambridge Soft. Corp., Cambridge, MA, USA). The concentrations of the AMA–OBP complexes were determined on the basis of emission spectra obtained by incubating AMA (0.1–10 µM) with saturating amounts of both OBP forms. [Ramoni, R. at al. *J. Phys.: Condens. Matter,* 2008]

3.9. Proteins fluorescent labelling

The fluorescent labelling of the proteins, was realized with the dye Oregon green 488 succinimidyl ester (6-isomer 488-X Mr = 622.5). We labelled randomly free amine groups of proteins according to a standard procedure described by the manufacturer (Molecular Probes).

The buffer employed for, bOBP and GCC-bOBP was Sodium Borate 20mM pH 8.3, (the optimal pH for random covalent modification using this dye) and the final concentration of fluorofore was 1 mM.

The samples were incubated for 1h and the reaction was terminated by the addition of Tris Base 10mM. For pOBP we used the same procedure, but in this case the buffer was PBS1x pH 7,4 with a two-hour incubation. After labelling, excess dye was removed by gel filtration chromatography on a column of Sephadex G-25, equilibrated with PBS.

3.10. Chemical denaturation by GdnHCl

Proteins (usually 5/10μM) in PBS buffer were denatured by addition of increasing amounts of PBS buffer containing 6MGdnHCl. The final concentration range of denaturant was 0–5 M. Measurements on the denatured protein forms were performed after, leaving the solutions 24 h at room temperature. By that time, all solutions were at the equilibrium, as shown by the absence of any further change of their spectroscopic properties.

The exact GdnHCl concentration was determined by refraction index using an Abbe refractometer (LOMO, Russia).

3.11. Fluorescence microscopy

A 2P laser (Mira, Coherent, Santa Clara, CA) pumped by 6.5 W of 532 nm light (green) from a Verdi solid state laser (Coherent) generates femtosecond 820 nm pulses at 80 MHz (magenta), it was used. The infrared (IR) laser beam, directly coupled to a microscope (Zeiss Axiovert 135, Zeiss, Jena, Germany), is expanded by a beam expander (BEX), attenuated by neutral density filters and passed to the X–Y scanner (SCN), which projects the scanned beam onto the objective (OBJ) (Zeiss Apo C40×, numerical aperture (NA) = 1.2 water immersion) and muscle fiber (MUS). The IR power impinging on the muscle is 65 mW. Fluorescent light (yellow) is collected by the objective, passed by the same scanner, and reflected by the dichroic mirror M3 into photomultipliers 1 and 2, which detect orthogonally polarized light passed by crossed analyzers AN1 and AN2. Since the fluorescent light is scanned again on the way to the detectors, it is termed descanned detection. Alternatively, mirror M5 can be substituted by a dichroic filter to pass the fluorescent light to another set of photomultipliers 3 and 4. Since the fluorescent light does not pass through the scanner, it is termed non-descanned detection.

Unless otherwise stated, all the experiments were performed in non-descanned mode. The 351 + 364 nm light from the ultraviolet (UV) laser (blue) (Enterprise, Coherent) is made collinear with the IR beam by the dichroic filter FT395. A fast-shutter SHT (Vincent Associates, Rochester, NY, model T132) is opened for 10 ms to admit UV light to the sample. [Ramoni R. at al., *J. Phys.: Condens. Matter, 2008]*

3.12. Fluorescence spectroscopy

Emission spectra were obtained with an ISS K2 spectrofluorometer. The excitation was set at 295 nm in order to exclude the tyrosine contribution to the overall fluorescence emission.

Front-face measurements were performed on bOBP immobilized onto CN in the absence and in the presence of AMA and the ligand.

3.13. Resonance Energy Transfer (RET)

Resonance energy transfer (RET) is an electrodynamic phenomenon that can be explained using classical physics. It has become widely used in all applications of fluorescence, including medical diagnostics.

RET occurs between two chromophores, a donor chromophore, initially in its electronic excited state, may transfer energy to an acceptor chromophore (in proximity, typically less than 10 nm) through non-radiative dipole–dipole coupling. When they are dissociated, the donor emission is detected upon the donor excitation, while, when the donor and acceptor are in proximity due to the interaction of the two molecules, the acceptor emission is predominantly observed because of the intermolecular RET from the donor to the acceptor.

This techniques is a useful tool to quantify molecular dynamics in biophysics and biochemistry, such as protein-protein interactions, protein-DNA interactions, and protein conformational changes.

In studies of protein structure the donor is often a tryptophan residue. However, extrinsic donors are often used because of the opportunity to position the donor in a desired location and to select the D-A pairs that are most suitable for a particular application. [Joseph R. Lakowicz, "*Principles of Fluorescence Spectroscopy*", third edition, 2006]

3.14. Optical spectroscopy of fluorescent labelled proteins

Absorbance spectra were measured on a Hitachi U-3210 spectrophotometer. Molar extinction coefficients were determined experimentally by dissolving a weighed amount of protein into neutral buffer and measuring the absorbance. The buffer used for this and most of the studies was PBS pH 7.4. The absorption spectrum of the labelled proteins were analyzed by adding the expected contributions of the tryptophan and tyrosine residues.

3.14.1. *Fluorescence Correlation Spectroscopy (Single Molecule Detection)*

A pulsed 470nm diode laser was used as the excitation source at a repetition rate of 20 MHz. All of the dynamic diffusion coefficient experiments were performed using one-photon excitation and a laser-synchronized gate in a detection channel.

It was used an Olympus FluoView 300 confocal scan head coupled to an IX71 inverted fluorescence microscope equipped with a water-immersion 60X 1.2 NA objective. Based on diffusion times for dye standards and ovalbumin, the estimated confocal volume was 1.4 femtoliters. The resulting fluorescence was collected through the same objective, separated from the laser light by a dichroic mirror and band-pass filter and focused onto an avalanche photodiode detector operated in single photon counting mode.

Spectra were recorded as a function of time (10 minutes each) and the diffusion times were determined from the autocorrelation of the fluorescence fluctuations, which were analyzed using software from PicoQuant, Inc., taking into consideration the contribution of triplet state blinking.

The values are obtained utilizing the Triplet State Model for FCS fits. It describes diffusion in the presence of triplet state blinking. The shape of the focal volume is approximated by a Gaussian profile.

The equation used for this fit is:

$$G_{(\tau)} = [1- T + Te^{(-\tau/\tau t)}] \; \Sigma \rho i \, (1+\tau/\tau i)^{-1} (1+ \tau/\tau i \kappa^2)^{-1/2}$$

$\kappa = z_0/ w_{0;}$ $Veff = \pi^{3/2} w_0^2 z_0$; $\langle C \rangle = \langle N \rangle / Veff \, N_A$; $Di = w_0^2/4\tau i$;

$\Sigma \rho i = 1/ \langle N \rangle (1-T)$

Veff [ft]= effective excitation volume determined by diffusion of free dye (Table 1); the reference conditions are used for calculation of the molecular diffusion coefficient from τ, which is the characteristic diffusion time obtained from fitting the autocorrelation of the fluorescence intensity fluctuations.

$z_{0[\mu m]}$ = effective focal radius along the optical axis at $1/e^2$ intensity; not fitted, calculated on the basis of Veff.

$w_{0[\mu m]}$ = effective lateral focal radius at $1/e^2$ intensity; not fitted, calculated on the basis of Veff.

ρi = contribution of the i^{th} diffusing species.

τi[ms] = diffusion time of the i^{th} diffusing species.

Di[μm^2/sec] = Diffusion costant of the i^{th} diffusing species; not fitted, calculated on the basis of Veff.

<N> = Avarage number of molecules in the focal volume; not fitted, calculated from G(0), the autocorrelation function at time=0.

<C> [nM]= Concentration of molecules in the focal volume; not fitted, calculated on the basis of Veff.

κ = length to diameter ratio of the focal volume.

T = Dark(triplet) fraction of molecules.

τ_T [ms] = Lifetime of the Dark (triplet) state.

3.14.2. *Time- resolved fluorescence anisotropy*

In a time-resolved fluorescence anisotropy experiment, the sample was repetitively excited with short (picosecond) pulses of polarized light.

Time-resolved fluorescence anisotropy measurements were carried out by time-correlated single-photon counting (TCSPC), using the FLASC 1000 sample chamber (Quantum Northwest, Liberty Lake, WA), which has a unique T format for simultaneous detection of horizontal (H), vertical (V) and variable polarization components of the emission. A beam-splitting Glan-Thompson polarizer (Karl Lambrecht, Chicago, IL) separates the H and V components.

The samples were excited at 5 MHz using the 470-nm laser diode from PicoQuant, Inc.. Instrument response functions (light scatter) and decay curves were collected to 100,000 and 40,000 counts in the peak channel, respectively. Decays were also collected from glycerol blank solutions for the same time as the sample, and were then subtracted from sample decays before analysis.

Fluorescence decay data were analyzed by nonlinear least-squares regression using the software package FluoFit (PicoQuant), which utilizes the Marquardt-Levenberg algorithm. The decay of the emission anisotropy was analyzed with

a double exponentials. The anisotropy parameters were obtained by fitting the vertically and horizontally polarized emission decay curves simultaneously.

3.15. Analytical Ultracentrifugation

Sedimentation velocity experiments were performed on a Beckman XL-A analytical ultracentrifuge equipped with absorption and fluorescence optics that allow scanning at multiple wavelengths and interfaced to a microcomputer for data acquisition. The sedimentation coefficient was determined from the movement of the boundary [Stafford, W.F. III, *Anal.Biochem.,* 1992] and corrected to standard conditions (20.0 C) and zero protein concentration using conventional methods [Van Holde K.E., *The Proteins*, 1985; Teller D.C., *Methods Enzymol.,* 1973].

The same PBS buffer, whose composition has been report above, was used for these experiments. Stock solutions of Oregon Green were prepared dissolving small amount of the dye in 100 µl of ethanol; these solutions were then diluted with PBS buffer 1:1000 and 1:2000. The concentration of the solutions was then determined by absorption at 492 nm. Fluorescence samples were finally diluted to a concentration of 10 and 50 nM in PBS containing 1mg/ml ovalbumin. All the centrifugations were realized at 50000 rpm at 20°C.

Sedimentation coefficients were calculated in SEDFIT either by assuming a single weight average frictional coefficient (f/fo) for all species (i.e., c(s) distribution) or by assuming a two-dimensional distribution of sedimentation and frictional coefficients (i.e., c(s,f/fo)). Buffer density and viscosity were fixed at 1.005 g/cm3 and 0.0102 Poise, respectively. Based on the amino acid sequence, the partial specific volume of proteins was estimated to be 0.73 cm3/g.

Data have been normalized for comparison.

3.16. SAW (Surface Acoustic Wave) biosensor system

SAW (Surface Acoustic Wave) biosensor system is composed of two identical 392 MHz 2-ports SAW resonators, consisted of gold/aluminium multilayered IDTs (interdigital transducers) produced using a 5 nm gold film on a 100 nm aluminum film and mounted on a TO39 package. bOBP was deposited on a SAW resonator by using the technique described below, while a second uncoated resonator was used as reference. SAW resonators were used as frequency-control element in the feedback branch of Pierce oscillator circuits. Two matching networks create the phase shift to fulfil the phase condition on the oscillator loop. A tuneable capacitor allows one to fine adjust the oscillation frequency to the serial resonance frequency of the SAW device [Benetti, M. at al., *IEEE Sensors Proc.,* 2008]. The differential frequency shift, due to the SAWs velocity changes as consequence of odorant concentration, was easily measured.

3.16.1. *OBPs deposition*

The proteins were deposited on the surface of the SAW device by means of droplet method. This method was optimized using a 155 MHz 2-port SAW resonator on ST-cut quartz. The IDTs were made of thin gold film. SAW resonators were mounted on a PCB and connected to two SMA connectors. Measurements were performed by an HP8753A Network Analyzer and data acquired by a PC, using National Instruments Labview software. The SAW resonator records frequency shifts before and after several depositions of proteins and its ligands showing different signals.

4. RESULTS

4.1. Proteins expression and purification

Heterologous expression of the recombinant proteins is an essential prerequisite for detailed physico-chemical characterization of distinct OBP types. The bOBP as well as GCCbOBP and pOBP were expressed in high quantities as soluble proteins, and were purified from the supernatant of *E.coli* extracts under native conditions employing Ni-nitrilotriacetic acid agarose and GST affinity chromatography. 5 to 30 mg of purified protein were obtained from 1 L of *E. coli* culture.

SDS-PAGE of the purified forms of OBP gave single bands at the expected molecular weights.

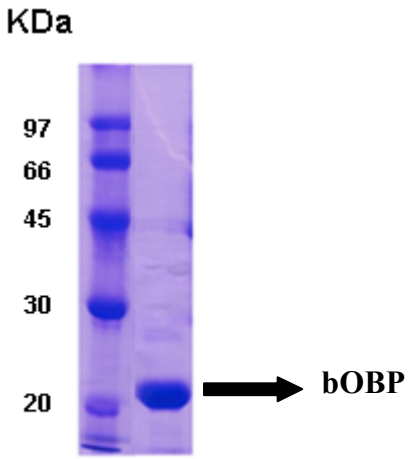

SDS-PAGE of purified bOBP

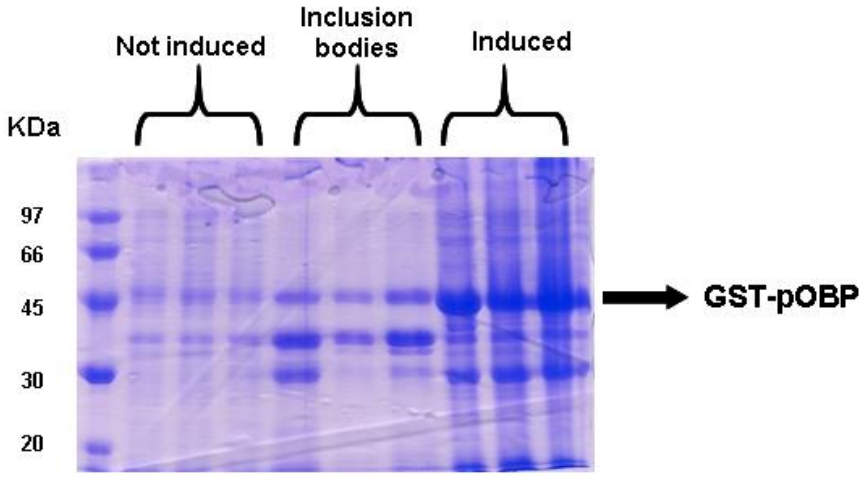

SDS-PAGE of expressed recombinant pOBP fused with GST (glutathione S-trasferase)

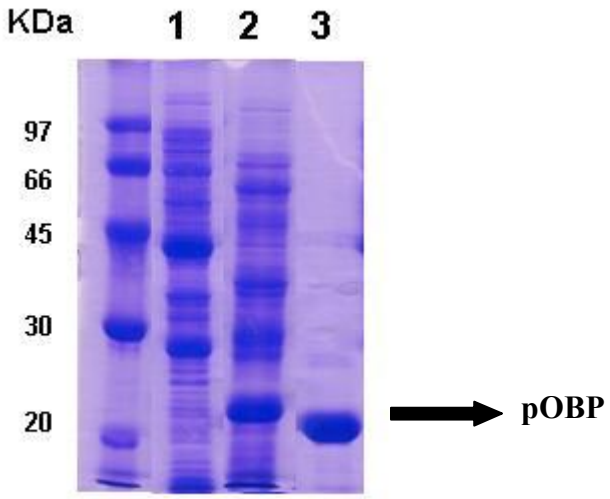

SDS-PAGE of purified pOBP. Lane 1 : crude extract, Lane 2: flow-through, Lane 3: eluated column fraction.

4.2. Production of ALLOpOBP

The Trp 16 in pOBP, that is conserved in the sequence of several OBPs, is located near the first strand of the barrel, and is deeply buried in the interior of the central cavity, being slightly exposed in pOBP.

We performed our experiments with standard protocols of analog incorporation (see methods), but after mass spectroscopy of purified pOBP ractions we realized that the final quantity of Alloprotein was only 4% of the total protein obtained.

4.3. Fluorescence Spectroscopy

To shed light on the structure and stability of OBPs and to investigate the possibility of their use as biological recognizing elements in biosensors, in the present project of Doctorate, I decided to characterize some structural, functional and stability properties of bOBP, mutant bOBP (GCCbOBP) and pOBP which had not been yet considered in previous studies.

The experiments of Fluorescence Correlation Spectroscopy (FCS) and time-resolved fluorescence anisotropy that were performed to study the stability of these proteins were realized by extrinsic fluorescence reporters. The aim of this approach was the characterization of the hydrodynamic properties of the OBPs. In particular I tried to establish first (1) if the mutant GCC-bOBP, after the modifications of its primary structure, has really acquired a monomer state. In addition (2) I wanted to test if the aggregation state of pOBP that, with other techniques had been demonstrated to be a monomer.

4.4. Labeling of proteins

For protein labelling we decided to use the dye Oregon green 488 succinimidyl ester (6-isomer 488-X Mr = 622.5) which is reported to be an excellent probe for the investigation of chemical physical properties of proteins, in fact, it has a very high extinction, a high quantum yield, and a very high photostability

making it is significantly less susceptible to photobleaching compared with other fluorescent probes. This probe has an excited-state lifetime of about 4ns.

The yield of GCC-bOBP labelling was between 0.8-0.9 molecule of probe per monomer , that of bOBP was between 0.6-0.7 molecules per monomer while that of pOBP less than 0.5 molecules per monomer. We also labelled chicken ovalbumin (with a very low efficiency of ~ 0.1 probe molecule/ monomer), which was used as a diffusion standard for FCS.

The yield of protein labelling was estimated from absorption spectra assuming that the extinction coefficients of the probe at the lowest energy maxima are unaffected by conjugation. The lowest energy absorption maximum for Oregon green 488 is near 492 nm, and the extinction coefficient is 68,000 $M^{-1}cm^{-1}$ (Molecular Probes). From the ratio between the lowest energy absorption maximum of the dye and its absorption value at 280 nm, it was determined that the extinction coefficient at 280 of Oregon green is about 20,200 $M^{-1}cm^{-1}$. These values were used to account for the contribution of the dyes to the absorbance at 280 nm of the dye-conjugated the proteins.

A caution in the measurements must be taken because the lowest energy absorption band of the dyes is red-shifted of 3–6 nm when conjugated with the proteins. A red or blue shift of 5 nm, in fact, could change the 280 nm absorption values as much as 20%, causing a systematic error to the estimation of labelling efficiency. The significance of this error obviously depends on the relative magnitude of the protein extinction coefficient. [Rusinova E. at al., *Anal. Biochem.*, 2002].

In addition, we noticed that it was not possible to remove the dye in excess, even after several rounds of dialysis. For this reason the yield of protein labelling was determined, in bands of proteins purified by SDS page.

4.5. Fluorescence correlation spectroscopy measurements

Fluorescence correlation spectroscopy have been widely used to study particle diffusion [Fahey, P. F. at al., *Science*, 1977; Koppel, D.E. et al., *Biophys. J*, 1976], chemical kinetics [Haupts, U. et al., *Proc. Natl. Acad. Sci. USA*, 1998; Starr, T. E.

& Thompson, N. L. *Biophys. J.*,2001], and molecular aggregation [Palmer, A. G. and Thompson, N. L. *Biophys. J.*, 1987; Qian, H. and Elson, E. L. *Proc. Natl. Acad. Sci. USA*, 1990] in solution. Recently FCS has evolved into a powerful method to study molecule dynamics at the single molecule level [Medina, M. A. and Schwille, P. Bioessays, 2002]

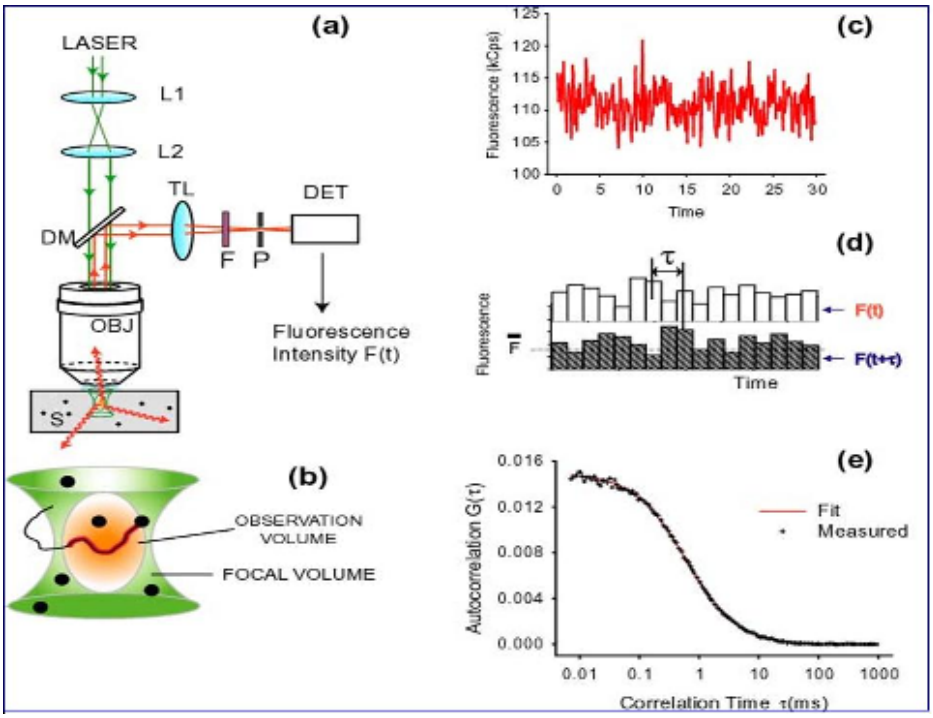

Fluorescence Correlation Spectroscopy (FCS) system

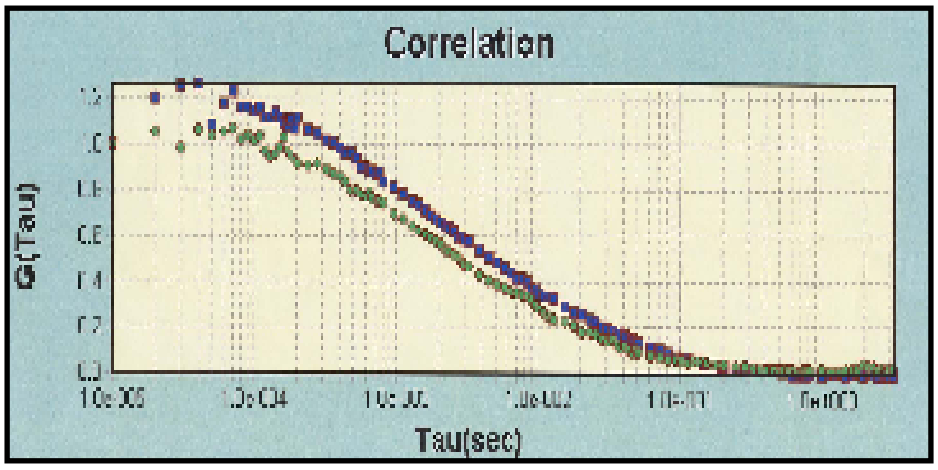

Autocorrelation spectra

This technique is a valuable tool in many scientific disciplines. In particular, such a spectroscopic technique has received a great deal of attention because of its remarkable potential for single-protein molecule detection.

In fluorescence correlation spectroscopy, are monitored temporal fluorescence fluctuations from the diffusion of single fluorescent molecules through a small optically delimited detection volume [reviewed by Bacia, K. and Schwille, P. *Methods*, 2003]. Excitation and detection are commonly performed using a similar laser-illuminated confocal setup as in scanning confocal microscopy. Fluctuations are processed online to yield an autocorrelation curve from which the particle mobility (diffusion coefficient) is derived. FCS works from the single molecule regime up to hundreds of molecules in the focus (from 10-nM to 1-μM concentration range). FCS is emerging as an important technique in biochemical studies to study diffusion as well as conformational transitions of macromolecules on timescales of microseconds and longer [Elson, E. L. *Annu. Rev. Phys. Chem.* **36:**379–406, 1985; Frieden, C. at al. *Adv. Protein Chem.*, 2002; Hess, S. T. at al. *Traffic*, 2001]. It involves measuring fluorescence fluctuations under conditions of thermodynamic equilibrium, in a small observation volume of about 1 fL. These fluctuations may result either from a change in the number of fluorophores in the observation volume due to diffusion, or can be due to a change in the fluorescence properties of the molecule as a consequence of chemical reactions or a conformational fluctuations.

The autocorrelation function for the fluorescence intensities, normalized by average intensity squared is given by:

$$G(\tau) = \frac{\langle \delta F(t+\tau)\ \delta F(t) \rangle}{\langle F(t) \rangle^2}$$

Where t is real time, τ is a time difference between two intensity measurements and δF(t) is the variance, which reflects the intensity fluctuation about the mean value – δF(t) = <F> - F(t). [Lakowicz J.R., "Principles of Fluorescence Spectroscopy", third edition, 2006].

We decided to do these experiments because an important parameter that can be obtained from FCS is the number and size of particles in the observation

volume, which is a very sensitive measure of the presence of aggregation or of a monomer-dimer equilibrium in solution at a very low concentration (typically 10–50 nM). In fact other techniques employed for the same purpose, as for instance exclusion chromatography or light scattering, usually require proteins concentrations higher one to three orders of magnitude. FCS is an equilibrium technique, no external perturbation is needed, it has high sensitivity and can be employed over wide timescales.

For the experiments we used the buffer (PBS1x) containing 1 mg/mL of unlabelled Ovalbumin to avoid non-specific binding of probe-labeled OBP to glass (coverslip) surfaces. We also checked using buffer without ovalbumin, and did not observe significant differences in diffusion times.

FCS measurements were also extended to unfolding protein unfolding investigations to determine the diffusion times and as a function of denaturant concentration. However, FCS measurements in the presence of Gdn are made more complex due to changes in viscosity and refractive index of the solution; FCS data need to be corrected for viscosity and refractive index changes as the guanidine hydrochloride concentration increases.

We recorded spectra as a function of time (10 minutes each) and the diffusion times were determined from the autocorrelation of the fluorescence fluctuations, which were analyzed using software (SymphoTime) from PicoQuant, Inc., taking into consideration the contribution of triplet state blinking.

For every measurement, we monitored the amplitude, that depends on the average number of fluorescent particles in the volume and hence on the concentration. . Based on diffusion times for dye standards and ovalbumin, the estimated confocal volume was 1.4 femtoliters.

The FCS data for OBPs yielded diffusion coefficients in the range of 90-120 μm^2/sec. [Table 1]

Each FCS measurement was performed several times (at least 5 times), and the obtained curves were always overlapping, indicating a high degree of reproducibility and accuracy.

Theoretical Diffusion Coefficient calculated for a sphere compared with Diffusion Coefficient of OVA and OBPs determined from FCS measurements.		
	Theoretical(sphere) translational D(µm^2/s)	Empirical translational D(µm^2/s)
OVA	**87**	**90**
bOBP	**89**	**60**
GCCb OBP	**113**	**120**
pOBP	**113**	**60**
Reference conditions for free dye: Veff= 1,6; κ = (z0/ w0) 8; z0= 2,640; w0= 0,330; D1= 390		

Table 1

These values were obtained utilizing the Triplet State Model for FCS fits. (See Material and Methods).

It describes diffusion in the presence of triplet state blinking. The shape of the focal volume is approximated by a Gaussian profile.

We interpreted our results using standard assumptions for partial specific volume (0.73 mL/g) and hydration (0.45 g/g protein) (scheme 1), and on this basis evaluated the deviation of shape of the protein molecules from rigid spheres. For the calculation of Rsphere, the Radius of the Hydrated Stokes' Sphere, we determined the hydrodynamic values expected if the molecules were rigid spheres. In this way, only shape parameters-asymmetry and flexibility-need be considered. We calculated Rp, the radius of an anhydrous sphere with a molecular weight equal to that of the molecule of interest, using the empirical equation $Rp = (6.723 * 10^{-9})* Mr^{1/3}$, where Mr is the molecular

weight obtained from equilibrium centrifugation [Teller, D. C., *Methods in Enzymol.* 1973].

The anhydrous molecular volume, Vp, can be calculated from Rp.

The hydration, δ, is used to generate V, the volume of the hydrated sphere.

$V = Vp (v + \delta / v)$

v is estimated using the method of Cohn and Edsall [Cohn, E.J. & Edsall, J.T., *Proteins, Amino Acids and Peptides as Ions and Dipolar Ions*, 1943; Laue, T.M. at al. *Biochemistry and Polymer Science*, 1992]

$v = \Sigma ni Mi vi / \Sigma ni Mi$

where ni, Mi, and vi are the number of moles, molecular weight and partial specific volumes, respectively, for the component amino acids of proteins.

For the purposes of this development, δ was estimated at 0.45 g of H2O/g of protein.

Rsphere, the radius of the hydrated Stokes' sphere, is easily calculated from V.

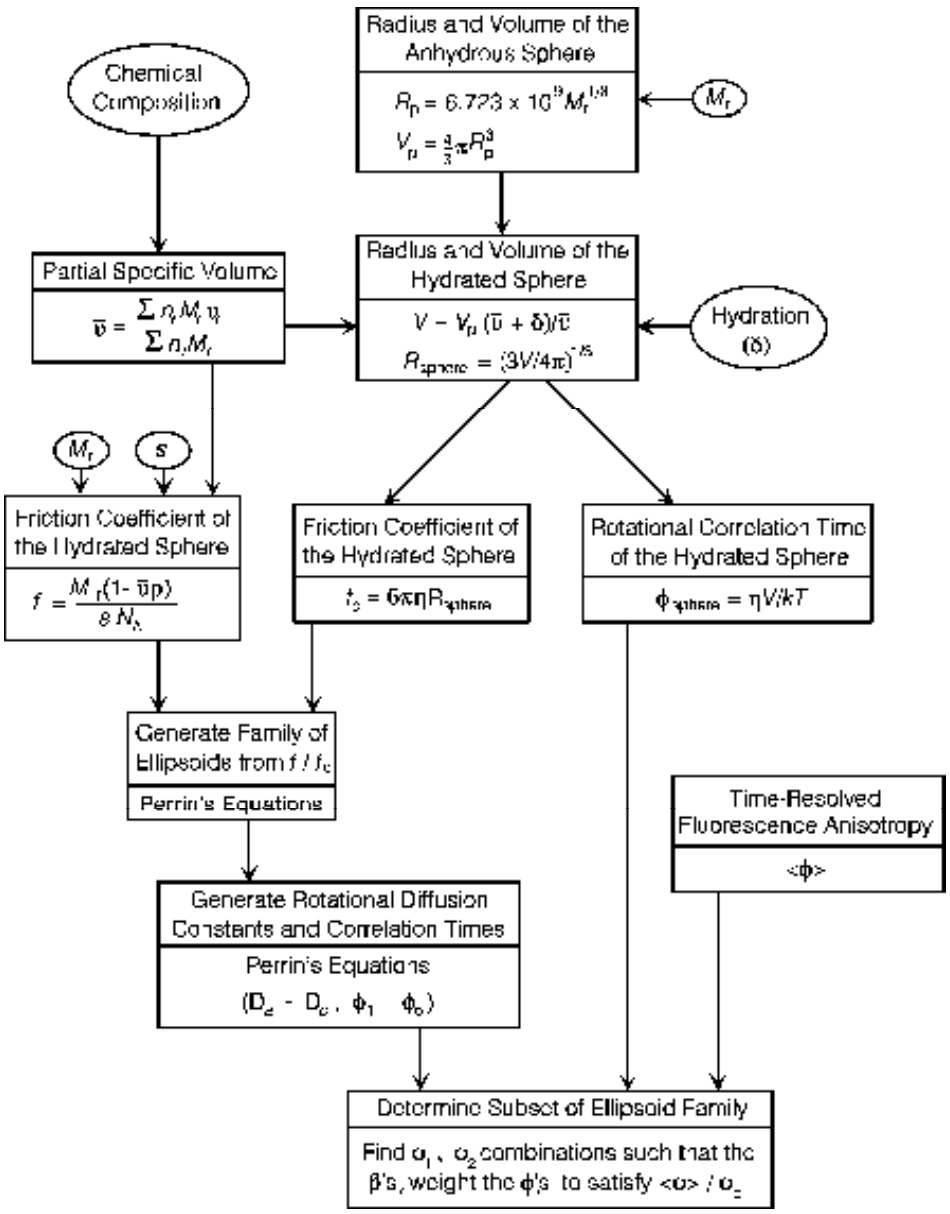

Scheme 1: Scheme for evaluation of hydrodynamic parameters showing inputs, assumptions, procedures, and equations where appropriate

[Waxman et al., *Anal. Biochem.*, 1993.]

4.6. Time-resolved fluorescence anisotropy measurements

Time-resolved fluorescence anisotropy decay is a well established experimental method for investigating hydrodynamic properties and structural dynamics of proteins [Badea M. and Brand L., Methods Enzymol., 1979]. This technique measures the time dependence of the depolarization of light emitted from a fluorophore experiencing angular (rotational) motions. For an intrinsic or extrinsic probe on a protein, these depolarizing motions include rotations of the entire macromolecule, segmental fluctuations of the domain containing the fluorophore, and local dynamics of the fluorophore about a covalent bond or within a non-covalent binding site. As a result, fluorescence anisotropy decay is useful for establishing relationships between structural dynamics and function by providing information about local motions within a specific region such as the active site of an enzyme. Time-resolved fluorescence anisotropy decay also yields overall size and shape parameters, which can provide additional information on biological function and interactions with other molecules.

So, Time-resolved fluorescence anisotropy decay data can provide important information regarding molecular flexibility or segmental motion. This is due to the short time frame (picoseconds to nanoseconds) over which molecular rotation is measured. The time dependence of the depolarization due to rotation is defined as

$$r(t) = \frac{I_{VV}(t) - I_{VH}(t)}{I_{VV}(t) + 2I_{VH}(t)}$$

where $I_{VV}(t)$ and $I_{VH}(t)$ represent the vertical and horizontal decays, respectively, obtained using vertical excitation. The denominator is the total intensity decay, $I(t)$.

$$I_{VV}(t) + 2I_{VH}(t) = I(t) = \sum_{i=1}^{n} \alpha_i e^{-t/\tau_i}$$

where τ_i is the lifetime and α_i is the amplitude of the ith component in the intensity decay, $I(t)$.

We have carried out time-resolved fluorescence anisotropy experiments with native proteins, and with increasing concentrations of Guanidine Hydrochloride from 0.5 to 5 M.

Time-Resolved Anisotropy of Oregon Green-Labeled bOBP, GCCbOBP and pOBP

Proteins	η	GdnHCl	χ^2	β_1	ϕ_1(ns)	β_2	ϕ_2(ns)	<r>	r_0
bOBP			1,26	0,0719	**15,1**	0,1152	**0,99**	0,086	0,187
GCCbOBP	/	0 M	1,25	0,0804	**7,2**	0,0956	**0,90**	0,075	0,176
pOBP			1,17	0,0379	**7,2**	0,1152	**0,68**	0,045	0,153
bOBP			1,21	0,0856	**7,3**	0,1604	**0,64**	0,085	0,246
GCCbOBP	1,02	0.5 M	1.17	0,0936	**4,4**	0,1240	**0,67**	0,073	0,217
pOBP			1,25	0,0902	**3,0**	0,2344	**0,30**	0,056	0,324
bOBP			1,21	0,0911	4,8	0,1533	0,55	0,075	0,244
GCCbOBP	1,04	1 M	1,17	0,0971	4,3	0,1580	0,56	0,075	0,255
pOBP			1,14	0,0791	4,1	0,1656	0,46	0,060	0,243
bOBP			1,14	0,0825	5,0	0,1620	0,61	0,077	0,244
GCCbOBP	1,07	1.5 M	1,22	0,0780	5,6	0,1500	0,73	0,073	0,228
pOBP			1,16	0,0758	3,1	0,1806	0,44	0,054	0,256
bOBP			1,16	0,0692	7,38	0,1780	0,78	0,080	0,247
GCCbOBP	1,10	2 M	1,20	0,0853	4,15	0,1506	0,63	0,07	0,236
pOBP			1,25	0,0961	1,8	0,1517	0,38	0,047	0,247
bOBP			1,18	0,1010	**2,8**	0,1786	**0,54**	0,070	0,28
GCCbOBP	1,13	2.5 M	1,10	0,0931	**3,4**	0,1424	**0,7**	0,07	0,235
pOBP			1,20	0,0806	**1,70**	0,1401	**0,55**	0,047	0,220
bOBP			1,20	0,1134	2.0	0,1462	0,58	0,065	0,26
GCCbOBP	1,17	3 M	1,14	0,1078	2,4	0,1292	0,62	0,065	0,237
pOBP			1,24	0,0750	1,5	0,1450	0,65	0,045	0,220

bOBP			1,17	0,1284	1,7	0,1427	0,51	0,06	0,271
GCCbOBP	1,22	3.5 M	1,20	0,1060	2,2	0,1316	0,62	0,064	0,237
pOBP			1,07	0,0740	2	0,1430	0,41	0,045	0,180
bOBP			1,14	0,1465	1,6	0,1580	0,4	0,06	0,304
GCCbOBP	1,27	4 M	1,20	0,1041	2,1	0,1488	0,6	0,063	0,253
pOBP			1,3	0,0850	1	0,1302	0,49	0,043	0,225
bOBP			1,22	0,0950	1,6	0,1640	0,7	0,06	0,259
GCCbOBP	1,41	4.5 M	1,18	0,0993	2,1	0,1284	0,66	0,06	0,227
pOBP			1,2	0,0780	1,05	0,1290	0,001	0,042	0,38
bOBP			1,09	0,0900	1,9	0,1740	0,7	0,06	0,264
GCCbOBP	1,51	5 M	1,23	0,1432	1,6	0,1321	0,44	0,06	0,275
pOBP			1,33	0,1001	1,12	0,1034	0,58		0,200

Table 2: The long correlation times, ϕ_1, and the short correlation times, ϕ_2, were fit as independent parameters at a timing resolution of 35 ps/channel at 20° C; β_1 and β_2 are the amplitudes of the respective correlation times, r_0 is the limiting anisotropy calculated from the sum of β_1 and β_2, $< r >$ is the steady-state calculated from the time-resolved parameters, and χ^2 is the reduced chi-squared statistic.

The anisotropy decays of the proteins were double exponential with a longer correlation time of 15 ns for bOBP and 7.25 ns for GCC-bOBP and pOBP respectively, representing the global motion for native proteins, and a shorter correlation time of 0.99 ns and 0.90 ns for bOBP and GCCbOBP and 0.68 ns for pOBP, representing segmental or local motions. We can see a considerable change of anisotropy decay just with a concentration 0.5M of denaturant and another change at 2.5M of guanidine hydrochloride for all proteins.

This suggests that at 0.5 M guanidine there is partial unfolding and/or subunit dissociation in the case of bOBP, assuming its native state is dimeric, and partial unfolding of the mutant bOBP and pOBP, assuming the latter proteins are monomeric in the native state.

4.7. Analytical Ultracentrifugation Experiments

The analytical ultracentrifuge is still one of the most versatile, rigorous and accurate technique for determining the molecular weight and the hydrodynamic properties of a protein or other macromolecule.

We performed ultracentrifugation experiments to better understand the global structure and assembly (monomer-dimer) of the different OBPs considered in this thesis. In particular, we run sedimentation equilibrium and sedimentation velocity experiments to obtain the molecular weight and the translational frictional coefficient of these proteins. The translational frictional coefficient is a single parameter that depends on the size, shape, and flexibility of the molecule. The purpose was to evaluate if bOBP and the GCCbOBP mutant are a dimer and a monomer respectively. We also compared the values of the friction coefficients determined by sedimentation velocity to those predicted from the FCS experiments. This can helped to establish if these proteins are asymmetric, as suggested by the time-resolved anisotropy data. In other words, our goal was to put together the FCS, time-resolved anisotropy and AUC results to develop a comprehensive hydrodynamic picture of the properties – monomer-dimer equilibrium and folding stability – of the different Odorant Binding Proteins considered here.

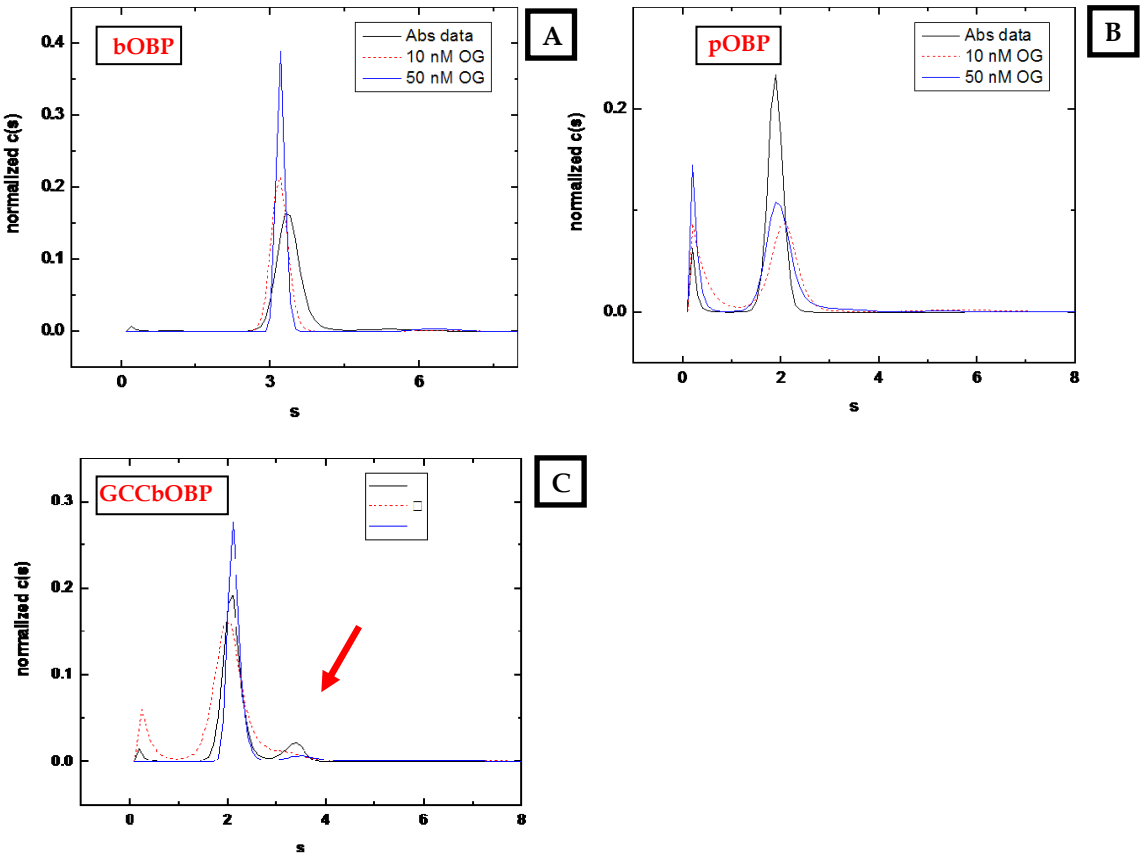

Ultracentrifugation spectra: (A) Bovine wild-type (bOBP) 3.2 - 3.4s, 90 -94%~37-39 kDa (dimer); **(B)** Pork wild-type (pOBP) 1.9-2.1 s, ~61-89 %~19kDa (monomer); **(C)** Bovine mutant (GCCbOBP) 2.0 to 2.1s, 75-86 % ~21-22 kDa (monomer) plus ~10% or more of larger s ~3.3s in the abs data (red arrow

From experimental results it possible to confirm that bOBP is a very tight (high affinity) dimer. There is no evidence of dissociation between the two subunits even at concentrations as low as 10 nM (fluorescence data). The bOBP mutant (GCC-bOBP) is mostly monomer at low (10 nM) concentrations. However, at higher concentrations there is a significant evidence for the formation of dimers, according to an equilibrium whose Kd value can be estimated in the

micromolar range. This indicates that the mutations introduced in the hinge sequence and the removal of the inter-domain disulphide bridge do not completely eliminate the attitude of bOBP to form dimers. These measurements confirm the FCS data showing that, at concentrations between 1 and 10 nM, the GCC-bOBP mutant behaves like a monomer. The behaviour of pOBP in ultracentrifugation indicates the presence of a monomer and, in lower quantities, of other forms with higher dimensions. Since pOBP is reported to be more unstable than bOBP or GCC-bOBP this behaviour could be due the formation of irregular aggregates instead of definite multimeric protein forms.

4.8. Fluorescence-based biosensor

In the present study we carried out preliminary experiments to understand if is possible to use as advanced nano-biosensors a mutant form of the bovine odorant-binding protein (bOBP) immobilized onto carbon nanotubes. In particular, after immobilization of the protein on the carbon nanotubes we developed a competitive resonance energy transfer (RET) assay between the protein tryptophan residues located at the positions 17 and 133 (W17 and W133) and the 1-amino-anthracene (AMA), a molecule that fits in the binding site of bOBP. The bOBP–AMA complex emitted light in the visible region upon excitation of the Trp donors.

However, the addition of an odorant molecule to the bOBP–AMA complex displaced AMA from the binding site making the carbon nanotubes colorless.

On the basis of bOBP structure, it is possible to notice that the molecule 1-amino-anthracene (AMA) fits very well into the bOBP binding site. A static analysis of the 3D structure of bOBP shows that the protein tryptophan residues are located in proximity to AMA, that is AMA and the protein indole residues are at a distance (Foster distance) allowing a resonance energy transfer (RET) phenomenon. We questioned whether it would be possible to design a carbon nanotubes (CTs) competitive RET assay based on the Trp donor–AMA acceptor for sensing the presence of odorant molecules in the environment. [Ramoni, R. at al. *J. Phys. Condens. Matter*, 2008]

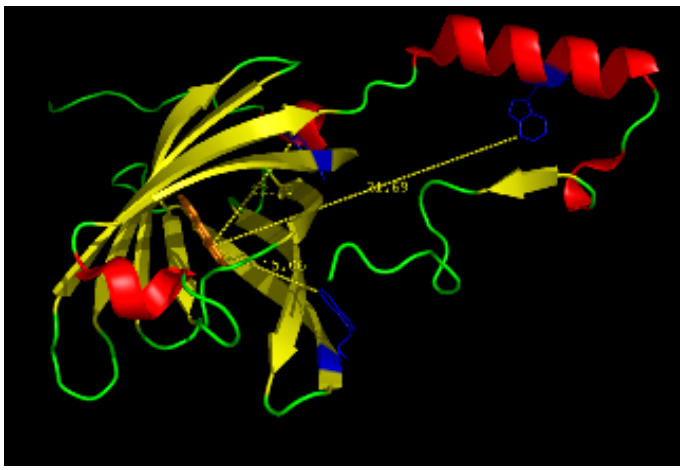

Structure of bOBP

We verified that bOBP could be immobilized onto CTs by simple incubation of the CTs-bOBP at room temperature for 10 min in aqueous buffers (phosphate buffer, pH 6.5). In fact, after several washings of the bOBP-treated CTs, the absorbance and fluorescence measurements confirmed that a large amount of bOBP was still present on the CTs surface.

We recorded emission spectra of CTs-bOBP alone, upon addition of AMA and upon addition of an excess of 1-octen-3-ol, the natural ligand of bovine OBP [Ramoni R. at al., *J. Biol. Chem.*, 2001].

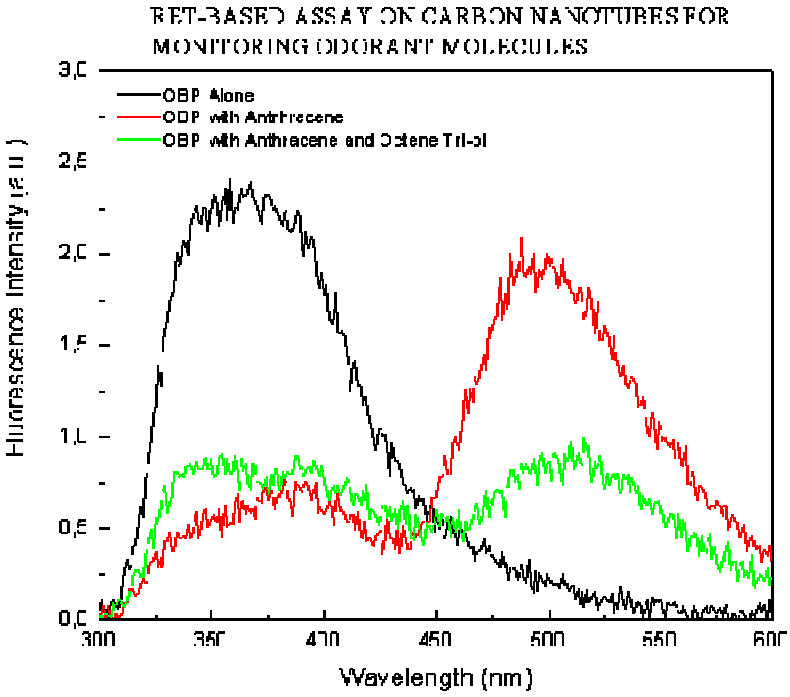

Fluorescence emission spectra of bOBP alone, in the presence of AMA and AMA-ligand

The resonance energy transfer process observed upon addition of AMA shows that the close interaction between the Trps of bOBP and AMA results in a high efficiency process of RET between the donor and acceptor. Since 1-octen-3-ol is present in large excess, the addition of the ligand to the bOBP–AMA complex results in a displacement of AMA from the bOBP binding site, and in turn to a decreased efficiency of the RET.

As the emission of AMA was in the visible region of light, we wondered whether it would be possible to design a light on/off nano CT-based biosensor. It is possible to observe a spectacular emission of blue light due to RET upon excitation of Trp at 290 nm. In fact, the CTs become completely blue in color. The addition of the competitive odorant molecule, 1-octen-3-ol, displacing AMA from the OBP ligand binding site, makes the CTs colorless.

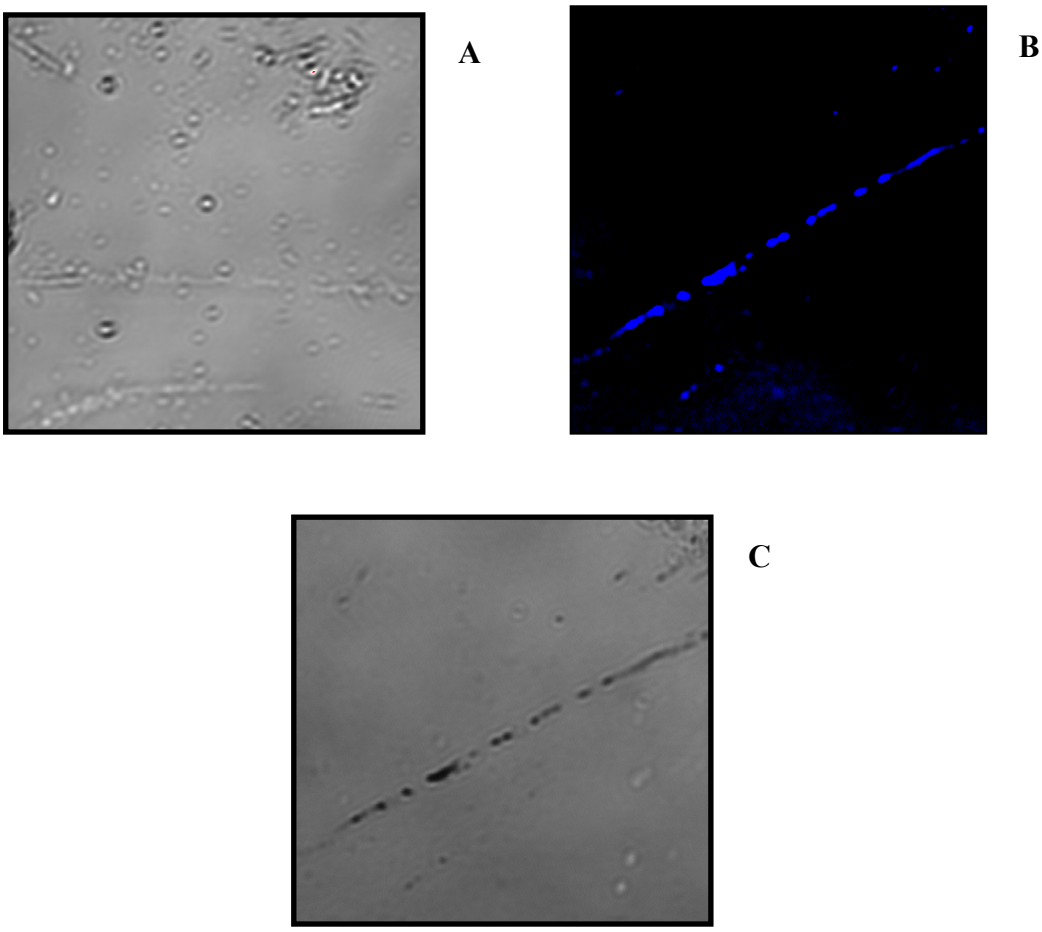

The confocal microscopy images of bOBP-treated CTs alone (A), in the presence of AMA (B), and after addition of 1-octen-3-ol (C)

4.9. Surface acoustic wave biosensor based on the utilizing of OBPs

The protein utilized to perform these experiments was bovine OBP. To optimize bOBP deposition on interdigital transducers (IDTs), the protein was deposited by means of the droplet method (see methods above) on the surface of a 155 MHz 2-port SAW resonator on ST-cut quartz. To promote the protein adhesion, the IDTs were made of thin gold film. SAW resonators were mounted on a PCB and connected to two SMA connectors (fig. 1).

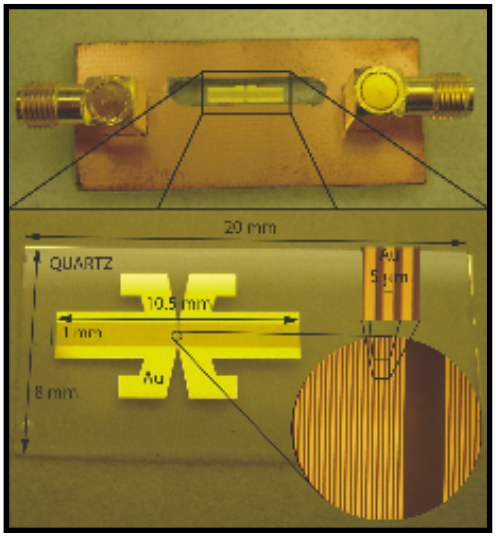

Figure 1. SAW device for optimization of deposition.

By means of two identical 392 MHz 2-ports SAW resonators, consisted of gold/aluminium multilayered IDTs, a differential configuration was implemented. In this way parasitic phenomena due to temperature variations could be reduce. Each SAW resonator was used as a frequency control element in a Pierce oscillator.

The bOBP was deposited on one resonator, the other was used as reference. The differential frequency shift, due to the SAWs velocity changes as consequence of odorant concentration, was easily measured.

The frequency shift in the resonator response (S_{21}) after deposition shows the presence of the protein on the IDTs surface as reported in fig. 2, where the SAW resonator transfer function before and after two depositions of bOBP is shown. The frequency shift after a deposition of 20 µl of bOBP (c=10mM) is about 5 KHz.

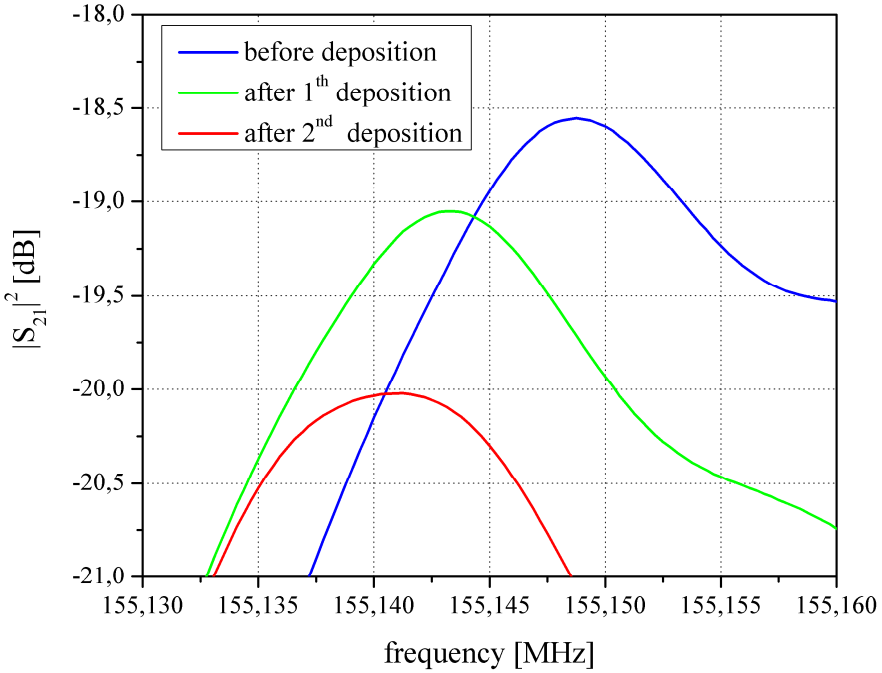

Figure 2. frequency response of the 2-port resonator before and after bOBP deposition.

The concentration of 1-octen-3-ol in a particular weight of boletus was measured by using gas chromatography technique [Bogus law Buszewski, A. at al. " *Journal of Chromatography B*, 2008].

To perform SAW sensor measurements, dried boletus was placed in a chamber, where pure nitrogen was fluxed. The odorant flux was diluted by a further nitrogen flux to obtain different concentrations of 1-octen-3-ol. The mixture was carried to the SAW sensor placed in a measure chamber. The differential frequency shift, due to the SAW velocity changes as consequence of odorant concentration, was measured by a frequency meter and data monitored and acquired by a PC. In fig. 3 the experimental setup is shown.

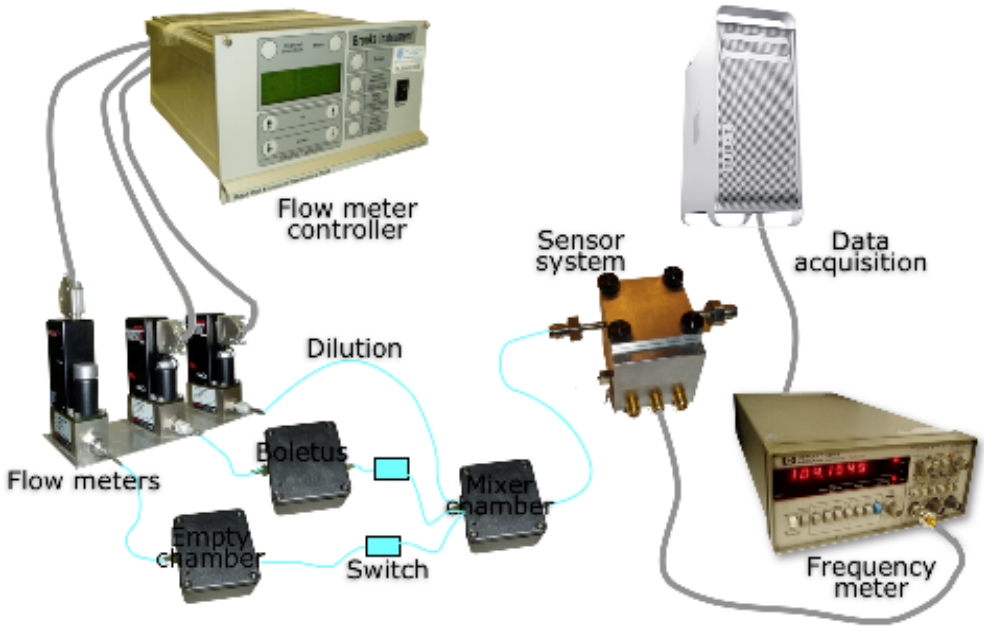

Fig. 3 SAW sensor measurements setup.

Real time monitoring of protein-odorant interaction was performed as suggested by SAW biosensor time response. In fig. 5 SAW sensor time responses for 6 different 1-octen-3-ol concentrations are reported.

To obtain the response curve, the frequency shift of SAW biosensor system at different 1-octen-3-ol concentrations was measured. In fig. 4 the SAW sensor frequency response for 1-octen-3-ol concentrations up to 8 ppm is reported. A resolution of 44 ppb and a sensor sensitivity of 314 Hz/ppm were obtained. The device sensing mechanism is related to change in SAW phase velocity, induced by the mass loading upon interaction between the bOBP and the odorant molecules in air.

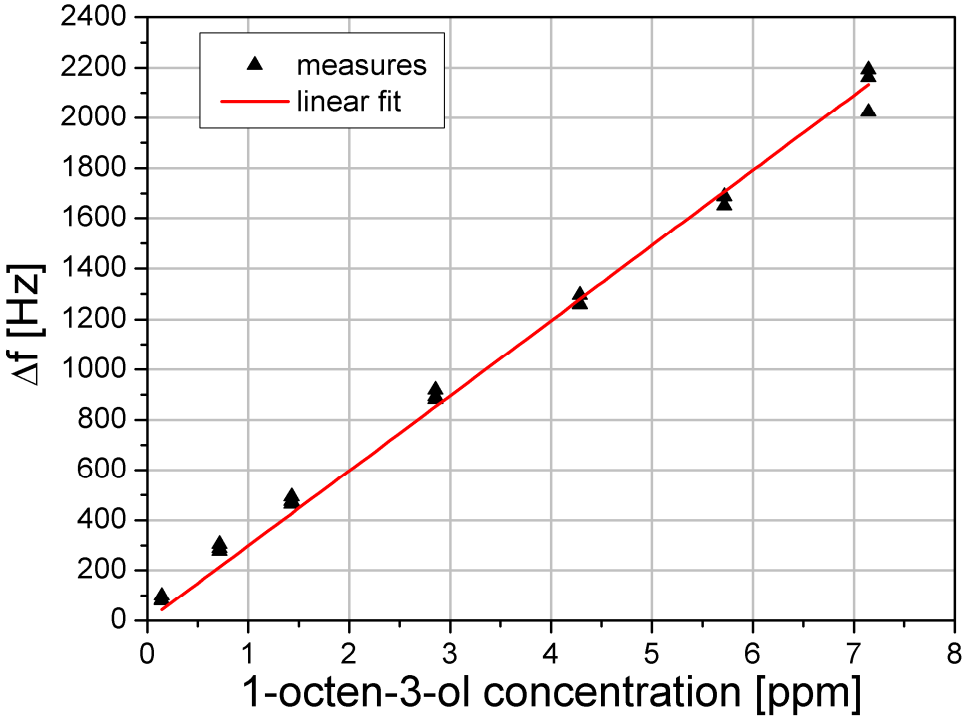

Fig. 4 SAW sensor response curve

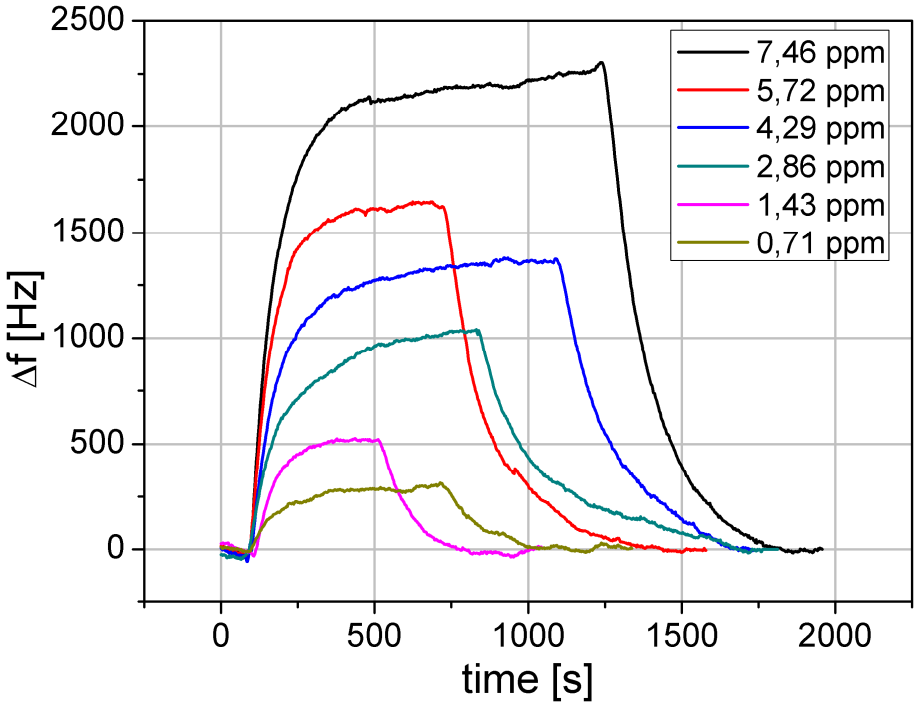

Figure 5 SAW sensor time responses for 6 different 1-octen-3-ol's concentrations

We demonstrated that OBPs are able to bind odorant molecules, after deposition on the SAW transducer surface. The OBPs preserve their function, we can considerate their application to realize future biosensors to detect various analytes.

5. DISCUSSION AND CONCLUSION

In this study, we considered the following OBP forms: porcine OBP (pOBP), a typical monomeric lipocalin [Spinelli, S. at al., *Biochem*, 1998] bovine OBP (bOBP), a dimer with domain swapping [Tegoni, M. at al. *Nat. Struct. Biol.* 1996] and GCC-bOBP, a deswapped monomerica mutant derived from bovine OBP [Ramoni, R. at al. *Biochim. Biophys. Acta*, 2008]. The aim was that of defining if these proteins, that bind a wide spectrum of ligands with different chemical structures, can be employed as biological recognition elements in Biosensors. The choice of investigating and characterizing OBPs was based on the following background:

1. bOBP and pOBP are two of the of the best characterized lipocalins [Tegoni, M. at al., *Biochim. Biophys. Acta*, 2000]
2. Prevoius studies have shown that mammalian OBPs are characterized by high stability and retain their functionality even after relevant chemical modifications [Grolli, S. at al., FEBS, 2006]
3. OBPs, and in particular the bovine form, tolerate mutations even when they involve residues playing a key role in protein structure and stabilization.

The initial part of my study has been devoted to the production of an alloprotein (a protein that contains unnatural amino acids) of pOBP that might allow to evaluate the formation of the ligand binding complex through variations of the intrinsic emission fluorescence of the protein.

The Alloprotein was prepared according to standard protocols for the incorporation of synthetic analogs of the amino acid tryptophan.

Unfortunately we had many problems of incorporation, in fact after mass spectroscopy of the purified protein, we realized that the final yield of Alloprotein was only 4% of the total, a very low quantity, obviously, not useful to continue with our experiments.

At first we thought that the reason of our unsuccess could be the plasmid used because we had a very low level of expression of the heterologous protein by E.coli. After we realized that the low yield of incorporation could be related to specific characteristics of porcine OBP structure and folding. In fact, comparing our data with those reported in the literature, it turned out that Human Tissue Factor, and other proteins with beta structures similar to those present in lipocalins [Zemsky, J. at al. *Proteins*, 1999], due to problems of folding, incorporate tryptophan analogs at the same low levels we obtained with ALLO-pOBP.

In particular based on the three dimensional structure of pOBP, we speculate that the folding of the protein requires the interactions of the Trp side chain and possibly hydrogen bond formation with the 5-hydroxy of 5HW or the 7-pyridinium of 7AW. Since, this avenue was not fruitful, we shifted our focus to experiments based on Fluorescence Correlation Spectroscopy (FCS) and time-resolved fluorescence anisotropy to study the stability of these proteins making use of extrinsic fluorescence reporters.

The concept of this approach is to do a characterization of hydrodynamic properties of the different OBPs to establish (1) if bOBP is a stable dimer even at low protein concentrations and the mutant monomeric is a monomer, and, (2) to understand the stability of pOBP, which is reported to be a monomer. Our longer-term goal is to use the OBPs and mutants as specific detectors for target odours in biosensors, for example for food quality analysis, homeland security or in others fields. So it is important to study the factors regulating the stability of these proteins, and establish general guidelines that could enable us, or other scientists, to approach a variety of different specific problems in biosensor applications. To this end, we have been studying the behaviour of proteins in their native form, after denaturation with guanidine hydrochloride and after renaturation (unfolding and refolding).

OBPs can represent an interesting and simple model for studying the phenomenon of protein assembly and how the formation of dimers and oligomers can depend upon single amino acid mutations.

We know from the crystal structure that bOBP is a dimer and presents the uncommon phenomenon of domain-swapping. This OBP is devoid of cysteine residues that could permit disulfide bridge formation, therefore electrostatic and hydrophobic interactions are the forces that bind together the two units of the dimer. Domain swapping between the two subunits could confer greater stability to this OBP. In contrast, porcine OBP is a monomer, and the alpha-helical domain that in the bovine OBP makes contact with the main domain of the second subunit, is folded back on the beta-barrel of the same protein. This different behaviour of the two OBPs could be related to a glycine residue, present in the pig OBP and absent in the bovine protein, that confers great flexibility to the polypeptide chain, thus allowing a compact structure only in the porcine OBP, and to the presence of an interdomain disulphide bridge that, in monomerica Lipocalins stabilizes the spatial relationship between the beta barrel and the alpha-helix. Previous studies [Ramoni, R. at al. *Biochem. J.*, 2002] have shown that deleting such a glycine in porcine OBP does not produce a dimeric protein with domain swapping, while introducing this amino acid in the bovine OBP has the opposite effect. Further investigations have also demonstrated that the introduction of two cysteine residue at the appropriate positions has been effective to estabilish in bOBP the interdomain disulphide bridge that characterize the foding of monomeric lipocalins [Ramoni, R. at al. *Biochim. Biophys. Acta*, 2008]. Since we were interested in developing biotechnological applications with the OBPs, we decided to investigate novel aspects concerning the aggregation state and stability of these protein forms that, to date, have not yet been approached. In particular we set up fuorescence correlation spectroscopy experiments (FCS) and time-resolved fluorescence anisotropy experiments both in native and denaturing conditions (increasing concentrations of Guanidine Hydrochloride from 0.5 to 5M).

Finally analytical ultracentrifugation (AUC) experiments helped us to better understand the global structure and assembly (monomer-dimer) of the OBPs. In particular, we carried out sedimentation equilibrium and sedimentation velocity experiments to obtain the molecular weight and the translational frictional coefficient of these proteins.

In other words, our goal was to put together the FCS, time-resolved anisotropy and AUC results to develop a comprehensive hydrodynamic picture of the comparative properties – monomer-dimer equilibrium and folding stability – of the different Odorant Binding Proteins.

We obtained these new informations:

- bOBP is a stable dimer even at very low protein concentration
- Mutant bOBP (GCCbOBP) is mostly in a monomeric form at low concentrations (10 nM)
- Mutant bOBP (GCCbOBP) at high concentrations, is present also in a dimeric form, with a dissociation costant (kd) in a micro molar range
- In spite of mutation (+Gly122), the protein has tendency dimerize, even if there are weak interactions
- pOBP is a monomeric form but AUC experiments show the formation of aggregated species.
- This could be aggregation and this behaviour could be expected if the pig protein is less stable than bOBP or the bovine mutant (GCCbOBP)
- The time-resolved anisotropy global analysis confirms the dimeric form of bOBP and the monomeric form of the bovine mutant (GCCbOBP). The guanidine hydrochloride denaturation experiments indicate two phases for unfolding (and dissociation in the case of bOBP). The first phase occurs about 0.5 M in denaturant, and the second phase occurs at about 2.5 M denaturant.

The high stability and the retained functionality in different conditions let us to consider the OBPs as good candidates for design ,through protein engineering

techniques, for the production of specific 'protein based' recognition elements for the detection of different analytes to be applied in Biosensor technology.

With regard to this it can be mentioned that Elegant studies, realized on the Bilin Binding Portein [Nygren P.A. & Skerra A. ,*J. of Immunol. Methods*, 2004] have already shown the possibility to use the lipocalin's scaffold as a "ligand pocket" for biosensing molecules of Biotechnological interest.

Finally, during our studies we realized two prototypes of biosensors OBP.

About the fluorescence based biosensor, the results shown above demonstrate that bOBP can serve as a probe for the development of an optical biosensor for odorant molecules present in the environment. Additional studies are needed to obtain a bOBP-based sensor that displays larger spectral changes, as we feel that it is important to covalently immobilize bOBP onto CTs. In addition, the use of different fluorophores for RET assays could allow larger spectral variations since RET is a through-space interaction which occurs whenever the donor and the acceptor are within the Forster distance (Ro) and does not require change in the probe microenvironment. For these reasons, we are confident that bOBP can be used with long wavelength donors and acceptors to devise a sensor for odorant and, in general, volatile molecules to use for safety and homeland security. Since the measurements can be easily performed by using an LED as an excitation source, one may envisage a polarization-based device with an external calibrated standard. The main advantage of using this method is the obtainment of ratiometric polarization measurements that are not influenced by light instability and sample perturbation. Finally, one can imagine a variety of OBP mutants covering a wide range of ligand binding constants, each labeled with a different fluorophore.

As consequence, the recombinant bOBP appears to be a valuable source for the development of innovative and stable CT-based biosensors for safety and homeland security. [Ramoni, R. at al., *J. Phys. Condens. Matter*, 2008]

The second prototype of biosensor was a "Surface acoustic wave (SAW) device".

Surface acoustic wave (SAW) devices are widely used in sensor applications in both physical and chemical fields. In particular SAW biosensors are currently used in medicine, environment monitoring, biotechnology, food industry and security applications. In the latter case SAW biosensors are very attractive as detectors of narcotics and explosives.

In this work we carried out experiments using bOBP to realize a SAW biosensor able to measure small concentrations of 1-octen-3-ol , a boletus odorant, that has been characterized as the natural ligand of bOBP. The experimental results have shown that the prototype we have realized has a good sensibility and can detect low levels of 1-octen-3-ol showing a clear signal of binding.

The sensor system, in fact, showed a resolution of 44 ppb and a sensor sensitivity of 314 Hz/ppm.

In our opinion, this first example of biosensor OBP-based is a clear indication of the potential applicability of mammalian Odorant Binding Proteins for the production of biological recognition elements for the detection of small hydrophobic molecules, which are the ligands of this type of protein.

In particular, we expect, in the future, to obtain through molecular engineering techniques, mutants of this protein with improved affinity and defined specificity towards OBP ligands like, for istance, 6-12 carbon atom aliphatic aldehydes [Grolli, S. at al., FEBS, 2006], that are the volatile degradation products of lipid peroxidation. Such mutants could be conveniently employed as sensing elements in biosensor to be used to monitor the degree of oxidative stress in different matrixes of biological origin especially in food industries.

Taking into account other classes of OBP ligands, as for instance the components of explosive mixtures, with the same approach, it would be possible to prepare OBP mutants to be applied as sensing elements in biosensors used for inspection purposal of by operators of the homeland security.

Finally the new and ulterior data about Odorant Binding Proteins aggregation stat and stability obtained through our studies, could provide information on the structural elements of the proteins that might determine and modify their specificity towards unique ligands.

References

Arruda, L.K. at al. "Cloning of cockroach allergen, Bla g 4, identifies ligand binding proteins (or calycins) as a cause of IgE antibody responses." *Biol. Chem.* **270:** 31196-31201, 1995

Avouris, P. at al. "Excited state interactions of 7-azaindole with alcohol and water" *Photochem Photobiol* **24:** 211-216, 1976

Bacia, K. and Schwille, P."A dynamic view of cellular processes by in vivo fluorescence auto- and cross-correlation spectroscopy" *Methods* **29:** 74–85, 2003

Badea, M. and Brand L. "Time-resolved fluorescence measurements." *Methods Enzymol.* **61:**378–425, 1979

Bartsch, S. and Tschesche, H. "Cloning and expression of human neutrophil lipocalin cDNA derived from bone marrow and ovarian cancer cells." FEBS Lett. ***357***: 255-259, 1985

Benetti, M.; Cannata, D.; Di Pietrantonio, F.; Marchiori, C.; Persichetti, P.; E. Verona, *IEEE Sensors Proc.,* Lecce 1024 – 1027, 26-29 Oct. 2008

Benetti, M., Cannatà, D., D'Amico, A., Di Pietrantonio, F., Macagnano, A. and Verona, E. IEEE Sensors Proc., Vienna, pp. 753-756, 24-27 Oct. 2004.

Bianchet, M.A. at al., "The three-dimensional structure of bovine odorant binding protein and its mechanism of odor recognition". *Nat. Struct. Biol.* **3**: 934-939, 1996

Bishop, R. E., Penfold, S. S., Frost, L. S., Holtje, J.-V. and Weiner, J. H., *J. Biol. Chem.* ***270*:** 23097-23103, 1995

Bogus law Buszewski, A. at al. "Identication of volatile organic compounds secreted from cancer tissues and bacterial cultures" *Journal of Chromatography B* **868:** 88-94, 2008

Chapman, C.F. & Marconcelli, M. "Excited-state tautomerization of 7-azaindole in water" *J Phys Chem* **96:** 8430-8441

Chen, Y. at al. "Fluorescent species of 7-azaindole and 7-azatryptophan in water" J Phys Chem 97: 1770-1780

Cohn, E.J. & Edsall, J.T. "Density and apparent specific volume of proteins" *Proteins, Amino Acids and Peptides as Ions and Dipolar Ions* pp.370-381, New York, Reinhold, 1943

D. D. Stubbs', Sang-Hun Lee, W. D. Hunt, "Cocaine detection Using Surface Acoustic Wave Immunoassay Sensors", 2002 IEEE lnternational Frequency Control Symposium and PDA Exhibition.

D'Auria, S. at al."The tryptophan phosphorescence of porcine and mutant bovine odorant-binding proteins: a probe for the local protein structure and dynamics" J Proteome Res. **7:** 1151-1158, 2008

Elson, E. L. "Fluorescence correlation spectroscopy and photobleaching recovery" *Annu. Rev. Phys. Chem.* **36:**379–406, 1985

Fahey, P. F. at al."Lateral diffusion in planar lipid bilayers" *Science* **195:** 305–306, 1977

Flower, D.R. at al."Mouse oncogene protein 24p3 is a member of the lipocalin protein family" *Biochem Biophys Res Commun.* **180(1):**69-74, 1991

Flower , D.R. "Structural relationship of streptavidin to the calycin protein superfamily." *FEBS Lett.* **333(1-2):**99-10, 1993

Flower, D.R. "The lipocalin protein family: structure and function" *Biochem J.* **318(Pt 1):** 1-14 Review, 1996

Flower D.R., "Multiple molecular recognition properties of the lipocalin protein family". *J Mol Recognit. m. Biophys. Acta* ,**1482**: 9-24, 2000

Frieden, C. at al. "What fluorescence correlation spectroscopy can tell us about unfolded proteins" *Adv. Protein Chem.* **62:**91–110, 2002

Ganfornina, M.D. at al. "Lazarillo, a new GPI-linked surface lipocalin, is restricted to a subset of neurons in the grasshopper embryo". *Development* **12**1**:** 123–134, 1995

Godovac-Zimmermann J. "The structural motif of beta-lactoglobulin and retinol-binding protein: a basic framework for binding and transport of small hydrophobic molecules" *Trends Biochem. Sci*. **13(2):** 64-66, 1988

Grolli, S. at al. "Odorant binding protein has the biochemical properties of a scavenger for 4-hydroxy-2-nonenal in mammalian nasal mucosa" *FEBS J.* **273(22):**5131-42**,** 2006

Guiraudie, G. at al. "Functional Characterization of Olfactory Binding Proteins for Appeasing Compounds and Molecular Cloning in the Vomeronasal Organ of Pre-pubertal Pigs" *Chem. Senses* **28:** 609-619, 2003

Haupts, U. at al. "Dynamics of fluorescence fluctuations in green fluorescent protein observed by fluorescence correlation spectroscopy" *Proc. Natl. Acad. Sci. USA.* **95:**13573–13578, 1998

Hess, S. T. at al. "Biological and chemical applications of fluorescence correlation spectroscopy: a review" *Traffic* **2:**789–796, 2001

Koppel, D. E. at al. "Dynamics of fluorescence marker concentration as a probe of Mobility" *Biophys. J.* **16:**1315–1329, 1976

Laemmli, U.K. "Cleavage of structural proteins during the assembly of the head of bacteriophage T4." *Nature* **227:** 680-685, 1970

Lakowicz Joseph R., "*Principles of Fluorescence Spectroscopy*", third edition (2006)

Laue, T.M. at al. "Computer-aided interpretation of analytical sedimentation data for proteins" *Biochemistry and Polymer Science.* **pp.**90-125, 1992

Maniatis, T. at al. Molecular Cloning: A Laboratory Manual *Cold Spring Harbor Lab., Cold Spring Harbor, NY*, 1982

Medina, M. A. and Schwille, P. "Fluorescence correlation spectroscopy for the detection and study of single molecules in biology" *Bioessays* **24:** 758–764, 2002

Nygren P.A. & Skerra A. "Binding proteins from alternative scaffolds" Review *J. of Immunol. Methods* **290:** 3–28, 2004

Palmer, A. G. and Thompson, N. L. "Molecular aggregation characterized by high order autocorrelation in fluorescence correlation spectroscopy" *Biophys. J.* **52:**257–270, 1987

Paolini, S. at al. "Amino acid sequence, post-translational modifications, binding and labelling of porcine odorant-binding protein." *Chem. Senses* **23:** 689–698, 1998

Parisi, M. at al. "Unfolding and refolding of porcine odorant binding protein in guanidinium hydrochloride: equilibrium studies at neutral pH" *Biochim. Biophys. Acta* **1652:** 115-125, 2003

Pelosi, P. at al. "Identification of a specific olfactory receptor for 2-isobutyl-3-methoxypyrazine" *Biochem J.* **201(1):**245-8, 1982

Pelosi, P. at al. " Odorant-binding proteins: structural aspects". *Ann. N. Y. Acad. Sci.*, **855**, 281–293, 1998

Qian, H. and Elson, E. L. "Distribution of molecular aggregation by analysis of fluctuation moments" *Proc. Natl. Acad. Sci. USA* **87:** 5479–5483, 1990

Ramoni, R. at al. "The insect attractant 1-octen-3-ol is the natural ligand of bovine odorant-binding protein" *J. Biol. Chem.* **276:** 7150–5, 2001

Ramoni, R. at al. "Control of domain swapping in bovine odorant-binding protein." *Biochem. J.* **365:** 739–748, 2002

Ramoni, R. at al. "Carbon nanotube-based biosensors" *J. Phys. Condens. Matter* **20:** 474201-474206, 2008

Ramoni, R. at al. "Deswapping bovine odorant binding protein" *Biochim Biophys Acta.* **1784(4):**651-7, 2008

Ross, J.B.A. at al. "Spectral enhancement of proteins: Biological incorporation and fluorescence characterization of 5-hydroxytryptophan in bacteriophage A ci repressor" *Biochem.* **89:** 12023-12027, 1992

Rusinova at al."Alexa and Oregon Green dyes as fluorescence anisotropy probes for measuring protein–protein and protein–nucleic acid interactions." *Analytic. Biochem.* **308:** 18–25, 2002

Silhavy, T.J. at al. "Experiments with gene fusions" *New York: Cold Spring Harbor,* 1984

Spinelli, S. at al., "The structure of the monomeric porcine odorant binding protein sheds light on the domain swapping mechanism" *Biochem* **37:** 7913-7918

Stafford, W.F. III "Boundary analysis in sedimentation transport experiments: a procedure for obtaining sedimentation coefficient distributions using the time derivative of the concentration profile" *Anal. Biochem.* **203:** 295-301, 1992

Starr, T. E. & Thompson, N. L. "Total internal reflection with fluorescence correlation spectroscopy: combined surface reaction and solution diffusion" *Biophys. J.* **80:**1575–1584, 2001

Tegoni, M. at al., "Domain swapping creates a third putative combining site in bovine Odorant Binding Protein dimer". *Nat. Struct. Biol*. **3**: 863–867, 1996

Tegoni, M. at al. "Mammalian odorant binding proteins", *Biochim. Biophys. Acta*, **1482**: 229-240, 2000

Tegoni, M. at al. "Structural aspects of sexual attraction and chemical communication in insects", *Trends Biochem Sci.***, 29(5):** 257-64, 2004 Review

Teller, D. C. "Characterization of proteins by sedimentation equilibrium in the analytical ultracentrifuge." *Methods in Enzymol.* 27: 346-441. Edited by C. H. W. Hirs and S. N. Timasheff. New York, Academic Press,1973

Van Holde, K. E. "Sedimentation analysis of proteins." *The Proteins* I: 225-291. Edited by H. Neurath and R. L. Hill. 3rd ed. New York, Academic Press, 1975

Waxman et al., "Determination of the tryptophan: tyrosine ratio in proteins", *Anal. Biochem.* **32:** 3005-3012, 1993

Vincent, F. at al. "Complexes of porcine odorant binding protein with odorant molecules belonging to different chemical classes"*J Mol Biol.* **300(1):** 127-39, 2000

Zagalsky, P. F., Mummery, R. S. and Winger, L. A. *Comp. Biochem. Physiol.* ***110B*****:** 385-391, 1995

Zemsky, J. at al. "Probing local environments of tryptophan residues in proteins: comparison of 19F nuclear magnetic resonance results with the intrinsic fluorescence of soluble human tissue factor" *Proteins* **37:**709–716, 1999**8(3):**185–195, 1995

PUBLICATIONS

Experiences in foreign Laboratories

From May 2009 to August 2009 she attended the J.B. Alexander Ross's laboratory at University of Montana, Montana

From 16 to 29 May 2008 she attended the Kostantin Turoverov's laboratory in Accademy of Science of San Petersburg, Russian;

Publications on International Journal

10- Nanostructured Silver-Based Surfaces: New Emergent Methodologies for an Easy Detection of Analyte
M. Staiano, E. G. Matveeva, M. Rossi, **Roberta Crescenzo**, Z. Gryczynski, I. Gryczynski, L. Iozzino, I. Akopova and S. D'Auria
ACS Appl. Mater. Interfaces, *(2009), 1 (12), pp 2909–291.*

9 - Wild-type and mutant bovine odorant-binding proteins to probe the role of the quaternary structure organization in the protein thermal stability
A. Marabotti, A. Scirè, M. Staiano, **Roberta Crescenzo**, V. Aurilia, F. Tanfani, and S. D'Auria
Journal of Proteome Research (2008) 7(12):5221-9

8 - Nanobeads-based Assays. The case of gluten detection
I. Venditti, I. Fratoddi, M. V. Russo, S. Bellucci, **Roberta Crescenzo**, L. Iozzino, M. Staiano, V. Aurilia, A. Varriale, M. Rossi, and S. D'Auria
J. Phys.: Condens. Matter 20 (2008) 474202 (3pp)

7 - Carbon nanotube-based biosensors
R. Ramoni, M. Staiano, S. Bellucci, I. Grycznyski, Z. Grycznyski, **Roberta Crescenzo**, L. Iozzino, S. Bharill, V. Conti, S Grolli and S. D'Auria
J. Phys.: Condens. Matter 20 (2008) 474201 (4pp)

6 - Advanced spectroscopy techniques for the detection of gluten in food
Crescenzo Roberta, and S. D'Auria
Agro Food Industry Hi-Tech (2008) 19,2, 14-17

5 - Molecular strategies for protein stabilization: The case of a trehalose/maltose-binding protein from *Thermus thermophilus*
A. Scire`, A. Marabotti, V. Aurilia, M. Staiano, P. Ringhieri, L. Iozzino, **Roberta Crescenzo**, F. Tanfani, and S. D'Auria.
Proteins. 2008 May 27 [Epub ahead of print] PMID: 18506781

4 - Mutant bovine odorant-binding protein: Temperature affects the protein stability and dynamics as revealed by infrared spectroscopy and molecular dynamics simulations
A. Marabotti, T. Lefèvre, M. Staiano, **Roberta Crescenzo**, A. Varriale, M. Rossi, M. Pézolet and D'Auria S.
Proteins. 2008 Aug;72(2):769-78

3 - Kissper, a kiwi fruit peptide with channel-like activity: Structural and functional features
M. Antonietta Ciardiello, D. Meleleo, G. Saviano, **Roberta Crescenzo**, V. Carratore, L. Camardella, E. Gallucci, S. Micelli, T. Tancredi, D. Picone and M. Tamburrini.
J Pept Sci. 2008 Jun;14(6):742-54

2 - New perspectives in protein-based biosensors: The glucokinase from B. stearothermophilus and the odorant-binding protein from C. familiaris as probes for non-consuming analyte sensors
I. M. Kuznetsova, O. Povarova, O. Stepanenko, K. K.Turoverov, Roberta Crescenzo, A. Varriale, M. Staiano and S. D'Auria
Proceedings of SPIE - The International Society for Optical Engineering 6733, 2007 art. no. 673318

1 - A strategic fluorescence labeling of D-galactose/D-glucose-binding protein from Escherichia coli helps to shed light on the protein structural stability and dynamics
V. Scognamiglio, A. Scirè, V. Aurilia, M. Staiano, **Roberta Crescenzo**, C. Palmucci , E. Bertoli , M. Rossi , F. Tanfani, and S. D'Auria.
J Proteome Res. 2007 Nov;6(11):4119-26

research articles Journal of proteome research

Wild-Type and Mutant Bovine Odorant-Binding Proteins To Probe the Role of the Quaternary Structure Organization in the Protein Thermal Stability

Anna Marabotti,[†,#] Andrea Scirè,[‡,#] Maria Staiano,[§] Roberta Crescenzo,[§] Vincenzo Aurilia,[§] Fabio Tanfani,[‡] and Sabato D'Auria*[,§]

Istituto di Scienze dell'Alimentazione, CNR, Avellino, Italy, Istituto di Biochimica, Università Politecnica delle Marche, Ancona, Italy, and Laboratory for Molecular Sensing, IBP-CNR, Naples, Italy

Received July 14, 2008

The exploration of events taking place at different timescales and affecting the structural and dynamics properties of proteins, such as the interactions of proteins with ligands and the subunits association/dissociation, must necessarily be performed by using different methodologies, each of which specialized to highlight the different phenomena that occur when proteins are exposed to chemical or physical stress. In this work, we investigated the structure and dynamics of the wild-type bovine odorant-binding protein (wt-bOBP), which is a domain-swapped dimeric protein, and the triple mutant deswapped monomeric form of the protein (m-bOBP) to shed light on the role of the quaternary and tertiary structural organization in the protein thermal stability. Difference infrared spectra, 2D-IR correlation spectroscopy and molecular dynamics simulations were used to probe the effect of heating on protein structure and dynamics in microsecond and nanoseconds temporal ranges, respectively. The obtained results show that there is a heating-induced transition toward a less structured state in m-bOBP, that it is detectable around 70−80 °C. On the contrary, in wt-bOBP this transition is almost negligible, and changes are detectable in the protein spectra in the range of temperature between 75 and 85 °C. A detailed 3D inspection of the structure of the two proteins that takes into the account the spectroscopic results indicates that (a) ion pairs and hydrophobic interactions appear to be the major determinants responsible for the protein stability and (b) the protein intersubunit interactions confer an increased resistance toward the thermal stress.

Keywords: Odorant-binding protein • Lipocalins • FT-IR • MD

Introduction

Odorant-binding proteins (OBPs) are small extracellular proteins belonging to the lipocalin superfamily.[1] They have been supposed to have an important role in peri-receptorial events related to the odor detection by carrying, deactivating, and/or selecting the odorant molecules.[1,2] In particular, OBPs reversibly bind odorant molecules with dissociation constants in the nano/micromolar range.[3−5] OBPs have been identified in a variety of species, including pig, rabbit, mouse and rat.[6] The structure of OBPs presents a conserved folding pattern in which an 8-stranded β-barrel flanks a α-helix structure at the C-terminal end of the protein. The β-barrel structure forms a central apolar cavity whose role is to bind and transport the hydrophobic odorant molecules.[7] Bovine OBP (bOBP) shows a peculiar 3D structure, characterized by domain "swapping".[8] In solution at neutral pH, it appears as a dimer in which each monomer is composed by the classical lipocalin fold, with a large buried cavity internal to the β-barrel forming the binding site for odorant molecules. The absence of a Gly after position 121 in the sequence and the lack of the disulphide bridge between the C-terminal and the β-barrel, which are both strictly conserved in other sequences of mammalian OBPs, were identified as the determinants for the domain swapping. This hypothesis is supported by the finding that a mutant bOBP in which a glycine residue was inserted after position 121 showed a monomeric structure. Recently a "deswapped" triple mutant bOBP (Gly 122+, W64C, H156C) has been obtained, in which a Gly residue is inserted after position 121 and the two residues in position 64 and 156 are replaced by Cys residues, in order to restore the disulphide bridge common to the lipocalin family.[9]

In some recent works,[10−12] we demonstrated the high stability exhibited by the porcine odorant-binding protein toward the high temperatures and the chemical denaturant agents such as guanidine hydrochloride. In particular, these investigations pointed out the role of the hydrophobic interac-

* To whom correspondence should be addressed. Dr. Sabato D'Auria, Laboratory for Molecular Sensing, IBP-C.N.R., Via Pietro Castellino, 111, 80131 Naples, Italy. Phone, +39-0816132250; fax, +39-0816132277; e-mail, s.dauria@ibp.cnr.it.
[#] These authors have equally contributed to the work.
[†] Istituto di Scienze dell'Alimentazione, CNR.
[‡] Università Politecnica delle Marche.
[§] Laboratory for Molecular Sensing, IBP-CNR.

10.1021/pr800528b CCC: $40.75

Published on Web 10/28/2008

tions in the stability and dynamics of the pOBP and the mutant monomeric form bOBP (m-OBP).

In this work, we investigated the stability of the wild-type dimeric form of bOBP (wt-OBP) and the triple mutant monomeric form of bOBP (m-OBP) by Fourier-transform-infrared (FT-IR) spectroscopy and molecular dynamics (MD) simulation experiments. Difference infrared spectra and generalized 2D-IR analysis of infrared band intensities of the obtained absorbance spectra was performed in order to highlight the presence of molten globule-like states in the two proteins. MD simulations allowed us to hypothesize a molecular explanation of the phenomena occurring in the proteins at the early stages of the experiments in the presence of heating.

The obtained results offer a representation with the molecular explanation of what happens to the structure of these two proteins at high temperatures.

Materials and Methods

Materials. Deuterium oxide (99.9% ^2H_2O), ^2HCl, NaO^2H, and deuterated ethanol (EtO^2H) were purchased from Aldrich (Sigma-Aldrich S.r.l., Milan, Italy). 1-Octen-3-ol was obtained from Sigma. All the other chemicals were commercial samples of the purest quality.

Protein Production. A 6×His affinity tag was placed at the N-terminal of the two bOBP forms by PCR using specific primers. The fused cDNAs were subcloned in the expression vector pT7−7 and the expression of the proteins was made in BL21-DE 3 *Escherichia coli*. The purification of the proteins was obtained by affinity chromatography with a Ni-NTA Agarose (Quiagen, Germany) according to the manufacturer's instructions, followed by a second chromatographic step on the anion exchange column Recourse Q (Amersham Biosciences, Italy), in FPLC. The purity of the two protein preparations was determined by SDS-PAGE and protein concentrations were calculated based on the absorbance values at 280 nm (48 000 M^{-1} cm^{-1} for bOBP).

Infrared Spectroscopy. FT-IR spectra were recorded by means of a 1760-X Perkin-Elmer Fourier-transform infrared spectrometer using a deuterated triglycine sulfate detector and a normal Beer-Norton apodization function. Twenty-four hours before the experiments and during data acquisition, the spectrometer was continuously purged with dry air at a dew point of −70 °C. Prior to FT-IR spectra recording, the protein samples were equilibrated in a deuterium oxide (^2H_2O) medium. Typically, 1.5 mg of wt-bOBP or m-bOBP, dissolved in the buffer used for their purification, was centrifuged in a "10 K Centricon" microconcentrator (Amicon) at 3000*g* and at 4 °C and concentrated into a volume of approximately 40 μL. Then, 300 μL of 50 mM Tris/^2HCl buffer, prepared in ^2H_2O p^2H 7.4, were added and the sample was concentrated again. The p^2H value corresponds to the pH meter reading +0.4.[13] The concentration and dilution procedure was repeated several times in order to completely replace the original buffer with the Tris buffer p^2H 7.4. In the last wash, the sample was brought to a volume of approximately 40 μL and then used for the infrared analysis.

bOBP displays a very high affinity toward 1-octen-3-ol in the nanomolar range.[3,5,11−13] In our experiments in order to study the effect of 1-octen-3-ol on bOBP structure, 0.5 μL of EtO^2H odorant solution was added to 40 μL of the concentrated protein solution, obtaining a 3/1 ligand/protein molar ratio. These conditions ensured the saturation of the protein with the ligand.

The protein samples were placed in a thermostatted Graseby Specac 20500 cell (Graseby Specac, Orpington, Kent, U.K.) fitted with CaF_2 windows and a 25-μm Teflon spacer.

Spectra of buffer were acquired under the same scanning and temperature conditions. In the thermal-denaturation experiments, the temperature was raised by 5 °C steps from 20 to 95 °C. Additional spectra were obtained at 98 and 99 °C. Before spectra acquisition, samples were maintained at the desired temperature for the necessary time for stabilization of the cell temperature (6 min). Spectra were processed using the SPECTRUM software from Perkin-Elmer. Subtraction of ^2H_2O was adjusted to the removal of the ^2H_2O bending absorption close to 1220 cm^{-1}.[14] Second derivative spectra were calculated over a 9 data-point range (9 cm^{-1}). The deconvoluted parameters were set with a gamma value of 2.5 and a smoothing length of 60.

2D-IR Correlation Spectroscopy. Generalized 2D-IR analysis of IR band intensities of absorbance spectra was performed according to the method of Noda. To obtain synchronous and asynchronous plots, 2Dshige program (Shigeaki Morita, Kwansei-Gakuin University, 2004−2005) was used.[15,16]

Synchronous plots, covering 45−80 °C, or 45−85 °C, or 45−99 °C temperature ranges were generated. Asynchronous maps were obtained analyzing the IR absorbance spectra in the 45−99 °C temperature range. These temperature ranges allowed us to better describe the thermal unfolding events.[17]

Molecular Dynamics Simulations. We started from two files available in PDB database[18] for wt-bOBP: 1OBP.pdb[8] and 1G85.pdb.[19] In the first file, a ligand classified as "unknown" is present and was deleted, whereas in the second file, the natural ligand, 1-octen-3-ol, is bound to the protein. These coordinates were used to perform MD simulations at high temperature in water, in the absence or in the presence of the ligand. Simulations were carried out using the program GROMACS version 3.3.2[20,21] running in parallel (MPI) on a cluster with 40 × 86_64 Opteron processors. The GROMOS96 force field[22] was used throughout the simulations. The topology of the protein was created using GROMACS utilities, whereas the topology of the ligand was created using the PRODRG[23] beta server, available at http://davapc1.bioch.dundee.ac.uk/cgi-bin/prodrg_beta. Each system was then included in a cubic box of 0.9 nm per side filled with water (SPC model)[24] (30 834 and 30 189 water molecules, respectively, in the absence and presence of ligand). Twenty-one and 19 Na^+ ions, respectively, for 1OBP.pdb and 1G85.pdb, to neutralize the net negative charge of the system, were added to the solvent. Periodic boundary conditions were used to exclude surface effects.

A preliminary energy minimization step with a tolerance of 1000 (kJ/mol)/nm was run with the Steepest Descent method. All bonds were constrained using LINCS.[25] After minimization, a short MD simulation (20 ps) with position restraints was applied to each system to soak the water molecules into the macromolecule. A time step of 2 fs was used in both cases, and the systems were coupled with a temperature bath at 300 K and a pressure of 1 atm using Berendsen's method.[26] Long-range electrostatics were handled using the PME method.[27] The cutoff for Coulomb interactions and for van der Waals interactions were set at 0.9 nm and at 1.4 nm, respectively.

The final MD simulations were carried out with a time-step of 2 fs and without any position restraints. To compare results with previous experiments made on m-bOBP,[11] the simulations were set in the same way, that is, 1 ns-long simulation at 300 K and four 600 ps-long simulations at 333 K, 348 K, 353 K, 368

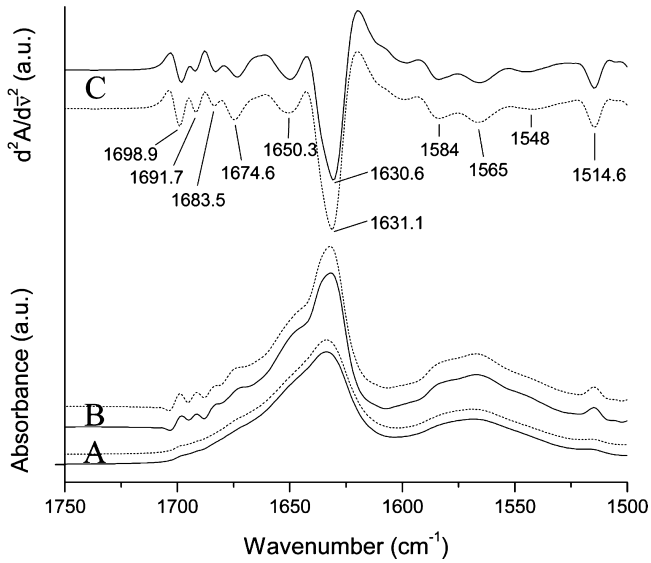

Figure 1. Absorbance (A), deconvoluted (B) and second derivative (C) spectra of wt-bOBP (continuous lines) and of m-bOBP (dotted lines). The spectra were obtained at 20 °C. The ordinate axis reports the arbitrary units for absorbance (A) and deconvoluted (B) spectra and for second derivative spectra (C).

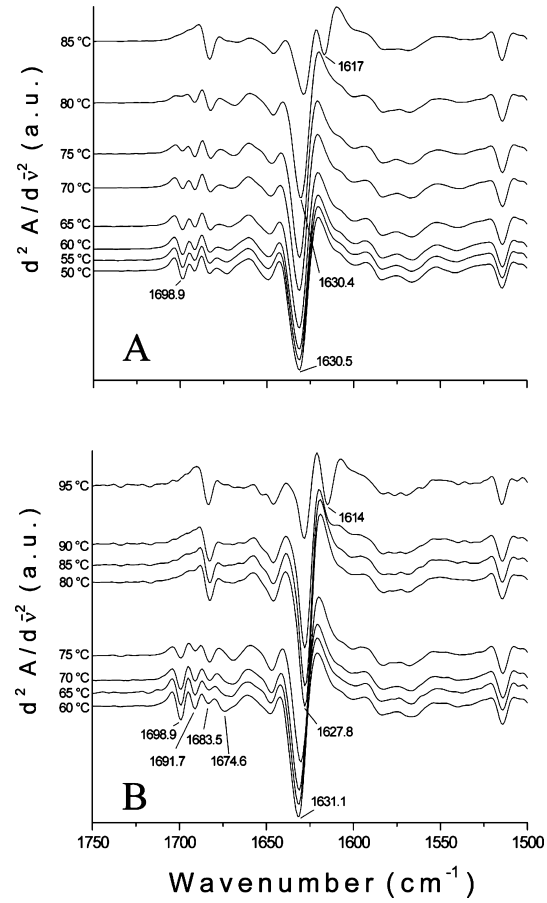

Figure 2. Second derivative spectra of wt-bOBP (A) and of m-bOBP (B) as a function of the temperature. Panels A and B show spectra in the 50−85 °C and in the 60−95 °C range, respectively. The ordinate axis reports the arbitrary units for second derivative spectra (C).

K for each system. Moreover, an additional 1 ns-long step at 373 K was made, for a global duration of 4.4 ns. The final conformation of each simulation was used as input for the following simulation at higher temperature.

Several analyses were conducted using programs built within GROMACS, and results were visualized and elaborated with the aid of the freely available program Grace (http://plasma-gate.weizmann.ac.il/Grace). The energy components were extracted from the energy files generated by the program, and analyzed to verify the stabilization of the system. The rmsd values were obtained from a least-squares fit of the respective non-hydrogen atoms (main-chain and side-chain). For each temperature step, an "average" structure was calculated on the whole protein excluding hydrogen atoms, and also for ligand when it was present in the system. These structures were saved in pdb format, and they were subsequently minimized with the Steepest Descent method as described above. Relative percentages of secondary structure elements were determined on these "average" structures using the DSSP program.[28] Other analyses were carried out with the Insight II package (Version 2000.1, Accelrys, Inc.; 2000). In particular, identification of salt bridges was made directly on average structures obtained as above-described, according to Kumar and Nussinov.[29]

Results and Discussion

Figure 1 shows the absorbance (A), deconvoluted (B) and second derivative (C) spectra of wt-bOBP (continuous lines) and of m-bOBP (dotted lines). In particular, the resolution enhanced spectra show the presence of the same number of amide I′ (1700−1600 cm^{-1} region) component bands having also similar intensity and position. The amide I′ region contains information on protein secondary structure.[30] The intense band close to 1630 cm^{-1} and the small band close to 1650 cm^{-1} indicate a predominance of β-structure with a minor content of α-helices, respectively. This finding is in agreement with the secondary structural content determined from the 3D structure of the two proteins.[19] The minor bands in the 1690−1670 cm^{-1} region may also contain information on β-sheet structures. However, it is noteworthy that this band assignment is less certain since peptide bonds located in turns and β-sheets may absorb in this region.[31,32]

The bands below 1620 cm^{-1} are due to amino acid side chain absorption.[33,34] In particular, the 1514.6 cm^{-1} band is due to tyrosine residues, whereas the 1584 and 1565 cm^{-1} bands are due to ionized carboxyl groups of aspartic and glutamic acid residues, respectively. The small 1548 cm^{-1} band is associated with residual amide II band absorption and its low intensity indicates that a small amount of amide hydrogens were not exchanged with deuterium during the preparation of the protein sample.[35]

Figure 2 displays the second derivative spectra of wt-bOBP and of m-bOBP in the range of temperature where conformational changes occurred. In particular, panels A and B of Figure 2 show spectra in the 50−85 °C and in the 60−95 °C range, respectively. The spectra of wt-bOBP (A) indicate that the protein is stable till 80 °C since the main β-sheet band intensity is scarcely affected by the temperature and the spectrum is similar to the spectrum obtained at 50 °C. At 85 °C, the intensity of the main β-sheet band decreases significantly and a new band at 1617 cm^{-1} appears, indicating thermal denaturation and protein aggregation, respectively.[36] A more detailed analysis of the spectra indicates that, in the 70−80 °C temperature interval, a decrease in intensity of the 1698.9 cm^{-1} band and a

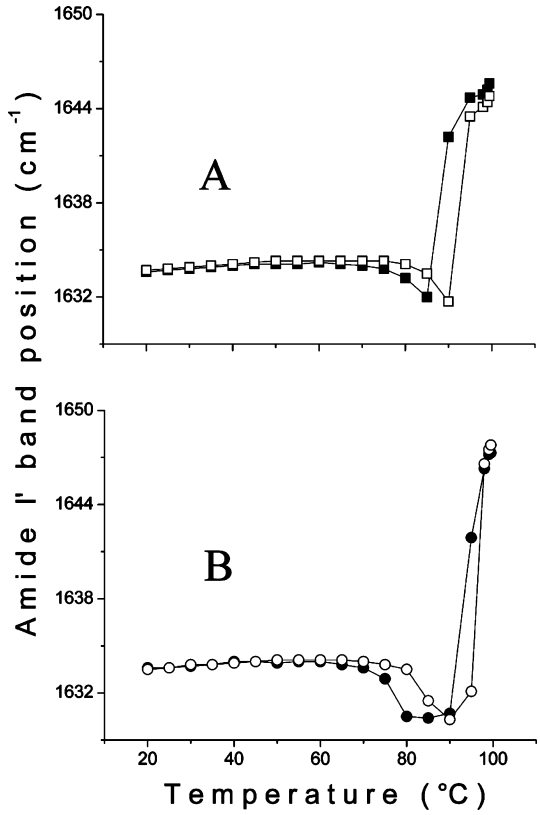

Figure 3. Thermal denaturation curves of wt-bOBP (A) and of m-bOBP (B) in the absence and in the presence of 1-octen-3-olo at pD 7.4. In the thermal-denaturation experiments, the temperature was raised by 5 °C steps from 20 to 95 °C. Additional spectra were obtained at 98 and 99 °C. The curves were obtained by plotting the amide I′ band position in absorbance spectra as a function of the temperature. (A) The wt-bOBP in the absence (■) and in the presence (□) of 1-octen-3-olo. (B) The m-bOBP in the absence (•) and in the presence (○) of 1-octen-3-olo.

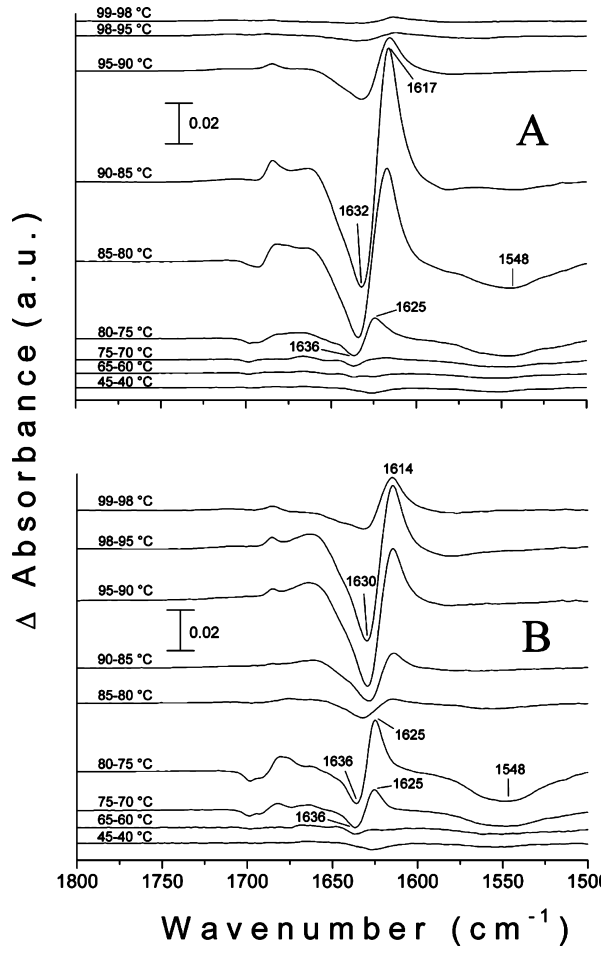

Figure 4. Difference spectra of wt-bOBP (A) and m-bOBP (B) in the 40−99 °C temperature range, In the thermal-denaturation experiments, the temperature was raised by 5 °C steps from 20 to 95 °C. Additional spectra were obtained at 98 and 99 °C. Each trace (difference spectrum) was obtained by subtracting the original absorbance spectrum recorded at the lower temperature from the one recorded at higher temperature (e.g., 85 − 80 °C).

small downshift in wavenumber of the main β-sheet band take place. These minor changes in the spectra may indicate some conformational changes occurring in the 70−80 °C interval. The analysis of m-bOBP spectra (Figure 2B) indicates that its secondary structural organization is more thermostable than wt-bOBP since both the decrease in intensity of the main β-sheet band and the appearance of the new band at 1614 cm^{-1} start occurring at 95 °C. Moreover, the spectra indicate that the protein main β-sheet band at 80 °C shifts significantly to a lower wavenumber. In addition, the m-bOBP minor bands in the 1690−1670 cm^{-1} region change their position, or it changes their intensity, or these bands disappear at all. These phenomena are more marked in m-bOBP than in wt-bOBP, suggesting more pronounced conformational changes in the mutant protein (Figure 2).

Figure 3 shows the thermal denaturation curves of wt-bOBP and m-bOBP obtained by monitoring the position of the amide I′ band in the absorbance spectra as a function of temperature.[35−37] In both protein samples, two transitions were observed. The first transition is indicated by a slight decrease of the amide I′ band, while the second one is indicated by a steady increase in the amide I′ band maximum. In the absence of the ligand, the first transition occurs within 75−85 °C for wt-bOBP and within 70−80 °C for m-bOBP; the second transition is observed within 85−99 °C and 90−99 °C for wt-bOBP and m-bOBP, respectively. The presence of 1-octen-3-ol increases the thermal stability of the two proteins shifting the first transition and second transition to higher temperatures. This behavior is similar to that already described for the porcine odorant-binding protein[37] and a thermostable thioredoxin[35] in which the first transition was ascribed to the formation of a molten globule-like state, and the second transition was attributed to protein thermal denaturation.[35,37]

By comparing our data with the results reported in other studies,[35,37] it is most likely that a molten globule-like state could be also present at specific temperatures in wt-bOBP and m-bOBP. To ascertain the presence of molten globule-like states in the two proteins, we analyzed the difference spectra (Figure 4)[35,37,38] and we used the generalized 2D-IR analysis of IR spectra obtained at different temperatures.[39]

Figure 4 shows the difference spectra from 45 to 99 °C. These spectra were derived from the series of absorbance spectra recorded at stepwise increasing temperatures, by subtracting each one of them from the spectrum recorded at the next higher temperature (e.g., the 85 °C − 80 °C difference spectrum corresponded to the spectrum recorded at 85 °C, after subtraction of the spectrum recorded at 80 °C). Both negative and positive peaks reflect the total changes in a particular band

which is present in the two IR spectra to be subtracted, and their characteristics depend on several factors.[40] Negative bands in the amide I′ region reflect protein denaturation[35] and/or band-shifts in case that positive adjacent bands of similar intensity are also present.[37]

The latter case is applicable to the 80 °C − 75 °C difference spectrum of wt-bOBP (Figure 4A) and to the 75 °C − 70 and 80 °C − 75 °C difference spectra of m-bOBP (Figure 4B). In fact, a 1636 cm^{-1} negative band and a 1625 cm^{-1} positive band of similar intensity are found within this temperature range. Since the band at 1636 cm^{-1} belongs to β-sheet, the band-shift to 1625 cm^{-1} indicates that the β-sheets became more exposed to the solvent (^2H_2O), allowing the protein to exchange residual amide hydrogens that were not exchanged during the preparation of protein sample. In fact, further $^1H/^2H$ exchange is supported by the appearance of a negative broadband close to 1545 cm^{-1} due to a decrease in intensity of the residual amide II band. The data indicate that between 75−80 °C and between 70−80 °C there are not significant changes of the secondary structure contents of wt-bOBP and m-bOBP (see also Figure 2), whereas the tertiary structures of the two proteins undergo a relaxation process with an additional $^1H/^2H$ exchange. This phenomenon could describe a protein less-folded state in which the secondary structural elements of the two proteins are still preserved. We could associate this protein less-folded state with the presence of molten globule-like states.[41] It is worth nothing that the presence of a molten globule-like state is well described by the 75 °C − 70 and 80 °C − 75 °C difference spectra obtained in m-bOBP (Figure 4B). On the contrary, the presence of a molten globule-like state is less evident in wt-bOBP (Figure 4A), as its presence is only reported by the 80 °C − 75 °C difference spectrum.

The difference spectra (85 °C − 80 °C), (90 °C − 85 °C) and (95 °C − 90 °C) in Figure 4A show a negative band close to 1632 cm^{-1} due to protein denaturation, and they also show the presence of a positive band at 1617 cm^{-1} due to protein aggregation (intermolecular interactions) brought about by thermal denaturation.[35,42]

Concerning the m-bOBP protein (Figure 4B), the presence of a small negative band in the 85 °C − 80 °C difference spectrum indicates that the protein denaturation starts between 80 and 85 °C as in the case of wt-OBP (Figure 4A), but to a very low extent. This information is not revealed in Figure 3B, thus, indicating that the analysis of difference spectra is a powerful tool to study protein conformational changes. The (99 °C − 98 °C) trace points out that at 99 °C the protein still undergoes to denaturation and aggregation processes (1614 cm^{-1} band), the latter started between 90 and 85 °C.

In summary, the difference spectra suggest the presence of a temperature-induced molten globule like state in the m-bOBP between 70 and 80 °C; then, at higher temperatures, the protein undergoes denaturation and aggregation. On the contrary, the formation of the molten globule-like state is less evident in wt-bOBP.

Figure 5 shows synchronous and asynchronous spectra of dynamic spectral intensity variations induced by the increase in temperature for wt-bOBP and m-bOBP. A synchronous spectrum represents the simultaneous or coincidental changes of spectral intensities measured at two discrete and independent wavenumbers $\nu 1$ and $\nu 2$ (on *x*- and *y*-axes, respectively). An asynchronous spectrum represents sequential or unsynchronized changes of spectral intensities measured at $\nu 1$ and $\nu 2$.[16,39] Auto peaks are present only on the diagonal of a synchronous map; these peaks represent the main changes in spectral intensity as a consequence of an external perturbation. Cross-peaks are present in either synchronous or asynchronous maps at the off-diagonal positions and they can be positive or negative. The sign of synchronous cross-peaks becomes positive if the spectral intensities at corresponding wavenumbers are either increasing or decreasing together. Negative synchronous cross-peaks indicate that one of the spectral intensities is increasing while the other is decreasing. The sign of asynchronous cross-peaks becomes positive if the intensity

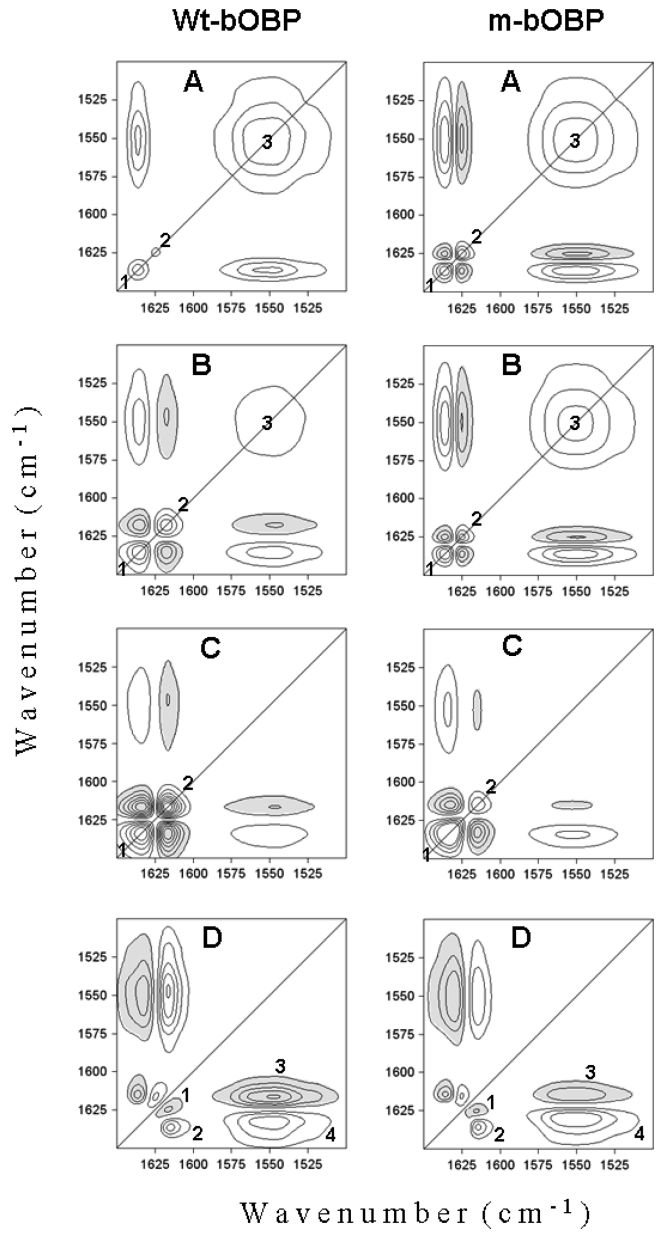

Figure 5. Synchronous and asynchronous spectra for wt-bOBP and m-bOBP in the 1650−1500 cm^{-1} spectral range. Left and right columns refer to wt-bOBP and m-bOBP, respectively. Synchronous spectra, maps (A−C); asynchronous spectra, maps (D). Gray and white spots represent negative and positive peaks, respectively. Multiple lines in the maps reflect the intensity of the peaks. Synchronous maps (A), (B), and (C) were obtained analyzing the IR absorbance spectra in the 45−80, 45−85, and 45−99 °C temperature ranges, respectively. Asynchronous maps (D) were obtained analyzing the IR absorbance spectra in the 45−99 °C temperature range.

Table 1. Data Obtained from Synchronous and Asynchronous Maps Reported in Figure 5[a]

Synchronous Maps				
	Wt-bOBP		m-bOBP	
maps	auto peaks (cm^{-1})	cross peaks at $\nu1$, $\nu2$ (cm^{-1})	auto peaks (cm^{-1})	cross peaks at $\nu1$, $\nu2$ (cm^{-1})
A	1 (1636)[b]	(1548↓[c], 1636↓[b])+	1 (1636)[c]	(1548↓[c], 1636↓[b])+,
	2 (1625)[b]		2 (1625)[b]	(1548↓[c], 1625↑[b])−,
	3 (1548)[c]		3 (1548)[c]	(1625↑b, 1636↓[b])−
B	1 (1632)[d]	(1548↓[c], 1617↑[e])−,	1 (1636)[b]	(1548↓[c], 1636↓[b])+,
	2 (1617)[b]	(1548↓[c], 1632↓[d])+,	2 (1625)[b]	(1548↓[c], 1625↑[b])−,
	3 (1548)[c]	(1617↑[e], 1632↓[d])−	**3** (1548)[c]	(1625↑[b], 1636↓[b])−
C	1 (1632)[d]	(1548↓[c], 1617↑[e])−,	1 (1630)[d]	(1548↓b, 1614↑[e])−,
	2 (1617)[e]	(1548↓[c], 1632↓[d])+,	2 (1614)[e]	(1548↓b, 1630↓[d])+,
		(1617↑[e], 1632↓[d])−		(1614↑d, 1630↓[d])−

Asynchronous Maps			
	Wt-bOBP	m-bOBP	
	Cross peaks at $\nu1$, $\nu2$ (cm^{-1})	Cross peaks at $\nu1$, $\nu2$ (cm^{-1})	
D	1 (1617[e], 1625[b])−	1 (1614[e], 1625[b])−	
	2 (1617[e], 1636[b])+	2 (1617[e], 1636[b])+	
	3 (1548[c], 1617[e])−	3 (1548[c], 1614[e])−	
	4 (1548[c], 1632[d])+	4 (1548[c], 1630[d])+	

[a] The arrows ↑ and ↓ indicate the increase and decrease of peak intensity, respectively. (+) and (−) represent positive and negative peaks, respectively. [b] Peaks involved in band shift. [c] $^1H/^2H$ exchange. [d] Denaturation. [e] Aggregation.

Table 2. Sequence of Temperature-Induced Events for wt-bOBP and m-bOBP[a]

Temperature (°C)	Wt-bOBP Bands involved in intensity changes (cm^{-1})	m-bOBP Bands involved in intensity changes (cm^{-1})
45−99°C	**A**	**A**
	1636↓[b], 1625↑[b], 1548↓[c] (band shift[b] and $^1H/^2H$ exchange[c])	1636↓[b], 1625↑[b], 1548↓[c] (band shift[b] and $^1H/^2H$ exchange[c])
	B	**B**
	1632↓[d], 1617↑[e], (denaturation[d], aggregation[e])	1630↓[d], 1614↑[e], (denaturation[d], aggregation[e])

[a] Symbols (↑) and (↓) mean the increase and the decrease of the band intensity, respectively. For wt-bOBP and m-bOBP, the sequence of events is the same: (A) followed by (B). The events reported in (A) or (B) occur concomitantly. [b] Peaks involved in band shift. [c] $^1H/^2H$ exchange. [d] Denaturation. [e] Aggregation.

change at $\nu1$ occurs predominantly before $\nu2$. On the other hand, it becomes negative if the change occurs after $\nu2$. This rule is reversed if the synchronous cross peak at $\nu1$ and $\nu2$ is negative. Multiple lines in the maps reflect the intensity of the peaks. The combination of synchronous and asynchronous plots provides useful information on the sequential order of the events following a perturbation on protein structure.[16,39]

The synchronous maps were calculated considering the 45−80 °C (maps A), 45−85 °C (maps B), and 45−99 °C (maps C) temperature intervals and the 1650−1500 cm^{-1} spectral range. This separation of IR spectra in different temperature sets and in a specific spectral range was done because it allows a more detailed description of the spectral events.[17]

Table 1 summarizes the information contained in Figure 5. For instance, in maps (A), the auto peaks (1 and 2) represent the shift of the 1636 cm^{-1} band to 1625 cm^{-1}. From the maps, it appears that in wt-bOBP the shift event is less marked than in m-bOBP. The auto peak (3) represents the decrease in intensity of the residual amide II band at 1548 cm^{-1} ($^1H/^2H$ exchange) that occurs concomitantly to the shift. The positive cross-peak (1548↓, 1636↓)+ indicates that the 1636 cm^{-1} and the 1548 cm^{-1} bands intensities are either decreasing together. In m-bOBP (map A), the negative cross-peak (1548↓, 1625↑)− indicates that the 1625 cm^{-1} band intensity is increasing while the 1548 cm^{-1} band intensity is decreasing. The auto peaks (1−3) in the map (B) of m-bOBP describe the same phenomenon, that is, band shift and $^1H/^2H$ exchange, while the auto peaks (1 and 2) in the map (B) of wt-bOBP are due to denaturation and aggregation, respectively. The auto peak (3) ($^1H/^2H$ exchange) occurs as a consequence of the protein denaturation (auto peak 1). In the maps (C), the auto peaks 1 and 2 describe the same event that is the denaturation and the aggregation processes, respectively.

The asynchronous maps (D) have been calculated in the 45−99 °C temperature range (see also Table 1), and together with synchronous maps (C) (45−99 °C) allowing us to calculate the sequence of the events occurred upon the increase of temperature (Table 2). In maps D, four asynchronous cross-peaks are present. As an example on how a sequence of event can be obtained, according to the rules previously described, we consider the positive cross-peak 2 (1617, 1636)+. This cross-peak indicates that the 1617 cm^{-1} band intensity change occurs after the change in intensity of the 1636 cm^{-1} band. In fact a positive asynchronous cross-peak indicate that the intensity change at $\nu1$ occurs predominantly before $\nu2$, but in this case, the rule is reversed because the corresponding synchronous cross peak at $\nu1$ and $\nu2$ (1617↑, 1632↓)− is negative (see maps C of wt-bOBP). The complete sequential order of the heating-induced events and their description is described in Table 2. In both wt-bOBP and m-bOBP, the increase of temperature causes as a first event the $^1H/^2H$ exchange with a concomitant band shift of the main β-sheet band. This phenomenon is more marked in m-bOBP than in wt-bOBP, and it also present in the spectra obtained in the temperature interval between 45

and 85 °C. After the $^1H/^2H$ exchange and the band shift of the main β-sheet band, the protein denaturation and the aggregation processes occur concomitantly.

The data support the idea that the $^1H/^2H$ exchange and a concomitant band shift of the main β-sheet band describe a less-folded state in which the secondary structural elements are maintained and it may be associated with the presence of a molten globule-like state.[41] It must be pointed out, however, that in wt-bOBP the molten globule-like state is slightly visible, probably because the temperature of its existence is very close to the temperature of denaturation of the protein.

MD simulations were carried out on wt-bOBP in water, both in the absence and in the presence of ligand, to analyze at a molecular level the effect of temperature on the dynamics and stability of this protein. Although the time scale is not sufficient to simulate phenomena like the global unfolding of the protein, it allows to detect the first traces of destabilization of the structures, if such phenomena are present, as shown also in previous works.[10,11]

The global behavior of the protein toward increasing temperature was analyzed in terms of variation of two parameters: radius of gyration (Rg) and solvent accessible surface area (SASA). For both parameters, a slight decrease during the first simulation at room temperature (from 2.13 to 2.07 nm for Rg; from 180 to 170 nm^2 for SASA) is followed by the stabilization around the last value for the rest of simulation, even at 373 K. Both hydrophobic and hydrophilic components contribute equally to the formation of the SASA. Taken together, these data would indicate that the compactness of the molecule is preserved, and high temperatures do not influence the exposure of the protein amino acid residues to the solvent.

The average structures obtained at different temperatures confirm that the overall structure of wt-bOBP is preserved even during the simulation experiments at 373 K. When present, the ligand is kept in the cavity of the protein, in both subunits (Figure 6). The two lipocalin-type β-barrels forming the central part of the two subunit of wt-bOBP are highly stable and they show no deformations or alterations. DSSP analysis shows that the percentage of β-strands has only minimal variations at the different temperatures investigated (Table 3). wt-bOBP is richer in α-helices if compared to both m-bOBP and pOBP (porcine OBP), since in its structure there is not only the helical segment encompassing residues 126−138 as in the monomeric proteins, but also short helices involving residues 11−15, 27−31 and 149−154 of both subunits. Comparing the results of simulations in the absence and in the presence of the ligand, it is possible to note that these short helical segments are better preserved when ligand is inside the protein. In the absence of the ligand, some of them are altered during simulations, and therefore, these segments are classified by DSSP as less regular structures such as H-bonded turns or bends, then decreasing the percentage of helices (Table 3). Finally, the loops connecting the β-strands of the protein and the unstructured N-terminal and C-terminal portions are highly flexible and show high conformational variability among the different simulations (Figure 6). By comparing the behavior of wt-bOBP with the previous simulations on the m-bOBP,[11] it is possible to notice that in the dimeric protein the percentage of β-structures oscillates around a constant value, whereas in the deswapped form it is slightly decreasing starting from the simulation at 348 K, although the main structural elements are preserved at high temperature also in this case.[11] This information may support the hypothesis of the formation of a molten globule state as suggested by infrared experiments. From these data, one can argue that the dimeric form of wt-bOBP may add further elements to stabilize the protein against thermal stress.

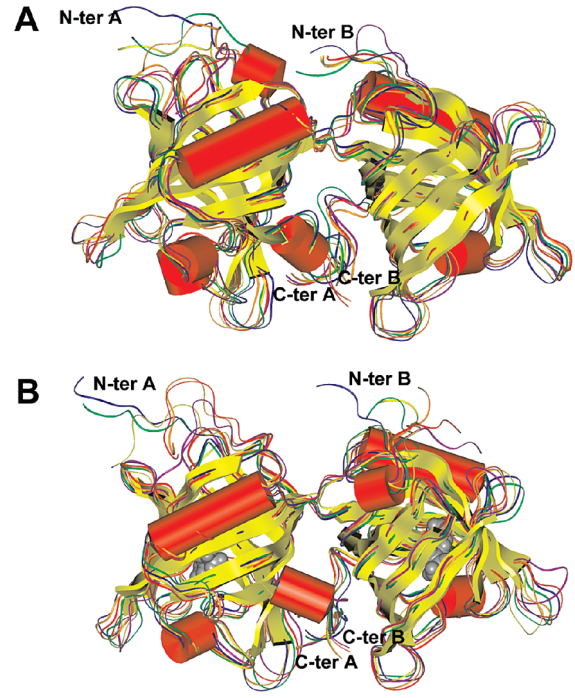

Figure 6. Superposition of average structures of wt-bOBP without (A) and with (B) ligand at different temperatures. Cα trace is colored according to temperature: 300 K (blue), 333 K (green), 348 K (yellow), 353 K (orange), 368 K (red), 373 K (violet). Secondary structures are represented as red cylinders (helix) and yellow arrows (β-sheet). N-ter and C-ter of each subunit are labeled. Ligand is in CPK mode and colored in gray.

Table 3. Percentage of Secondary Structure Elements in Average Structures Obtained by MD Simulations

secondary structures	300 K	333 K	348 K	353 K	368 K	373 K
Wild-Type bOBP without Ligand						
Helices[a]	12.30	14.88	15.21	14.57	13.91	13.92
β-strands[b]	47.57	46.93	47.25	46.60	44.01	48.54
others[c]	22.65	20.71	22.33	23.63	23.96	22.65
coils[d]	17.48	17.48	15.21	15.21	18.12	14.89
Wild-Type bOBP with Ligand						
Helices[a]	16.94	17.26	15.98	16.94	17.26	15.34
β-strands[b]	49.20	47.92	47.92	46.65	47.60	47.28
others[c]	17.57	18.53	20.45	19.48	20.12	20.77
coils[d]	16.29	16.29	15.65	16.93	15.02	16.61

[a] Marked as "H", "G" and "I" in DSSP output. [b] Marked as "E" in DSSP output. [c] Marked as "B", "T" and "S" in DSSP output. [d] Structures not classified in DSSP output.

As we already did in other investigations on different proteins,[10,11] in this work, we analyzed the role of salt bridges in stabilizing the structure of wt bOBP. This protein possesses 61 negatively charged and 52 positively charged amino acid residues, and it is of interest to check if the presence of salt bridges on the protein surface could contribute to the protein stability. In fact, it has been showed by several authors the critical role played both by networks of buried salt bridges located at the protein C-terminal domain of proteins as well as exposed salt bridges on the protein surface in enhancing the stability of proteins isolated from organisms living at high temperature.[43−45]

Table 4. Conserved Ion Pairs in Average Structures Obtained by MD Simulations[a]

ion pairs	300 K	333 K	348 K	353 K	368 K	373 K
			Wild-Type bOBP without Ligand			
D53A-K70A	OD1-NZ: 3.1 OD2-NZ: 3.0 c-c: 3.0	OD1-NZ: 3.6 OD2-NZ: 2.9 c-c: 3.3	OD1-NZ: 3.4 OD2-NZ: 2.8 c-c: 3.1	OD1-NZ: 3.6 OD2-NZ: 3.0 c-c: 3.3	OD1-NZ: 2.9 c-c: 3.6	OD1-NZ: 3.1 OD2-NZ: 3.5 c-c: 3.2
D82B-K108B	-	OD1-NZ: 3.6 OD2-NZ: 2.9 c-c: 3.2	OD1-NZ: 3.4 c-c: 3.9	OD1-NZ: 3.2 c-c: 3.7	-	OD1-NZ: 3.6 OD2-NZ: 2.9 c-c: 3.3
D107A-K29A	-	OD2-NZ: 3.4 c-c: 3.7	OD1-NZ: 3.9 OD2-NZ: 3.3 c-c: 3.5	-	OD2-NZ: 3.3 c-c: 3.7	OD2-NZ: 3.5 c-c: 3.7
E32B-R37B	-	OE1-NH2: 3.5 OE2-NH1: 3.2 OE2-NH2: 3.8 c-c: 3.4	OE1-NH2: 3.2 OE2-NH1: 3.9 OE2-NH2: 3.6 c-c: 3.4	OE1-NH1: 3.9 OE1-NH2: 3.4 OE2-NH1: 3.8 OE2-NH2: 3.8 c-c: 3.4	OE1-NH1: 3.8 OE1-NH2: 3.5 c-c: 3.7	OE1-NH2: 3.1 c-c: 3.6
E84B-R60B	-	-	OE2-NH1: 3.7 OE2-NH2: 3.2 c-c: 4.0	OE1-NH1: 3.5 OE1-NH2: 3.3 OE2-NH1: 3.9 OE2-NH2: 3.4 c-c: 3.3	OE1-NH1: 3.2 OE1-NH2: 3.6 OE2-NH1: 3.6 OE2-NH2: 3.2 c-c: 3.3	OE1-NH2: 3.0 OE2-NH1: 3.9 c-c: 3.6
E153B-R18A	OE1-NH2: 3.2 OE2-NH2: 4.0 c-c: 3.4	OE2-NH2: 3.9 c-c: 4.0	OE2-NH1: 3.9 OE2-NH2: 3.3 c-c: 3.6	OE2-NH2: 3.4 c-c: 3.8	-	-
			Wild-Type bOBP with Ligand			
D53A-K70A	-	-	OD1-NZ: 3.3 OD2-NZ: 3.0 c-c: 3.2	OD1-NZ: 3.9 OD2-NZ: 3.1 c-c: 3.5	OD1-NZ: 3.7 OD2-NZ: 3.0 c-c: 3.3	OD1-NZ: 3.0 OD2-NZ: 3.7 c-c: 3.3
D107A-K29A	OD1-NZ: 3.8 c-c: 3.7	OD1-NZ: 3.4 c-c: 3.7	OD2-NZ: 3.0 c-c: 3.9	-	OD2-NZ: 3.3 c-c: 4.0	-
E32B−K59B	OE1-NZ: 3.6 OE2-NZ: 3.3 c-c: 3.3	OE1-NZ: 3.4 OE2-NZ: 3.4 c-c: 3.3	OE1-NZ: 3.0 c-c: 3.8	-	-	OE1-NZ: 3.4 OE2-NZ: 3.8 c-c: 3.7
E153B-R18A	OE2-NH2: 3.9 c-c: 4.0	OE1-NH2: 3.5 OE2-NH2: 3.3 c-c: 3.2	OE1-NH2: 3.3 OE2-NH2: 3.6 c-c: 3.2	OE1-NH2: 3.1 OE2-NH2: 3.6 c-c: 3.2	OE1-NH2: 3.4 OE2-NH2: 3.5 c-c: 3.1	OE2-NH2: 3.4 c-c: 3.3

[a] Only ion pairs conserved in at least 4 simulations at different temperatures are shown. When a ion pair is present, the distances (in Å) between the atoms and between the centroids (c) of the charged groups are reported in the table.

Using the criteria suggested by Kumar and Nussinov,[29] we were able to detect many salt bridges in the structure of the protein, but only few of them are conserved in many average structures obtained by MD simulations (Table 4). The most interesting one is probably the ion pair between E153 of subunit B and R18 of subunit A. In wt-bOBP, the segment 123−159 of each monomer is stacked against the β-barrel of the other monomer, and in this way, the α-helix of each monomer (segment 126−138) is placed close to where the helix would be in a classic lipocalin fold.[19] This ion pair allows to connect the β-barrel of subunit A to the C-terminal portion of subunit B, and probably this interchain bridge plays a fundamental role in keeping the correct reciprocal positioning of the two subunits of wt-bOBP (Figure 7). The ligand may play an important role in increasing stability in this dimeric protein influencing somehow this ion pair. In fact, in the absence of the ligand, this ion pair is lost at high temperatures, whereas when the ligand is present, this ion pair is conserved even at 373 K. E153 is inserted in a short helical segment, and as discussed above, the absence of ligand may induce an alteration of this secondary structure that prevent the formation of this salt bridge. The other ion pairs are structurally localized mainly at the larger moiety of the β-barrel, and all except the one between D53 and K70 involve at least a residue inserted in a loop. Therefore, as already shown for m-bOBP,[11] this may suggest the importance of these interactions in bringing together highly mobile portions of the protein, contributing to the overall protein stability. In both cases, hydrophobic interactions in the core of the β-barrel structure and ion pairs seem to play a major role in protecting these proteins against high temperature shock.

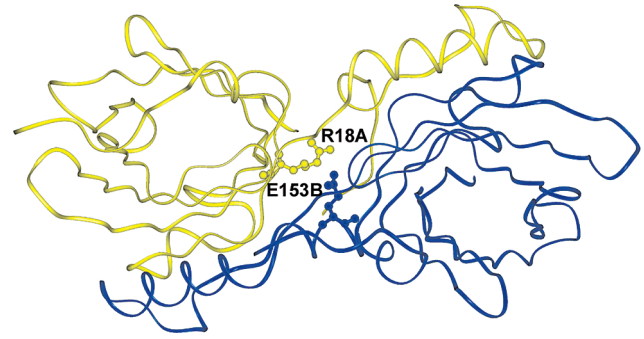

Figure 7. Ion pair between E153 (B subunit) and R18 (A subunit) in wt-bOBP. The subunit A of wt-bOBP is shown in yellow, whereas subunit B is shown in blue. The two residues are represented in ball and stick mode.

In conclusion, FT-IR analysis and MD simulations are able to highlight phenomena that take place at different timescales, allowing to elucidate both the preliminary molecular events

and the long-range behavior of the proteins. FT-IR shows that both wt-bOBP and m-bOBP are characterized by a remarkable resistance of their global structural organization to high temperatures (considering also that they are not deriving from thermophilic organisms). The domain swapping occurring in wt-bOBP, however, seems to induce more stabilization of the three-dimensional structure with respect to the monomeric structure of the triple deswapped mutant as revealed by difference infrared spectra and 2DIR correlation analysis of infrared spectra obtained at different temperatures. Indeed, in m-bOBP, a molten globule-like state seems to appear around 75 °C, whereas this seems not the case in the wild-type protein. On the contrary, difference spectra indicated that a marked loss of secondary structure occurs at lower temperature in wt-bOBP when compared with m-bOBP, although the onset of denaturation is the same for both proteins. MD simulations elucidate the molecular processes that occur in the early phases of the experiment and allow the interpretation of the macroscopic phenomena registered with the long timescale technique, suggesting a role for elements such as the presence of ion pairs and hydrophobic interactions, or secondary structure formation/disruption in protein structure stabilization.

Abbreviations: Amide I′, amide I band in ^2H_2O medium; FT-IR, Fourier transform-infrared; wt-bOBP, wild-type bovine odorant-binding protein; m-bOBP, mutant bovine odorant-binding protein; MD, molecular dynamics.

Acknowledgment. This work was in the frame of the CNR Commessa "Diagnostica avanzata ed alimentazione" (S.D., M.S., V.A.). This work was also supported by the ASI project MoMa No. 1/014/06/0 (M.S.; S.D.), the CNR Bioinformatics Project (A.M.), the NATO grant CBP.EAP.CLG 982437 (M.S.), and by a grant from Università Politecnica delle Marche (A.S., F.T.). The authors wish to thank to Prof. Roberto Ramoni, University of Parma for providing the genes of the wild-type and the mutant OBPs and the PDB files of the protein structures, Dr. Umberto Amato for hosting MD simulations on the cluster "Lilligrid" located at the IAC-CNR, Naples, and Dr. Angelo Facchiano, Laboratory of Bioinformatics, ISA, Avellino, for providing tools for the calculation of the percentage of secondary structures using DSSP program and for the determination of distances between ion pairs, starting from a PDB file.

References

(1) Grzyb, J.; Latowski, D.; Strzalka, K. *J. Plant Physiol.* **2006**, *163*, 895–915.
(2) Briand, L.; Eloit, C.; Nespoulous, C.; Bezirard, V.; Huet, J. C.; Henry, C.; Blon, F.; Trotier, D.; Pernollet, J. C. *Biochemistry* **2002**, *41*, 7241–7252.
(3) Pevsner, J.; Snyder, S. H. *Chem. Senses* **1990**, *15*, 217–222.
(4) Flower, D. R.; North, A. C. T.; Sansom, C. E. *Biochim. Biophys. Acta* **2000**, *1482*, 9–24.
(5) Boudjelal, M.; Sivaprasadarao, A.; Findlay, J. B. C. *Biochem. J.* **1996**, *317*, 23–27.
(6) Tegoni, M.; Pelosi, P.; Vincent, F.; Spinelli, S.; Campanacci, V.; Grolli, S.; Ramoni, R.; Cambillau, C. *Biochim. Biophys. Acta* **2000**, *1482*, 229–240.
(7) Flower, D. R. *Biochim. Biophys. Acta* **2000**, *1482*, 46–56.
(8) Bianchet, M. A.; Bains, G.; Pelosi, P.; Pevsner, J.; Snyder, S. H.; Monaco, H. L.; Amzel, L. M. *Nat. Struct. Biol.* **1996**, *3*, 934–939.
(9) Ramoni, R.; Spinelli, S.; Grolli, S.; Conti, V.; Merli, E.; Cambillau, C.; Tegoni, M. *Biochim. Biophys. Acta* **2008**, *1784* (4), 651–657.
(10) Stepanenko, O. V.; Marabotti, A.; Kuznetsova, I. M.; Turoverov, K. K.; Fini, C.; Varriale, A.; Staiano, M.; D'Auria, S. *Proteins* **2008**, *71*, 35–44.
(11) Marabotti, A.; Lefevre, T.; Staiano, M.; Crescenzo, R; Varriale, A.; Rossi, M.; Pezolet, M.; D'Auria, S. *Proteins* **2008**, *72*, 769–778.
(12) D'Auria, S.; Staiano, M.; Varriale, A.; Gonnelli, M.; Marabotti, A.; Rossi, M.; Strambini, G. *J. Proteome Res.* **2008**, *7*, 1151–1158.
(13) Salomaa, P.; Schaleger, L. L.; Long, F. A. *J. Am. Chem. Soc.* **1964**, *86*, 1–7.
(14) Tanfani, F.; Galeazzi, T.; Curatola, G.; Bertoli, E.; Ferretti, G. *Biochem. J.* **1997**, *322*, 765–769.
(15) Morita, S.; Ozaki, Y.; Noda, I. *Appl. Spectrosc.* **2001**, *55*, 1618–1621.
(16) Noda, I.; Ozaki, Y. *Generalized Two-Dimensional Correlation Spectroscopy. Applications in Vibrational and Optical Spectroscopy*; Wiley: New York, 2004.
(17) Fabian, H.; Mantsch, H. H.; Schultz, C. P. *Proc. Natl. Acad. Sci. U.S.A.* **1999**, *96*, 13153–13158.
(18) Berman, H.; Henrick, K.; Nakamura, H.; Markley, J. L. *Nucleic Acids Res.* **2007**, *35* (Database issue), D301–D303.
(19) Ramoni, R; Vincent, F.; Grolli, S.; Conti, V.; Malosse, C.; Boyer, F. D.; Nagnan-Le Meillour, P.; Spinelli, S.; Cambillau, C.; Tegoni, M. *J. Biol. Chem.* **2001**, *276*, 7150–7155.
(20) Lindahl, E.; Hess, B.; van der Spoel, D. *J. Mol. Model.* **2001**, *7*, 306–317.
(21) van der Spoel, D.; Lindahl, E.; Hess, B.; Groenhof, G.; Mark, A. E.; Berendsen, H. J. *J. Comput. Chem.* **2005**, *26*, 1701–1718.
(22) van Gunsteren, W. F.; Billeter, S. R.; Eising, A. A.; Hunenberger, P. H.; Kruger, P.; Mark, A. E.; Scott, W. R. P.; Tironi, I. G.; *Biomolecular Simulation: The GROMOS96 Manual and User Guide*; Vdf Hochschulverlag AG an der ETH Zurich: Zurich, Switzerland, 1996; p 1042.
(23) Schuettelkopf, A. W.; van Aalten, D. M. F. *Acta Crystallogr., D* **2004**, *60*, 1355–1363.
(24) Berendsen, H. J. C.; Postma, J. P. M.; van Gunsteren, W. F.; Hermans, J. In *Intermolecular Forces*; Pullman B., Ed.; Reidel D. Publishing Company: Dordrecht, The Netherlands, 1981; p 331−342.
(25) Hess, B.; Bekker, H.; Berendsen, H. J. C.; Fraaije, J. G. E. M. *J. Comput. Chem.* **1997**, *18*, 1463–1472.
(26) Berendsen, H. J. C.; Postma, J. P. M.; Di Nola, A.; Haak, J. R. *J. Phys. Chem.* **1984**, *81*, 3684–3690.
(27) Essmann, U.; Perera, L.; Berkowitz, M. L.; Darden, T.; Lee, H.; Pedersen, L. G. *J. Chem. Phys.* **1995**, *103*, 8577–8593.
(28) Kabsch, W.; Sander, C. *Biopolymers* **1983**, *22*, 2577–2637.
(29) Kumar, S.; Nussinov, R. *J. Mol. Biol.* **1999**, *293*, 1241–1255.
(30) Arrondo, J. L. R.; Muga, A.; Castresana, J.; Goni, F. M. *Prog. Biophys. Mol. Biol.* **1993**, *59*, 23–56.
(31) Krimm, S.; Bandekar, J. *Adv. Protein Chem.* **1986**, *38*, 181–364.
(32) Byler, D. M.; Susi, H. *Biopolymers* **1986**, *25*, 469–487.
(33) Barth, A.; Zsherp, C. *Q. Rev. Biophys.* **2002**, *35*, 369–430.
(34) Barth, A. *Biochim. Biophys. Acta* **2007**, *1767*, 1073–1101.
(35) Pedone, E.; Bartolucci, S.; Rossi, M.; Pierfederici, F. M.; Scirè, A.; Cacciamani, T.; Tanfani, F. *Biochem. J.* **2003**, *373*, 875–883.
(36) Ausili, A.; Cobucci-Ponzano, B.; Di Lauro, B.; D'Avino, R.; Perugino, G.; Bertoli, E.; Scirè, A.; Rossi, M.; Tanfani, F.; Moracci, M. *Proteins* **2007**, *67*, 991–1001.
(37) Paolini, S.; Tanfani, F.; Fini, C.; Bertoli, E.; Pelosi, P. *Biochem. Biophys. Acta* **1999**, *1431*, 179–188.
(38) Ausili, A.; Scirè, A.; Damiani, E.; Zolese, G.; Bertoli, E.; Tanfani, F *Biochemistry* **2005**, *44*, 15997–16006.
(39) Noda, I. *Appl. Spectrosc.* **1993**, *47*, 1329–1336.
(40) Umemura, J.; Cameron, D. G.; Mantsch, H. H. *Biochim. Biophys. Acta* **1980**, *602*, 32–44.
(41) Ptitsyn, O. B. The molten globule state. In *Protein Folding*; Creighton, T. E., Ed.; W. H. Freeman and Company: New York, 1992; pp 243−300.
(42) Seshadri, S.; Khurana, R.; Fink, A. L. *Methods Enzymol.* **1999**, *309*, 559–576.
(43) Knapp, S.; de Vos, W. M.; Rice, D.; Ladenstein, R. *J. Mol. Biol.* **1997**, *267*, 916–932.
(44) Goldman, A. *Structure* **1995**, *3*, 1277–79.
(45) Fessas, D.; Staiano, M.; Barbiroli, A.; Marabotti, A.; Schiraldi, A.; Varriale, A.; Rossi, M.; D'Auria. S *Proteins* **2007**, *67*, 1002–9.

PR800528B

J. Phys.: Condens. Matter **20** (2008) 474202 (3pp) doi:10.1088/0953-8984/20/47/474202

Nanobeads-based assays. The case of gluten detection

Iole Venditti[1], Ilaria Fratoddi[1], Maria Vittoria Russo[1], Stefano Bellucci[2], Roberta Crescenzo[3], Luisa Iozzino[3], Maria Staiano[3], Vincenzo Aurilia[3], Antonio Varriale[3], Mosè Rossi[3] and Sabato D'Auria[3,4]

[1] Department of Chemistry, 'Sapienza' University of Rome, Piazzale Aldo Moro 5, Box 34 Rome 62, 00185 Rome, Italy
[2] INFN—Laboratori Nazionali di Frascati, Frascati, Italy
[3] Laboratory for Molecular Sensing, IBP-CNR, Via Pietro Castellino, 111 80131 Naples, Italy

E-mail: s.dauria@ibp.cnr.it

Received 23 April 2008, in final form 4 June 2008
Published 6 November 2008
Online at stacks.iop.org/JPhysCM/20/474202

Abstract

In order to verify if the use of nanobeads of poly[phenylacetylene-(co-acrylic acid)] (PPA/AA) in the ELISA test would affect the immune-activity of the antibodies (Ab) and/or the activity of the enzymes used to label the Ab anti-rabbit IGg, in this work we immobilized the horse liver peroxidase labelled Ab anti-rabbit IGg onto PPA/AA nanobeads. The gluten test was chosen as the model to demonstrate the usefulness of these nanobeads in immunoassays. The synthesis of PPA/AA nanobeads was performed by a modified emulsion polymerization. Self-assembly of nanospheres with mean diameter equal to 200 nm was achieved by casting aqueous suspensions. The materials were characterized by traditional spectroscopic techniques, while the size and dispersion of the particles were analysed by scanning electron microscopy (SEM) measurements. The obtained results show that the immobilization process of the Abs onto PPA/AA did not affect either the immune-response of the Abs or the functional activity of the peroxidase suggesting the usefulness of PPA/AA for the design of advanced nanobeads-based assays for the simultaneous screening of several analytes in complex media.

Abbreviations

PPA/AA	poly[phenylacetylene-(co-acrylic acid)]
SEM	Scanning electron microscopy

1. Introduction

A large effort is currently devoted in research to develop chemical approaches which allow the preparation of materials with mesoscale dimensions. It is now recognized that nanoparticles have the potential to regulate cellular processes such as protein–protein interactions, protein–nucleic acid interactions and enzyme activity. Scaffolds with large surfaces are of particular interest for biomolecular recognition.

In this field, organic materials (e.g. polystyrene, polyacrylates) have the advantage of greater synthetic flexibility in comparison with inorganic ones (e.g. titanium, silicon) [1, 2]. Among the wide number of literature reports, some examples will be cited. Cellular uptake of polystyrene and PLGA (poly(lactic-co-glycolic acid)) nanoparticles for oral delivery of anticancer drugs was successfully demonstrated [3], as well as the enhancement of recombinant protein production induced by PLGA nanospheres [4]. Highlights on the up to date research efforts and paradigms concerning protein–nanoparticle interactions appeared recently [5].

Micro and nanospheres of uniform size and shape play a dramatic role in biomolecule–nanoparticle activity and performance. Generally, emulsion polymerization or co-polymerization of monomers [6] are the most suitable chemical methods to prepare micro-nanospheres. Since many applications and properties of these particles are significantly influenced by the morphology and surface properties of the particles, interest has been increasingly focused on the control of the particle size and its distribution and the control of the distribution of functional groups. In this framework, π conjugated polymers such as polyphenylacetylene (PPA) and

[4] Author to whom any correspondence should be addressed.

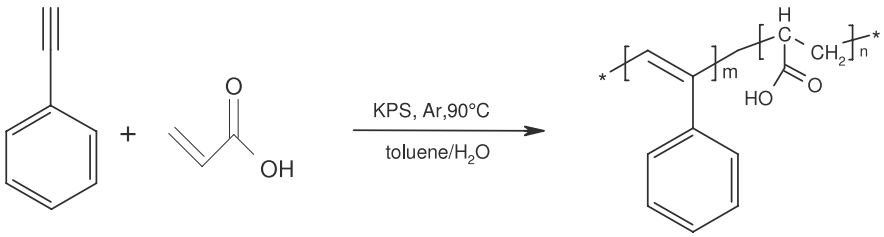

Figure 1. Modified emulsion synthesis of PPA/AA.

its copolymers are of particular interest because PPA is a semiconductor luminescent polymer and it is a candidate for cell and protein immobilization due to its biocompatibility [7].

Our research has been focussed on the synthesis of a novel material, i.e. poly[phenylacetylene-(co-acrylic acid)] (PPA/AA), at the micro and nanoscale, which is a material suited for the investigation of scientific aspects related to biotechnology because the functional groups are expected to strongly interact with biomolecules such as antibodies, enzymes and nucleic acids.

In this work we immobilized horse liver peroxidase labelled Abs anti-rabbit IGg onto PPA/AA nanobeads and we checked their functional properties before and after the immobilization process. The obtained data demonstrate that the immobilized biomolecules retain their functional properties suggesting their utilization for the design of new nanobeads-based assays.

2. Experimental details

2.1. Instruments and materials

Deionized water was obtained with Millipore-Q RG(CPMQ00 4R1) and degassed for 30 min with argon before use; phenylacetylene (PA) (Aldrich 99% pure) was distilled under reduced pressure before use; acrylic acid (AA) (Aldrich 99% pure) and potassium persulfate (KPS) (Aldrich 99.99% pure), were used as received; other solvents and materials were reagent grade (Aldrich).

FTIR spectra were recorded as nujol mulls or as films deposited from $CHCl_3$ solutions by using CsI cells, on a Bruker Vertex 70 spectrophotometer. UV–vis spectra were carried out on a Varian Cary100 spectrophotometer; the samples were analysed as solutions in common organic solvents.

The morphology and the diameter of the beads and their poly-dispersity were determined by an SEM-LEO1450VP instrument on metallized samples; nanobead dimensions were calculated from the SEM images of films deposited by casting, using an image analysis software tool (Scion Image for Windows, Scion Corp, Beta 4.0.2) and the poly-dispersity index (PI) was obtained using the formula:

$$\mathrm{PI} = (d_{\max} - d_{\min})/d_{\text{average}},$$

where d is the particle diameter in nm.

2.2. Synthesis of polymeric nanobeads

Poly[phenylacetylene-(co-acrylic acid)] (PPA/AA) nanospheres were prepared by a modified emulsion synthesis. The PPA/AA nanobeads were prepared by following this typical procedure: 50 ml of deionized water, 1 ml of toluene, 1 ml (0.936 g, 0.01 mol) of PA and 0.2 ml (5.255 g, 0.07 mol) of AA, were degassed for 15 min and then stirred in an Argon atmosphere, at 90 °C for 1 h; then 5 ml of KPS water solution (20 mg ml^{-1}) was added and the reaction was refluxed under vigourous stirring in an Argon atmosphere for 20 h; polymerization was stopped by opening the flask (yield ∼70% of crude product) and the light yellow emulsion was filtered, redispersed and centrifuged with deionized water seven times, in order to remove the unreacted chemicals.

UV–vis spectra in a $CHCl_3$ solution showed continuous absorption in the λ range 200–400 nm. IR (cm^{-1}): 3050 ($\nu_{\text{aromatic CH}}$), 1670 (ν_{COOH}), 1597 ($\nu_{\text{aromatic C=C}}$), 770 ($\nu_{\text{CH}}$). SEM images show mono-dispersed spheres with diameter 200–210 nm and PI 0.8.

2.3. ELISA test

We used the following procedure. (1) We applied a sample of known concentration of gliadin to the plate surface. The plate walls were then coated with specific antibodies anti-gliadin, diluted into the same buffer used for the antigen. A concentrated solution of non-interacting protein, such as bovine serum albumin (BSA) was added to all plate walls. The plate was washed, and a detection antibody specific to the antigen of interest was applied to all plate walls. The plate was washed to remove any unbound detection antibody. After this wash, only the antibody–antigen complexes remained attached to the wall. Secondary antibodies, previously immobilized onto PPA/AA nanobeads were added to the walls. These secondary antibodies were conjugated to the substrate-specific enzyme. The plate was washed so that the excess of unbound enzyme–antibody conjugates was removed. The substrate was added to the walls and a chromogenic signal was detected at 620 nm.

3. Results and discussion

Poly[phenylacetylene-(co-acrylic acid)] nanospheres were synthesized by using a modified emulsion technique, as reported in figure 1.

In analogy to synthetic procedures for the preparation of alike copolymers [8], the KPS initiator, PA/toluene and PA/initiator ratios and the reaction time were optimized in order to achieve monodisperse nanospheres with a mean diameter of 200 nm, whose SEM image is reported in figure 2.

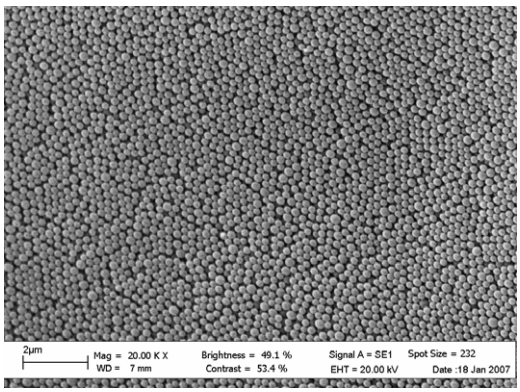

Figure 2. SEM image of PPA/AA nanobeads, mean diameter 200 nm.

We used these beads as a solid support to immobilize the horse liver peroxidase labelled Abs anti-rabbit IGg. After rinsing the PPA/AA beads in distilled water several times at room temperature, the PPA/AA nanobeads were soaked in a 10 mM PBS buffer, pH 7.4. These nanobeads were incubated with a solution 20 μg ml^{-1} of horse liver peroxidase labelled Abs anti-rabbit IGg at room temperature for 1.0 h. After incubation, the nanobeads were washed several times with a PBS buffer, pH 7.4 and used for the last step of the ELISA test. In the discarded washing solutions we did not find an appreciable amount of Ab. This result suggested that almost all the Ab molecules were attached to the nanobeads. For this experiment, we decided to use a well known Ab–Ag system used in the detection of gliadin in food for coeliac patients. We choose gluten as the model since we already worked on this system by using different detection methodologies [9–11].

The ELISA tests were performed by using the commercial secondary antibodies attached to the PPA/AA nanobeads or free in solution. The goal of this experiments was to understand if the immobilization of secondary antibodies onto the PPA/AA nanobeads could affect the binding features of the Abs and/or the enzyme activity of the horse liver peroxidase.

The results obtained show that there is no difference for the detection of gluten when we use secondary Abs immobilized onto PPA/AA nanobeads or secondary Abs in free solution.

The results obtained by using different concentrations of Ab anti-gliadin and secondary Ab immobilized onto the nanobeads are shown in figure 3. The results obtained indicate that the immobilization process of horse liver peroxidase labelled Ab anti-rabbit IGg onto PPA/AA nanobeads does not perturb the functional features of the Abs as well as the activity of the enzyme, suggesting a more general utilization of these nanobeads in ELISA tests.

4. Conclusions

In conclusion, the results obtained in this work show that there is a strong interaction between the nanobeads of PPA/AA and anti-gliadin antibodies and that the immobilized antibodies retain their immunological activity. These results suggest a potentially wider utilization of the PPA/AA nanobeads for the design of new assays that allow a simultaneous screening of different analytes that are present in complex media.

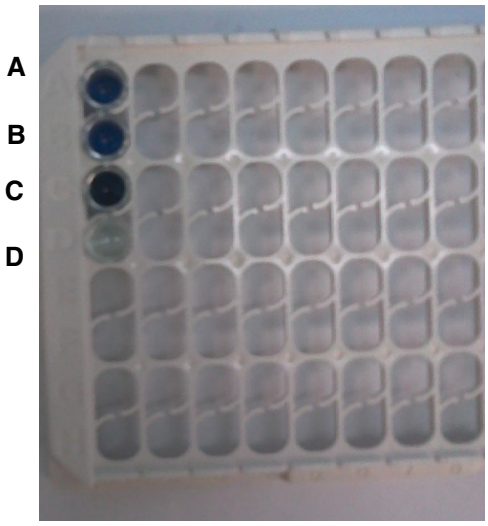

Figure 3. ELISA test performed by using secondary Abs immobilized onto the nanobeads PPA/AA. (A) Gliadin (25 μg ml^{-1}) + Ab anti-Gliadin dil.1:100 000; (B) Gliadin (25 μg ml^{-1}) + Ab anti-Gliadin dil.1:50 000; (C) Gliadin (25 μg ml^{-1}) + Ab anti-Gliadin dil.1:10 000; (D) negative control-Gliadin (25 μg ml^{-1}) + Ab-Gliadin dil.1:10 000.
(This figure is in colour only in the electronic version)

Acknowledgments

The authors thank Dr Paolo Bazzicalupo for the useful discussion. This work was in the frame of the CNR Commessa Diagnostica avanzata ed alimentazione (SD). This work was also supported by ASI project MoMa No. 1/014/06/0 (MS; SD), by Regione Campania grant L R N.5 del 28.03.2002 'Un semplice e rapido biosensopre a fluorescenza per pazienti celiaci' (SD; M.S;AV), by NATO grant CBP.EAP.CLG 982437 (SD), and by NATO grant CBP.NR.NRCLG.983088 (MS).

References

[1] Reese C E, Guerrero C D, Weissman J M, Lee K and Asher S A 2000 *J. Colloid Interface Sci.* **232** 76
[2] Muller M, Zentel R, Maka T, Romanov S G and Torres C M S 2000 *Chem. Mater.* **12** 2508
[3] Win K Y and Feng Si-S 2005 *Biomaterials* **26** 2713
[4] Ryu J H, Kim M S, Lee G M, Choi C Y and Kim B-S 2005 *Biomaterials* **26** 2173
[5] Lynch I and Dawson K A 2008 *Nanotoday* **3** 40
[6] Capek I 2002 *Adv. Colloid Interface Sci.* **99** 77
[7] Panzavolta F, Soro S, D'Amato R, Palocci C, Cernia E and Russo M V 2005 *J. Mol. Catal.* B **32** 67
[8] Venditti I, D'Amato R, Russo M V and Falconieri M 2007 *Sensors Actuators* B **126** 35
[9] De Stefano L, Rossi M, Staiano M, Mamone G, Parracino A, Rotiroti L, Rendina I, Rossi M and D'Auria S 2006 *J. Prot. Res.* **5** 1241–5
[10] Staiano M, Scognamiglio V, Mamone G, Rossi M, Parracino A, Rossi M and D'Auria S 2006 *J. Prot. Res.* **5** 2083–6
[11] Varriale A, Rossi M, Staiano M, Terpetschnig E, Barbieri B, Rossi M and D'Auria S 2007 *Anal. Chem.* **79** 4687–9

J. Phys.: Condens. Matter **20** (2008) 474201 (4pp) doi:10.1088/0953-8984/20/47/474201

Carbon nanotube-based biosensors

Roberto Ramoni[1], Maria Staiano[2], Stefano Bellucci[3], Ignacy Gryczynski[4], Zygmunt Gryczynski[4], Roberta Crescenzo[1,2], Luisa Iozzino[2], Shashank Bharill[4], Virna Conti[1], Stefano Grolli[1] and Sabato D'Auria[2,5]

[1] Dipartimento di Produzioni Animali, Università degli Studi di Parma, Italy
[2] Laboratory for Molecular Sensing, IBP, CNR, Naples, Italy
[3] INFN—Laboratori Nazionali di Frascati, Frascati, Italy
[4] University of North Texas, Forth Worth, TX, USA

E-mail: s.dauria@ibp.cnr.it

Received 21 April 2008, in final form 22 April 2008
Published 6 November 2008
Online at stacks.iop.org/JPhysCM/20/474201

Abstract

An easy and rapid detection of hazardous compounds is crucial for making on-the-spot irreversible decisions at airport security gates, luggage storage rooms, and other crowded public places, such as stadia, concert halls, etc.

In the present study we carried out a preliminary investigation into the possibility of utilizing as advanced nano-biosensors a mutant form of the bovine odorant-binding protein (bOBP) immobilized onto carbon nanotubes. In particular, after immobilization of the protein on the carbon nanotubes we developed a competitive resonance energy transfer (RET) assay between the protein tryptophan residues located at the positions 17 and 133 (W17 and W133) and the 1-amino-anthracene (AMA), a molecule that fits in the binding site of bOBP. The bOBP–AMA complex emitted light in the visible region upon excitation of the Trp donors. However, the addition of an odorant molecule to the bOBP–AMA complex displaced AMA from the binding site making the carbon nanotubes colorless.

The results presented in this work are very promising for the realization of a color on/color off b-OBP-based biosensor for the initial indication of hazardous compounds in the environment.

(Some figures in this article are in colour only in the electronic version)

1. Introduction

Odorant-binding proteins (OBPs) are small extracellular proteins belonging to the lipocalin superfamily. They have been supposed to play a role in peri-receptorial events of odor detection by carrying, deactivating, and/or selecting odorant molecules [1–3]. The OBPs share a conserved folding pattern, an eight-stranded β-barrel flanked by an α-helix at the C-terminal end of the polypeptide chain. The β-barrel creates a central apolar cavity whose role is to bind and transport hydrophobic odorant molecules. These proteins reversibly bind odorant molecules with dissociation constants in the nano-/micromolar range. Although their functions are still not fully understood, OBPs are also believed to participate in the deactivation of odorant molecules [4–6]. OBPs have been identified in a variety of species, including pig, rabbit, mouse, and rat. Bovine OBP (bOBP) shows a peculiar three dimensional (3D) structure, characterized by domain 'swapping'. In solution at neutral pH it appears as a dimer in which each monomer is composed of the classical lipocalin fold, with a large buried cavity internal to the beta-barrel forming the binding site for odorant molecules. The absence of a Gly after position 121 in the sequence and the lack of the disulfide bridge between the C-terminal and the beta-barrel, which are both strictly conserved in other sequences of mammalian OBPs, were identified as the determinants for the domain swapping. This hypothesis is supported by the finding that a mutant bOBP in which a glycine residue was inserted after position 121, showed a monomeric structure. Recently a 'deswapped' triple mutant bOBP (Gly 122+, W64C, H156C) has been obtained, in which a Gly residue is inserted after position 121 and the two residues in positions 64 and 156

[5] Address for correspondence: Laboratory for Molecular Sensing, IBP—National Research Council, Via Pietro Castellino, 111—80131 Naples, Italy.

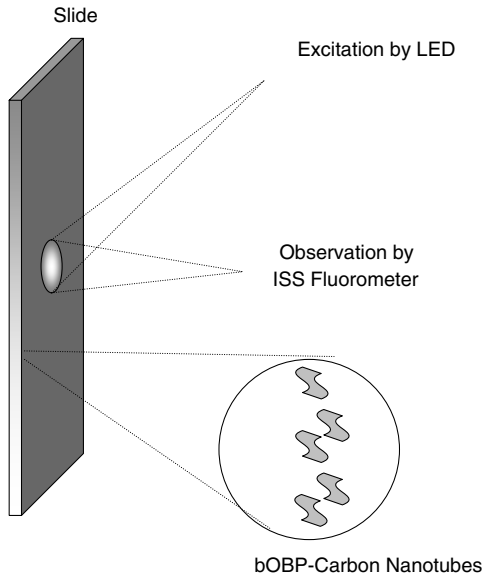

Figure 1. Experimental sample geometry for fluorescence front-face measurements.

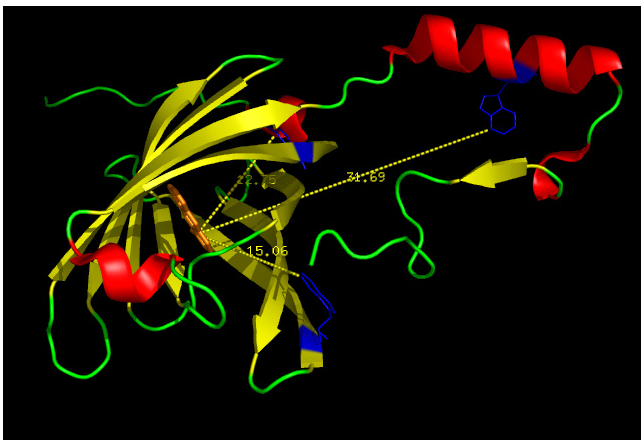

Figure 2. Structure of bOBP.

are replaced by Cys residues, in order to restore the disulfide bridge common to the lipocalin family [7–9]. This protein has been over-expressed in *E. coli* and it has been demonstrated that it binds compounds that are usually utilized for the preparation of explosives and/or compounds produced upon an explosion [10, 11].

In this work we utilized this mutant form of bOBP to develop a new sensing concept: a light on/off carbon nanotube-based biosensor for easy and rapid detection of harmful analytes present in the environment.

2. Materials and methods

2.1. Materials

Carbon nanotubes were from Sigma. All the chemicals from different commercial sources, were of the purest grade available. A brief description of bovine OBP purification and the functionality test with 1-amino-anthracene is given below [9, 12].

3. Protein production

A 6xHis affinity tag was placed at the N-terminal of bOBP formed by polymerase chain reaction (PCR) using specific primers. The fused cDNAs were sub-cloned in the expression vector pT7-7 and the expression of the proteins, in BL21-DE 3 *E. coli*, was realized as reported above for the recombinant form of the mutant bOBP [9]. The purification of the proteins was obtained by affinity chromatography with an Ni-NTA agarose (Quiagen, Germany) according to the manufacturer's instructions, followed by a second chromatographic step on the anion exchange column Recourse Q (Amersham Biosciences, Italy), in FPLC. The purity of bOBP preparation was determined by SDS-PAGE and protein concentrations were calculated based on the absorbance values at 280 nm ($48\,000\ M^{-1}\ cm^{-1}$ for bOBP). Functionality of the bOBP form was determined by direct titrations using the fluorescent ligand 1-amino-anthracene as previously reported [9, 12]. Briefly, 1 ml samples of 1 μM OBP, in 20 mM Tris-HCl buffer pH 7.8, were incubated overnight at 4 °C in the presence of increasing concentrations of AMA (0.156–10 μM). Fluorescence emission spectra between 450 and 550 nm were recorded with a Perkin-Elmer LS 50 luminescence spectrometer (excitation and emission slits of 5 nm) at a fixed excitation wavelength of 380 nm and the formation of the AMA–OBP complex was followed as an increase of the fluorescence emission intensity at 480 nm. The dissociation constants of the AMA–OBP complexes were determined from the hyperbolic titration curves using the nonlinear fitting program of Sigma Plot 5.0 (Cambridge Soft. Corp., Cambridge, MA, USA). The concentrations of the AMA–OBP complexes were determined on the basis of emission spectra obtained by incubating AMA (0.1–10 μM) with saturating amounts of both OBP forms.

4. Fluorescence microscopy

A 2P laser (Mira, Coherent, Santa Clara, CA) pumped by 6.5 W of 532 nm light (*green*) from a Verdi solid state laser (Coherent) generates femtosecond 820 nm pulses at 80 MHz (*magenta*). The infrared (IR) laser beam, directly coupled to a microscope (Zeiss Axiovert 135, Zeiss, Jena, Germany), is expanded by a beam expander (BEX), attenuated by neutral density filters and passed to the X–Y scanner (SCN), which projects the scanned beam onto the objective (OBJ) (Zeiss Apo C 40×, numerical aperture (NA) = 1.2 water immersion) and muscle fiber (MUS). The IR power impinging on the muscle is 65 mW. Fluorescent light (*yellow*) is collected by the objective, passed by the same scanner, and reflected by the dichroic mirror M3 into photomultipliers 1 and 2, which detect orthogonally polarized light passed by crossed analyzers AN1 and AN2. Since the fluorescent light is scanned again on the way to the detectors, it is termed descanned detection. Alternatively, mirror M5 can be substituted by a dichroic filter to pass the fluorescent light to another set of photomultipliers 3 and 4. Since the fluorescent light does not

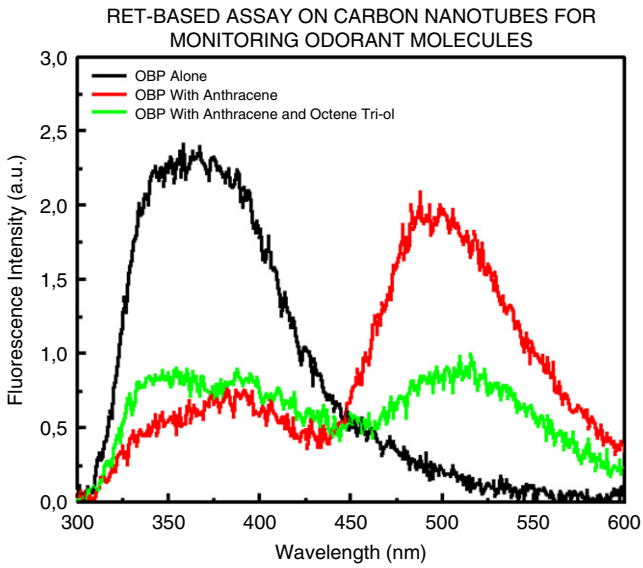

Figure 3. Fluorescence emission spectra of bOBP alone, in the presence of AMA and AMA ligand.

pass through the scanner, it is termed non-descanned detection. The significant advantage of this mode of detection is that the distance between the detectors and the sample is shortened and that the fluorescent light does not enter the microscope at all, and hence does not pass through the scanner or is not attenuated by the internal optics. Unless otherwise stated, all the experiments were performed in non-descanned mode. The 351 + 364 nm light from the ultraviolet (UV) laser (*blue*) (Enterprise, Coherent) is made collinear with the IR beam by the dichroic filter FT395. A fast-shutter SHT (Vincent Associates, Rochester, NY, model T132) is opened for 10 ms to admit UV light to the sample.

5. Fluorescence spectroscopy

Emission spectra were obtained with an ISS K2 spectrofluorometer. The excitation was set at 295 nm in order to exclude the tyrosine contribution to the overall fluorescence emission. Front-face measurements were performed on bOBP immobilized onto CN in the absence and in the presence of AMA and the ligand according to figure 1.

6. Results and discussion

In figure 2 is shown the structure of bOBP. In particular it is possible to notice that the molecule 1-amino-anthracene (AMA) fits very well into the bOBP binding site. A static analysis of the 3D structure of bOBP shows that the protein tryptophan residues are located in proximity to AMA, that is AMA and the protein indole residues are at a distance (Foster distance) allowing a resonance energy transfer (RET) phenomenon. We questioned whether it would be possible to design a carbon nanotubes (CTs) competitive RET assay based on the Trp donor–AMA acceptor for sensing the presence of odorant molecules in the environment.

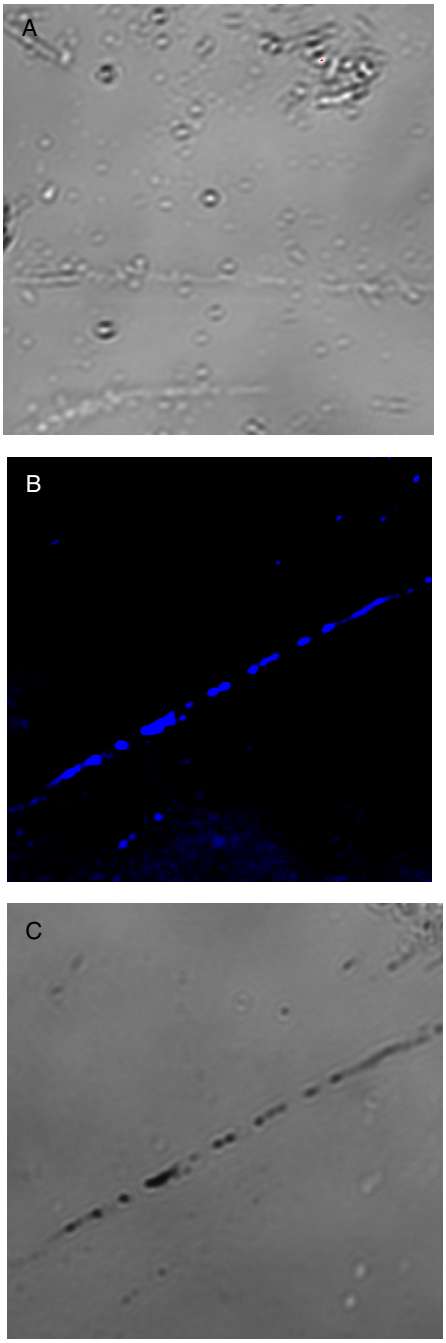

Figure 4. Optical microscope image of CTs (A) with bOBP–AMA (B), and CTs with bOBP–AMA-ligand (C).

We verified that bOBP could be immobilized onto CTs by simple incubation of the CTs-bOBP at room temperature for 10 min in aqueous buffers (phosphate buffer, pH 6.5). In fact, after several washings of the bOBP-treated CTs, the absorbance and fluorescence measurements confirmed that a large amount of bOBP was still present on the CTs surface.

Figure 3 shows the emission spectra of CTs-bOBP alone (black line), upon addition of AMA (red line) and upon addition of an excess of 1-octen-3-ol, the natural ligand of bovine OBP [12].

The resonance energy transfer process observed upon addition of AMA shows that the close interaction between the

Trps of bOBP and AMA results in a high efficiency process of RET between the donor and acceptor. Since 1-octen-3-ol is present in large excess, the addition of the ligand to the bOBP–AMA complex results in a displacement of AMA from the bOBP binding site, and in turn to a decreased efficiency of the RET.

As the emission of AMA was in the visible region of light, we wondered whether it would be possible to design a light on/off nano CT-based biosensor.

Figure 4 shows the confocal microscopy images of bOBP-treated CTs alone (figure 4(A)), in the presence of AMA (figure 4(B)), and after addition of 1-octen-3-ol (figure 4(C)). It is possible to observe a spectacular emission of blue light due to RET upon excitation of Trp at 290 nm. In fact, the CTs become completely blue in color. The addition of the competitive odorant molecule, 1-octen-3-ol, displacing AMA from the OBP ligand binding site, makes the CTs colorless.

The results shown above demonstrate that bOBP can serve as a probe for the development of an optical biosensor for odorant molecules present in the environment. Additional studies are needed to obtain a bOBP-based sensor that displays larger spectral changes, as we feel that it is important to covalently immobilize bOBP onto CTs. In addition, the use of different fluorophores for RET assays could allow larger spectral variations since RET is a through-space interaction which occurs whenever the donor and the acceptor are within the Forster distance (R_o) and does not require change in the probe microenvironment. For these reasons, we are confident that bOBP can be used with long wavelength donors and acceptors to devise a sensor for odorant and, in general, volatile molecules to use for safety and homeland security. Since the measurements can be easily performed by using an LED as an excitation source, one may envisage a polarization-based device with an external calibrated standard. The main advantage of using this method is the obtainment of ratiometric polarization measurements that are not influenced by light instability and sample perturbation. Finally, one can imagine a variety of OBP mutants covering a wide range of ligand binding constants, each labeled with a different fluorophore.

In conclusion, the recombinant bOBP appears to be a valuable source for the development of innovative and stable CT-based biosensors for safety and homeland security.

Acknowledgments

This work was carried out in the framework of the CNR Commessa Diagnostica avanzata ed alimentazione (SD). This work was also supported by the ASI project MoMa No. 1/014/06/0 (MS; SD) and by NATO grant CBP.EAP.CLG 982437 (SD).

References

[1] Briand L, Eloit C, Nespoulous C, Bezirard V, Huet J C, Henry C, Blon F, Trotier D and Pernollet J C 2002 *Biochemistry* **41** 7241–52
[2] Lobel D, Jacob M, Volkner M and Breer H 2002 *Chem. Senses* **27** 39–44
[3] Spinelli S, Ramoni R, Grolli S, Bonicel J, Cambillau C and Tegoni M 1998 *Biochemistry* **37** 7913–8
[4] Dal Monte M, Centini M, Anselmi C and Pelosi P 1993 *Chem. Senses* **18** 713–21
[5] Herent M, Collin S and Pelosi P 1995 *Chem. Senses* **20** 601–8
[6] Tegoni M, Ramoni R, Bignetti E, Spinelli S and Cambillau C 1996 *Nat. Struct. Biol.* **3** 863–7
[7] Vincent F, Spinelli S, Ramoni R, Grolli S, Pelosi P, Cambillau C and Tegoni M 2000 *J. Mol. Biol.* **300** 127–39
[8] Ramoni R, Vincent F, Ashcroft A E, Accornero P, Grolli S, Valencia C, Tegoni M and Cambillau C 2002 *Biochem. J.* **365** 739–48
[9] Ramoni R, Spinelli S, Grolli S, Conti V, Merli E, Tegoni M and Cambillau C 2008 *Biochim. Biophys. Acta* **1784** 651–7
[10] Ramoni R, Bellucci S, Grycznyski I, Grycznyski Z, Grolli S, Staiano M, Debellis G, Micciulla F, Pastore R, Tiberia A, Conti V, Merli E, Varriale A, Rossi M and D'Auria S 2007 *J. Phys.: Condens. Matter* **19** 395012–9
[11] D'Auria S, Staiano M, Varriale A, Scognamiglio V, Parracino A, Rossi M, Campopiano S, Cennamo N and Zeni L 2006 *Proteins Peptide Lett.* **13** 349–52
[12] Ramoni R, Vincent F, Grolli S, Conti V, Malosse C, Boyer F D, Nagnan-Le Meillour P, Spinelli S, Cambillau C and Tegoni M 2001 *J. Biol. Chem.* **276** 7150–5

Advanced spectroscopy techniques for the detection of gluten in food


Sabato D'Auria

ROBERTA CRESCENZO, SABATO D'AURIA*
Laboratory for Molecular Sensing
IBP-CN, Via Pietro Castellino, 1111 80131 Napoli, Italy

ABSTRACT: In this review article we report some of the most recent optical methodologies described for the detection of gluten. In particular, we show three different approaches that allow an easy and high sensitive detection of toxic prolamines in food for celiac patients. The first methodology is based on the use of a chip of porous silicon on which a protein that recognizes gliadin has been immobilized. The second methodology describes a fluorescence biosensor for gluten based on the phenomenon of resonance energy transfer that happen between donor and acceptor molecules. Finally, a method based on fluorescence correlation spectroscopy that allows the detection of gluten even if it is present at very low concentration in food for celiac patients is reported.

POROUS SILICON CHIP FOR GLIADIN DETECTION

There is a strong need of integrated and automated bio-analytical systems in medical, food, agricultural, environmental and defence testing. At present the main market is shared between blood glucose, pregnancy, antibody-based infectious diseases and biological warfare agent detection. The interaction between an analyte and a biological recognition system is normally detected in biosensors by the transducer element which converts the molecular event into a measurable effect, such as an electrical or optical signal. Due to its sponge-like structure, porous silicon (PSi) is a useful material to be used as a transducer. In fact, its surface has a specific area of the order of 200 m^2 cm^{-3} - 500 m^2 cm^{-3}, and, as a consequence, an effective interaction with liquid or gaseous substances can be assured. PSi optical sensors are based on changes of photoluminescence or reflectivity when exposed to the target analytes which substitute the air into the PSi pores. The effect depends on the chemical and physical properties of each analyte. However, due to this specific sensing mechanism, these devices are not able to discriminate the single components that are present in a complex mixture. In order to enhance the sensor selectivity through specific interactions, it was proposed to chemically or physically modify the PSi surface in order to covalently bind specific biomolecules to the porous silicon surface (1-4). Among different probes of biological nature, ligand binding proteins are particularly good candidates in designing highly specific biosensors for small analytes (5-6): in particular, the glutamine-binding protein (GlnBP) from *E. coli* is a monomeric protein composed of 224 amino-acid residues (26 kDa) responsible for the first step in the active transport of L-glutamine across the cytoplasm membrane. The GlnBP consists of two similar globular domains, the large domain (residues 1 to 84 and 186 to 224) and the small domain (residues 90 to 180), linked by two peptide. The deep cleft formed between the two domains contains the ligand-binding site. The GlnBP binds L-glutamine with a dissociation constant K_d of 5 x 10^{-9} M[8] as well as poly-glutamine residues (7-10). Since gluten proteins are rich of gln residues we questioned if GlnBP were able to bind amino acid sequences present in gluten proteins such as gliadin, a protein toxic for celiac patients. In order to check it, we covalently bound GlnBP to a CNBr-activated Sepharose 4B resin and a gliadin PT were passed through the column. The column was washed with three volumes of phosphate buffer saline and the peptide(s) bound to GlnBP were eluted with 0.2 M glycine/HCl pH 3.0. The eluted fractions were utilized for mass spectrometric experiments. MALDI-TOF analysis on the isolated gliadin digest gave a complex peptide profile, which was difficult to rationalize due to the high sequence variability amongst the components of the gliadin fraction. In fact, the main difficulty in gliadin structural analysis lies in high protein heterogeneity owed to numerous duplications, and subsequent divergences of the gliadin multi-gene family encoding a polymorphic set of polypeptides. With tandem MS analysis for identification of some derived PT peptides, we were able to determine gliadin sequences in elute fraction. Figure 1 shows the nano ESI-MS/MS spectrum of the triply charged ion at m/z 784.37 (M=2351.11 Da), corresponding to the sequences XXQPQPQQQQQQQQQQQL (X indicates an unidentified residue) corresponding to that of wheat alfa-gliadin with only the last 13 amino acid residues of peptide (11). This result prompts us to develop a new methodology for sensing toxic sequences for celiac patients. First of all, we immobilized GlnBP to a porous silicon wafer and tested the strength of the covalent bond between the labeled GlnBP and the porous silicon surface by washing the chip in a demi-water flux. We found that the fluorescence emission was very high and homogeneous on the whole surface. In the presence of gliadin PT, GlnBP undergoes to a

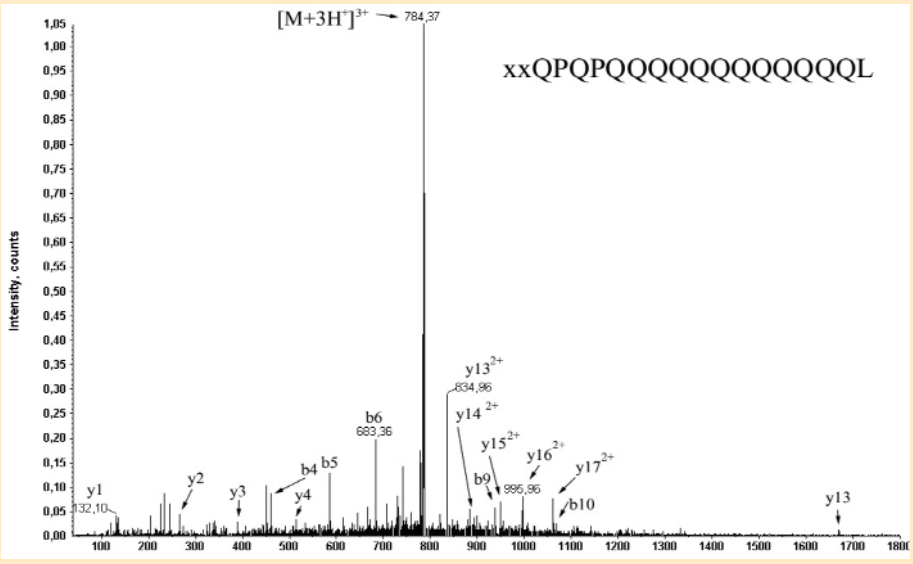

Figure 1. MS/MS spectra of triple ion charged 784.37 (M=2351.11 Da)

large conformational change in its global structure to accommodate the ligand inside the binding site. The ligand binding event was detected as a fringes shift in wavelength which corresponds to a

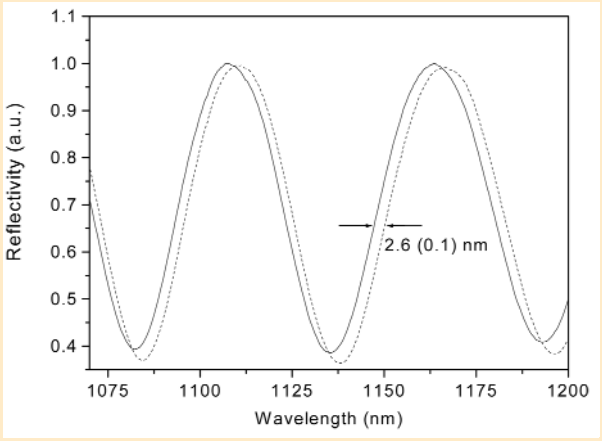

Figure 2. Fringes shift due to protein-protein interaction. Continuous curve: porous silicon + GlnBP. Dashed curve: porous silicon + GlnBP + PT-gliadin. Wavelength shift between the continuous curve and the dashed curve is 2.6 (0.1) nm

defined red-shift of 2.6±0.1 nm (Figure 2).

We also measured the signal response to the protein concentration after the ligand interaction. The sensor displays a linear response between 2.0 µM and 10 µM as a consequence it is possible to calculate the sensitivity of the optical interferometer to the concentration of PT-gliadin by estimating the slope of the curve: s_{ω}= 421 (13) nm/ M. The sensor response saturates approximately at 35 µM, which means that about the 45 percent of the spotted proteins have bound the respective peptide. The rationale of the proposed strategy is that gluten proteins (gliadins and glutenins) are characterized by a high content of glutamine (gln) residues and, consequently, they represent a substrate for the GlnBP. Ideally, a method to determine gliadin should be applicable in a wide range of food, irrespective of processing and should be directly related with toxicity. Until now, none of the produced methods are considered to be fully satisfactory (12-13). On the other hand, the use of reducing agents, that are present in the proposed solvent, can improve the extraction of prolamines but affect their immunochemical quantification (14). From this point of view our method can potentially work also in reducing conditions, so overcoming the problem related to prolamin extraction. In conclusion, in this work we have presented useful data for the development of an optical protein micro-sensor, based on porous silicon nano-technology, for an easy and rapid detection of gliadin.

FRET FOR GLIADIN DETECTION

In recent years, fluorescent sensors have been developed based upon the natural affinity and specificity between a protein and its substrate (15-16). Site-directed mutagenesis has allowed alterations in amino acid sequences, resulting in changes in protein binding constants and insertion of new positions for reporter group labeling. Such amino acid changes have allowed the signal transduction of the binding event to be evaluated by using a variety of physical and chemical techniques (17-18). In particular, optical methods of detection using fluorescence energy transfer, polarization, and solvent sensitivity have been shown to offer high signal- to-noise ratios and the potential to construct simple and robust devices (19-20). As a result, the use of such methods has allowed for the development of highly sensitive optical protein biosensors for a variety of analytes, including amino acids, sugars, and metabolic byproducts. Since in our previous work we demonstrated that GlnBP can bind amino acid sequence contained in gluten we wondered if a fluorescence resonance energy transfer (FRET) assay for sensing toxic sequences for celiac patients could be developed.

We labeled GlnBP and PT-gliadin with fluoresceine isothiocyanate and rhodamine isothiocyanate, respectively. In Figure 3 it is shown the SDS-PAGE of the labeled fluoresceine-GlnBP and rhodamine PT-gliadin upon exposure to UV light. The emission spectra of fluoresceine-labeled GlnBP alone and upon addition of rhodamine-labeled PT-gliadin showed the presence of FRET between fluorescein and rhodamine. The fluorescence resonance energy transfer process observed upon addition of rhodamine-labeled PT-gliadin indicates a close interaction between GlnBP and PT-gliadin . Figure 4 shows the variation of the fluorescence intensity ratio (I_{520nm}/I_{572nm}) at different concentrations of rhodamine- PT-gliadin. The obtained results indicate that the sensitivity of this assay is up to 1.0 µg of PT-gliadin addition that means 33 nM if we consider the average molecular weight of gliadin before enzyme digestion (30000 Da) and the volume of the FRET assay (1ml). Figure 4 also shows the effect of the unlabeled PT-gliadin on the fluorescein-GlnBP - rhodamine PT-gliadin complex fluorescence emission. In the presence of 250 nmol unlabeled PT-gliadin a marked reduction of the FRET efficiency is observed as a consequence of the competition between unlabeled PT-gliadin and rhodamine-labeled PT-gliadin. This result suggests the use of this assay for determining the presence of gliadin in food (11).

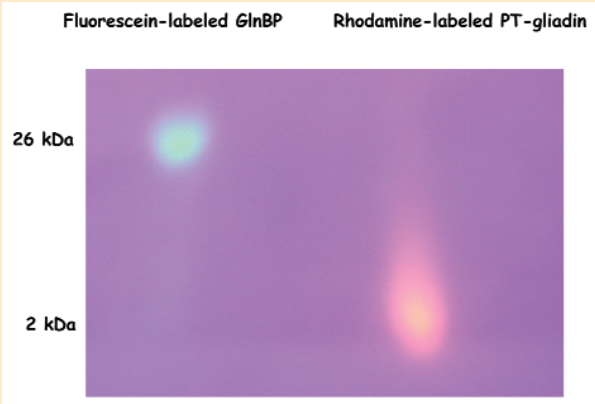

Figure 3. SDS-PAGE of fluorescein-labeled GlnBP (lane 1) and rhodamine-labeled PT-gliadin (lane 2). The protein bands were visualized by UV illumination

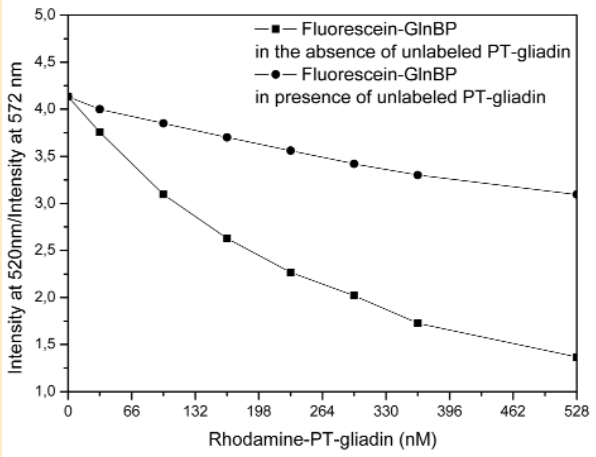

Figure 4. Effect of rhodamine-labeled PT-gliadin on the emission of fluorescein-labeled GlnBP in the absence (closed squares) and in the presence (closed circles) of 250 nmol unlabeled PT-gliadin.
Figure5. Fluorescence correlation curves of fluorescein-labeled-GP (square curve), and fluorescein-labeled-GP/anti-GP antibodies complex (circle curve)

SINGLE MOLECULE DETECTION METHODOLOGY FOR GLIADIN DETECTION

Celiac disease (CD) is an inflammatory disease of the small intestine affecting genetically susceptible people (21-23) following gluten feeding.

At present, a strict gluten-free lifelong diet is mandatory for celiac patients for both intestinal mucosal recovery and prevention of complicating conditions. However, full adherence to diet is difficult, essentially because of very low amount of gluten can precipitate the disease; consequently, inadvertent gluten consumption can easily occur. Gluten proteins of wheat have been grouped into two classes according to their solubility: gliadins, soluble in aqueous alcohols, and insoluble glutenins. While gliadins occur in flour predominantly as monomers, glutenins are present in an aggregated state with molecular weights (mw) up to several millions. Gliadin proteins are primarily responsible of CD. Reversed-phase HPLC (RP-HPLC) can separate gliadin in more than 30 components according to their polarity. The amino acid compositions of single components together with the determination of N-terminal amino acid sequences indicated the existence of only three protein types in the gliadin fraction: ω–, α– and γ– gliadins (24). The high content of proline residues makes gliadins very resistant to gastric, pancreatic and intestinal proteases. The gastrointestinal stability of certain gluten peptides can have implications for their immunoactivity in CD (25). Another important biochemical feature of gliadins is that they represent an ideal substrate for tissue transglutaminase (tTG) (26): this enzyme catalyses deamidation of certain glutamine to glutamate residues; following this post-translational modification, most gliadin peptides become able to elicit a T cell response (27). On the basis of these data, to develop immunoassays able to exactly determine the content of gluten remains a hard task. More in particular, such a method should determine gluten and related toxic prolamines in a wide range of food, irrespective of processing and should be directly related with toxicity. Until now, none of the produced methods are considered to be fully satisfactory. To date a series of enzyme-linked immuno-adsorbent assay (ELISA) have been developed for the analysis of gliadin in food based on the detection of ω-gliadin (28) or a pentapeptide (QQPFP) (29). However, some concern about the usefulness of these immunoassays exist; moreover, the use of reducing agents, that are present in the proposed solvent, can improve the extraction of prolamines but affect their immunochemical quantification (30). In this work, we explored the ability of a very innovative competitive immunoassay to detect toxic prolamins such as gliadin peptides (GP). This assay is based on the ability of the fluorescence correlation spectroscopy methodology to detect and to investigate the molecular properties of biomolecules at the level of a single-molecule. In fact, the detection of a single molecule represents the ultimate level of sensitivity and it has been a long standing goal of analytical methods. Because of its high sensitivity, and because a bright signal appears against a dark background, fluorescence is one obvious choice for single molecule detection. There are several methods for detection of single or small numbers of fluorophores. Fluorescence correlation spectroscopy (FCS) measures fluctuations in the small number of molecules in a focused laser beam. FCS is based on the analysis of time-dependent intensity fluctuations which are the result of some dynamic process, typically translation diffusion into and out of a small volume defined by a focused laser beam and a confocal aperture. When the fluorophore diffuses into a focused light beam, there is a burst of emitted photons due to multiple excitation-emission cycles from the same fluorophore. If the fluorophore diffuses rapidly out of the volume photon burst is short lived. If the fluorophore diffuses more slowly, the photon burst displays a longer duration. By correlation analysis of the time-dependent emission one can determine the diffusion coefficient of the fluorophore. The study of interaction between fluorescein-labeled GP and unlabeled anti-GP antibodies was carried out in a three step procedure. In particular, in the first step we studied the diffusion of the fluorescein-labeled-GP alone (10 nM). We registered a diffusion coefficient value of 120,935 μm²/s. In the second step, we measured the diffusion coefficient of the fluorescein-labeled-GP upon addition of un-labeled-anti-GP mouse polyclonal antibodies. The formation of the complex fluorescein-labeled-GP/ un-labeled-anti-GP Abs was detected as dramatic variation of the diffusion coefficient that passed from 120,935 μm²/s to 50,307 μm²/s (see Table 1). The results of the analysis are shown in Figure 5 where the fluorescence correlation curve of fluorescein-labeled GP and the fluorescence correlation curve of fluorescein-labeled GP/anti-GP Abs complex are reported. The last step of the assay was realized by the addition of un-labeled GP to the complex fluorescein-labeled-GP/ un-labeled-anti-GP Abs. In particular, we were looking for a competition reaction between the fluorescein-labeled-GP and unlabeled-GP. In Table 2 are reported the effects of the addition of increasing amounts of un-labeled GP on the diffusion coefficient of the fluorescent complex. It appears that the addition of 0.006 ppm of un-labeled GP causes a large variation of the diffusion coefficient complex from 50,307 μm²/s to 65,4322 μm²/s. Further additions of un-labeled GP results in a marked increase of the diffusion coefficient complex indicating a significant presence of free-labeled GP (31). In conclusion, in this work we present a new generation analytical tool to evaluate the presence of trace quantities of gluten in food. The combination of high-avidity IgG antibodies together with the innovative immunoassay strategy in the proposed system resulted in a gluten-detection limit of 0.006 ppm lower than 3.2 ppm recently reported for R5-ELISA (32) and much lower than the existing threshold of 20-200 ppm. Our method is fully compatible with the quantitative cocktail extraction procedure for heat-processed foods (32).

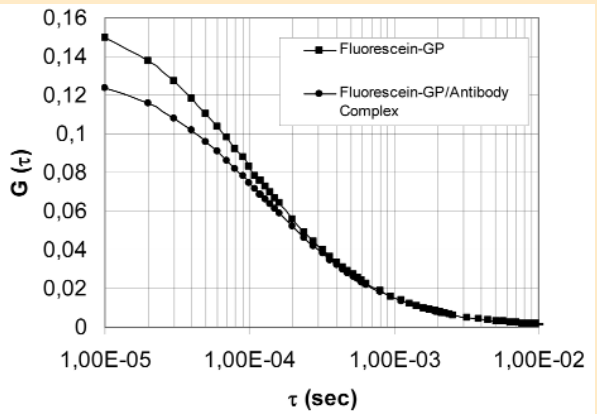

Figure 5

	D (um²/s)	W0 (μm)	Z0 (μm)	CPS	Chi-square
Fluorescein-GP	120.935	0.385659	1.97126	5792	4.2
Fluorescein-GP+Anti-GP Ab	50.307	0.385659	1.97126	7913	6.7

Table 1. Analysis of FCS data showed in Figure 5

Un-labeled GP (ppm)	D (um²/s)	W0 (μm)	Z0 (μm)	CPS	Chi-square
0.0	50.307	0.385659	1.97126	7913	2.3
0.006	65.4322	0.385659	1.97126	6991	2.6
0.012	69.9851	0.385659	1.97126	7303	2.9
0.018	70.9851	0.385659	1.97126	7207	2.6

Table 2. Effect of addition of un-labeled GP to the fluorescein-GP-anti-GP-Ab complex on the diffusion coefficient as monitored by FCS

ACKNOWLEDGEMENTS

This work is in the frame of the CNR Commessa Diagnostica avanzata ed alimentazione.

REFERENCES AND NOTES

1. S. Borini, M. Staiano et al., Recent Patents on DNA & Genes, 1, pp. 1-7 (2007).
2. M. Staiano, M. de Champdore' et al., Curr Opin Chem Biol., 1, pp. 3-9 (2007).

3. M. Rocchia, S. Borini et al., Ultrasensitive and SingleMolecule Detection Technologies II, SPIE Vol. 6444; doi: 10.1117/12.697923 (2007), Edited by J Enderlein, Z Grycznyski
4. S. Borini, S. D'Auria et al., Lab Chip, 5(10), pp. 1048-1052 (2005).
5. M. Staiano, P. Bazzicalupo et al., Mol BioSyst., 1(5-6), pp. 354-362 (2005).
6. S. D'Auria, J.R. Lakowicz, Curr Opin Biotechnol., 12, pp. 99-104 (2001).
7. S. D'Auria, A. Scirè et al., Proteins, 58, pp. 80-87 (2005).
8. C.D. Hsiao, Y.J. Sun et al., J Mol Biol., 262, pp. 225-242 (1996).
9. C.F. Higgins, Annu Rev Cell Biol., 8, pp. 67-113 (1992).
10. M.D. Adams, D.L. Oxender, J Biol Chem., 264, pp. 15739-15742 (1989).
11. M. Staiano, V. Scognamiglio et al., J Proteome Res, 5(9), pp. 2083-2086 (2006).
12. H. Arentz-Hansen, S.N. McAdam et al., Gastroenterology, 123, pp. 803-809 (2002).
13. J.H. Skerrit, A.S. Hill, J. Agric. Food Chem., 38, pp. 1771-1778 (1990).
14. L. Sorell, J.A. Lopez et al., FEBS Lett., 439, pp. 46-50 (1998).
15. P.R. Coulet, G. Bardeletti, Biochem. Soc. Trans., 19, pp. 1-4 (1991).
16. H.W. Hellinga, J.S. Marvin, Trends Biotechnol., 16, pp. 83-189 (1998).
17. J.J. Ramsden, J. Mol. Recogn., 10, pp. 109-120 (1997).
18. V. V. Sorochinskii, B.I. Kurganov, Appl. Biochem. Microbiol., 33, pp. 515-529 (1997).
19. K.A. Giuliano, P.L. Post et al., Annu. Rev. Biophys. Biomol. Struct., 24, pp. 405-434 (1995).
20. K.A. Giuliano, D.L.Taylor, Trends Biotechnol., 16, pp. 135-140 (1998).
21. M. Maki, P. Collin, Lancet, 349, pp. 1755-1759 (1997).
22. A. Tursi, G. Giorgetti et al., Hepatogastroenterology, 48, pp. 462-464 (2001).
23. H. Wieser, A. Mödl et al., Lebens. Unters. Forsch., 185, pp. 371-378 (1987).
24. M.A Silva, E. Guizaldeis et al., Agro Food Industry hi-tech, 18, p. 5 (2007).
25. L. Shan, O. Molberg et al., Science, 297, pp. 2275-2279 (2002).
26. O. Molberg, S.N. McAdam et al., Nat. Med., 4, pp. 713-717 (1998).
27. Y. van de Wal, Y. Kooy, et al., J. Immunol., 161, pp. 1585-1588 (1998).
28. J.H. Skerrit, A.S. Hill, J. Agric. Food Chem., 38, pp. 1771-1778 (1990).
29. L. Sorell, J.A. Lopez et al., FEBS Lett., 439, pp. 46-50 (1998).
30. A.I. Margheritis, V.V. Dona et al., Proceedings of the 17thmeeting of the Working group on prolamin Analysis and Toxicity, pp. 3-6 (2002).

Readers interested in having a list of references are kindly invited to write to the author at: s.dauria@ibp.cnr.it

PROTEINS
STRUCTURE ■ FUNCTION ■ BIOINFORMATICS

Molecular strategies for protein stabilization: The case of a trehalose/maltose-binding protein from *Thermus thermophilus*

Andrea Scirè,[1] Anna Marabotti,[2] Vincenzo Aurilia,[3] Maria Staiano,[3] Paola Ringhieri,[3] Luisa Iozzino,[3] Roberta Crescenzo,[3] Fabio Tanfani,[1] and Sabato D'Auria[3]*

[1] Institute of Biochemistry, Faculty of Sciences, Università Politecnica delle Marche, Ancona, Italy
[2] Institute of Food Science, CNR, Avellino, Italy
[3] Laboratory for Molecular Sensing, IBP-CNR, Naples, Italy

ABSTRACT

The trehalose/maltose-binding protein (MalE1) is one component of trehalose and maltose uptake system in the thermophilic organism *Thermus thermophilus*. MalE1 is a monomeric 48 kDa protein predominantly organized in α-helix conformation with a minor content of β-structure. In this work, we used Fourier-infrared spectroscopy and in silico methodologies for investigating the structural stability properties of MalE1. The protein was studied in the absence and in the presence of maltose as well as in the absence and in the presence of SDS at different p^2H values (neutral p^2H and at p^2H 9.8). In the absence of SDS, the results pointed out a high thermostability of the MalE1 α-helices, maintained also at basic p^2H values. However, the obtained data also showed that at high temperatures the MalE1 β-sheets underwent to structural rearrangements that were totally reversible when the temperature was lowered. At room temperature, the addition of SDS to the protein solution slightly modified the MalE1 secondary structure content by decreasing the protein thermostability. The infrared data, corroborated by molecular dynamics simulation experiments performed on the structure of MalE1, indicated that the protein hydrophobic interactions have an important role in the MalE1 high thermostability. Finally, the results obtained on MalE1 are also discussed in comparison with the data on similar thermostable proteins already studied in our laboratories.

Proteins 2008; 73:839–850.

Key words: FTIR; protein structure; trehalose/maltose-binding protein; *Thermus thermophilus*.

INTRODUCTION

The general interest in biomolecules isolated from thermophilic organisms was originally due to the biotechnological advantages offered by the utilization of these high stable molecules in industrial processes.[1] In fact, enzymes and proteins isolated from thermophilic microorganisms exhibit a high stability in conditions usually used for denaturing proteins such as high temperature, ionic strength, extreme pH values, elevated concentration of detergents, and chaotropic agents.[2,3] In addition, proteins and enzymes that are stable and active over 100°C represent a good model for shedding light, at a molecular level, on the adaptation of life at high temperature.[4,5]

The trehalose/maltose-binding protein (MalE1) is one component of trehalose and maltose (Mal) uptake system, which is in the thermophilic organism *Thermus thermophilus* mediated by a protein-dependent ATP-binding cassette (ABC) system transporter.[6] MalE1 from *T. thermophilus* is a monomeric 48 kDa protein belonging to the class of sugar-binding proteins. This class of proteins presents a structure organized in two globular domains connected by a hinge region made of two or three short polypeptide segments. The two domains are formed by noncontiguous polypeptide stretches and exhibit similar tertiary structure. The ligand-binding site is located in the deep cleft between the two domains, and the binding is accompanied by a movement of the two lobes as well as by conformational changes in protein hinge region.

In some recent works,[2,4] we investigated the structure and the stability of a trehalose/maltose-binding protein from *T. litoralis* (TMBP) by

Abbreviations: DSC, differential scanning calorimetry; FTIR, Fourier-transform infrared; Amide I′, amide I in ^2H_2O medium; MalE1, maltose-binding protein from *Thermus thermophilus*; MalE1/mal, MalE1 in the presence of maltose; MalE1/0.5SDS, MalE1 in the presence of 0.5% SDS; MalE1/1.5SDS, MalE1 in the presence of 1.5% SDS; TMBP, trehalose/maltose-binding protein from *T. litoralis*; MD, molecular dynamics.

This work is dedicated to Prof. Helena Santos for her outstanding contribution to the study of the thermophilic periplasm binding proteins.
Grant sponsor: NATO; Grant number: CBP.EAP.CLG 982437; Grant sponsors: ASI (project MoMa No. 1/014/06/0), Università Politecnica delle Marche.
Andrea Scirè and Anna Marabotti contributed equally to this work.
*Correspondence to: Dr. Sabato D'Auria, Laboratory for Molecular Sensing, IBP-CNR, Via Pietro Castellino, 111, 80131 Naples, Italy. E-mail: s.dauria@ibp.cnr.it
Received 15 January 2008; Revised 16 April 2008; Accepted 17 April 2008
Published online 27 May 2008 in Wiley InterScience (www.interscience.wiley.com).
DOI: 10.1002/prot.22114

FTIR,[2] fluorescence spectroscopy,[2] and differential scanning calorimetry (DSC)[4] in a range of temperature between 20 and 120°C. We found that at neutral pH, TMBP was very stable respect to high temperature. In fact, it was not possible to register any DSC endothermic peak as a consequence of the protein denaturation. However, when TMBP was incubated at basic pH values (pH 9.0), we observed a clear protein denaturation DSC profile. The conclusions of that work were that ionic interactions played a crucial role in the stability of TMBP.

In this work, we have investigated the structural features of MalE1 by FTIR spectroscopy. The structural analysis was performed both in the absence and in the presence of SDS at different temperatures and pH values. The obtained data have been discussed taking into account the information earned by a detailed inspection of a model of the three-dimensional structure of the protein as well as by molecular dynamics (MD) simulation experiments performed on this model at different temperatures and pH values.

METHODS

Materials

Deuterium oxide (99.9% ^2H_2O), ^2HCl, and NaO^2H were purchased from Aldrich. Hepes, CAPSO, and SDS were obtained from Sigma. All other chemicals were commercial samples of the purest quality.

Production of the recombinant protein MalE1

BL21 Rosetta strain, containing pTRCGEMal1, constructed as described in Ref. 6, was cultivated at 37°C in Luria-Bertani medium containing 100 g/mL ampicillin and 50 g/mL chloramphenicol. Strain DH5, containing pTRCGTMal2, was cultivated in the same medium with 100 g/mL ampicillin. When an OD_{610} of 1.0 was reached, the expression of GST-MalE1 or GSTMalE2 fusion proteins was induced by adding 0.5 m*M* IPTG (isopropyl-D-thiogalactopyranoside). After 3 h of incubation, the cells were harvested (7000*g*, 10 min, 4°C); suspended in phosphate-buffered saline (pH 7.3) containing (per milliliter of suspension) DNase I (10 g) and the protease inhibitors phenylmethylsulfonyl fluoride (80 g), leupeptin (20 g), and antipain (20 g); and ruptured by sonication. To remove cell debris, the extracts were centrifuged (18,000*g*, 1 h, 4°C) and filtered through 0.22 µm-pore-size-filters (Schleicher & Schuell). The extracts were applied to a GSTprepFF16/10 column and eluted with 50 m*M* Tris–HCl and 10 m*M* glutathione (Sigma) (pH 8.0). The fractions containing GST-MalE1 or GST-MalE2 were treated with enterokinase (Novagen) or thrombin (Amersham Biosciences), respectively, for 16 h at 22°C. To separate GST from MalE1 or MalE2, the samples were applied to a MonoQ fast-flow column equilibrated with 20 m*M* Tris–HCl (pH 7.6). Elution was carried out with a linear NaCl gradient (0.0*M* to 1.0*M*). The fractions containing MalE1 were eluted before applying the gradient. Those fractions were concentrated, and the purity of the samples was evaluated by sodium dodecyl sulfate-polyacrylamide gel electrophoresis (SDS-PAGE).

Preparation of samples for FTIR analysis

About 1.5 mg of protein, dissolved in the buffer used for its purification, were concentrated to a volume of ~50 µL using a "30 K Centricon" micro concentrator (Amicon) at 3000*g* and at 4°C. Afterwards, 250 µL of 25 m*M* Hepes/NaO^2H p^2H 7.5 (buffer A), or 250 µL of 25 m*M* Hepes/NaO^2H, 10 m*M* maltose p^2H 7.5 (buffer B), or 250 µL of 25 m*M* CAPSO/NaO^2H p^2H 9.8 (buffer C), were added and the protein solution was concentrated again. The p^2H corresponds to the pH meter reading +0.4.[7] The concentration-dilution procedure was repeated several times, to replace completely the original buffer with buffer (A) or (B) or (C). Altogether, the washings took 24 h, which is the time of contact of the protein with the ^2H_2O medium prior to infrared analysis. In the last washing, the protein solution was concentrated to a final volume of 40 µL and used for FTIR measurements. For the analysis in the presence of SDS, an appropriate amount of 10% SDS solution prepared in ^2H_2O was added to the final concentrated protein solution.

FTIR measurements

The concentrated protein samples were placed in a thermostatic Graseby Specac 20500 cell (Graseby-Specac, Orpington, Kent, UK) fitted with CaF_2 windows and a 25 µm Teflon spacer. FTIR spectra were recorded by means of a Perkin-Elmer 1760-x Fourier transform infrared spectrometer using a deuterated triglycine sulphate detector and a normal Beer-Norton apodization function. To eliminate spectral contributions due to atmospheric water vapor, the spectrometer was continuously purged with dry air at −73°C dew-point using a Parker Balston 75-62 FTIR purge gas generator. MalE1 was analyzed at p^2H 7.5 and at p^2H 7.5 in the presence of 10 m*M* maltose. An external bath circulator (HAAKE F3) was used for the thermal denaturation experiments. Temperature was raised in 5°C steps from 20 to 95°C; additional spectra were acquired at 98, 99, and 99.5°C. Temperature in the cell was controlled by a thermocouple placed directly onto the CaF_2 windows. Before spectrum acquisition, samples were maintained at the desired temperature for the time necessary for the stabilization of temperature inside the cell (6 min). MalE1 was extremely heat-resistant. Indeed the protein maintained for 60 min at 99.5°C did not denature. For this reason, MalE1 was analyzed also at p^2H 9.8, at p^2H 7.5 in the presence of 0.5% SDS,

and at p^{2}H 7.5 in the presence of 1.5% SDS. In the absence of SDS and at high temperatures, we did not observe protein denaturation, but a rearrangement of the protein β-sheets. To check the reversibility of this phenomenon that it was particularly evident when MalE1 was kept at p^{2}H 9.8, we heated the protein sample up to 99.5°C and then we cooled it down to 20°C collecting the spectra at the same temperatures reported for the thermal denaturation experiments (see above). Spectra were collected and processed using the SPECTRUM software from Perkin-Elmer. Spectra of buffers and samples were acquired at 2 cm^{-1} resolution under the same scanning and temperature conditions. The protein spectrum was obtained by subtracting the buffer spectrum from the spectrum of the protein solution, measured at the same temperature. Subtraction of ^2H_2O was adjusted to the removal of the ^2H_2O bending absorption close to 1220 cm^{-1}.[8] The deconvoluted parameters were set with a gamma value of 2.5 and a smoothing length of 65. Second derivative spectra were calculated over a 13-data-point range (13 cm^{-1}). The concentration of SDS in the sample was checked using a calibration curve obtained by monitoring the intensity of the symmetric methylene stretching vibration band (2854 cm^{-1}) of SDS[9] as a function of SDS concentration.

Analysis of protein structure and molecular dynamics simulations

The three-dimensional structure of MalE1 from *T. thermophilus* has not been yet determined by experimental methods, but a model of the structure, obtained by homology modeling methods, is available in the ModBase database.[10] The model was created by ModPipe,[11] an automated modeling pipeline relying on the programs PSI-BLAST[12] and MODELLER,[13] using the structure of TMBP[14] as a template.

Before starting simulations, to evaluate the effective pKa of the charged residues, the algorithm developed by Bashford and Karplus[15] and implemented in the server H^{++}[16] was applied to the model. Then, to simulate two different pH conditions (pH 7 and 10), residues, whose pKa indicate different protonation states at these two different pH values, were protonated accordingly. In particular, E122, E402, D206, D145, and D386 show a pKa between 7 and 10; therefore, they were protonated at pH 7 and unprotonated at pH 10. The pKa of all His was estimated below 7; therefore, all His residues were neutral both at pH 7 and 10.

Simulations were carried out using the program GROMACS version 3.3.1,[17,18] running in parallel (MPI) on a Linux cluster with 40 × 86_64 processors. The OPLS-AA force field[19,20] was used throughout the simulations. A cubic box, containing ~18,300 water molecules (TIP3P model[21]) and nine Cl$^-$ ions to neutralize the net positive charge of the protein, was used to solvate MalE1. Periodic boundary conditions were applied to eliminate surface effects.

A preliminary energy minimization with a tolerance of 1000 kJ/mol/nm was applied using the Steepest Descent method. All bonds were constrained using LINCS.[22] After minimization, the system was submitted to a short MD simulation with position restraints to better "soak" the water molecules into the macromolecule. We run the position-restrained MD for 20 ps, with a time step of 2 fs, with the system coupled to a temperature bath at 300 K using Berendsen's method of bath coupling.[23] Berendsen's pressure coupling was also used. Long-range electrostatics were handled using the PME method.[24] Cut-off were set at 0.9 nm for Coulomb interactions, and at 1.4 nm for van der Waals interactions. The final MD simulations were carried out with a time-step of 2 fs and without any position restraints. Three subsequent MD simulations (the final conformation of each simulation was used as input for the following simulation at higher temperature) were carried out with the Berendsen's method of bath coupling at 300, 330, and 370 K. The run at 300 K was made for 1 ns; each of the other two simulations was carried out for 2 ns; therefore, the global simulation is 5 ns long.

Several analyses were conducted using programs built within GROMACS package. The energy components were extracted from the energy files generated by the program and analyzed to verify the stabilization of the system. For each simulation, an "average" structure of the protein was calculated on the whole protein minus hydrogen atoms. Then, for each simulation, the real structure with the smallest RMSD from the average was selected as the representative structure of the population in that run.

The content in secondary structures was evaluated using DSSP.[25] Solvent accessibility of amino acid residues was evaluated using the program NACCESS[26] by rolling a probe atom of 1.40 Å in radius on the van der Waals surface of the protein models. Only the relative accessibilities of side chains were taken into account. The evaluation of cavities was made using AVP with a probe radius of 0.5 Å as suggested by the authors.[27] Other analyses were carried out using the utilities available in the Insight II package (Version 2000.1, Accelrys; 2000). In particular, the presence of a salt bridge was inferred for pairs of oppositely charged residues (Asp or Glu with Arg, Lys or His) according to criteria reviewed by Kumar and Nussinov,[28] taking also into account the protonation state of the residues.

RESULTS AND DISCUSSION

FTIR spectra

Figure 1 shows the absorbance (A), deconvoluted (B), and second derivative (C) spectra (1750–1500 cm^{-1} spectral

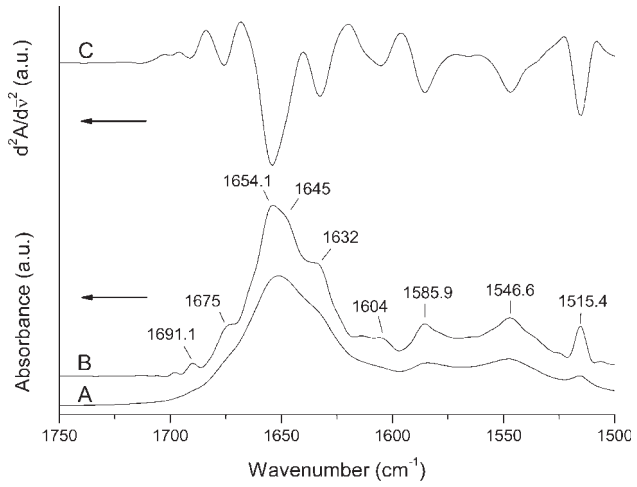

Figure 1

Absorbance (**A**), deconvoluted (**B**), and second derivative (**C**) FTIR spectra of MalE1 at p^{2}H 7.5, 20°C.

region) of MalE1 in 25 m*M* Hepes/NaO^{2}H p^{2}H 7.5 at 20°C, after digital subtraction of the buffer spectrum. The most important band in structural studies of proteins is the amide I band, located between 1700 and 1600 cm^{-1}. The amide I' band consists of a series of components bands, which occur as a result of the secondary structures present in proteins. Resolution enhancement of the absorbance spectra, as deconvoluted and second derivatives spectra, allows the identification of these structures.[29,30] The deconvolution and second derivative spectra of MalE1 evidence a number of component bands. In particular, five component bands corresponding to peptide bonds in various conformations are visible in the amide I' region. The main band at 1654.1 cm^{-1} is characteristic of α-helix,[29,30] and the shoulder at 1645 cm^{-1} can be assigned to unordered structures.[29] The bands at 1632 and 1691.1 cm^{-1} are related to β-sheets, whereas the presence of the 1675 cm^{-1} could be due to β-sheets and/or turns.[31] The bands below 1620 cm^{-1} are assigned to absorptions of amino acid side chains[32,33] except for the 1546.6 cm^{-1} band, which is due to the residual amide II band, i.e., the amide II band (1600–1500 cm^{-1} range) after ^{1}H/^{2}H exchange of the amide hydrogens of the polypeptide chain.[34] The amide II band is also important for conformational studies, and it is particularly sensitive to the exchange of amide hydrogen with deuterium. In experiments performed in H_2O medium, the intensity of the band is about 2/3rd that of the amide I band, while in ^2H_2O medium it decreases significantly.[34] The bigger the intensity decrease, the bigger the ^{1}H/^{2}H exchange. A big ^{1}H/^{2}H exchange indicates that the protein structure is very accessible to the solvent (^2H_2O). The fact that the infrared spectrum of MalE1 displays a residual amide II band indicates that at 20°C the protein segments were not completely accessible to the solvent.

Figure 2 shows the effect of p^{2}H, maltose, and SDS on the deconvoluted spectra of MalE1. The presence of maltose does not have an apparent visible effect on the secondary structure of the protein, since the amide I′ band of MalE1/mal is perfectly superimposed to the amide I′ band of the control spectrum [Fig. 2(A)]. Figure 2(A) shows that in MalE1/mal spectrum the residual amide II band intensity is slightly higher with respect to the control spectrum. Since the intensity of the residual amide II band is an indicator of the accessibility of solvent to the peptide backbone, the result indicates that the sugar makes MalE1 structure more compact. At p^{2}H 9.8, the spectrum profile is similar to the control (p^{2}H 7.5) [Fig. 2(B)], but the amide I′ band (1700–1600 cm^{-1}) is slightly shifted to lower wavenumbers and the residual amide II band intensity is lower. The shift is frequently observed when the secondary structure elements of a protein become more exposed to the solvent, and since the amide I′ band shows only tiny differences with respect to the control, the large decrease in intensity of the residual amide II band is most likely due to a more relaxed tertiary structure.[34–36] The reason for the high decrease in residual amide II band intensity at p^{2}H 9.8 could reflect changes in ionic interactions within the structure of MalE1, causing an higher exposure of structural elements to the ^2H_2O medium.

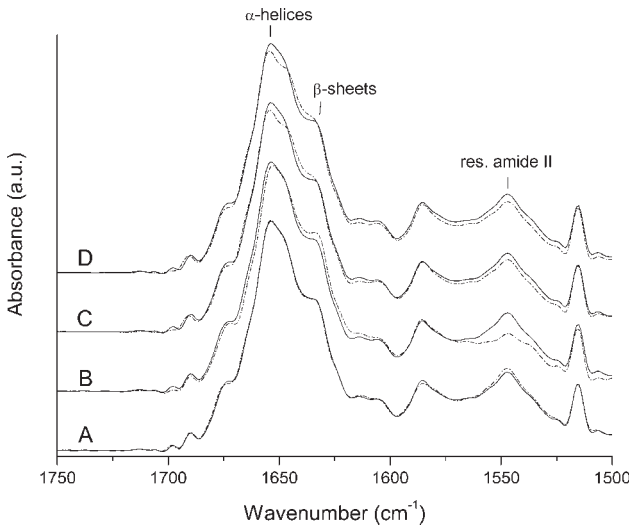

Figure 2

Comparison of deconvoluted spectra of MalE1 under different conditions. All spectra were obtained at 20°C. Continuous lines in spectra (**A–D**) represent the spectrum of the protein at p^{2}H 7.5 (control). (A) dashed line, MalE1 at p^{2}H 7.5 in the presence of 10 m*M* maltose (MalE1/mal); (B) dashed line, MalE1 at p^{2}H 9.8; (C, D) dashed lines, MalE1 at p^{2}H 7.5 in the presence of 0.5% SDS (MalE1/0.5SDS) and 1.5% SDS (MalE1/1.5SDS), respectively.

In the presence of 0.5% SDS [Fig. 2(C)] and 1.5% SDS [Fig. 2(D)], the deconvoluted spectrum of MalE1 is slightly different with respect to the control spectrum. In particular, the α-helix and the β-sheet band intensity is lower and higher, respectively. Also, the residual amide II band intensity is affected by the presence of the detergent, but to a lower extent compared to the decrease observed for MalE1 at p^{2}H 9.8. These data indicate that SDS induces small but significant changes in the secondary structure of the protein and allows the solvent to a deeper contact with the polypeptide.

Thermal stability

Proteins from hyperthermophilic organisms are particularly heat-resistant. In many cases, they unfold at temperatures below but close to 100°C, allowing the thermal denaturation process to be followed by spectroscopic techniques. In other cases, these proteins have a T_m above 100°C and in this case the unfolding process may be studied under high pressure or in the presence of destabilizing agents.[37,38] MalE1 belongs to the latter case; in fact, this protein showed to retain most of its secondary structure even prolonging the analysis at 99.5°C for 60 min. This great thermostability was compromised only when SDS was added to the protein solution.

Figure 3 displays the effect of temperature on absorbance [Spectra 3(A–E)] and second derivative spectra [Spectra 3(A*–E*)] of MalE1 under different experimental conditions. MalE1 absorbance spectra at p^{2}H 9.8 [Fig. 3(A)], p^{2}H 7.5 [Fig. 3(B)], and p^{2}H 7.5 + maltose [Fig. 3(C)] clearly point out that the increase in temperature has small effect on the amide I′ band, indicating a high protein thermostability. On the other hand, the spectra of MalE1 in the presence of 0.5% or 1.5% SDS [Fig. 3(D,E)] are affected by the temperature to a larger extent as compared to spectra shown in Figure 3(A–C). In particular, the width and the intensity of the amide I′ band increases and decreases, respectively, with the increase in temperature, indicating that SDS lowers the protein thermostability.

More detailed information on temperature-dependent spectral changes can be obtained by second derivative spectra shown in Figure 3(A*–E*). In particular, Figure 3(A*) (p^{2}H 9.8) and Figure 3(B*) (p^{2}H 7.5) show that the α-helix band (band close to 1654 cm^{-1}) decreases slightly in intensity and shifts to lower wavenumbers, and the phenomenon is more marked at p^{2}H 9.8 than at p^{2}H 7.0. In the presence of maltose [Fig. 3(C*)], the α-helix band is not affected by high temperatures, indicating that the sugar stabilizes the structure of MalE1. The most evident change with the increase in temperature is the decrease in intensity of the bands related to β-sheet structures at ~1632 cm^{-1} and at ~1675 cm^{-1} [Fig. 3(A*–C*)]. This result may indicate a temperature-dependent loss of β-sheets. However, this decrease is accompanied by a shift of the 1675 cm^{-1} band to lower wavenumbers and by an increase in intensity at about 1639 cm^{-1}, positions that are also characteristic of β-sheets.[30] Hence, the concomitant decrease in intensity of the 1632 cm^{-1} band and the appearance of the 1639 cm^{-1} band may suggest a temperature-dependent rearrangement of β-sheets, even though it is not excluded that the decrease in intensity of the 1632 cm^{-1} band is due to loss, at least in part, of β-sheets. The decrease in intensity of the 1632 cm^{-1} band and the concomitant appearance of the 1639 cm^{-1} band is more marked at p^{2}H 9.8 [Fig. 3(A*)] with respect to the control [Fig. 3(B*)], while in the presence of maltose [Fig. 3(C*)], the phenomenon is similar to the control. These data suggest that the loss of β-sheets or their possible rearrangement

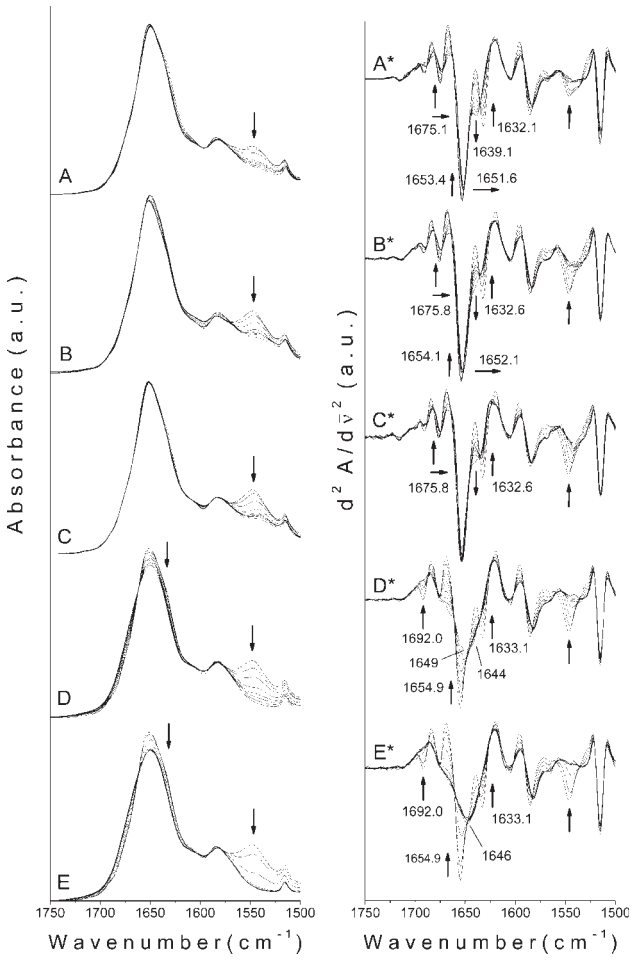

Figure 3

Thermal stability of MalE1 under different conditions. Each plot shows the superimposed absorbance (**A–E**) and second derivative (**A*–E***) spectra of MalE1 at 20, 40, 60, 80, 90, 95, 98, and 99.5°C. The arrows indicate the decrease, or increase, or shift of the corresponding band with the increase in temperature. MalE1 at p^{2}H 9.8 (A, A*); at p^{2}H 7.5 (B, B*) (control); at p^{2}H 7.5 + 10 mM maltose (C, C*); at p^{2}H 7.5 + 0.5% SDS (D, D*); and at p^{2}H 7.5 + 1.5% SDS (E, E*).

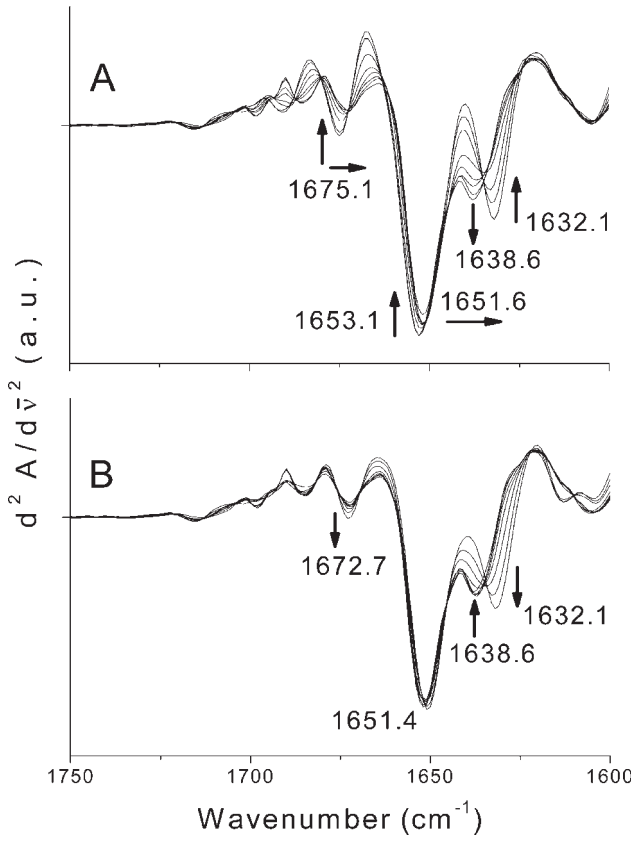

Figure 4

Reversibility of secondary structural changes induced by high temperatures at p^2H 9.8. A protein sample of MalE1 was heated up to 99.5°C and then the sample was cooled down to 20°C (see "Methods" section). The figure shows the superimposed second derivative spectra of MalE1 at increasing (**A**) or decreasing (**B**) temperatures. The spectra shown in (A) and (B) were obtained at 20, 40, 60, 80, 90, 95, 98, and 99.5°C. The arrows indicate the decrease, or increase, or shift of the corresponding band with the increase (A) or decrease (B) in temperature.

is facilitated by a relaxed structure [see above and Fig. 2(B)]. The temperature-dependent rearrangement of β-sheets may have a physiological meaning, since the β-sheets rearrangement occurs when the temperature gets close to the optimal growth temperature of *Thermus thermophilus* (about 75°C).

To check the reversibility of the loss and/or conformational changes involving the protein β-sheets at high temperatures, we repeated the experiment on MalE1 kept at p^2H 9.8 by heating the protein sample up to 99.5°C and then we cooled it down to 20°C (see "Methods" section for details). For this experiment, we used a new preparation of MalE1. The spectra are reported in Figure 4, which shows that the heating experiment [Fig. 4(A)] gives the same results as the previous experiment reported in Figure 3(A*). Moreover, Figure 4(B) shows that the 1638.6 cm^{-1} band, formed at high temperatures at the expense of the 1632.1 cm^{-1} band [Fig. 4(A)], decreases its intensity with decreasing of the temperature, and concomitantly the 1632.1 cm^{-1} band appears and increases its intensity. This experiment indicates that the shift of the 1632.1 cm^{-1} band to higher wavenumbers (1638.6 cm^{-1}) is reversible and that it could be due to rearrangements of the protein β-sheets.

Figure 3(D*,E*) shows the temperature-dependent changes of infrared spectra of MalE1 in the presence of 0.5% SDS and 1.5% SDS, respectively. The presence of 0.5% SDS reduces significantly the thermostability of the protein, since the α-helix band decreases in intensity gradually with increasing of temperature. At 99.5°C, the spectrum is characterized by a broad band centered at 1649 cm^{-1} and a shoulder at about 1644 cm^{-1}, reflecting a protein predominantly in a random conformation with some residual α-helices. In the presence of 1.5% SDS, the

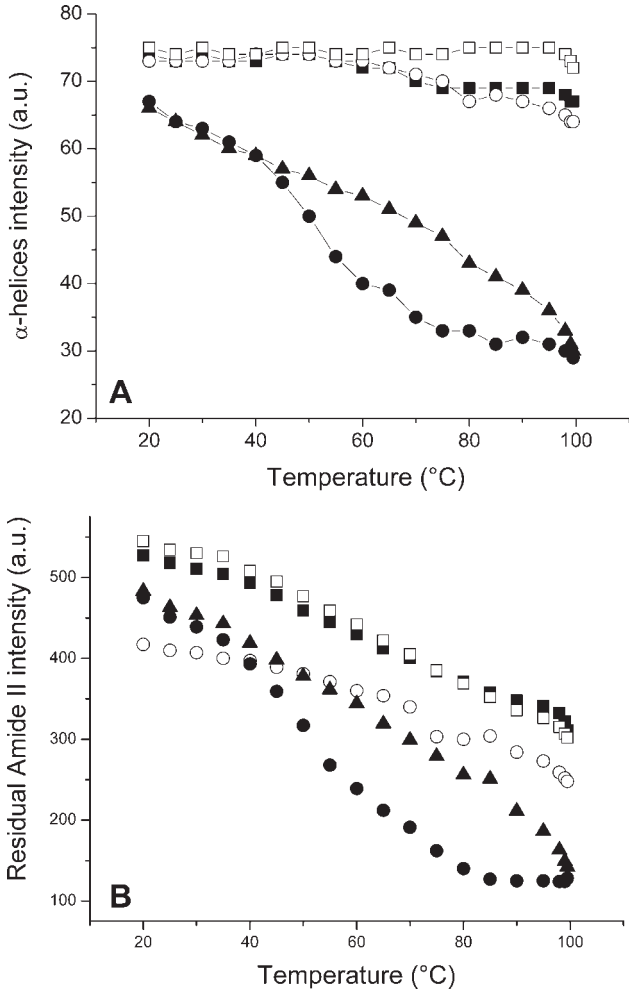

Figure 5

Temperature-induced decrease in intensity of the α-helix and residual amide II band. (**A**, **B**) Intensity of the α-helix and residual amide II bands from second derivative and absorbance spectra, respectively, of MalE1 at p^2H 9.8 (○), at p^2H 7.5 (■), at p^2H 7.5 + 10 mM maltose (□), at p^2H 7.5 + 0.5% SDS (▲), and at p^2H 7.5 + 1.5% SDS (●) plotted versus temperature.

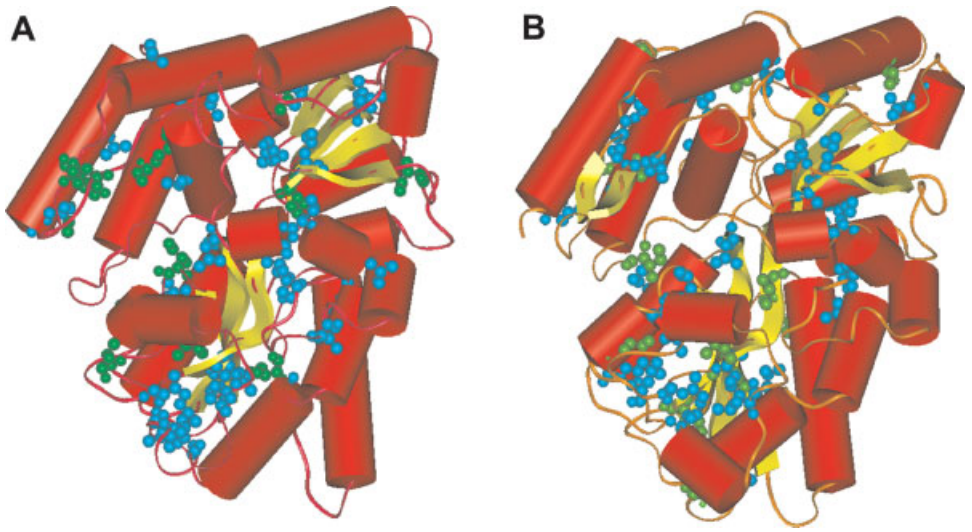

Figure 6

Structure comparison between MalE1 and TMBP. Panel **A**: structure of MalE1. Panel **B**: structure of TMBP. Backbone is represented as a ribbon; α-helices are represented as red cylinders and β-sheets as yellow arrows. Amino acids Ile (green) and Leu (cyan) are in CPK mode.

α-helix band decreases in intensity more rapidly, and at 80°C and at higher temperatures, the protein spectrum is characterized by a broad band centered at 1646 cm^{-1}, position that is characteristic for unordered structures. The destabilizing effect of SDS and the negligible effect of p^2H [Fig. 3(A,A*)] on the protein structure suggest that hydrophobic interactions have an important role in MalE1 thermostability. It also appears that ionic interactions may have a minor role in the protein thermostability with respect to the hydrophobic ones.

Both absorbance and second derivative spectra show that the residual amide II band intensity decreases with the increase in temperature. This effect is due to further $^1H/^2H$ exchange that may be caused by increased molecular dynamics at high temperature and/or by protein denaturation.[34] In the case of MalE1/0.5SDS and MalE1/1.5SDS, the temperature-dependent decrease in intensity of the residual amide II band reflects mainly the thermal denaturation of the protein [Fig. 3(D*,E*)]. Figure 5 shows in synthesis the spectral changes occurring with the increase in temperature. As previously observed in Figure 3, the presence of 1.5% SDS affects markedly the thermostability of MalE1, since the intensity of the α-helix band decreases from 40 to 80°C [Fig. 5(A)] very rapidly as compared to the sample in the presence of 0.5% SDS in which the decrease is constant with the increase in temperature [Fig. 5(A)]. On the other hand, the decrease in intensity of the α-helix band for the sample at p^2H 7.5 and p^2H 9.8 is very similar, while in the presence of maltose the α-helix band intensity is not affected by temperature, even at the highest values, indicating that the sugar confers an extra stability to this secondary structure element. The intensity of the residual amide II band in the spectra of the protein in the absence of SDS decreases continuously with the increase in temperature [Fig. 5(B)]. This result could be due to increased molecular dynamics at high temperature and not to the unfolding of the protein, since the intensity of the MalE α-helix band is only marginally affected by temperature [Figs. 3(A*–C*) and 5(A)]. However, it should be pointed out that the intensity of residual amide II band in the spectra of the protein in the presence of SDS decreases similarly to the decrease in intensity of the α-helix band, suggesting that in this case the phenomenon is mainly due to the denaturation of the protein structure.

Analysis of protein structure

The structure of MalE1 as it appears from the model is very similar to that of TMBP and of other proteins of the ABC transporters family (see Fig. 6). The protein is

Table I

Percentage of the Secondary Structure Content in MalE1 Compared to TMBP

Secondary structures	MalE1	TMBP
Helices[a]	47.8	47.0
Extended β-strands[b]	11.2	15.9
Others[c]	23.5	21.9
Random coil[d]	17.5	15.2

[a]Marked as "H," "G," and "I" in DSSP output.
[b]Marked as "E" in DSSP output.
[c]Marked as "B," "S," and "T" in DSSP output.
[d]Not classified in DSSP output.

Table II
Analysis of Salt Bridges in MalE1

Residue 1	Residue 2	Distance (Å) (atom 1–atom 2)[a]	Distance (Å) centroid 1–centroid 2[b]	% Solvent accessibility residue 1[c]	% Solvent accessibility residue 2[c]
D154	R152	2.74 (OD2–NH2) 3.23 (OD2–NE)	3.39	37.8	10.1
D206	R273	2.99 (OD1–NH1) 3.08 (OD1–NH2)	4.06	0.3	0.2
E172	R246	3.89 (OE2–NH1)	3.98	44.6	21.2
E258	R261	3.63 (OE1–NH2) 3.18 (OE2–NH2)	3.98	37.9	14.9

[a]Distance between the Asp or Glu side-chain carboxyl oxygen atoms and side-chain nitrogen atoms of Arg, Lys, or His involved in salt bridges.
[b]Distance between the centroids of the side-chain charged groups in oppositely charged residues.
[c]% of solvent exposure calculated on the side chain of the corresponding residue. Residues are considered buried if this percentage is $\leq$10%, partially exposed for a percentage between 10 and 30%, totally exposed for a percentage $\geq$30%.

composed of two domains connected by a hinge region; the cleft between the two domains hosts the sugar-binding site. After sugar binding, the protein shifts in its "closed" form with a rearrangement of the reciprocal positions of the two domains. Since the template used to model the structure of MalE1 binds maltodextrin,[14] also the structure modeled for MalE1 is in "closed" form although no sugar is present.

The comparison of the content in secondary structures between the model of MalE1 and the crystal structure of its template (Table I) shows that the content of helices in both proteins is almost the same, but MalE1 has a lower content in β-sheets and a higher content in residues in different β-structures such as isolated β-bridges or H-bonded turns (marked as "other structures" in Table I) and in random coil conformation. The composition in amino acids show that MalE1 has a lower content in acidic residues, but a higher content in basic residues, with a number of charged residues almost equivalent to that of TMBP. Therefore, potentially a high number of ionic pairs could be formed. However, a careful inspection made on the protein structure showed only few interactions that could be configured as salt bridges on the protein structure (Table II). Although the model of MalE1 could suffer of potential errors in the placement of side chains that impairs the correct formation of ionic pairs on its structure, the relative importance of these interactions to stabilize the protein structure seems lower than in TMBP, in which several ionic pairs were found as potential structural feature to induce thermostability. Most of the salt bridges found in TMBP were formed by buried or partially exposed residues, and were found to create networks to crosslink noncontiguous regions of the structure, especially in the C-terminal domain.[4] On the contrary, in MalE1, there is only one ionic pair involving buried residues, i.e. D206-R273, which is equivalent to the salt bridge between R255 and E186 in TMBP. It is worth noting that from the analysis of pKa of single residues, the pKa of D206 is estimated to be higher than 7; therefore, at pH 7, this residue may be protonated and not able to form a salt bridge. Another potential ionic pair involves R273 and E209, but it was not inserted in Table II, since the geometry of this interaction is not that of "canonical" salt bridges. All these salt bridges, including the others showed in Table II are not part of a big network as in TMBP, rather they appear isolated, especially in the N-terminal domain.

We also analyzed the presence of clusters of hydrophobic residues in the interior of the structure, since this is commonly considered as a determinant for thermal stability.[39] MalE1 shows a lower number of aromatic residues than TMBP (especially Phe), but the number of bulky aliphatic residues such as Ile, Leu, and Val is almost equivalent. Looking at the model [Fig. 6(A)], we can see a number of Ile + Leu clusters both in the C-terminal and in the N-terminal domain: in the former, a big cluster involves I427, L428, I424, I226, and I219, and there are also other smaller clusters formed by L155, L270, L256; L407, L237, L203; L420, I399. In the latter domain, two clusters are visible in the structure, formed by L140, L137, L111, L115, I127 and L335, L316, L331. Similar clusters are also present in TMBP [Fig. 6(B)]. Finally, the calculation of the volume of cavities in the interior of the proteins with the program AVP (Table III) shows that the volume of buried voids in MalE1 is 47 Å^3 whereas in TMBP it is 738 Å^3. On the contrary, the volume of surface cavities is almost equivalent in the two proteins (1150 Å^3 for MalE1 and 1256 Å^3 for TMBP). Therefore, the very tight packing of buried residues can be considered as a major determinant for the thermostability of this protein.

Table III
Analysis of Cavities in MalE1 and TMBP

	MalE1 (Å^3)	TMBP (Å^3)
Total buried voids	47	738
Total surface voids	1150	1256
Total voids	1197	1994

Table IV
Percentage of the Secondary Structure Content in MalE1 at Different pH and Temperatures

Secondary structures	MalE1 (pH 7 300 K)	MalE1 (pH 7 330 K)	MalE1 (pH 7 370 K)	MalE1 (pH 10 300 K)	MalE1 (pH 10 330 K)	MalE1 (pH 10 370 K)
Helices[a]	42.5	38.9	41.0	39.9	41.2	39.9
Extended β-strands[b]	10.3	10.6	8.0	9.3	7.5	4.9
Others[c]	22.9	27.3	26.5	29.1	28.4	31.0
Random coil[d]	24.3	23.2	24.5	21.7	22.9	24.2

[a]Marked as "H", "G" and "I" in DSSP output.
[b]Marked as "E" in DSSP output.
[c]Marked as "B," "S," and "T" in DSSP output.
[d]Not classified in DSSP output.

Molecular dynamics simulations

The behavior of MalE1 in different conditions of pH and temperature was simulated using MD. Although the timescale applied (5 ns total) is not sufficient to follow the total rearrangement of secondary structures in the protein, these experiments can identify the first structural variations that take place in the protein. These variations were calculated with the aid of DSSP program[25] on the representative structures of each simulation and are reported in Table IV (Note: the difference between the percentage of secondary structures of the model and of the simulation may be ascribed to the fact that the crystals of the template were grown at 18°C,[14] and therefore

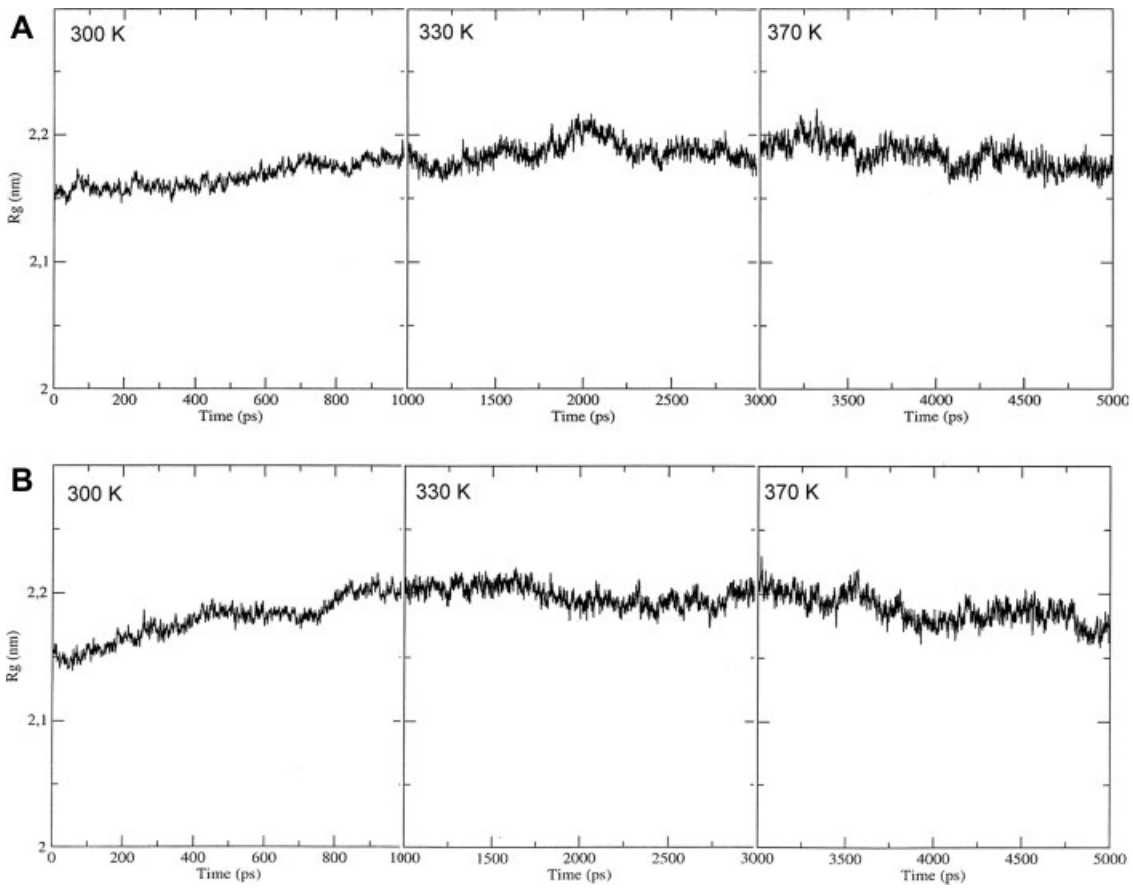

Figure 7
Variation of radius of gyration (R_g) of MalE1 during MD simulations. The calculations were performed separately on the three trajectories resulting from GROMACS simulations at 300, 330, and 370 K. Panel **A**: R_g of the protein at pH 7. Panel **B**: R_g of the protein at pH 10.

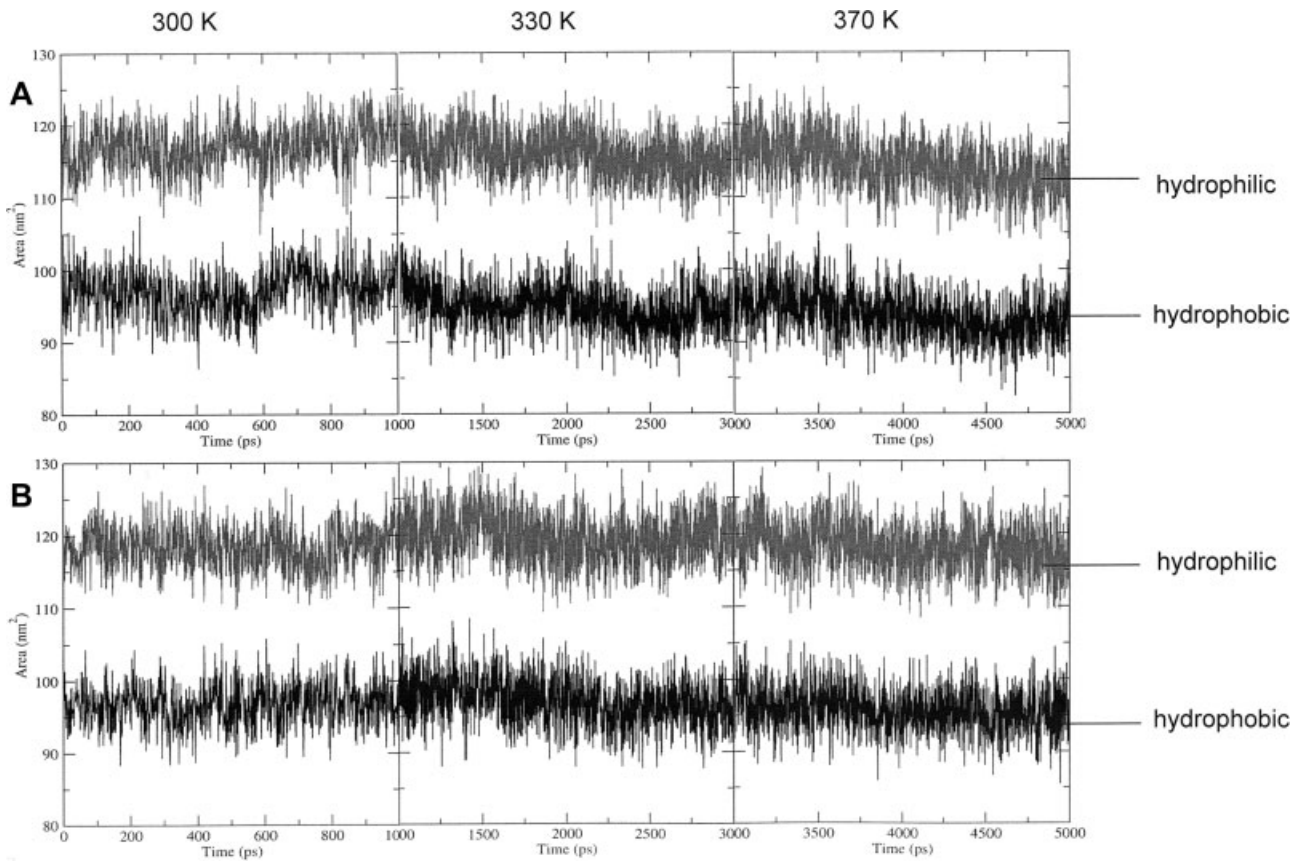

Figure 8

Variation of solvent-accessible surface area of MalE1 during MD simulations. The calculations were performed separately on the three trajectories resulting from GROMACS simulations at 300, 330, and 370 K. Traces corresponding to hydrophobic and hydrophilic area are labeled. Panel **A**: parameter calculated on the trajectories at pH 7. Panel **B**: parameter calculated on the trajectories at pH 10.

the structure of the model may be more "relaxed" at higher temperature).

The simulations performed at pH 7 at increasing temperatures confirm a higher resistance of helices to thermal stress. On the contrary, extended β-strands seem to be less thermostable, and at 370 K their percentage is decreasing. The percentage of random coil, however, is practically unchanged; therefore, it can be assumed that at high temperatures β-sheets undergo alterations, but residues involved do not loose completely their structural organization; rather, they switch to different (and probably less stable) structures such as H-bonded turns or residues in isolated β-bridges.

At basic pH, MalE1 shows a slight decrease in the percentage of helices, but their presence is constant at high temperature. Again, β-sheets appear less resistant and their percentage is consistently decreasing at 370 K. Also, in this condition, these structures seem to be partially transformed in other structures, but in this case the percentage of residues in random coil structures increases at increasing temperatures. These results are in agreement with the experimental ones obtained with FTIR and may be considered as a "molecular portrait" of the early stages of destabilization of secondary structures in MalE1.

Interesting information come also from the analysis of the variation of radius of gyration (R_g) and of solvent-accessible surface during the simulations (Figs. 7 and 8). The R_g of the protein increases slightly at increasing temperatures, but it then stabilizes around a value of 2.18 nm. The basic pH seems not to have impact on this parameter, since the behavior of the system is more or less the same. This should support the fact that this protein is not sensitive to the change of pH of the medium (see Fig. 7). This resistance is also visible in the analysis of solvent-accessible surface of MalE1. As shown in Figure 8, neither pH nor temperature is able to influence the exposure of hydrophobic residues. The solvent-accessible surface area of hydrophilic residues is slightly influenced by the pH, since in basic conditions the hydrophilic component of this parameter is little bit higher than the corresponding value at neutral pH; however, these values

remain stable or even are decreasing at increasing temperatures. These data corroborate the hypothesis that MalE1 is made of a compact hydrophobic core, and that this is the main determinant for its thermostability.

CONCLUSIONS

The analysis of infrared spectra indicates that MalE1 is a protein predominantly in α-helix conformation with a minor content of β-structure. This finding is corroborated by the *in silico* experiments. At neutral p^2H, the protein is extremely thermostable. In particular, the protein preserves its α-helical conformation even when maintained for prolonged time at 99.5°C. The high thermostability of the α-helices is maintained also at p^2H 9.8, and it is even higher at p^2H 7.5 in the presence of maltose. On the other hand, the β-conformation is temperature-sensitive. The infrared data suggest that at high temperatures rearrangements of the β-structure take place. This sensitivity of β-sheet towards high temperature is also observed at p^2H 9.8 and at p^2H 7.5 both in the absence and in the presence of maltose.

Molecular dynamics simulations performed at increasing temperature and different pH conditions are in agreement with these conclusions, and show a molecular portrait of the protein in which a compact hydrophobic core remains stable, but the β-sheets of the protein are transforming in less organized (and presumably more flexible) structures, whereas α-helices are conserved. The presence of SDS slightly modifies the secondary structure of MalE1 by decreasing the protein thermostability. In the presence of SDS, a temperature-dependent loss of α-helices and β-sheet takes place and the β-sheet rearrangement is not observed. The infrared data, corroborated by the inspection of the 3D structure of MalE1, indicate that hydrophobic interactions may play an important role in the high thermostability of MalE1.

In conclusion, this work suggests that even if MalE1 and TMBP present a very similar structural architecture, they show two different strategies for stabilizing their structure at the extreme environmental conditions that represent the natural habitat of the microorganisms from whose these proteins have been isolated.

ACKNOWLEDGMENTS

The authors are grateful to Prof. Helena Santos for providing the *E. coli* strain containing the plasmid with the gene of MalE1, to Dr. Umberto Amato for hosting MD simulations on the cluster "Lilligrid" located at the IAC-CNR, Naples, and to Dr. Angelo Facchiano, Laboratory of Bioinformatics, ISA, Avellino, for providing a tool for the calculation of the percentage of secondary structures using DSSP program, starting from a PDB file. This work was in the frame of the CNR-Commessa Diagnostica avanzata ed alimentazione (SD) and of CNR-Bioinformatics Project (AM).

REFERENCES

1. Brock TD. Life at high temperatures. Science 1985;230:132–138.
2. Herman P, Staiano M, Marabotti A, Varriale A, Scirè A, Tanfani F, Vecer J, Rossi M, D'Auria S. D-Trehalose/D-maltose-binding protein from the hyperthermophilic archaeon *Thermococcus litoralis*: the binding of trehalose and maltose results in different protein conformational states. Proteins 2006;63:754–767.
3. D'Auria S, Nucci R, Rossi M, Gryczynsky I, Gryczynsky Z, Lakowicz JR. The β-glycosidase from the hyperthermophilic archaeon *Sulfolobus solfataricus*: enzyme activity and conformational dynamics at temperatures above 100°C. Biophys Chem 1999;81:23–31.
4. Fessas D, Staiano M, Barbiroli A, Marabotti A, Schiraldi A, Varriale A, Rossi M, D'Auria S. Molecular adaptation strategies to high temperature and thermal denaturation mechanism of the D-trehalose/D-maltose-binding protein from the hyperthermophilic archaeon *Thermococcus litoralis*. Proteins 2007;67:1002–1009.
5. D'Auria S, Moracci M, Febbraio F, Tanfani F, Nucci R, Rossi M. Structure-function studies on β-glycosidase from *Sulfolobus solfataricus*. Mol Bases Thermostabil Biochim 1998;80:949–957.
6. Silva Z, Sampaio MM, Henne A, Böhm A, Gutzat R, Boos W, da Costa MS, Santos H. The high-affinity maltose/trehalose ABC transporter in the extremely thermophilic bacterium *Thermus thermophilus* HB27 also recognizes sucrose and palatinose. J Bacteriol 2005; 187:1210–1218.
7. Salomaa P, Schaleger LL, Long FA. Solvent deuterium isotope effects on acid–base equilibria. J Am Chem Soc 1964;86:1–7.
8. Tanfani F, Galeazzi T, Curatola G, Bertoli E, Ferretti G. Reduced beta-strand content in apoprotein B-100 in smaller and denser low-density lipoprotein subclasses as probed by Fourier-transform infrared spectroscopy. Biochem J 1997;322:765–769.
9. Bellamy LJ. The infrared spectra of complex molecules. London: Chapman and Hall; 1975.
10. Pieper U, Eswar N, Davis FP, Braberg H, Madhusudhan MS, Rossi A, Marti-Renom MA, Karchin R, Webb BM, Eramian D, Shen MY, Kelly L, Melo F, Sali A. MODBASE, a database of annotated comparative protein structure models, and associated resources. Nucleic Acids Res 2006;34(Database Issue):D291–D295.
11. Eswar N, John B, Mirkovic N, Fiser A, Ilyin VA, Pieper U, Stuart AC, Marti-Renom MA, Madhusudhan MS, Yerkovich B, Sali A. Tools for comparative protein structure modeling and analysis. Nucleic Acids Res 2003;31:3375–3380.
12. Altschul SF, Madden TL, Schäffer AA, Zhang J, Zhang Z, Miller W, Lipman DJ. Gapped BLAST and PSI-BLAST: a new generation of protein database search programs. Nucleic Acids Res 1997;25:3389–3402.
13. Sali A, Blundell TL. Comparative protein modelling by satisfaction of spatial restraints. J Mol Biol 1993;234:779–815.
14. Diez J, Diederichs K, Greller G, Horlacher R, Boos W, Welte W. The crystal structure of a liganded trehalose/maltose-binding protein from the hyperthermophilic archaeon *Thermococcus litoralis* at 1.85 Å. J Mol Biol 2001;305:905–915.
15. Bashford D, Karplus M. pKa's of ionizable groups in proteins: atomic detail from a continuum electrostatic model. Biochemistry 1990;29:10219–10225.
16. Gordon JC, Myers JB, Folta T, Shoja V, Heath LS, Onufriev A. H^{++}: a server for estimating pKas and adding missing hydrogens to macromolecules. Nucleic Acids Res 2005;33(Web Server Issue): W368–W371.
17. Lindahl E, Hess B, van der Spoel D. GROMACS 3.0: a package for molecular simulation and trajectory analysis. J Mol Model 2001; 7:306–317.

18. van der Spoel D, Lindahl E, Hess B, Groenhof G, Mark AE, Berendsen HJC. Gromacs: fast, flexible and free. J Comput Chem 2005; 26:1701–1718.
19. Jorgensen WL, Maxwell DS, Tirado-Rives J. Development and testing of the OPLS all-atom force field on conformational energetics and properties of organic liquids. J Am Chem Soc 1996;118:11225–11236.
20. Kaminski GA, Friesner RA, Tirado-Rives J, Jorgensen WL. Evaluation and reparametrization of the OPLS-AA force field for proteins via comparison with accurate quantum chemical calculations on peptides. J Phys Chem B 2001;105:6474–6487.
21. Jorgensen WL, Chandrasekhar J, Madura JD, Impey RW, Klein ML. Comparison of simple potential functions for simulating liquid water. J Chem Phys 1983;79:926–935.
22. Hess B, Bekker H, Berendsen HJC, Fraaije JGEM. LINCS: a linear constraint solver for molecular simulations. J Comput Chem 1997; 18:1463–1472.
23. Berendsen HJC, Postma JPM, van Gunsteren WF, Di Nola A, Haak JR. Molecular dynamics with coupling to an external bath. J Chem Phys 1984;81:3684–3690.
24. Essmann U, Perera L, Berkowitz ML, Darden T, Lee H, Pedersen LG. A smooth particle mesh Ewald method. J Chem Phys 1995;103: 8577–8593.
25. Kabsch W, Sander C. Dictionary of protein secondary structure: pattern recognition of hydrogen-bonded and geometrical features. Biopolymers 1983;22:2577–2637.
26. Hubbard SJ, Campbell SF, Thornton JM. Molecular recognition. Conformational analysis of limited proteolytic sites and serine proteinase protein inhibitors. J Mol Biol 1991;220:507–530.
27. Cuff AL, Martin AC. Analysis of void volumes in proteins and application to stability of the p53 tumour suppressor protein. J Mol Biol 2004;344:1199–1209.
28. Kumar S, Nussinov R. Salt bridge stability in monomeric proteins. J Mol Biol 1999;293:1241–1255.
29. Byler DM, Susi H. Examination of the secondary structure of proteins by deconvolved FTIR spectra. Biopolymers 1986;25:469–487.
30. Arrondo JL, Muga A, Castresana J, Goni FM. Quantitative studies of the structure of proteins in solution by Fourier-transform infrared spectroscopy. Prog Biophys Mol Biol 1993;59:23–56.
31. Krimm S, Bandekar J. Vibrational spectroscopy and conformation of peptides, polypeptides, and proteins. Adv Protein Chem 1986;38: 181–364.
32. Chirgadze YN, Fedorov OV, Trushina NP. Estimation of amino acid residue side-chain absorption in the infrared spectra of protein solutions in heavy water. Biopolymers 1975;14:679–694.
33. Barth A, Zscherp C. What vibrations tell us about proteins? Q Rev Biophys 2002;35:369–430.
34. Pedone E, Saviano M, Bartolucci S, Rossi M, Ausili A, Scirè A, Bertoli E, Tanfani F. Temperature-. SDS-, and pH-induced conformational changes in protein disulfide oxidoreductase from the archaeon *Pyrococcus furiosus*: a dynamic simulation and Fourier transform infrared spectroscopic study. J Proteome Res 2005;4:1972–1980.
35. Pedone E, Bartolucci S, Rossi M, Pierfederici FM, Scirè A, Cacciamani T, Tanfani F. Structural and thermal stability analysis of *Escherichia coli* and *Alicyclobacillus acidocaldarius* thioredoxin revealed a molten globule-like state in thermal denaturation pathway of the proteins: an infrared spectroscopic study. Biochem J 2003;373:875–883.
36. Ausili A, Scirè A, Damiani E, Zolese G, Bertoli E, Tanfani F. Temperature-induced molten globule-like state in human alpha 1-acid glycoprotein: an infrared spectroscopic study. Biochemistry 2005;44: 15997–16006.
37. D'Auria S, Barone R, Rossi M, Nucci R, Barone G, Fessas D, Bertoli E, Tanfani F. Effects of temperature and SDS on the structure of beta-glycosidase from the thermophilic archaeon *Sulfolobus solfataricus*. Biochem J 1997;323:833–840.
38. Gogliettino MA, Tanfani F, Scirè A, Ursby T, Adinolfi BS, Cacciamani T, De Vendittis E. The role of Tyr41 and His155 in the functional properties of superoxide dismutase from the archaeon *Sulfolobus solfataricus*. Biochemistry 2004;43:2199–2208.
39. Danson MJ, Hough DW. Structure, function and stability of enzymes from the Archaea. Trends Microbiol 1998;6:307–314.

PROTEINS
STRUCTURE ■ FUNCTION ■ BIOINFORMATICS

Mutant bovine odorant-binding protein: Temperature affects the protein stability and dynamics as revealed by infrared spectroscopy and molecular dynamics simulations

Anna Marabotti,[1] Thierry Lefèvre,[2] Maria Staiano,[3] Roberta Crescenzo,[3] Antonio Varriale,[3] Mosè Rossi,[3] Michel Pézolet,[2] and Sabato D'Auria[3]*

[1] Istituto di Scienze dell'Alimentazione, CNR, Avellino, Italy
[2] CERSIM/CREFSIP, Département de Chimie, Université Laval, Québec, Québec, Canada G1V 0A6
[3] Istituto di Biochimica delle Proteine, CNR, Via Pietro Castellino, 111 80131 Naples, Italy

ABSTRACT

Bovine odorant-binding protein (bOBP), a member of the lipocalin family, presents the so-called 3D "domain-swapped" protein structure. In fact, in solution, it appears as a dimer in which each monomer is composed by the classical lipocalin fold, with a central β-barrel followed by a stretch of residues and the α-helix domain protruding out of the barrel and crossing the dimer interface. Recently, a deswapped mutant form of bOBP was obtained, in which a Gly residue was inserted after position 121 and the two residues in position 64 and 156 were replaced by Cys residues for restoring the disulfide bridge common to the lipocalin family. In this work, we used Fourier transform infrared spectroscopy and molecular dynamics simulations to investigate the effect of temperature on the structural stability and conformational dynamics of the mutant bOBP. The spectroscopic and molecular simulation data pointed out that the hydrophobic regions of the protein matrix appear to be an important factor for the protein stability and integrity. In addition, it was also found that the mutant bOBP is significantly stabilized by the binding of the ligand, which may have an impact on the biological function of bOBP. The obtained results will allow for a better use of this protein as probe for the design of advanced protein-based biosensors for the detection of compounds used in the fabrication of explosive powders.

Proteins 2008; 72:769–778.

Key words: odorant-binding protein; FTIR spectroscopy; protein dynamics; protein conformation.

INTRODUCTION

Bovine odorant-binding protein (bOBP) has been the first vertebrate OBP to be detected in the nasal mucosa of cows,[1] and the first one for which the three-dimensional (3D) structure was determined.[2,3] Although it is considered as a member of the lipocalin family,[4,5] it shows a peculiarity in its 3D structure, since it is a "domain-swapped" protein.[3] In solution at neutral pH it appears as a dimer in which each monomer is composed by the classical lipocalin fold, with a central β-barrel followed by a stretch of residues and the α-helix domain protruding out of the barrel and crossing the dimer interface. A large buried cavity internal to the β-barrel is present in each monomer, forming the binding site for odorant molecules.[6] The absence of a Gly residue, Gly121, which is strictly conserved in other sequences of mammalian OBPs[6] and seems to play a crucial role in the formation of a turn in that part of the structure was identified as the determinant for the domain swapping. This hypothesis is supported by the finding that a mutant bOBP in which a glycine residue was inserted after position 121 showed a monomeric structure.[7] Another peculiarity of bOBP is the absence of the disulfide bridge between the C-terminal and the β-barrel, which is strictly conserved in the lipocalin family; in fact, the two Cys residues forming the bridge are not present in the sequence of bOBP.[6] Also the absence of this disulfide bridge seems to play a role in the domain swapping.[7]

In this work, we have characterized the structural features and the stability of a deswapped triple mutant bOBP (Gly 122+, W64C, H156C), in which a Gly residue is inserted after position 121 and the two residues in position 64 and 156 are replaced by Cys residues, to restore the disulfide bridge common to the lipocalin family. A comparison of the structural features of this mutant with those of pig

Grant sponsor: CNR-Bioinformatics Project (ISA-CNR); this work was also supported by the ASI project MoMa No. 1/014/06/0
*Correspondence to: Sabato D'Auria, Institute of Protein Biochemistry, Italian National Research Council, Via Pietro Castellino, 111 80131 Naples, Italy. E-mail: s.dauria@ibp.cnr.it.
Received 12 November 2007; Revised 13 December 2007; Accepted 18 December 2007
Published online 7 February 2008 in Wiley InterScience (www.interscience.wiley.com).
DOI: 10.1002/prot.21966

OBP (pOBP), whose structure in the absence[8] and presence of ligands[9] is well known, is investigated elsewhere (D'Auria *et al.*), by means of phosphorescence spectroscopy together with a detailed analysis of their structures. In this article, Fourier transform infrared (FTIR) spectroscopy and molecular dynamics (MD) simulations have been used to detect temperature-induced effects on bOBP stability. It is well-known that infrared active amide I vibration is quite sensitive to conformational changes induced by either temperature of pressure.[10–13] On the other hand, MD simulation is a powerful technique to identify more precisely structural features associated with experimental results obtained from spectroscopic techniques. Previous studies on pOBP[14] showed that, although this protein is not extracted by a thermophilic organism, it possesses a high resistance to thermal stress, and the determinants were identified in the hydrophobic interactions and ionic networks occurring in the 3D structure. Our work shows that the mutant bOBP protein is highly thermostable too, and that the presence of the ligands in its interior cavity further enhances this stability allowing the design of stable protein-based biosensors for the detection of explosive compounds.

METHODS

OBP purification and functionality test with 1-aminoanthracene

A 6xHis affinity tag was placed at the N-terminal of the mutant bOBP form (Gly 122+, W64C, H156C) by PCR using specific primers. The fused cDNA was subcloned in the expression vector pT7-7 and the expression of the protein was realized in BL21-DE 3 *E. coli*. The purification of the protein was performed by affinity chromatography with a Ni-NTA Agarose (Quiagen, Germany) according to the manufacturer's instructions, followed by a second chromatographic step on the anion exchange column Resourse Q (Amersham Biosciences, Italy), in FPLC. The purity of bOBP preparation was determined by SDS-PAGE, and protein concentration was calculated based on the absorbance values at 280 nm (48,000 M^{-1} cm^{-1}). Functionality of the recombinant bOBP was determined by direct titration using the fluorescent ligand 1-amino-anthracene (AMA) as previously reported.[7] Briefly, 1 mL sample of 1 μ*M* bOBP in 20 m*M* Tris-HCl buffer pH 7.8 was incubated overnight at 4°C in the presence of increasing concentrations of AMA (0.156–10 μM). Fluorescence emission spectra between 450 and 550 nm were recorded by ISS K2 fluorometer (excitation and emission slits of 2 nm) at a fixed excitation wavelength of 380 nm, and the formation of the AMA–bOBP complex was followed as the increase of the fluorescence emission intensity at 480 nm.

Molecular dynamics simulations

The coordinates of the mutant bOBP are currently "on hold" in the PDB database[15] and were kindly provided to us by Dr. Ramoni (R. Ramoni, personal communication). They include a ligand of the protein, which is inserted in the interior of the β-barrel. These coordinates were used to perform molecular dynamics simulations at high temperature in water, in the absence or in the presence of the ligand. Simulations were carried out using the program GROMACS version 3.3.1,[16,17] running in parallel (MPI) on a cluster with 40 × 86_64 Opteron processors. The GROMOS96 force field[18] was used throughout the simulations. A cubic box, containing 7955 water molecules (SPC model)[19] and 5 Na^+ ions to neutralize the net negative charge of the protein was used to solvate bOBP. Periodic boundary conditions were used to exclude surface effects. A preliminary energy minimization step with a tolerance of 1000 kJ/(mol nm) was run with the Steepest Descent method. All the bonds were constrained using LINCS.[20] After minimization, a short MD simulation with position restraints was applied to better "soak" the water molecules into the macromolecule. This position-restrained MD was 20 ps long, with a time step of 2 fs, coupling the system to a temperature bath at 300 K using Berendsen's method.[21] Berendsen's pressure coupling was also used. Long-range electrostatics were handled using the PME method.[22] Cut-off were set at 0.9 nm for Coulomb interactions, and at 1.4 nm for van der Waals interactions. The final MD simulations were carried out with a time-step of 2 fs and without any position restraints. Five subsequent MD simulations (the final conformation of each simulation was used as input for the following simulation at higher temperature) were carried out to gradually increase the temperature from 300 to 368 K for bOBP in the presence and in the absence of ligand, with the Berendsen's method of bath coupling.[21] Four simulations of 600 ps for each system were carried out at 333, 348, 353, and 368 K, whereas the simulation at 300 K was 1 ns long, for a global duration of 3.4 ns. Several analyses were conducted using programs built within GROMACS, and results were visualized and elaborated with the aid of the freely available program Grace (http://plasma-gate.weizmann.ac.il/Grace). The energy components were extracted from the energy files generated by the program and analyzed to verify the stabilization of the system. The RMSD values were obtained from a least-square fit of the respective nonhydrogen atoms (main-chain and side-chain). For each temperature step, an "average" structure of the protein was calculated on the whole protein minus hydrogen atoms. These structures were saved in pdb format, and they were subsequently minimized with the Steepest Descent method as described earlier. Relative percentages of secondary structure elements were determined on these "average" structures using the DSSP program.[23]

Solvent accessibility of amino acid residues was evaluated using the program NACCESS[24] by rolling a probe atom of 1.40 Å in radius on the van der Waals surface of the protein models. Only the relative accessibilities of side chains were taken into account. Other analyses were carried out with the Insight II package (Version 2000.1, Accelrys; 2000). In particular, identification of salt bridges was made directly on average structures obtained as described earlier, according to Kumar and Nussinov.[25]

Infrared spectroscopy

FTIR spectroscopy was used to investigate the mutant bOBP's thermal stability and heat-induced secondary structure changes. The protein was dissolved directly in D_2O (CDN Isotopes, Sainte-Claire, PQ, Canada) for 1 h at a concentration of 10 mg mL^{-1}. For experiment with the ligand, 1-octen-3-ol (Sigma-Aldrich, Oakville, Ontario, Canada) was mixed with D_2O and mechanically vortexed to obtain a cloudy emulsion. The protein was immediately dissolved in this solution for 1 h at 10 mg mL^{-1} and a ligand:bOBP molar ratio of 3:1. A volume of 27 μL of the protein solution was deposited between the two CaF_2 windows of a Biocell™ from Biotools (Jupiter, FL) manufactured with a calibrated path length of 50 μm. The transmission spectra were recorded at a resolution of 2 cm^{-1} using a Nicolet Magna 560 spectrometer (Thermo Electron Corporation, Madison, WI) equipped with a narrow band MCT detector and continuously purged with dry air. For each spectrum, 128 scans were coadded and apodized with a Happ-Genzel function. The temperature was computer controlled using a Omega temperature controller (Stamford, CT). The temperature of the samples was increased between 293 and 353 K with steps of 5 K allowing an equilibration period of 5 min at each desired temperature before recording the spectra. The whole data treatment of the amide I′ band was made with Grams/AI 8.0 (Thermo Electron Corporation, Waltham, MA). Water vapor was subtracted, the subtraction factor being optimized using the autosubtract function. For each temperature, the spectrum of D_2O at the appropriate temperature was subtracted from that of the protein solution. For the study of the amide I′ region, a linear baseline correction was performed between 1700 and 1595 cm^{-1}. Spectra were smoothed following the Savitzky-Golay procedure using a polynomial of order 2 and intervals of 37 points. This treatment did not affect the shape of the amide I′ band. All spectra were normalized to obtain an absorbance of 1 at peak maximum. Difference spectra were calculated by subtracting the spectrum recorded at 293 K from all other spectra using a subtraction factor of 1.

RESULTS AND DISCUSSION

Molecular dynamics simulations

Molecular dynamics simulations were carried out on mutant bOBP in water, both in the absence and in the presence of ligand, to analyze at a molecular level the effect of temperature on the dynamics and stability of this protein. Analyses of the energies of the MD simulations (data not shown) confirm that the total energy and its components (potential and kinetic energies) and the temperature are stable during each MD step, and that the equilibrium after the heating during the simulations is reached in less than 5 ps.

The simulation experiments performed at increasing temperature in the absence of the ligand showed a high stability of mutant bOBP toward the thermal perturbation. No major effects were detected on the overall tertiary structure of the protein (but we have to point out that the timescale of the simulation is not sufficient to find phenomena such as the unfolding of the protein). Looking at the average structures obtained at different temperatures, it is possible to note that the central β-sheet typical of the structure of this family of proteins is conserved also during the simulation experiments at 368 K, and also the helix-connecting strands β8 and β9 is stable during all the simulations (see Fig. 1). However, the DSSP analysis on these structures shows that the percentage of secondary structure elements, in particular β-sheets, is decreasing as temperature increases, and at the same time the percentage of residues in coil conformation is increasing (Table I). The highest conformational variability is focused in the loops connecting the β-strands of the protein (see Fig. 1). RMSD calculated on the superposed average structures of the protein during the simulation experiments confirms that the major conformational fluctuations are present in the following segments: 45–51 (loop 2), 72–78 (loop 4), 107–112 (loop 7), and C-terminal portion. This behavior is very similar to that simulated previously for pOBP[14] and confirms a notable thermal stability of this protein, although it is not isolated from thermophilic organisms. It also confirms that the mutations introduced in bOBP are able to drive the protein to mimic the behavior of the porcine protein. As for pOBP, the amino acid residues forming the walls of the β-barrel structure are mainly hydrophobic and sequestered from the solvent. Therefore, the hydrophobic interactions could be responsible for the high stability at high temperatures.

When present, the ligand is kept in the center of the β-barrel and interacts mainly with hydrophobic residues [Fig. 1(B)]. Simulations at high temperature show that the ligand does not leave the protein, although its conformational motility is higher as temperature increases. The DSSP analysis (Table I) shows that in the presence of the ligand, there is a higher percentage of residues in structured environments with respect to the ligand-free structure, both at low and high temperature, although also in this last case it is possible to see that the percentage of residues in coil conformation increases. The conformational flexibility of the highly flexible loops discussed earlier is reduced in amplitude although the

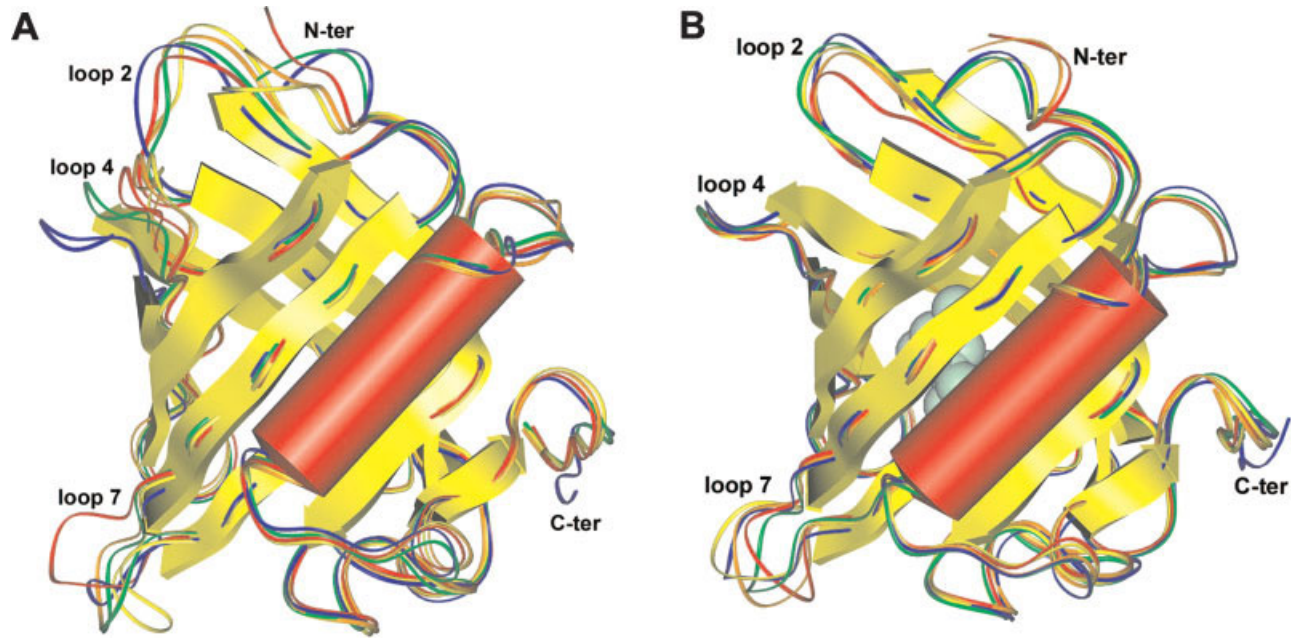

Figure 1

*Superposition of average structures of mutant bOBP without (**A**) and with (**B**) ligand at different temperatures. Cα trace is colored according to temperature: 300 K (blue), 333 K (green), 348 K (yellow), 353 K (orange), 368 K (red). Secondary structures are represented as follows: red cylinder (helix) and yellow arrows (β-sheet). Highly mobile loops (loop 2, loop 4, loop 7), N-ter, and C-ter are labeled. Ligand is in CPK mode and colored in grey.*

ligand does not interact directly with those residues, but probably this is an indirect stabilizing effect of the overall structure of the mutant protein.

The mutant bOBP contains two tryptophan residues (W17 and W133) and five tyrosine residues (Y21, Y39, Y55, Y79, Y83). W17 is the last residue before the first strand of the β-barrel, whereas W133 is in the middle of the α-helix. The superposition of the average structures (see Fig. 2) shows that W17 keeps a stable position in all simulations, both in the absence and in the presence of ligand, whereas the average position of W133 is more variable, especially when the ligand is not bound to the protein. Y21 lies near W133 and its conformation is conserved in all simulations, as well as Y39 and Y83, whereas Y55 and Y79 are more variable especially in the absence of ligand. Two Lys residues (K121 and K143) lies near W17 and W133, respectively, with their side chain parallel to the indole ring of the adjacent Trp. The mean distance between W133 and K143 increases when the temperature increases, more markedly when the ligand is

Table I

Percentage of Secondary Structure Elements in Average Structures Obtained by MD Simulations

Residues	MD at 300 K	MD at 333 K	MD at 348 K	MD at 353 K	MD at 368 K
Mutant bOBP without ligand					
Helices[a]	11.4	11.4	11.4	11.4	11.4
β-Structures[b]	47.7	47.7	45.6	45.0	44.7
Others[c]	24.8	25.5	24.9	24.1	23.5
Coils[d]	16.1	15.4	18.1	19.5	20.4
Mutant bOBP with ligand					
Helices[a]	11.4	11.4	11.4	11.4	11.4
β-Structures[b]	49.7	49.7	48.3	47.7	45.6
Others[c]	25.5	26.8	26.9	25.5	26.9
Coils[d]	13.4	12.1	13.4	15.4	16.1

[a]Marked as "H," "G," and "I" in DSSP output.
[b]Marked as "E" in DSSP output.
[c]Marked as "B," "T," and "S" in DSSP output.
[d]Structures not classified in DSSP output.

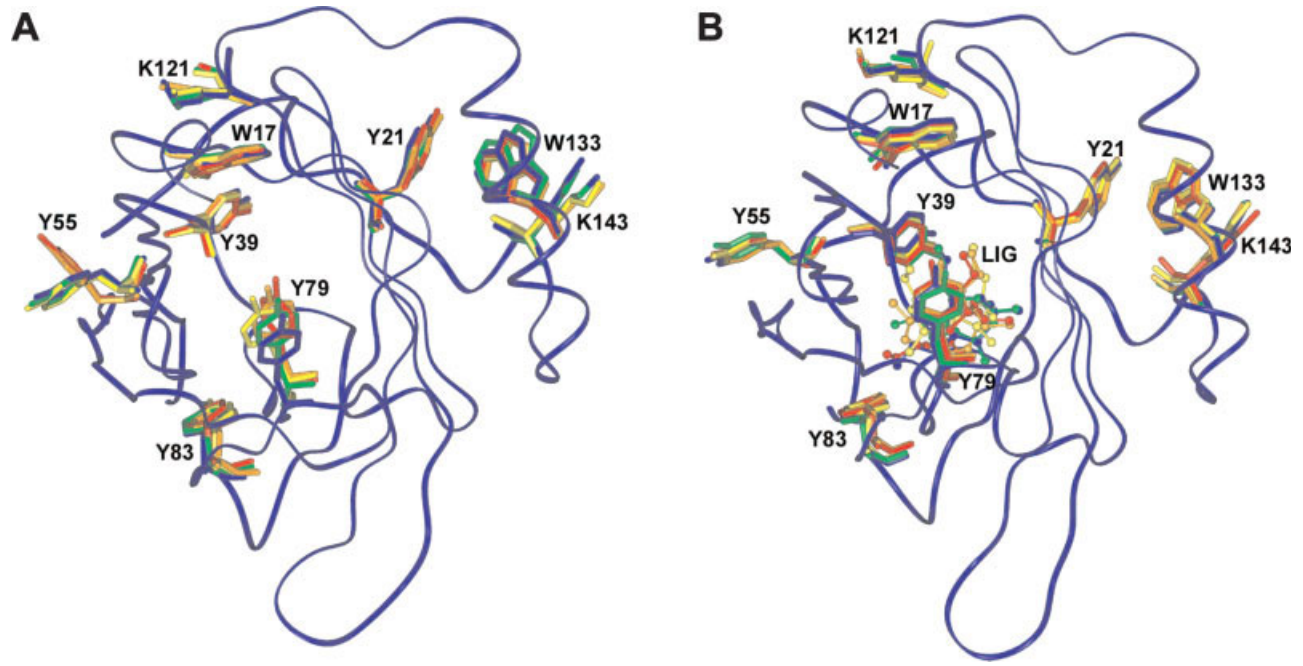

Figure 2

*Trp, Tyr, and Lys residues in mutant bOBP without (**A**) and with (**B**) ligand at different temperatures. Only the Cα trace of average structure at 300 K is shown, for reasons of clarity. Trp and Tyr residues, as well as Lys 121 and Lys 143, are in stick mode and labeled. The ligand is in ball-and-stick mode and labeled. The color code is the same as for Figure 1.*

absent, whereas the distance between W17 and K121 is more or less constant in the absence of the ligand, and slightly increases in the complex.

We also analyzed the relative solvent accessibility of these residues, calculated with NACCESS[24] (Table II). W17 is completely buried in the protein structure,

Table II
Relative Solvent Accessibility

Residue	MD at 300 K	MD at 333 K	MD at 348 K	MD at 353 K	MD at 368 K
Mutant bOBP without ligand					
W17	0	0.3	0.4	0.1	0.2
W133	22.0	28.6	23.5	20.8	22.2
Y21	28.3	28.2	27.0	25.9	28.7
Y39	7.5	5.8	4.9	4.1	7.2
Y55	39.6	42.6	41.8	29.8	27.3
Y79	8.3	2.3	0	3.4	2.3
Y83	11.9	11.4	11.0	9.5	10.6
K121	29.1	29.2	37.3	42.2	31.3
K143	70.5	59.5	52.3	53.0	59.5
Mutant bOBP with ligand					
W17	0	0.2	0	0	0
W133	21.2	22.1	21.0	25.3	24.0
Y21	24.6	26.8	24.3	30.8	32.3
Y39	5.3	3.0	3.2	3.1	4.1
Y55	46.8	49.4	39.8	40.0	39.3
Y79	5.4	5.0	5.3	10.1	4.9
Y83	14.5	14.1	9.5	9.9	11.5
K121	28.3	30.1	29.4	31.8	28.3
K143	66.5	64.3	55.4	76.4	57.1
Ligand	0.22	1.69	0.9	0	0

This parameter was calculated on side chains of Trp and Tyr residues and of selected Lys residues of mutant bOBP (see text) and is expressed here in percentage.

Table III
Ion Pairs Between Charged Residues

Ion pair	MD at 300 K	MD at 333 K	MD at 348 K	MD at 353 K	MD at 368 K
Mutant bOBP without ligand					
E32-K37	OE1-NZ: 3.53 OE2-NZ: 3.90 c-c: 3.67	–	OE1-NZ: 3.67 OE2-NZ: 3.09 c-c: 3.28	–	OE1-NZ: 3.02 OE2-NZ: 3.53 c-c: 3.16
E32-K59	**OE1-NZ: 3.25** **c-c: 3.67**	**OE2-NZ: 3.26** **c-c: 3.83**	**OE2-NZ: 3.31** **c-c: 3.81**	**OE2-NZ: 3.10** **c-c: 3.70**	**OE2-NZ: 3.20** **c-c: 3.54**
K49-D53	–	–	OD1-NZ: 3.02 OD2-NZ: 3.12 c-c: 3.05	OD1-NZ: 3.48 c-c: 3.98	–
D53-K70	OD1-NZ: 3.83 OD2-NZ: 3.21 c-c: 3.54	–	–	–	OD1-NZ: 3.37 c-c: 3.54
R60-E84	**NH1-OE2: 3.28** **NH2-OE2: 3.46** **c-c: 3.70**	**NH1-OE1: 3.94** **NH1-OE2: 3.26** **NH2-OE1: 3.53** **NH2-OE2: 3.79** **c-c: 3.46**	**NH1-OE1: 3.21** **NH2-OE1: 3.44** **c-c: 3.75**	**NH1-OE1: 3.39** **NH2-OE1: 3.32** **NH2-OE2: 3.41** **c-c: 3.52**	**NH1-OE1: 3.86** **NH1-OE2: 3.31** **NH2-OE1: 3.59** **NH2-OE2: 3.87** **c-c: 3.51**
H98-D128	NE2-OD1: 3.10 c-c: 3.59	NE2-OD1: 3.52 NE2-OD2: 3.45 c-c: 3.87	NE2-OD2: 3.70 c-c: 4.01	NE2-OD1: 3.32 NE2-OD2: 3.43 c-c: 3.78	–
Mutant bOBP with ligand					
E32-K37	OE1-NZ: 3.84 OE2-NZ: 2.97 c-c: 3.40	–	OE1-NZ: 3.72 OE2-NZ: 3.83 c-c: 3.70	–	OE1-NZ: 3.97 OE2-NZ: 3.28 c-c: 3.57
E32-K59	**OE1-NZ: 3.22** **c-c: 4.02**	**OE1-NZ: 3.21** **c-c: 3.77**	**OE1-NZ: 3.22** **OE2-NZ: 3.86** **c-c: 3.36**	**OE1-NZ: 3.05** **OE2-NZ: 3.73** **c-c: 3.26**	**OE1-NZ: 3.69** **OE2-NZ: 3.11** **c-c: 3.26**
D53-H68	–	OD1-NE2: 3.12 OD2-NE2: 3.21 c-c: 3.88	OD1-NE2: 3.04 OD2-NE2: 3.52 c-c: 3.83	–	–
D53-K70	–	–	–	–	OD1-NZ: 3.31 c-c: 4.00
R60-E84	**NH1-OE1: 3.40** **NH2-OE1: 3.25** **NH2-OE2: 3.54** **c-c: 3.46**	**NH1-OE1: 3.24** **NH2-OE1: 3.40** **NH2-OE2: 3.64** **c-c: 3.45**	**NH1-OE1: 3.78** **NH1-OE2: 3.68** **NH2-OE2: 3.21** **c-c: 3.59**	**NH1-OE1: 3.38** **NH2-OE1: 3.74** **NH2-OE2: 3.34** **c-c: 3.47**	**NH1-OE1: 3.59** **NH1-OE2: 3.86** **NH2-OE2: 3.24** **c-c: 3.49**
H98-D128	NE2-OD1: 3.48 NE2-OD2: 3.26 c-c: 3.68	–	–	NE2-OD1: 3.23 NE2-OD2: 3.51 c-c: 3.98	–
K131-D128	–	NZ-OD1: 3.51 c-c: 3.95	NZ-OD1: 3.46 c-c: 4.00	–	–

Ion pairs in bold are conserved in all average structures.

whereas W133 is exposed to solvent. Among Tyr residues, Y55 is the most exposed one, whereas Y39 and Y79 (both localized near the ligand and in the opposite parts of the β-barrel) are the most buried. Both Lys residues are markedly exposed to solvent, and especially K143 which points out of the protein, whereas K121 is located in the upper part of the β-barrel. The solvent accessibility of these residues is quite constant during all simulations, with the exception of Y55 in the absence of ligand, whose value markedly decreases at higher temperatures, and Y21 in the presence of ligand, whose accessibility increases at higher temperatures. The ligand is constantly shielded from solvent.

Previously[14] we analyzed the role of salt bridges in stabilizing the structure of pOBP. The mutant bOBP is also very rich in charged residues (50, 1/3 of the total residues) which are equally distributed in positively and negatively charged; in particular, mutant bOBP contains 5 His residues which are absent in pOBP.[8] Charged residues are grouped especially in loops between the β-strands or in the α-helix, with the exception of strand β4 (near the mutation W64C) which contains five charged residues, all pointing on the external surface of the protein.

Using the criteria reviewed in Kumar and Nussinov,[25] we were able to detect several salt bridges in the structure of mutant bOBP (Table III). Similarly to pOBP,[14] it is noteworthy that only the ion pair between D53 and K70 (connecting strand β3 to strand β4 in the external part of the β-barrel structure) does not involve residues

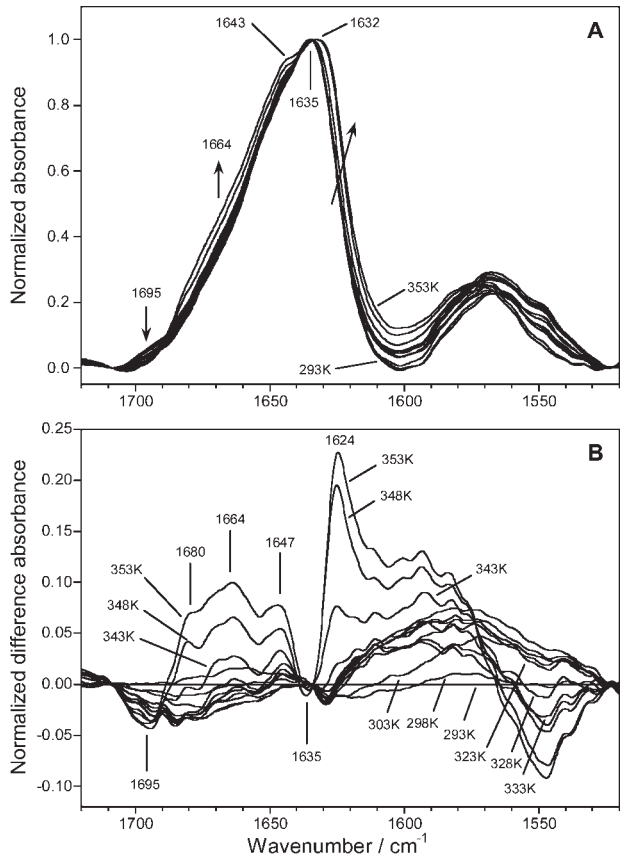

Figure 3

*Absorbance (**A**) and difference (**B**) spectra of mutant bOBP. Spectra were performed in 1% w/v D_2O and registered from 293 to 353 K (step of 5 K) in the amide I′ region. Arrows indicate the direction of spectral changes as temperature increases.*

placed in the protein loops. This underlines the importance of these interactions in bringing together these highly mobile portions of the protein, concurring to the overall protein stability, in addition to the stabilizing effect produced by the restored disulfide bridge connecting C64 and C156. Two ion pairs (R60-E84 and K59-E32) are conserved in all the average structures obtained by MD simulations. The first one connects loop L3 to loop L5, the second connects loop L1 to loop L3 and is placed near the disulfide bridge present in the mutant bOBP. Both salt bridges are present in the larger part of the β-barrel structure, near the C-terminal moiety. Interestingly, no salt bridge connect loops in the opposite part of the β-barrel, near the N-terminal moiety. A third conserved ion pair formed by H98-D128 joins the α-helix to the loop L6. In the absence of the ligand, this salt bridge is conserved in all structures with the exception of that at higher temperature (368 K), whereas in the presence of the ligand, the fluctuation of the two residues is more significant, and this ion pair is not always present. As for pOBP, other ion pairs are present sporadically in the structures.

We can conclude that, similarly to pOBP, the mutant bOBP shows a high resistance of its global structural organization to high temperatures, since its overall fold are practically unchanged in a wide range of temperature. Local perturbations in the protein conformation are especially present in highly mobile loops connecting the protein secondary structure elements, and a higher conformational freedom is especially present when ligand is absent from structure. Hydrophobic interactions in the core of the β-barrel structure and ion pairs seem to play a major role in protecting the protein against high temperature shock.

Infrared spectroscopy

Figure 3(A) shows the spectra of mutant bOBP in D_2O at different temperatures from 293 to 353 K in the 1720–1520 cm^{-1} region. The strong band between 1700 and 1600 cm^{-1} is because of the amide I′ vibration, a mode which is sensitive to polypeptide secondary structure.[26] The less intense band near 1560 cm^{-1} is because of the COO^- antisymmetric stretching vibration of acidic side-chains.[27] At 293 K, the maximum of the amide I′ band is observed at 1635 cm^{-1}. This indicates that bOBP in its native state is mainly composed of β-sheets, which is in agreement with the three-dimensional structure of the protein. The small component at 1695 cm^{-1} is also assigned to the β-sheet conformation. As the temperature increases, only minor changes occur up to 338 K, the temperature at which the spectrum abruptly changes. Most of the spectral modifications occur above this temperature. In particular, the maximum of the amide I′ band is shifted to 1632 cm^{-1}. The difference spectra [Fig. 3(B)] reveals that this shift is because of the appearance of a new component located near 1624 cm^{-1}, which is characteristic of the formation of β-sheets upon protein self-aggregation.[28,29] This observation is confirmed by experiments performed at higher temperatures and concentrations (not shown) that clearly display a further increase of this band. The appearance of the component at 1685 cm^{-1} [Fig. 3(B)] is assigned to antiparallel intermolecular β-sheets[26] and is also characteristic of protein aggregation.[28,29] The heat-induced aggregation of proteins via the formation of β-sheets is a common property of globular proteins. It has been extensively studied for β-lactoglobulin from bovine milk,[10,12] another protein of the lipocalin family.[30] As seen from Figure 3(B), the development of β-aggregation is concomitant with the loss of native intramolecular β-sheets (1635 and 1695 cm^{-1} components) and to the formation of nonnative turns (1664 cm^{-1} component) and unordered segments (1647 cm^{-1} component).

Figure 4(A) shows the comparison of the spectra at 293 K in the presence and absence of the ligand. Only

minor differences are observed at this temperature, showing that the secondary structure of the protein is only slightly altered by the ligand. The small narrowing of the amide I′ band indicates a more homogeneous distribution of conformations when the ligand is present. In particular, the decrease of the bandwidth in the 1680–1640 cm^{-1} range in the presence of the ligand indicates a slight rigidification of the turn (1674 cm^{-1} component) and α-helix/unordered (1648 cm^{-1} component) structures. This experimental observation suggests that the ligand mainly stabilizes the more "flexible" elements of bOBP, which nicely supports MD simulations.

The thermal stability of bOBP in the presence of the ligand is presented in Figure 5(A) from 293 to 353 K. Only minor heat-induced changes are observed during the whole heating process. As opposed to the protein in the absence of ligand (see Fig. 3), the difference spectra [Fig. 5(B)] reveal very small spectral alterations upon heating. Therefore, the thermal stability of mutant bOBP

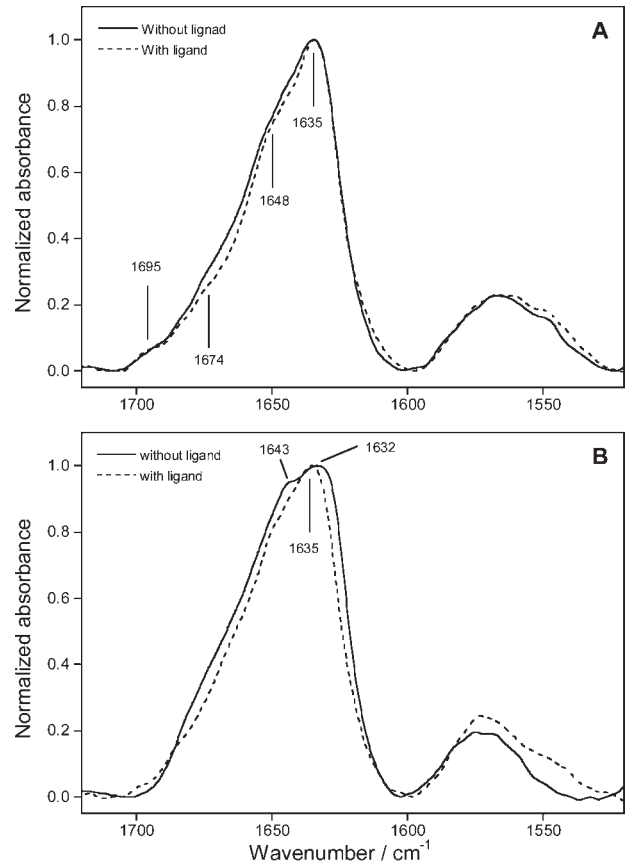

Figure 4

*Spectra of mutant bOBP in the absence and presence of 1-octen-3-ol. Spectra were performed in 1% w/v D_2O at 293 K (**A**) and 353 K (**B**) in the absence and presence of 1-octen-3-ol (ligand:protein molar ratio of 3:1).*

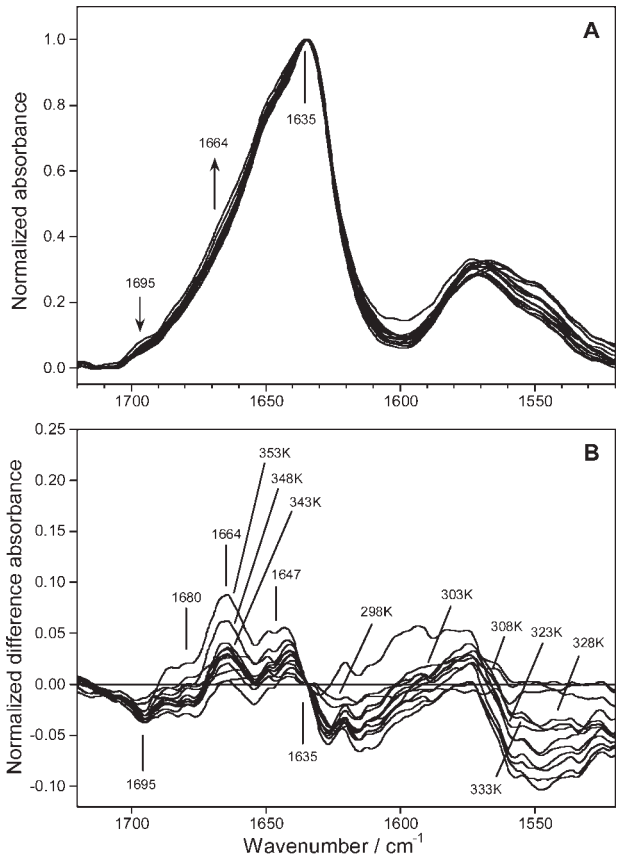

Figure 5

*Absorbance (**A**) and difference (**B**) spectra of mutant bOBP. Spectra were performed in 1% w/v D_2O in the presence of 1-octen-3-ol (ligand:protein molar ratio of 3:1) from 293 to 353 K (step of 5 K) in the amide I′ region. Arrows indicate the direction of spectral changes as temperature increases.*

appears to be much higher in the presence of the ligand. In particular, no formation of intermolecular β-sheets is observed showing that the protein aggregation is completely inhibited by the presence of the ligand at least up to 353 K. On the other hand, the components at 1664 and 1647 cm^{-1} slightly increase in intensity upon heating, as for unliganded bOBP. These bands increase at the expense of the 1635 and 1695 cm^{-1} components indicating that a few native intramolecular β-sheets are again converted into turns and unordered segments, which is in agreement with the MD simulations. Figure 4(B) presents the comparison of the amide I′ band of bOBP at 353 K in the presence and absence of the ligand. This figure emphasizes the strong difference in the shape of the amide I′ bands and the fact that pure bOBP is significantly denatured at high temperature, whereas it keeps in structural integrity in the whole temperature range in the presence of the ligand.

The heat-induced aggregation of globular proteins in general and β-lactoglobulin in particular is generally

acknowledged to stem from an initial (partial) unfolding of the protein.[30] Unfolding results in the exposure to water of the initially buried hydrophobic patches of the native protein.[31] This leads to the irreversible assembly of the polypeptide chains[31] accompanied by the formation of intermolecular β-sheets. The IR results suggests that, being located in the hydrophobic pocket formed by the β-barrel, the ligand stabilizes this structural motif and/or some flexible regions of the protein against unfolding, thus preventing aggregation. These results confirm the important role played by the hydrophobic effect on the protein stability.

In conclusion, the obtained spectroscopic results on the conformation stability of bOBP and the determination of the protein structure dynamics and solvent accessibility as assessed by MD simulations are in good agreement. The hydrophobic effect appears to be an important factor for the protein stability and integrity. The mutant protein is significantly stabilized by the ligand, which may have an impact on the biological function of bOBP.

The obtained results will be used for designing new protein-based fluorescence biosensors for the detection of explosive compounds.[32]

ACKNOWLEDGMENTS

The authors thank Prof. Roberto Ramoni, University of Parma, for providing the pdb file of the protein structure as well as the plasmid containing the obp gene, and Dr. Susan Costantini, Laboratory of Bioinformatics, ISA, Avellino, for providing a tool for the calculation of the percentage of secondary structures from a DSSP file. This work is in the frame of the CNR Commessa Diagnostica avanzata ed alimentazione (SD).

REFERENCES

1. Bignetti E, Cavaggioni A, Pelosi P, Persaud KC, Sorbi RT, Tirindelli R. Purification and characterisation of an odorant-binding protein from cow nasal tissue. Eur J Biochem 1985;149:227–231.
2. Bianchet MA, Bains G, Pelosi P, Pevsner J, Snyder SH, Monaco HL, Amzel LM. The three-dimensional structure of bovine odorant binding protein and its mechanism of odor recognition. Nat Struct Biol 1996;3:934–939.
3. Tegoni M, Ramoni R, Bignetti E, Spinelli S, Cambillau C. Domain swapping creates a third putative combining site in bovine odorant binding protein dimer. Nat Struct Biol 1996;3:863–867.
4. Flower DR, North AC, Sansom CE. The lipocalin protein family: structural and sequence overview. Biochim Biophys Acta 2000;1482:9–24.
5. Grzyb J, Latowski D, Strzalka K. Lipocalins—a family portrait. J Plant Physiol 2006;163:895–915.
6. Tegoni M, Pelosi P, Vincent F, Spinelli S, Campanacci V, Grolli S, Ramoni R, Cambillau C. Mammalian odorant binding proteins. Biochim Biophys Acta 2000;1482:229–240.
7. Ramoni R, Vincent F, Ashcroft AE, Accornero P, Grolli S, Valencia C, Tegoni M, Cambillau C. Control of domain swapping in bovine odorant-binding protein. Biochem J 2002;365:739–748.
8. Spinelli S, Ramoni R, Grolli S, Bonicel J, Cambillau C, Tegoni M. The structure of the monomeric porcine odorant binding protein sheds light on the domain swapping mechanism. Biochemistry 1998;37:7913–7918.
9. Vincent F, Spinelli S, Ramoni R, Grolli S, Pelosi P, Cambillau C, Tegoni M. Complexes of porcine odorant binding protein with odorant molecules belonging to different chemical classes. J Mol Biol 2000;300:127–139.
10. Casal HL, Köhler U, Mantsch HH. Structural and conformational changes of β-lactoglobulin B: an infrared spectroscopic study of the effect of pH and temperature Biochim Biophys Acta 1988;957:11–20.
11. Paolini S, Tanfani F, Fini C, Bertoli E, Pelosi P. Porcine odorant-binding protein: structural stability and ligand affinities measured by Fourier-transform infrared spectroscopy and fluorescence spectroscopy. Biochim Biophys Acta 1999;1431:179–188.
12. Lefevre T, Subirade M. Molecular differences in the formation and structure of fine-stranded and particulate β-lactoglobulin gels. Biopolymers 2000;54:578–586.
13. Marabotti A, Ausili A, Staiano M, Scirè A, Tanfani F, Parracino A, Varriale A, Rossi M, D'Auria S. Pressure affects the structure and the dynamics of the D-galactose/D-glucose-binding protein from *Escherichia coli* by perturbing the C-terminal domain of the protein. Biochemistry 2006;45:11885–11894.
14. Stepanenko OV, Marabotti A, Kuznetsova IM, Turoverov KK, Fini C, Varriale A, Staiano M, Rossi M, D'Auria S. Hydrophobic interactions and ionic networks play an important role in thermal stability and denaturation mechanism of the porcine odorant-binding protein. Proteins; Published online ahead of print, DOI: 10.1002/prot.21658.
15. Berman H, Henrick K, Nakamura H, Markley JL. The worldwide Protein Data Bank (wwPDB): ensuring a single, uniform archive of PDB data. Nucleic Acids Res 2007;35(Database Issue):D301–D303.
16. Lindahl E, Hess B, van der Spoel D. GROMACS 3.0: a package for molecular simulation and trajectory analysis. J Mol Model 2001;7:306–317.
17. van der Spoel D, Lindahl E, Hess B, Groenhof G, Mark AE, Berendsen HJ. GROMACS: fast, flexible and free. J Comput Chem 2005;26:1701–1718.
18. van Gunsteren WF, Billeter SR, Eising AA, Hunenberger PH, Kruger P, Mark AE, Scott WRP, Tironi IG. Biomolecular simulation: The GROMOS96 manual and user guide. Zurich, Switzerland: Vdf Hochschulverlag AG an der ETH Zurich; 1996. 1042 p.
19. Berendsen HJC, Postma JPM, van Gunsteren WF, Hermans J. Interaction models for water in relation to protein hydration. In: Pullman B, editor. Intermolecular forces. Dordrecht: Reidel D. Publishing Company; 1981, pp 331–342.
20. Hess B, Bekker H, Berendsen HJC, Fraaije JGEM. LINCS: a linear constraint solver for molecular simulations. J Comput Chem 1997;18:1463–1472.
21. Berendsen HJC, Postma JPM, Di Nola A, Haak JR. MD with coupling to an external bath. J Phys Chem 1984;81:3684–3690.
22. Essmann U, Perera L, Berkowitz ML, Darden T, Lee H, Pedersen LG. A smooth particle mesh Ewald method. J Chem Phys 1995;103:8577–8593.
23. Kabsch W, Sander C. Dictionary of protein secondary structure: pattern recognition of hydrogen bonded and geometrical features. Biopolymers 1983;22:2577–2637.
24. Hubbard SJ, Campbell SF, Thornton JM. Molecular recognition. Conformational analysis of limited proteolytic sites and serine proteinase protein inhibitors. J Mol Biol 1991;220:507–530.
25. Kumar S, Nussinov R. Salt bridge stability in monomeric proteins. J Mol Biol 1999;293:1241–1255.

26. Krimm S, Bandekar J. Vibrational spectroscopy and conformation of peptides, polypeptides, and proteins. Adv Protein Chem 1986;38:181–364.
27. Venyaminov SY, Kalnin NN. Quantitative IR spectrophotometry of peptide compounds in water (H_2O) solutions. I. Spectral parameters of amino acid residue absorption bands. Biopolymers 1990;30: 1243–1257.
28. Timasheff SN, Susi H, Stevens L. Infrared spectra and protein conformations in aqueous solution. II. Survey of globular proteins. J Biol Chem 1967;242:5467–5473.
29. Clark AH, Saunderson DH, Suggett A. Infrared and laser-Raman spectroscopic studies of thermally-induced globular protein gels. Int J Pept Protein Res 1981;17:353–364.
30. Papiz MZ, Sawyer L, Eliopoulos EE, North AC, Findlay JB, Sivaprasadarao R, Jones TA, Newcomer ME, Kraulis PJ. The structure of β-lactoglobulin and its similarity to plasma retinol-binding protein. Nature 1986;324:383–385.
31. Ferry JD. Protein gels. Adv Protein Chem 1948;4:1–78.
32. Ramoni R, Bellucci S, Grycznyski I, Grycznyski Z, Grolli S, Staiano M, Giannini G, Micciulla F, Pastore R, Tiberia A, Conti V, Merli E, Varriale A, Rossi M, D'Auria S. The protein scaffold of the lipocalin odorant binding protein is suitable for the development of biosensors for the detection of explosive components. J Opt Phys Solid Matter 2007;19:395012–395019.

Journal of Peptide Science
J. Pept. Sci. (2008)
Published online in Wiley InterScience (www.interscience.wiley.com). DOI: 10.1002/psc.992

JOURNAL OF PEPTIDE SCIENCE

Kissper, a kiwi fruit peptide with channel-like activity: Structural and functional features‡

M. ANTONIETTA CIARDIELLO,[a]* DANIELA MELELEO,[b] GABRIELLA SAVIANO,[c] ROBERTA CRESCENZO,[a] VITO CARRATORE,[a] LAURA CAMARDELLA,[a] ENRICO GALLUCCI,[b] SILVIA MICELLI,[b] TEODORICO TANCREDI,[d] DELIA PICONE[e] and MAURIZIO TAMBURRINI[a]

[a] Istituto di Biochimica delle Proteine, C.N.R., I-80131 Napoli, Italy
[b] Dipartimento Farmaco-Biologico, Università degli Studi di Bari, I-70126 Bari, Italy
[c] Dipartimento STAT, Università degli Studi del Molise, I-86170 Pesche (Is), Italy
[d] Istituto di Chimica Biomolecolare, C.N.R., I-80078 Pozzuoli (Na), Italy
[e] Dipartimento di Chimica, Università di Napoli Federico II, I-80126 Napoli, Italy

Received 19 October 2007; *Revised 31 October 2007*; *Accepted 4 November 2007*

Abstract: Kissper is a 39-residue peptide isolated from kiwi fruit (*Actinidia deliciosa*). Its primary structure, elucidated by direct protein sequencing, is identical to the *N*-terminal region of kiwellin, a recently reported kiwi fruit allergenic protein, suggesting that kissper derives from the *in vivo* processing of kiwellin. The peptide does not show high sequence identity with any other polypeptide of known function. However, it displays a pattern of cysteines similar, but not identical, to those observed in some plant and animal proteins, including toxins involved in defence mechanisms. A number of these proteins are also active on mammalian cells. Functional characterization of kissper showed pH-dependent and voltage-gated pore-forming activity, together with anion selectivity and channeling in model synthetic PLMs, made up of POPC and of DOPS : DOPE : POPC. A 2DNMR analysis indicates that in aqueous solution kissper has only short regions of regular secondary structure, without any evident similarity with other bioactive peptides. Comparative analysis of the structural and functional features suggests that kissper is a member of a new class of pore-forming peptides with potential effects on human health. Copyright © 2008 European Peptide Society and John Wiley & Sons, Ltd.

Keywords: kiwi fruit; peptide; amino acid sequence; NMR; membrane channels; ion transport

INTRODUCTION

Regular consumption of fruit and vegetables is generally associated with a reduction of the risk of several human pathologies, such as cardiovascular diseases, heart failure, microbial infections, cancer, Alzheimer's disease, cataract and other age-related functional degenerations [1–3]. These advantages are usually ascribed to rich vitamin and antioxidant and dietary fibre content, although other constituents may have beneficial effects on human health [4]. Recently, food containing significant amounts of bioactive molecules with effects beyond nutritional aspects and playing important roles in the prevention of chronic diseases has been referred to as 'functional food' [2,5]. The effects of dietary fruit and vegetables on health are yet to be fully explained, and might be associated with as yet unidentified components that are still to be characterized both chemically and functionally.

Biochemical and genetic studies have also identified several PR (Pathogenesis Related) proteins, playing a role in plant defence against pathogen agents. A number of these bioactive polypeptides have been found also in dietary plants and in some cases they show toxicity against human pathogens [6–8]. Therefore, isolation and characterization of these polypeptides could provide new insights for the production of novel drugs that are able to improve human resistance to infections.

Kiwi fruit is a food with significant effects on human health. In Chinese traditional medicine this fruit was used for the prevention and therapy of many different types of cancers [9]. More recently, a number of experimental data suggests the presence of biological activities associated to kiwi fruit extracts or to specific molecules isolated from this fruit, such as *in vitro* cytotoxicity for tumor cell lines and antimicrobial activity [9], protection against oxidative DNA damage [10] and cardiovascular protective properties [11]. Human trial data indicated that daily consumption of kiwi fruit promoted laxation in elderly people [12]. *In vitro* experiments showed that the PR protein thaumatin, isolated from kiwi fruit, displays antifungal and antiviral (anti-HIV) activities against human pathogens [13].

Abbreviations: FPLC, fast protein liquid chromatography; HSQC, heteronuclear single-quantum coherence; PLM, planar lipid membrane; POPC, palmitoyloleoylphosphatidylcholine; DOPS, dioleoylphosphatidylserine; DOPE, dioleoylphosphatidylethanolamine.

* Correspondence to: M. Antonietta Ciardiello, Istituto di Biochimica delle Proteine, CNR, Via Pietro Castellino 111, I-80131 Napoli, Italy; e-mail: ma.ciardiello@ibp.cnr.it

‡ The protein sequence data reported in this paper will appear in the Swiss-Prot and TrEMBL knowledgebase under the accession number P83975.

Unfortunately, an increasing number of individuals have to avoid consumption of kiwi fruit due to the presence of several allergens [13–17]. The isolation and characterization of molecules associated with the specific biological effects of kiwi fruit appears to be an important goal, which might enlarge our knowledge about a possibly safe pharmacological use of naturally occurring drugs. In particular, a proteomic analysis of the edible portion of ripe kiwi fruit may allow the identification of the polypeptides ingested during consumption and suggest their possible biological effects.

In the framework of a proteomic study on kiwi fruit (*Actinidia deliciosa*), we have undertaken the analysis of proteins and peptides found in the ripening fruit. Kiwi fruit pectin methylesterase inhibitor [18] and pectin methylesterase [19] have already been isolated and characterized, and the study of a possible influence on human health is under investigation. More recently, we have isolated kiwellin [17], a novel allergenic protein which is one of the three most abundant proteins present in the edible part of this fruit. We report here the purification, the characterization and the complete amino acid sequence of a novel peptide (henceforth named kissper), isolated in our laboratory. Furthermore, as a planar lipid bilayer system provides an elegant way to study membrane-active compounds, electrophysiological studies have been carried out on model synthetic PLMs made up of POPC or DOPS : DOPE : POPC as a surrogate for the intestinal lipids [20], and the solution structure of the peptide has been investigated by 2D NMR. The data obtained are discussed and compared with those of kiwellin and other peptides and proteins from various families, with related structural features and/or biological activities.

MATERIALS AND METHODS

Reagents

Kiwi fruits were purchased in Italy from a local farm; they were picked in mid October and stored for a week at room temperature until slightly soft. Trypsin was from Boehringer (Mannheim, Germany); bovine serum albumin, dithiothreitol, Tris, and 4-vinylpyridine from Sigma (Milan, Italy); DEAE-cellulose (type DE52) from Whatman (Brentford, UK). HPLC-grade acetonitrile was from Baker (Phillipsburg, NJ, USA). Salts and other analytical grade basic chemicals used in PLM studies were bought from Merck (Darmstadt, FRG, analytical grade), whereas biochemicals were from Sigma. POPC was purchased from Avanti Polar Lipids (Alabaster, AL, USA). Sequencer grade reagents were from Applied Biosystems (Foster City, CA, USA). All other reagents were of the highest commercially available quality.

Protein Purification and Characterization

FPLC ion-exchange chromatography was carried out on a Mono-Q HR 10/10 column (Amersham-Pharmacia, Milan, Italy), at a flow-rate of 3 ml/min, recording the absorbance at 280 nm.

Protein concentrations were determined by the BIO-RAD Protein Assay (BIO-RAD, Segrate, Italy), using calibration curves made with bovine serum albumin. When required, protein samples were concentrated by ultrafiltration using Centriplus YM-3 filters (Amicon, Millipore, Bedford, MA, USA).

Denaturation and alkylation was carried out by dissolving the peptide at a concentration of 2 mg/ml in 0.5 M Tris-HCl pH 7.8, containing 2 mM EDTA and 6 M guanidine hydrochloride. Dithiothreitol (ten-fold molar excess over the thiol groups of the protein) was added under nitrogen atmosphere, and the solution was kept at 37 °C for 1 h. 4-vinylpyridine (five-fold molar excess over the total thiols) was then added under nitrogen atmosphere, and the mixture was kept in the dark at room temperature for 30 min. At the end of the reaction, excess reagents were removed by gel filtration on a PD-10 column (Amersham-Pharmacia) equilibrated with 0.1% TFA.

Tryptic digestions on pyridylethylated samples (0.5 mg/ml) were carried out at an enzyme : protein ratio of 1 : 20 (w : w) in 1% ammonium bicarbonate, at 37 °C for 2 h.

Reverse-phase HPLC of kiwi extracts and of peptides derived from chemical or enzymatic cleavage was performed on a Vydac (Deerfield, IL, USA) C_8 column (0.21 × 25 cm), using a Beckman (Fullerton, CA, USA) System Gold apparatus. Elution was accomplished by a multistep linear gradient of eluant B (0.08% TFA in acetonitrile) in eluant A (0.1% TFA) at a flow rate of 1 ml/min. The eluate was monitored at 220 and 280 nm. The separated fractions were manually collected and analyzed as needed.

Amino acid sequencing was performed with an Applied Biosystems Procise 492 automatic sequencer, equipped with on-line detection of phenylthiohydantoin amino acids. Protein sequence analyses were performed using softwares available on the ExPASy Proteomics Server (www.expasy.org).

MALDI-TOF mass spectrometry was carried out on a PerSeptive Biosystems (Framingham, MA, USA) Voyager-DE Biospectrometry Workstation. Analyses were performed on premixed solutions prepared by diluting samples (final concentration 5 pmol/μl) in 4 volumes of matrix, namely 10 mg/ml α–cyano-4-hydroxycinnamic acid in 60% acetonitrile containing 0.3% TFA.

NMR

NMR measurements were performed on a sample prepared by dissolving 1 mg of freeze-dried peptide in 0.60 ml of 25 mM phosphate buffer (in 90% H_2O, 10% ^2H_2O), pH 3.5. NMR spectra were acquired at 300 K using a 600 MHz Bruker (Billerica, MA, USA) DRX spectrometer equipped with a cryoprobe. 2D ^{1}H-TOCSY [21], NOESY [22] and DQF-COSY [23], as well as ^{1}H-^{13}C and ^{1}H-^{15}N-HSQC [24] spectra were used for resonance assignments. The HDO solvent resonance was suppressed using the WATERGATE pulse sequence [25]. NOESY at different mixing times were acquired for assignment and structure calculations, TOCSY experiments were recorded with mixing times of 30 and 70 ms. The $^3J_{NHC\alpha H}$ coupling constants were measured for resolved NH amidic protons from a 1D spectrum. 2D

DOI: 10.1002/psc

data were typically apodized with a Gaussian window function and zero-filled to 1 K in F_1 prior to Fourier transform. NMRPipe [26] and NMRView [27] programs were used for data processing and spectral analysis, respectively. ^{1}H chemical shifts were referenced to the water signal at 4.70 ppm, ^{15}N chemical shifts were indirectly referenced to the ^{1}H chemical shifts according to magnetogiric ratios [28].

Cross-peaks of the NOESY spectrum at 300 ms mixing time were integrated by NMRView, transferred to the program package DYANA 1.0.6 [29], and converted to upper distance limits. Structure calculation was carried out by torsion angle dynamics. Eighty structures were calculated by TSSA, starting with a total of 10 000 MD steps and a default value of maximum temperature. The 20 best structures, in terms of target function, were considered as models of the solution structure of kisspер.

Planar Membrane Experiments

PLMs were composed of POPC or of DOPS : DOPE : POPC (27 : 27:18, w : w : w) in 1% *n*-decane and formed as previously described [30]. The measurements were carried out at pH 7.0, or at pH 3.5, and at 22 ± 1 °C. Bilayers were painted across a 0.3 mm diameter circular hole in a teflon divider separating two 4 ml teflon chambers. The membrane current was monitored with an oscilloscope and recorded on a chart recorder for data analysis. The *cis* and *trans* chambers were connected to the amplifier head stage by Ag/AgCl electrodes in series with a voltage source and a highly sensitive current amplifier. The single-channel instrumentation had a time resolution of 1–10 ms, depending on the magnitude of the single-channel conductance. The *cis*-side compartment, where kisspер was added, had a positive polarity. The painted PLMs were tested for integrity by checking the reflectance optically and also by their resistance and capacitance. After the membranes were formed, 4 or 8 µl of a 40 µg/ml kisspер solution in bidistilled water at pH 3.8 were added on the *cis* compartment and stirred to reach a final concentration of 0.04 and 0.08 µg/ml. To allow comparison of the results, particular attention was devoted to the standardization of the experimental conditions, such as (i) volume of the cell, (ii) stirring of the bathing solutions and (iii) modality of peptide addition.

The channel incorporation was studied as follows: (i) To define the mean channel conductance (central conductance Λ_c), the single-channel data were obtained from at least three experiments with usually more than 150 single events for each series performed on different days. Upward/downward (positive/negative applied voltage, respectively) current transition (event) was more frequent than terminating events. A histogram of the current amplitude distribution for each experiment was constructed and fitted by a Gaussian distribution function (GraphPad Prism version 3.0; GraphPad Software, Inc, http://www.graphpad.com). (ii) To identify the charge of the ion carrying the current, we measured the shift in the reversal potential induced by a change from a symmetrical to an asymmetrical KCl solution system. When the membrane conductance reached a virtually stable value, after kisspер addition on the *cis* side, the salt concentration on the *cis* side of the membrane was raised by the addition of a concentrated salt solution. A salt concentration gradient was set, with 1.5 M on one side (*cis*) and 0.3–1 M on the other (*trans*) (pH 7.0 and 3.5, respectively), in POPC PLM. In DOPS : DOPE : POPC PLM the concentration gradient was 1.0 M on the *cis* side and 0.5 M on the *trans* side. The reversal potential was determined by changing the holding potential step by step by ±2 mV. The permeability ratio was calculated using the Hodgkin-Goldman-Katz equation [31]:

$$V = (RT/F) \times \ln \{(P_K[K]_t + P_{Cl}[Cl]_c)/(P_K[K]_c + P_{Cl}[Cl]_t)\}$$

where $[X]_t$ and $[X]_c$ are the concentrations of the ion species X in the *trans* and *cis* compartments, respectively; R, T and F have their usual meanings.

In all the experiments that were performed, the conductance and capacitance of each membrane were tested by applying a voltage of ±200 mV for 10–15 min under stirring, to ensure that the membrane was stable. In all sets of experiments, the initial applied voltage was 80 mV and, if the channel insertion did not occur within 1 h, it was increased step by step until the first channel-like activity appeared (activation voltage and activation time). Then, the voltage could be lowered or increased and the voltage dependence studied at different voltage values. Results are expressed as means ± SE. Statistical significance was assessed using Students' *t*-tests.

RESULTS

Isolation and Purification of Kisspер

Ripe kiwi fruits were peeled and washed, and then homogenized in water (1 : 1, mass/vol). The pH of the homogenate was 3.5. After centrifugation at 10 400*g* for 20 min, the supernatant, representing the soluble fraction, was collected. Large proteins were precipitated with 0.1% TFA, at 0–4 °C for 30 min, and then removed by centrifugation at 12 100*g* for 20 min. An aliquot of the supernatant was analyzed by reverse-phase HPLC, as described under Materials and Methods, and the *N*-terminal amino acid sequence of several collected fractions was established by automated sequencing. Upon comparative analysis, one of the components (kisspер) showed the same *N*-terminal sequence of

DOI: 10.1002/psc

kiwellin [17], the kiwi fruit allergenic protein previously isolated and characterized.

In order to purify larger amounts of kissper, the supernatant obtained upon precipitation of the soluble fraction with TFA was dialyzed in 3500 Da MW cut-off tubings against 10 mM Tris-HCl, pH 8.0, and then loaded on a DE52 column (2.5 × 18 cm), equilibrated in the same buffer. The column was eluted with 0.5 M NaCl in the equilibrating buffer, and aliquots of the collected fractions were analyzed by reverse-phase HPLC. The fractions containing kissper were dialyzed against 10 mM Tris-HCl, pH 8.0, and then loaded on a Mono-Q HR 10/10 column, equilibrated in the same buffer. The column was eluted by a linear gradient from 0 to 0.3 M NaCl. The fractions from Mono-Q were analyzed by reverse-phase HPLC, and those containing kissper were concentrated by ultrafiltration. If needed, kissper was additionally purified to homogeneity by reverse-phase HPLC. Up to 3 mg of pure peptide was obtained from 300 g of ripe kiwi fruits.

Amino Acid Sequence

N-Terminal amino acid sequencing of kissper proceeded for 30 residues. After denaturation and alkylation of the sulfhydryl groups, kissper was digested with trypsin as described earlier, and the resulting peptides were analyzed by reverse-phase HPLC. The peaks were collected manually, vacuum-dried, redissolved in 0.1% TFA containing 20% acetonitrile and sequenced. The sequence established by alignment of the tryptic peptides with the sequence obtained from the *N*-terminus of intact kissper and with the sequence of kiwellin [17] corresponded to a 37-residue peptide, with Arg at the *C*-terminus, and accounting for a molecular weight of 3992.5 Da, whereas that obtained by MALDI-TOF mass spectrometry was 4154 Da. However, as shown in more detail below, this apparent contradiction was resolved by NMR analysis, since in the 2D spectra we were able to clearly identify the spin systems of 39 residues, including Gly38 and Thr39, following Arg37 in the primary structure of kiwellin and kissper, that were lost in the HPLC purification subsequent the trypsin cleavage. The molecular weight calculated for the complete sequence, containing 39 amino acid residues (Figure 1), was 4150.6 Da, in good agreement with that obtained by MALDI-TOF mass spectrometry. The amino acid sequence of kissper contained six cysteine residues and only one aromatic residue (His34).

Homology searches were carried out by using the Fasta3 Program. Search in the UniProt Data Bank showed the highest identity (69%) with the *N*-terminal region of both the putative kiwellin from potato leaves (UNIPROT accession number Q2HPL5) and the cDNA-derived sequence of Grip 22 from grape [32]. Search in the Swiss-Prot Data Bank, carried out using default parameters, showed from 31 to 47% sequence identities

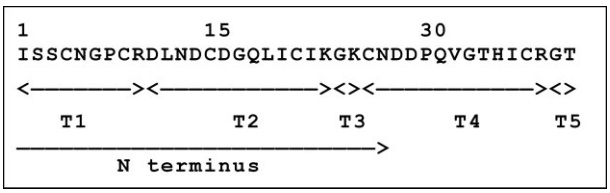

Figure 1 Amino acid sequence of kissper. The tryptic peptides (T1–T5) and the sequence portion elucidated by automated Edman degradation from the *N*-terminus are indicated below the sequence.

with the corresponding overlapping regions of several peptides and of small, as well as large, proteins (Figure 2) having a variety of functions, such as toxins (from scorpion, mollusc, snake and spider), protease inhibitors and other proteins containing the EGF-like cysteine-rich motif [33], including fibrillin, transforming growth factor and thrombomodulin.

Chemical Characterization of Disulfide Bridges

Digestion of 8 μg of native kissper was attempted (i) dissolving the sample in 20 μl of 5% formic acid, and incubating with pepsin at an enzyme : peptide ratio of 1 : 25 (w : w) at 37 °C for 2 h, and (ii) dissolving the sample in 20 μl of 1% ammonium bicarbonate, and incubating with trypsin at an enzyme : peptide ratio of 1 : 20 (w : w) at 37 °C for 2 h. Both hydrolysates were analyzed by reverse-phase HPLC, where the sample was eluted in a single peak at the same retention time of kissper, and by amino acid sequencing, where only the *N*-terminal sequence of kissper was observed. Therefore, the two digestions were ineffective.

Following an alternative strategy, an aliquot of kissper (16 μg) was dissolved in 50 μl of 70% formic acid, and incubated at 42 °C for 20 h to specifically cleave the Asp28-Pro29 bond of the sequence. After incubation, HPLC analysis (carried out as described earlier) showed only one peak, eluted at 26.7 min (not shown), whereas two amino acid sequences were determined, one proceeding from the *N*-terminal Ile and another proceeding from Pro29, in a molar ratio of 2 : 1, respectively, indicating that only 50% of kissper had been cleaved. After drying under vacuum, the sample was redissolved in water and dried again two times, in order to remove the residual acid, and then incubated with trypsin, as described above, for 5 h. Two peaks were obtained upon HPLC analysis (not shown). The peptide eluted at the retention time 26.7 min contained only the *N*-terminal amino acid sequence of kissper, whereas the one eluted at 27.3 min contained three sequences, proceeding from Ile1, Gly23 and Pro29, respectively. This result suggests that only the sample previously cleaved by the acidic treatment could be hydrolyzed by trypsin. The sample eluted at 27.3 min was successively dried under vacuum, and then incubated with pepsin, as

DOI: 10.1002/psc

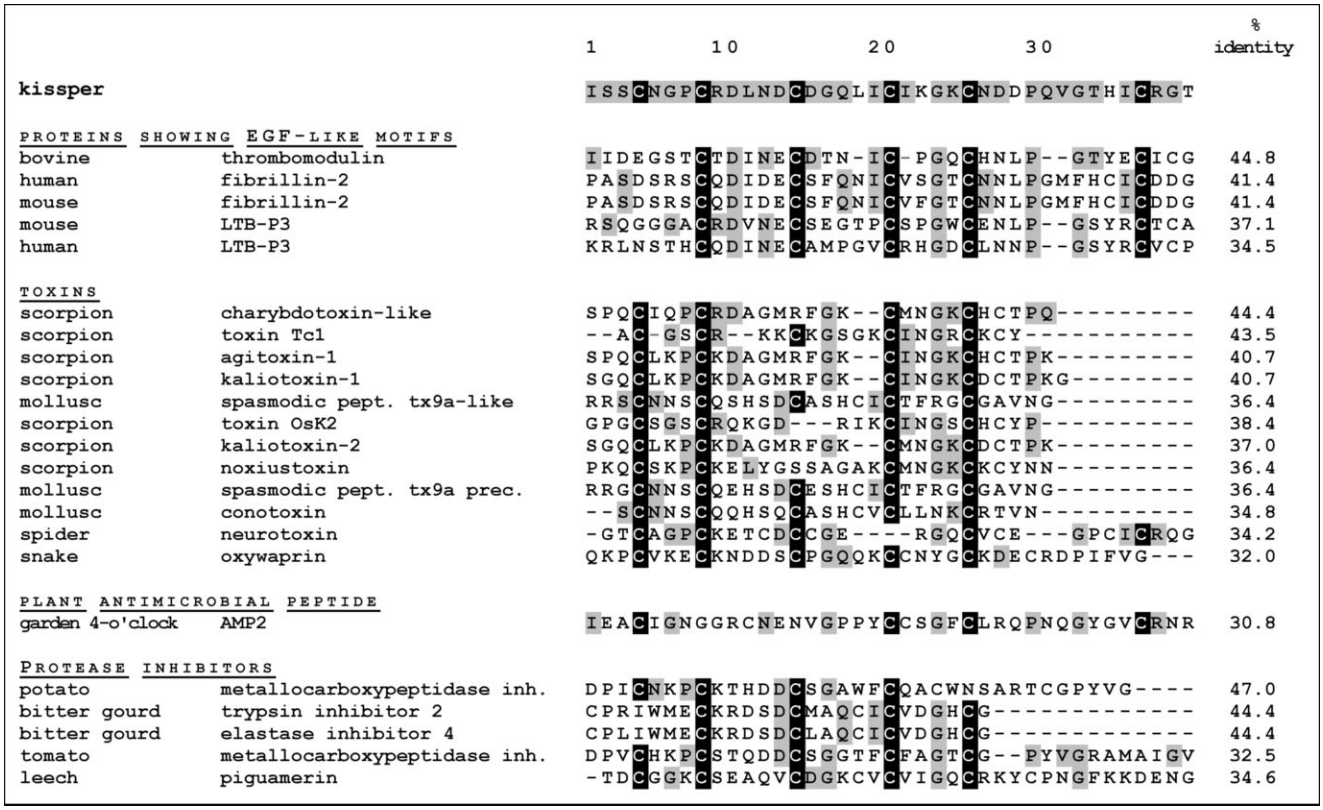

Figure 2 Alignment of the amino acid sequence of kissper with those of the most similar peptides and proteins available in the Swiss-Prot Data Bank, identified by the Fasta3 program. The cysteine residues of kissper conserved in other sequences are black-shadowed; other conserved residues are grey-shadowed. Accession numbers are the following: bovine thrombomodulin, P06579; human fibrillin-2 precursor, P35556; mouse fibrillin-2 precursor, Q61555; mouse latent transforming growth factor β-binding protein 3 precursor, Q61810; human latent transforming growth factor β-binding protein 3 precursor, Q9NS15; scorpion charybdotoxin-like peptide, P59886; scorpion toxin Tc1, P83243; scorpion agitoxin-1, P46110; scorpion kaliotoxin-1, Q9NII7; mollusc spasmodic peptide tx9a-like precursor, Q9GU57; scorpion toxin OsK2, P83244; scorpion kaliotoxin-2, P45696; scorpion noxiustoxin, P08815; mollusc spasmodic peptide tx9a precursor Q9GU58; mollusc conotoxin, P83390; spider neurotoxin PRTx32C1, P83904; snake oxywaprin, P83952; garden 4 o'clock antimicrobial peptide 2, P25404; potato metallocarboxypeptidase inhibitor, P01075; bitter gourd trypsin inhibitor 2, P10295; bitter gourd elastase inhibitor 4, P10296; tomato metallocarboxypeptidase inhibitor, P01076; leech piguamerin, P81499.

described above, for 20 h. Four peaks were obtained upon HPLC analysis (not shown). Both the peptides eluted at the retention times 26.9 and 27.4 min showed a single molecular mass in agreement with that derived from the entire sequence of kissper. The sample eluted at 25.2 min showed a single molecular mass of 1680 Da, and two amino acid sequences proceeding from Leu11 to Leu18 and from Gly23 to Asp28, respectively. This result allowed to clearly identify the disulfide bridge established between Cys14 and Cys25. The sample eluted at 25.9 min showed a single molecular mass of 2415 Da, and three amino acid sequences proceeding from Ile1 to Asp10, from Ile19 to Lys22 and from Pro29 to Arg37, respectively. This result (i) excluded disulfide bridges between Cys4 and Cys8 and between Cys20 and Cys36, and (ii) suggested two alternative disulfide bridge patterns, i.e. Cys4–Cys20/Cys8–Cys36 and Cys4–Cys36/Cys8–Cys20.

Solution Structure and Disulfide Bridges Connectivity

A conformational study was carried out by 2D NMR spectroscopy in a phosphate buffer solution at pH 3.5, i.e. at a pH value very close to that of both unripe and ripe kiwi fruit. Almost all proton signals were well resolved in the TOCSY experiment, but the β protons of the five aspartate, the three asparagine and the six cysteine residues were in a crowded spectral region. To overcome this problem, TOCSY, NOESY and ^{1}H-^{15}N-HNSQC spectra were acquired at different temperatures. Spin system identification of individual resonances and sequence specific assignment of kissper were carried out by the usual combination of TOCSY, DQF-COSY and NOESY spectra, according to the standard procedure [34]. The good dispersion of the NH chemical shifts, which can be diagnostic of the presence of nonrandom structures in solution, is well evident in the ^{1}H-^{15}N-HSQC spectrum reported in Figure 3(a) with the assignment of all amide resonances.

DOI: 10.1002/psc

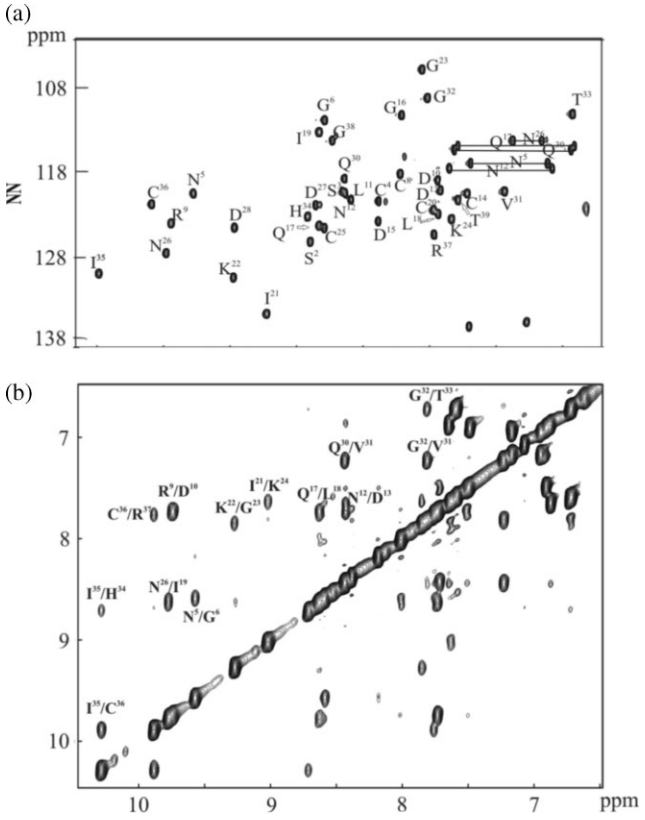

Figure 3 (a) ^{1}H-^{15}N HSQC spectrum of natural abundance 0.4 mM kissper in 25 mM phosphate buffer pH 3.5. Labels represent assignments for the cross peaks. The side chain -NH_2 amide protons of asparagine and glutamine residues are connected through horizontal lines. (b) Amide region of the 300 ms mixing time NOESY spectrum at 600 MHz on the sample of panel a. Cross peak labels identify inter-residue NOEs.

The proton assignment, reported in Table 1, was 97% complete, the missing resonances corresponding to Pro29 that could not be identified in the TOCSY or in the NOESY experiments, due to the strong overlap of resonances. The low field region of the NOESY spectrum with labeling of NH–NH connectivities is reported in Figure 3(b).

The careful analysis of NOESY data indicated that the peptide is characterized by the presence of multiple conformations, with almost all sequential $d_{NN}(i, i+1)$, typical of helical structures, alternated with strong $d_{\alpha N}(i, i+1)$, characteristic of extended structures. Nevertheless, the presence of several long-range effects, such as two d_{NN} involving residues 21–24 and 19–26, as well as a $d_{\alpha N}$ between residues 25–19 is consistent with the presence of a β-hairpin with the two short β-strands encompassing Ile19–Ile21 and Lys24–Asn26, connected through a central loop centered on Lys22–Gly23. Moreover, sequential $d_{NN}(i, i+1)$ in the *C*-terminal region in combination with $d_{NN}(i, i+2)$ and $d_{\alpha\beta}$ $(i, i+3)$, are indicative of a short helical stretch encopassing residues 32–35.

To define a plausible structure of kissper in aqueous environment, and also to facilitate the assignment of ambiguous NOE cross-peaks, preliminary structure calculations were performed with the DYANA package. A total of 237 upper distance limits were derived from the cross-peaks integrals of the NOESY spectrum at 300 ms mixing time, and five $^{3}J_{NH-\alpha CH}$ coupling constants values were extracted directly from the 1D proton spectrum, due to the good resolution of the related amide resonances.

Eighty structures were calculated from the refined list of structural constraints excluding disulfide bridges and dihedral angles constraints. As already described, the chemical characterization of disulfide bridges in kissper peptide allowed only the identification of a Cys14–Cys25 bridge. Since the Cys4–Cys8 and Cys20–Cys36 bridges were also excluded on the basis of biochemical data, to elucidate the two remaining disulfide bridges we repeated structural calculations considering all possible combinations of the remaining cysteine residues, i.e. either Cys4–Cys20/Cys8–Cys36 and Cys4–Cys36/Cys8–Cys20, keeping fixed the Cys14–Cys25 bridge. The best 20 structures, in terms of both target function and constraint violations, correspond to the disulfide bridges Cys4–Cys36 and Cys8–Cys20. However, on the basis of this preliminary NMR study, the alternative combination cannot be excluded. Figure 4 shows a representative structural model of kissper, with the secondary structure elements and the 4–36, 8–20 and 14–25 disulfide bridges pattern, as visualized by the program MOLMOL [35].

Insertion of Kissper into POPC and DOPS : DOPE : POPC PLM and Channel-Like Activity

In order to analyze the ability of kissper to induce ion conductance, PLMs of POPC and of DOPS : DOPE : POPC were used. Furthermore, the incorporation and pore formation of kissper as a function of pH were investigated in POPC PLM.

In five different experiments in POPC PLM, the addition of 0.04 μg/ml (10 nmol/l) of kissper to the *cis* side of the medium (KCl 1 M, pH 7.0) facing the membrane did not produce any conductance variation for a long period of time (>24 h), upon application of voltage as high as 140 mV (Figure 5(a)). In contrast, in experiments carried out at pH 3.5, step-like variations in membrane current compatible with single channel activity, were manifested in short time (about 13 min) when a constant voltage of 40 mV was applied to the membrane. This result was confirmed in new experiments carried out initially at pH 7.0, then lowering the pH to 3.5 by addition of a small amount of concentrated HCl solution, checking the pH during and at the end of the experiments.

Under all the responsive potentials tested, we observed alternating periods of bursting channel

DOI: 10.1002/psc

Table 1 Proton chemical shift values of 0.4 mM kissper in 25 mM phosphate buffer (in 90% H_2O, 10% ^2H_2O), at pH 3.5 and 300 K. The figures in square brackets report the ^{15}N chemical shifts of backbone amide nitrogens

Residues	HN [HN]	HC_α	HC_β	HC_γ	HC_δ	Others
Ile[1]	—	3.84	1.77	1.32–1.13	0.77	—
Ser[2]	8.69 [120.2]	4.68	4.09–3.63	—	—	—
Ser[3]	8.44 [114.4]	4.40	3.80	—	—	—
Cys[4]	8.18 [115.5]	3.80	2.73–2.80	—	—	—
Asn[5]	9.57 [114.5]	4.18	2.97	—	—	7.49–6.90
Gly[6]	8.59 [106.1]	3.58–4.39	—	—	—	—
Pro[7]	—	4.80	2.16–1.81	—	—	—
Cys[8]	8.02 [112.3]	4.65	3.13–2.95	—	—	—
Arg[9]	9.74 [118.0]	4.26	1.58	1.75	3.10	7.50
Asp[10]	7.73 [113.2]	4.22	2.74–2.88	—	—	—
Leu[11]	8.39 [114.4]	3.78	1.95–1.67	1.57	0.85	—
Asn[12]	8.43 [115.3]	4.70	2.73–2.84	—	—	7.65–6.88
Asp[13]	7.71 [114.2]	4.72	3.09–2.73	—	—	—
Cys[14]	7.51 [114.7]	5.11	2.52–2.73	—	—	—
Asp[15]	8.18 [117.8]	4.32	2.38	—	—	—
Gly[16]	8.01 [105.5]	3.68	—	—	—	—
Gln[17]	8.63 [118.4]	4.21	1.86	2.22	—	7.58–6.71
Leu[18]	7.75 [117.0]	4.20	1.79	1.15	0.65–0.48	—
Ile[19]	8.63 [107.4]	4.58	1.65	1.09–0.82	0.82	—
Cys[20]	7.76 [116.6]	4.67	2.74–2.16	—	—	—
Ile[21]	9.02 [128.6]	4.13	1.65	1.35–0.81	0.81	—
Lys[22]	9.28 [124.4]	3.70	1.90	1.34	1.72	—
Gly[23]	7.85 [100.1]	3.92	—	—	—	—
Lys[24]	7.63 [117.7]	5.21	1.58	1.10	1.33	—
Cys[25]	8.59 [118.6]	5.17	2.91–2.38	—	—	—
Asn[26]	9.77 [121.5]	4.90	2.68–2.48	—	—	7.17–6.95
Asp[27]	8.65 [116.0]	4.22	2.20–1.98	—	—	—
Asp[28]	9.26 [118.5]	4.62	2.49–3.03	—	—	—
Pro[29]	—	—	—	—	—	—
Gln[30]	8.44 [112.9]	4.05	2.03	2.27–2.33	—	—
Val[31]	7.23 [114.4]	3.96	2.15	0.93	—	—
Gly[32]	7.81 [103.5]	3.66–3.90	—	—	—	—
Thr[33]	6.72 [105.3]	3.98	4.20	1.06	—	—
His[34]	8.71 [117.3]	4.75	2.87–3.13	—	—	7.07–8.38
Ile[35]	10.29 [123.9]	3.70	1.91	1.51–1.09	0.76	—
Cys[36]	9.89 [115.9]	4.92	3.24–3.01	—	—	—
Arg[37]	7.76 [119.5]	4.24	1.80	1.58	3.08	7.07
Gly[38]	8.53 [108.4]	3.92	—	—	—	—
Thr[39]	7.58 [115.3]	4.06	—	1.06	—	—

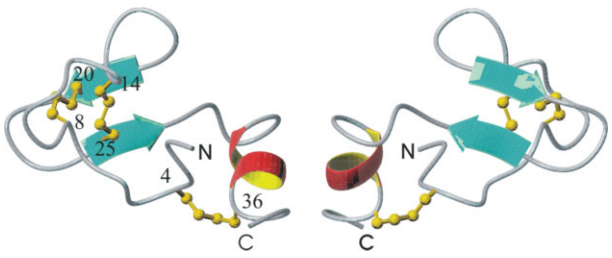

Figure 4 MOLMOL ribbon representation of a kissper solution structure as derived by structure calculations performed with DYANA package. The two models correspond to the front and rear views of the calculated structure. On the left model the labels evidence the pattern of the three disulfide bridges.

activity followed by quiescent periods in which a return of the current to the baseline was observed (Figure 5(b)). At pH 7.0, when the peptide concentration in the medium was doubled (0.08 μg/ml, corresponding to 20 nmol/l), the channel activity was elicited, in about 24 h, with an applied voltage of 80 mV, and could be registered at higher positive and negative voltages (Figure 5(c)). However, for applied voltage higher than ±120 mV the membrane, after a high rate of channel formation, resulted destabilized. In the same experimental conditions, but at pH 3.5, the channel activity was triggered by a lower applied potential (20 mV) and arised in a shorter time (about 9 min).

DOI: 10.1002/psc

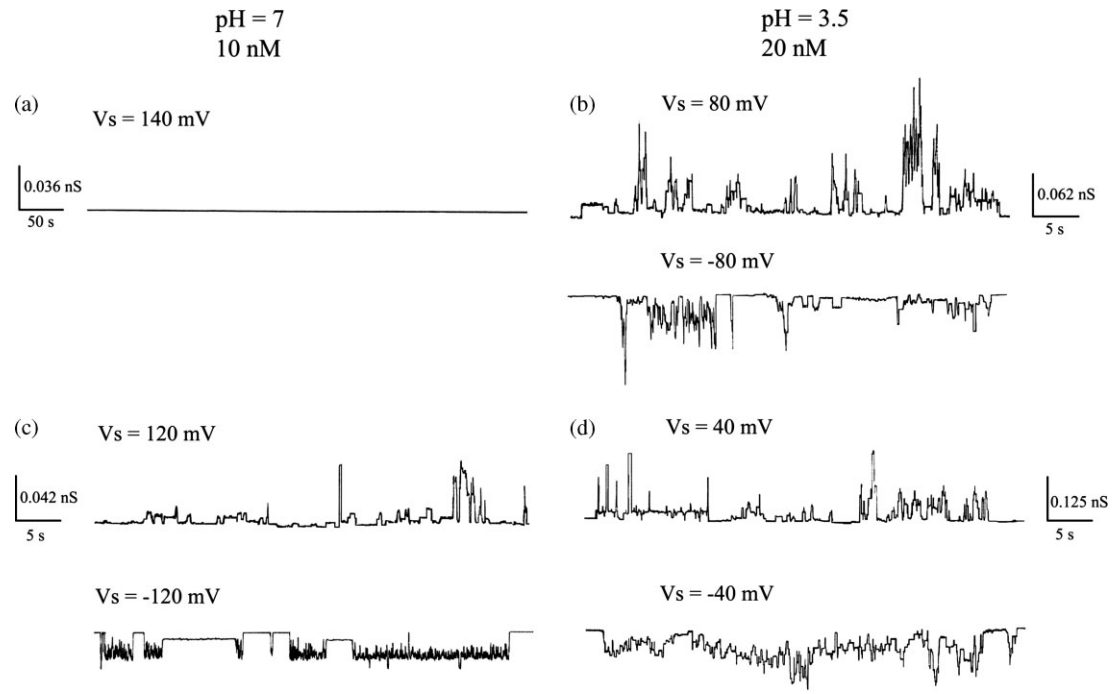

Figure 5 Chart recordings of kissper channel formation in POPC PLM at different pH values of the medium (a and c, pH = 7.0; b and d, pH = 3.5), at various holding potential (indicated on the top of the tracing), and at different kissper concentrations (a and b, 0.04 μg/ml; c and d, 0.08 μg/ml). Channel opening and closing are represented by upward/downward (for positive applied voltage) or downward/upward (for negative applied voltage) deflections, respectively. Each trace represents a fragment of the recorded activity obtained in individual experiments at different times. Experimental conditions: 1 M KCl; kissper was present on the *cis* side of the membrane; temperature was 22 °C.

Furthermore, in these conditions the channel activity was paroxystic and even at low potential the count of the total number of single-channel-like events was difficult (Figure 5(d), −40 mV). An increasing in the potential resulted in an irreparable destabilization of the membrane.

In order to test the effect of membrane composition upon kissper incorporation and channel-like activity, a PLM made up of DOPS : DOPE : POPC (27 : 27:18, w : w : w) was used. This membrane is characterized by the presence of the net negative charge of DOPS and of the neutral DOPE, a nonlamellar-forming lipid. Experiments carried out by using DOPS : DOPE : POPC PLM at pH 7.0, upon addition of 0.04 μg/ml of kissper on the *cis* side, showed channel-like activity when a constant voltage of 80 mV was applied (Figure 6(a)). The range of channel-like activity registered was very high (from 60 to 140 mV), and the peptide addition stabilized the membrane even at potential values higher than 140 mV, although the conductance events were not observed. By doubling the kissper concentration (0.08 μg/ml), the voltage at which the pore-forming activity arised was lower (60 mV) and the range of channel-like activity reduced (from 20 to 60 mV and from −20 to −40 mV) (Figure 6(b)). In this case, higher positive or negative applied voltages induced a paroxystic pore-forming activity that in a short time (minutes) broke the membrane, thus precluding the possibility to calculate channel-like activity (Figure 6(c)).

All single events were used to calculate the channel amplitude. Current amplitudes analyzed in the different experiments revealed the existence of one main conductance level. The central value of the single-channel conductance ± SE was obtained by constructing a histogram of the amplitude distribution and fitting the data by a Gaussian distribution function (Figure 7).

Table 2 summarizes the results obtained under different experimental conditions and with both PLMs. In particular, the Table shows (i) the activation voltage, i.e. the lowest applied voltage that induces channel-like activity across membrane, (ii) the activation time, i.e. the time at which the first conductance variation is evident after kissper addition, (iii) the range of activity, i.e. the range of the applied voltages to detect channel-like activity, (iv) the central conductance ($\Lambda_c \pm$ SE), (v) the channel occurrence frequency, i.e. the mean number of openings in a period of 60 s, (vi) the total number of events, and (vii) the effect of kissper on membrane stability. All data are reported as a function of membrane composition, pH variation and kissper concentration. The analysis of the lifetime of the channel with the known equation [30] was difficult as the events were preponderant over the terminating events, the latter being less than 100 (minimum number of channels for an appropriate

DOI: 10.1002/psc

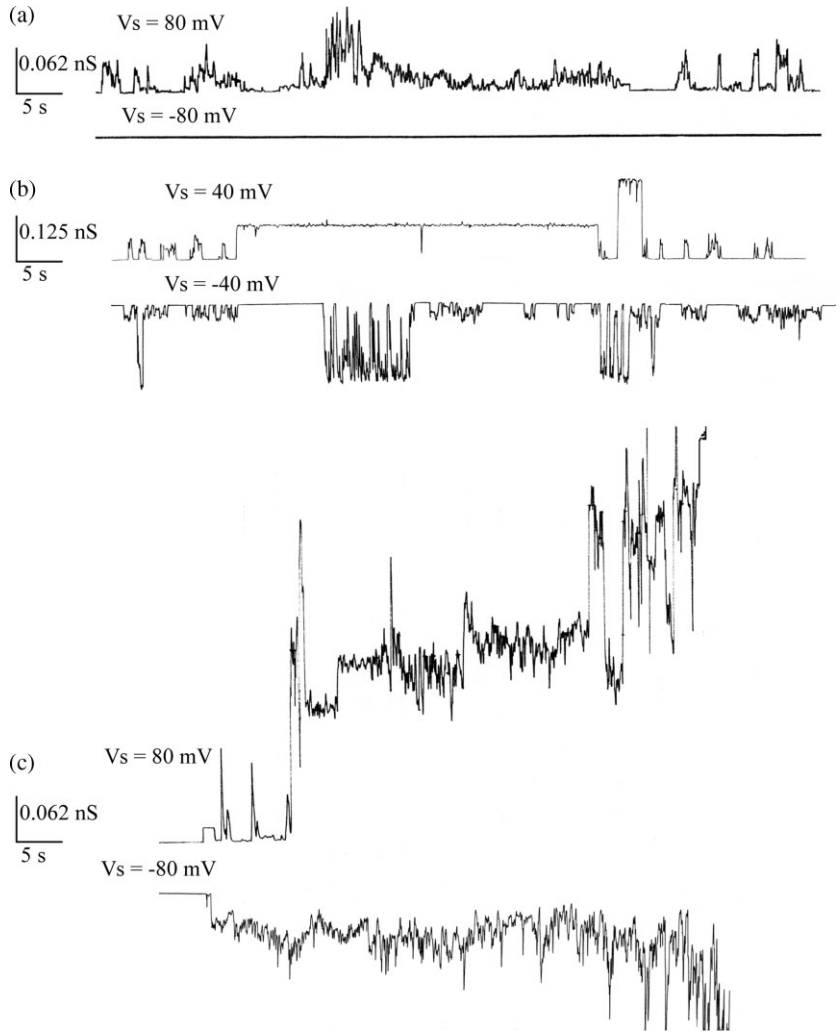

Figure 6 Chart recordings of kissper channel formation in DOPS : DOPE : POPC PLM at various holding potential (indicated on the top of the tracing), and at different kissper concentrations (a, 0.04 μg/ml; b and c, 0.08 μg/ml). Channel opening and closing are represented by upward/downward (for positive applied voltage) or downward/upward (for negative applied voltage) deflections, respectively. Each trace represents a fragment of the recorded activity obtained in individual experiments at different times. Experimental conditions: 1 M KCl; kissper was present on the *cis* side of the membrane; pH 7.0; temperature was 22 °C.

statistics). However, the duration of the observed channels, although variable (see Figures 5 and 6), and despite the different PLMs, pH or kissper concentration used, was within a similar lifetime range (from 0.85 to 15.75 s).

It can be observed that the kissper channel-like activity can be affected by both PLM composition and pH conditions. In all the experimental conditions used, kissper channel conductance resulted potential-dependent, independently of both the pH value of POPC PLM and the membrane composition (Figure 8).

In POPC PLM (at different pH values) and in DOPS : DOPE : POPC PLM (at pH 7.0), the ion selectivity of the channel was determined in asymmetrical conditions, i.e. in the presence of a salt gradient. At zero current value, the voltage difference represents the reversal potential. Approximately the same result was obtained with I–V curve, where the measured amplitude of the channel events at each membrane potential was used to calculate the reversal potential. In this case for kissper channels in POPC PLM at pH 7.0 and 3.5, in an asymmetrical condition of KCl concentration of 1.5–0.3 M and 1.5–1.0 M *cis*/*trans* side respectively, the reversal potential was 5.76 and 5.38 mV, giving, by using the Goldman-Hodgkin-Katz equation, a calculated P_{K^+}/P_{Cl^-} of 0.71 and 0.31, respectively. In DOPS : DOPE : POPC membrane, in an asymmetrical concentration of KCl of 1.0–0.5 M *cis*/*trans* at pH 7.0, the reversal potential of kissper channel was 6.24 mV giving a calculated P_{K^+}/P_{Cl^-} of 0.47.

DISCUSSION

Kissper is a 39-residue peptide isolated in good yield from the edible part of kiwi fruit, whose amino acid

DOI: 10.1002/psc

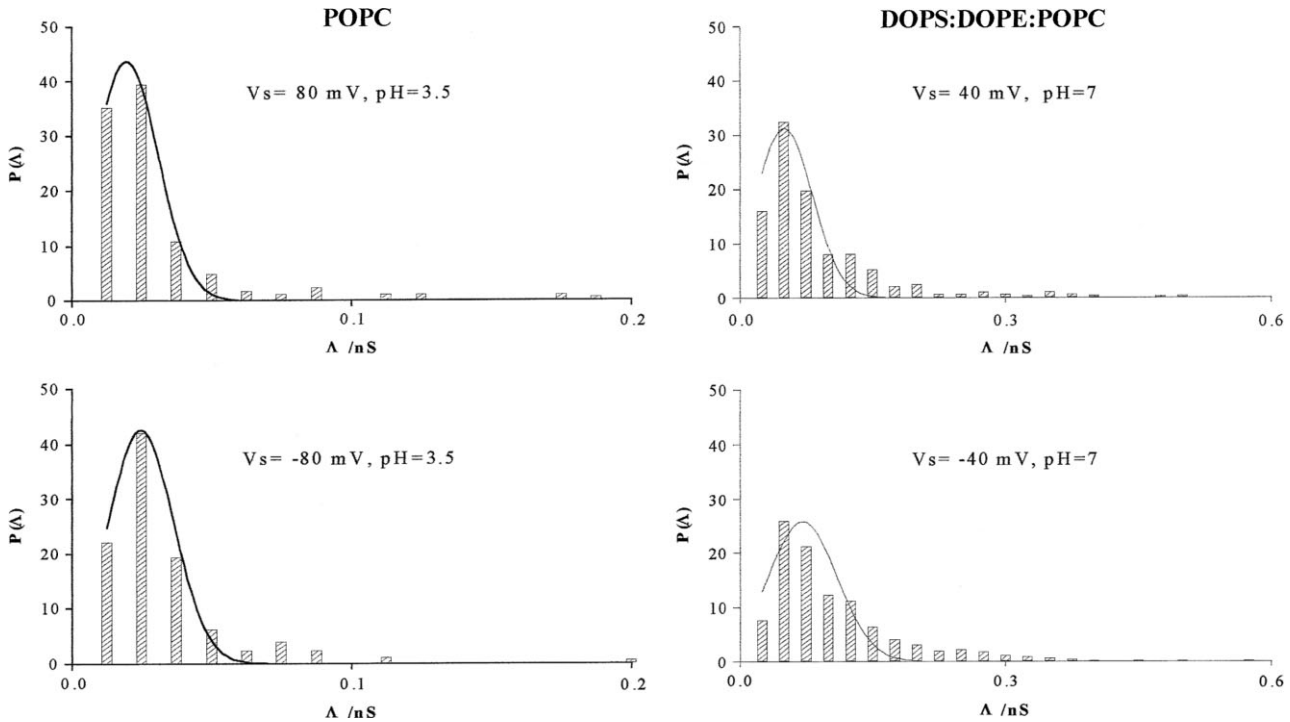

Figure 7 Amplitude histograms of kissper channel conductance relative to the experiments reported in Figures 5 and 6. The histogram of the probability [P(Λ)] for the occurrence of a given conductivity unit was fitted by a Gaussian, which is shown as a solid curve.

sequence showed 100% identity with the first 39 residues of the *N*-terminal region of kiwellin, the allergenic protein previously isolated from the same source and characterized [17]. Therefore, it may be hypothesized that kissper derives from the processing of the precursor kiwellin, through the cleavage of the peptide bond between Thr39 and Thr40.

Kissper, as well as the entire sequence of the precursor kiwellin, has a very high identity with the putative kiwellin from potato leaves (UNIPROT accession number Q2HPL5), and the cDNA-derived sequence of the hypothetical protein Grip22 from grape [32], whose mRNA is differentially expressed during fruit ripening. However, no information about the function of kiwellin and both the homologous proteins from grape and potato is so far available.

Homology search and comparative analysis of fold prediction showed a rather low structural similarity of kissper with other peptides and proteins with known function. However, kissper showed a cysteine pattern similar to those observed in proteins and peptides displaying the so-called EGF-like cysteine-rich motif [33], such as mammalian fibrillins, scorpion, snake and insect toxins, human endothelins, protease inhibitors, and antimicrobial peptides. Four or five cysteine residues out of the six of kissper sequence are indeed conserved in peptides and proteins belonging to these classes. Literature reports describe structural similarities between polypeptides showing the EGF-like motif and plant pore-forming peptides, including thionins and defensins, which are involved in defence mechanisms against pathogens [6,8,36].

The observation that most of these polypeptides display their function by interacting with membrane lipids or proteins [6,33,37,38] suggested a possible similar action mechanism for kissper. Attempts to test the kissper channel blocker activity provided unclear preliminary results (data not shown). In contrast, clear results were obtained when the kissper capacity to permeabilize synthetic membranes was tested. In fact, reconstitution of kissper in PLMs of both POPC, an ubiquitary plasma membrane phospholipid, and DOPS : DOPE : POPC, a surrogate of intestinal membrane, revealed peptide incorporation and channel-like activity. However, PLM composition affected the pore-forming activity that also showed concentration and voltage dependence. In both PLM systems tested, anion selectivity was observed. Kissper showed efficient incorporation into PLMs and ion channeling at concentration values generally lower than those reported for several pore-forming peptides, such as defensins, thionins, cecropins, cryptidin, duramycin, etc [39–43]. Furthermore, the channel-like activity of kissper was markedly affected by pH conditions. At neutral pH values, the ion transport was observed only within a limited range of experimental conditions. In contrast, under acidic pH conditions, in POPC PLM the channel-like activity was more efficient and the ion transport occurred even at voltage and peptide concentration ineffective at neutral pH. Furthermore,

DOI: 10.1002/psc

Table 2 Planar lipid membrane observations on kissper

PLM pH	Kissper (μg/ml)	Activ. voltage (mV)	Activ. time(min)	Range of activity (mV)	Λ_c at 80 mV (nS ± SE)	Lifetime channels (sec)	Occur. (even./min) ± SD	N events	Effect on membrane stability
POPC 3.5	0.04	40	13	±40 ÷ ±100	0.02 ± 0.0007	0.75 ÷ 12.2	0.96 ± 0.07	165	Unstable for Vs > ± 100 mV
POPC 7.0	0.08	80	1440	±60 ÷ ±120	0.025 ± 0.001	0.75 ÷ 17.2	1.77 ± 0.14	167	Unstable for Vs > ± 120 mV
POPC 3.5	0.08	20	9	±40 ÷ ±80	0.024 ± 0.001	0.75 ÷ 18.7	5.26 ± 0.03	367	Unstable for Vs > ± 80 mV
DOPS : DOPE : POPC 7.0	0.04	80	11	+60 ÷ +140	0.019 ± 0.001	0.75 ÷ 16.7	1.73 ± 0.11	255	Stable for Vs > ± 140 mV
DOPS : DOPE : POPC 7.0	0.08	60	180	+20 ÷ +60 − 20 ÷ −40	0.054 ± 0.003[a]	1.25 ÷ 13.7	2.69 ± 0.18	249	Unstable for Vs > − 40 and Vs > + 60 mV

[a] The central conductance is referred to an applied voltage of 60 mV.

at low pH the anion selectivity of the pores became much more marked.

It is worth recalling that an acidic-pH dependence of cytotoxicity and, in particular, of *in vitro* channel-forming activity has been described for other peptides [44,45] and for large toxins or toxin-like molecules [46–48]. A low-pH activation has been reported, for example, for bacteriocins, such as the *Escherichia coli* colicin E1, for the diphtheria, anthrax and cholera toxins [49], and for *Bacillus thuringiensis* toxins [50]. The acidic-pH dependence of these activities has been explained by assuming that the protonated state of one or more acidic amino acid side-chain(s) is a requirement for channel formation, membrane insertion and voltage gating [46]. Three aspartic residues (Asp408, Asp410, and Asp423) in the colicin E1 channel domain have been involved in critical pH-sensitive conformational transition of the activation process [49]. Intriguingly, kissper has five aspartic residues, and three of them are arranged into a Asp-Xaa-Asp-Xaa(12)-Asp pattern, similar to that observed in colicin E1. However, this hypothesis could be proved only by evaluating the effects of mutant peptides on the same processes or, alternatively, by performing an extensive characterization of the 3D structure of kissper in different environments. At the moment, we have undertaken a conformational study of this peptide in solution by 2D NMR. Preliminary results under acidic conditions (pH 3.5) in aqueous buffer and at a temperature of 300 K indicated that kissper, like many other typical disulfide-rich small proteins [51], shows a quite flexible 3D structure, despite the presence of the conformational constraints imposed by three disulfide

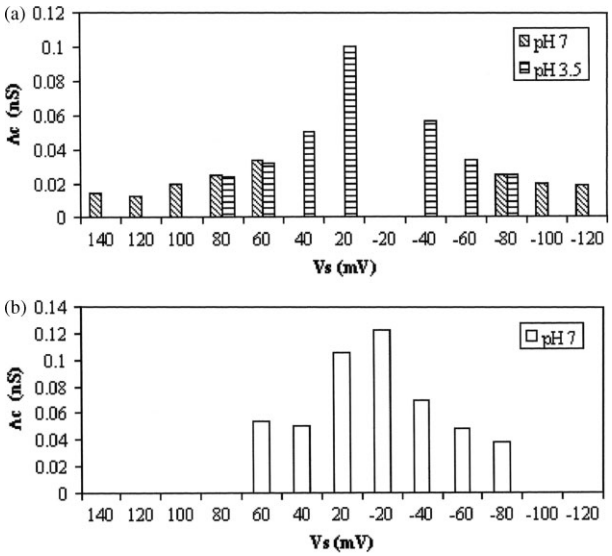

Figure 8 Conductance–voltage relationship for kissper channels at pH 7.0 and pH 3.5 in POPC (a) and at pH 7.0 in DOPS : DOPE : POPC (b) PLM. Experimental conditions: 1 M KCl; 0.08 μg/ml kissper, present on the *cis* side of POPC membrane; temperature was 22 °C.

DOI: 10.1002/psc

bridges involving the six cysteine residues, with only a small amount of regular secondary structure. A careful analysis of the NMR derived structures allowed the identification of a sizeable amount of molecules with short secondary structure elements that can be described as a short antiparallel β-sheet encompassing residues 19–21/24–26 and a short helix spanning residues 32–35. We believe that this helical stretch is unable to span a bilayer to form channels, for which perhaps an aggregate of molecules is necessary. However, a model for kissper pore structure cannot be described in the light of the existing data. For this purpose, it will be necessary to perform extensive characterization of kissper 3D structure under different biomimetic conditions.

The comparative analysis of the structural and functional properties of kissper suggested that, despite the similarities observed with a variety of large and small toxins and, in general, with proteins containing the EGF-like motif, it cannot be included in any of the known peptide families. Plant thionins, for instance, are cationic peptides of 45–54 residues, with eight conserved cysteine residues forming four intramolecular disulfide bridges [7,52] and with a typical 3D structure characterized by the so-called cysteine-stabilized $\alpha\beta$ motif [53], i.e. a triple-stranded antiparallel β-sheet connected to an α-helix through a disulfide bridge. Moreover, α-defensins, which have the same I–VI, II–IV, III–V cysteine pairing proposed for kissper, show a different size of the Cx_nC segments, are smaller than kissper, cationic, and are characterized by triple-stranded antiparallel β-sheet structures [54].

Kissper is a small, anionic, cysteine-rich member of a new family of peptides with pH-dependent and voltage-gated pore-forming activity, characterized by anion selectivity and channeling. Beyond the physiological role in the plant cell, the capacity of this food peptide to form channel-like pathways in a lipid bilayer, whose composition is similar to that found in intestinal cells, suggests potential biological effects on human health. The high amount of kissper found in ripe kiwi fruit and its strong resistance to proteolysis suggest that it could very likely affect the gastrointestinal physiology. In perspective, experiments on isolated intestinal tissue and, possibly, *in vivo* studies, will allow the characterization of the local and of possible systemic effects of kissper.

Furthermore, kissper functional properties suggest a potential pharmacological use of this peptide as it is or after appropriate modifications, for the treatment of pathologies involving nonoptimal ion transport mechanisms. For example, defective anion channels have been related to many pathologies, such as cystic fibrosis [55–57], for which channel replacement therapy has been proposed as a possible treatment [43]. In this context, peptides forming anionic channels may assume physiological relevance for the biological functions related to the ionic balance through the cell.

Acknowledgements

This work received financial support from MIUR (FIRB RBNE03B8KK).

REFERENCES

1. Roberfroid MB. Concepts in functional foods: the case of inulin and oligofructose. *J. Nutr.* 1999; **129**: 1398S–1401S.
2. Rutherfurd-Markwick KJ, Moughan PJ. Bioactive peptides derived from food. *J. AOAC Int.* 2005; **88**: 955–966.
3. Hartmann R, Meisel H. Food-derived peptides with biological activity: from research to food applications. *Curr. Opin. Biotechnol.* 2007; **18**: 163–169.
4. Eastwood MA. A molecular biological basis for the nutritional and pharmacological benefits of dietary plants. *Q. J. Med.* 2001; **94**: 45–48.
5. Kitts DD, Weiler K. Bioactive proteins and peptides from food sources. Applications of bioprocesses used in isolation and recovery. *Curr. Pharm. Des.* 2003; **9**: 1309–1323.
6. Froy O, Gurevitz M. Membrane potential modulators: a thread of scarlet from plants to humans. *FASEB J.* 1998; **12**: 1793–1796.
7. Almeida MS, Cabral KMS, Kurtenbach E, Almeida FCL, Valente AP. Solution structure of Pisum sativum defensin 1 by high resolution NMR: plant defensins, identical backbone with different mechanisms of action. *J. Mol. Biol.* 2002; **315**: 749–757.
8. Anaya-Lopez JL, Lopez-Meza JE, Baizabal-Aguirre VM, Cano-Camacho H, Ochoa-Zarzosa A. Fungicidal and cytotoxic activity of a Capsicum chinense defensin expressed by endothelial cells. *Biotechnol. Lett.* 2006; **28**: 1101–1108.
9. Motohashi N, Shirataki Y, Kawase M, Tani S, Sakagami H, Satoh K, Kurihara T, Nakashima H, Mucsi I, Varga A, Molnar J. Cancer prevention and therapy with kiwifruit in Chinese folklore medicine: a study of kiwifruit extracts. *J. Ethnopharmacol.* 2002; **81**: 357–364.
10. Collins AR, Harrington V, Drew J, Melvin R. Nutritional modulation of DNA repair in a human intervention study. *Carcinogenesis* 2003; **24**: 511–515.
11. Jung K-A, Song T-C, Han D, Kim I-H, Kim Y-E, Lee C-H. Cardiovascular protective properties of kiwifruit extracts in vitro. *Biol. Pharm. Bull.* 2005; **28**: 1782–1785.
12. Rush EC, Patel M, Plank LD, Ferguson LR. Kiwifruit promotes laxation in the elderly. *Asia Pac. J. Clin. Nutr.* 2002; **11**: 164–168.
13. Gavrovic-Jankulovic M, Cirkovic T, Vuckovic O, Atanaskovic-Markovic M, Petersen A, Gojgic G, Burazer L, Jankov RM. Isolation and biochemical characterization of a thaumatin-like kiwi allergen. *J. Allergy Clin. Immunol.* 2002; **110**: 805–810.
14. Pastorello EA, Conti A, Pravettoni V, Farioli L, Rivolta F, Ansaloni R, Ispano M, Incorvaia C, Giuffrida MG, Ortolani C. Identification of actinidin as the major allergen of kiwi fruit. *J. Allergy Clin. Immunol.* 1998; **101**: 531–537.
15. Lucas JSA, Lewis SA, Hourihane JOB. Kiwi fruit allergy: a review. *Pediatr. Allergy Immunol.* 2003; **14**: 420–428.
16. Bublin M, Mari A, Ebner C, Knulst A, Scheiner O, Hoffmann-Sommergruber K, Breiteneder H, Radauer C. IgE sensitization profiles toward green and gold kiwifruits differ among patients allergic to kiwifruit from 3 European countries. *J. Allergy Clin. Immunol.* 2004; **114**: 1169–1175.
17. Tamburrini M, Cerasuolo I, Carratore V, Stanziola AA, Zofra S, Romano L, Camardella L, Ciardiello MA. Kiwellin, a novel protein from kiwi fruit. Purification, biochemical characterization and identification as an allergen. *Protein J.* 2005; **24**: 423–429.

18. Camardella L, Carratore V, Ciardiello MA, Servillo L, Balestrieri C, Giovane A. Kiwi protein inhibitor of pectin methylesterase. Amino-acid sequence and structural importance of two disulfide bridges. *Eur. J. Biochem.* 2000; **267**: 4561–4565.
19. Ciardiello MA, Tamburrini M, Tuppo L, Carratore V, Giovane A, Mattei B, Camardella L. Pectin methylesterase from kiwi and kaki fruits: purification, characterization and role of pH in the enzyme regulation and interaction with the kiwi proteinaceous inhibitor. *J. Agric. Food Chem.* 2004; **52**: 7700–7703.
20. Schwarz S, Hostetler B, Ling S, Mone M, Waltkins J. Intestinal membrane lipid composition and fluidity during development in the rat. *Am. J. Physiol.* 1985; **248**: G200–G207.
21. Cavanagh J, Rance M. Suppression of cross-relaxation effects in TOCSY spectra via a modified DIPSI-2 mixing sequence. *J. Magn. Reson.* 1992; **96**: 670–678.
22. Jeener J, Meyer BH, Bachman P, Ernst RR. Investigation of exchange processes by two-dimensional nmr spectroscopy. *J. Chem. Phys.* 1979; **71**: 4546–4553.
23. Rance M, Sørensen OW, Bodenhausen G, Wagner G, Ernst RR, Wüthrich K. Improved spectral resolution in COSY 1H NMR spectra of proteins via double quantum filtering. *Biochem. Biophys. Res. Commun.* 1983; **117**: 479–485.
24. Bax A, Ikura M, Kay LE, Torchia DA, Tschudin R. Comparison of different modes of two-dimensional reverse correlation NMR for the study of proteins. *J. Magn. Reson.* 1990; **86**: 304–318.
25. Piotto M, Saudek V, Sklenar V. Gradient-tailored excitation for single-quantum NMR spectroscopy of aqueous solutions. *J. Biomol. NMR* 1992; **2**: 661–666.
26. Delaglio F, Grzesiek S, Vuister G, Zhu G, Pfeifer J, Bax A. NMRPipe: A multidimensional spectral processing system based on UNIX pipes. *J. Biomol. NMR* 1995; **6**: 277–293.
27. Johnson BA, Blevins RA. NMR View: a computer program for the visualization and analysis of NMR data. *J. Biomol. NMR* 1994; **4**: 603–614.
28. Wishart DS, Bigam CG, Yao J, Abildgaard F, Dyson HJ, Oldfield E, Markley JL, Sykes BD. 1H, 13C and 15N chemical shift referencing in biomolecular NMR. *J. Biomol. NMR* 1995; **6**: 135–140.
29. Güntert P, Mumenthaler C, Wüthrich K. Torsion angle dynamics for NMR structure calculation with the new program DYANA. *J. Mol. Biol.* 1997; **273**: 283–298.
30. Micelli S, Meleleo D, Picciarelli V, Gallucci E. Effect of sterols on beta-amyloid peptide (AbetaP 1–40) channel formation and their properties in planar lipid membranes. *Biophys. J.* 2004; **86**: 2231–2237.
31. Hill B. Selective permeability: impedence. *Ion Channels of Excitable Membranes*. Sinauer Associated, Inc. Publishers: Sunderland, MA, 2001; 441–470.
32. Davies C, Robinson SP. Differential screening indicates a dramatic change in mRNA profiles during grape berry ripening. Cloning and characterization of cDNAs encoding putative cell wall and stress response proteins. *Plant Physiol.* 2000; **122**: 803–812.
33. Oka T, Murata Y, Nakanishi T, Yoshizumi H, Hayashida H, Ohtsuki Y, Toyoshima K, Hakura A. Similarity, in molecular structure and function, between the plant toxin purothionin and the mammalian pore-forming proteins. *Mol. Biol. Evol.* 1992; **9**: 707–715.
34. Wüthrich K. *NMR of Proteins and Nucleic Acids*. Wiley: New York, 1986.
35. Koradi R, Billeter M, Wüthrich K. MOLMOL: a program for display and analysis of macromolecular structure. *J. Mol. Graph.* 1996; **14**: 51–55.
36. Pelegrini PB, Franco OL. Plant γ-thionins: Novel insights on the mechanism of action of a multi-functional class of defense proteins. *Int. J. Biochem. Cell Biol.* 2005; **37**: 2239–2253.
37. Xu CQ, Brone B, Wicher D, Bozkurt O, Lu WY, Huys I, Han YH, Tytgat J, Van Kerkhove E, Chi CW. BmBKTx1, a novel Ca2+-activated K+ channel blocker purified from the Asian scorpion Buthus martensi Karsch. *J. Biol. Chem.* 2004; **279**: 34562–34569.
38. Barona J, Batista CV, Zamudio FZ, Gomez-Lagunas F, Wanke E, Otero R, Possani LD. Proteomic analysis of the venom and characterization of toxins specific for Na+ and K+ channels from the Colombian scorpion Tityus pachyurus. *Biochim. Biophys. Acta* 2006; **1764**: 76–84.
39. Thevissen K, Ghazi A, De Sablanx GW, Brownlee C, Osborn RW, Broekaert WF. Fungal membrane responses induced by plant defensins and thionins. *J. Biol. Chem.* 1996; **21**: 15018–15025.
40. Wu M, Maier E, Benz R, Hancock REW. Mechanism of interaction of different classes of cationic antimicrobial peptides with planar bilayers and with the cytoplasmic membrane of Escherichia coli. *Biochemistry* 1999; **38**: 7235–7242.
41. Hughes P, Dennis E, Whitcross M, Llewellyn D, Gage P. The cytotoxic plant protein, b-purothionin, forms ion channels in lipid membranes. *J. Biol. Chem.* 2000; **14**: 823–827.
42. Yue G, Merlin D, Selsted ME, Lencer WI, Mafdara JL, Eaton DC. Cryptin 3 forms anion selective channels in cytoplasmic membranes of human embryonic kidney cells. *Am. J. Physiol. Gastrointest. Liver Physiol.* 2002; **282**: G757–G765.
43. Zeitlin PL, Boyle MP, Guggino WB, Molina L. A phase I trial of intranasal Moli1901 for cystic fibrosis. *Chest* 2004; **125**: 143–149.
44. Micelli S, Meleleo D, Picciarelli V, Gallucci E. Effect of pH-variation on insertion and ion channel formation of human calcitonin into planar lipid bilayers. *Front. Biosci.* 2006; **11**: 2035–2044.
45. Meleleo D, Gallucci E, Picciarelli V, Micelli S. Acetyl-[Asn^{30},Tyr^{32}]-calcitonin fragment 8–32 forms channels in phospholipid planar lipid membranes. *Eur. Biophys. J.* 2007; **36**: 763–770.
46. Shiver JW, Cramer WA, Cohn FS, Bishop LJ, de Jong PJ. On the explanation of the acidic pH requirement for in vitro activity of colicin E1. Site-directed mutagenesis at Glu-468. *J. Biol. Chem.* 1987; **262**: 14273–14281.
47. Oh KJ, Senzel L, Collier RJ, Finkelstein A. Translocation of the catalytic domain of diphtheria toxin across planar phospholipid bilayers by its own T domain. *PNAS* 1999; **96**: 8467–8470.
48. Zakharov SD, Lindeberg M, Griko Y, Salamon Z, Tollin G, Prendergast FG, Cramer WA. Membrane-bound state of the colicin E1 channel domain as an extended two-dimensional helical array. *PNAS* 1998; **95**: 4282–4287.
49. Musse AA, Merrill AR. The molecular basis for the pH-activation mechanism in the channel-forming bacterial colicin E1. *J. Biol. Chem.* 2003; **278**: 24491–24499.
50. Puntheeranurak T, Uawithya P, Potvin L, Angsuthanasombat C, Schwartz JL. Ion channels formed in planar lipid bilayers by the dipteran-specific Cry4B Bacillus thuringiensis toxin and its alpha1-alpha5 fragment. *Mol. Membr. Biol.* 2004; **21**: 67–74.
51. Harrison PM, Sternberg MJE. The disulphide beta-cross: from cystine geometry and clustering to classification of small disulphide-rich protein folds. *J. Mol. Biol.* 1996; **264**: 603–623.
52. Li S-S, Gullbo J, Lindholm P, Larsson R, Thunberg E, Samuelsson G, Bohlin L, Claeson P. Ligatoxin B, a new cytotoxic protein with a novel helix-turn-helix DNA-binding domain from the mistletoe Phoradendron liga. *Biochem. J.* 2002; **366**: 405–413.
53. White SH, Wimley WC, Selsted ME. Structure, function, and membrane integration of defensins. *Curr. Opin. Struct. Biol.* 1995; **4**: 521–527.
54. De Smet K, Contreras R. Human antimicrobial peptides: defensins, cathelicidins and histatins. *Biotechnol. Lett.* 2005; **27**: 1337–1347.
55. Du D, Sharma M, Lukacs GL. The DeltaF508 cystic fibrosis mutation impairs domain-domain interactions and arrests post-translational folding of CFTR. *Nat. Struct. Mol. Biol.* 2005; **12**: 17–25.
56. Shank LP, Broughman JR, Takeguchi W, Cook G, Robbins AS, Hahn L, Radke G, Iwamoto T, Schultz BD, Tomich JM. Redesigning channel-forming peptides: amino acid substitutions that enhance rates of supramolecular self-assembly and raise ion transport activity. *Biophys. J.* 2006; **90**: 2138–2150.
57. Gadsby DC, Vergani P, Csanady L. The ABC protein turned chloride channel whose failure causes cystic fibrosis. *Nature* 2006; **440**: 477–483.

DOI: 10.1002/psc

New perspectives in protein-based biosensors: The glucokinase from *B. stearothermophilus* and the odorant-binding protein *from C. familiaris* as probes for non-consuming analyte sensors

Irina M. Kuznetsova, Olga Povarova, Olesya Stepanenko, and Konstantin K. Turoverov[†]

Institute of Cytology, Russian Academy of Sciences, St. Petersburg, Russia

Roberta Crescenzo, Antonio Varriale, Maria Staiano, and Sabato D'Auria[‡]

Consiglio Nazionale delle Ricerche – Istituto di Biochimica delle Proteine
Via P. Castellino 111 –80131- Napoli, Italy

ABSTRACT

Glucose sensing and odorant molecules sensing are used as a models to explore the advantages and problems deriving from the use of either enzymes or odorant-binding proteins to develop stable optical biosensors. We report on a novel approach to address the problem of substrate consumption by sensors based on enzymes, namely the utilization of apo-enzymes as non-active forms of the protein which are still able to bind the substrate/ligand. We also show studies in which the isolation of an odorant-binding protein from the nose of the dog is used as non-consuming analyte probe for the realization of an integrated optical sensor.

Index terms: Biosensors, odor-binding proteins, glucose, biohazard

I. INTRODUCTION

In recent years, fluorescent sensors have been developed based upon the natural affinity and specificity between a protein and its substrate[1, 2]. Site-directed mutagenesis has allowed alterations in amino acid sequences, resulting in changes in protein binding constants and insertion of new positions for reporter group labeling. Such amino acid changes have allowed the signal transduction of the binding event to be evaluated by using a variety of physical and chemical techniques[3, 4]. In particular, optical methods of detection using fluorescence energy transfer, polarization, and solvent sensitivity have been shown to offer high signal- to-noise ratios and the potential to construct simple and robust devices[5, 6]. As a result, the use of such methods has allowed for the development of highly sensitive optical protein biosensors for a variety of analytes, including amino acids, sugars, and metabolic byproducts.

As a consequence, the modern biotechnology has resorted to the idea of using proteins and enzymes as components of sensors for biochemical analytes. The idea is to exploit the extremely wide range of selective affinities sculpted into the various proteins by biological evolution. The number of potential ligands specifically recognized by different proteins is very large and ranges from small molecules to macromolecules (including protein themselves). The advantages of using proteins as components of biosensors are many and include relatively low costs in design and synthesis, the fact that proteins are, at least in general, soluble in water, and finally, with the progresses of molecular genetics, the possibility of improving/changing some of the properties of the proteins by genetic manipulation. Many of the ligands that are

[†] email: kkt@mail.cytspb.rssi.ru

[‡] email: s.dauria@ibp.cnr.it

International Conf. on Lasers, Applications, and Technologies 2007: Environmental Monitoring and Ecological Applications; Optical Sensors in Bio, Chemical, and Engineering Technologies; and Femtosecond Laser Pulse Filamentation, edited by G. G. Matvienko, et al., Proc. of SPIE Vol. 6733, 673318, (2007) · 0277-786X/07/$18 · doi: 10.1117/12.753249

important in clinical medicine and in the food control industry are relatively small (MW up to 1000 Daltons). In these cases the enzymes appear to be the class of proteins endowed with the highest specificity and affinity. Other classes of proteins, such as receptors, transporters, antibodies etc., often present lower specificity although they offer other advantages such as the fact that they can specifically recognize a wide range of much larger ligands[7, 8].
However, a broad use of proteins as probes for the development of sensors requires that some problems be addressed. Protein stability, which is one of the problems, has been improved using a variety of protocols in the preparation of the sensor (immobilization and/or cross linking of the proteins, addition of stabilizing agents, etc.). A second approach to improve stability is the use of naturally thermostable proteins isolated from thermophilic organisms. In addition, the use of enzymes as probes for biosensors poses the additional problem of substrate consumption. One solution, adopted in the two examples reported in this article, has been the use of coenzyme-depleted enzymes (apo-enzymes) which are still able to bind the substrate, but not to transform it or use ligand binding proteins as specific probes for the target analytes.

II. THE THERMOSTABLE GLUCOKINASE FROM B. STEAROTHERMOPHILUS AS NON-CONSUMING GLUCOSE SENSOR

Close control of blood glucose is essential to avoid the long-term adverse consequences of elevated blood glucose, including neuropathies, blindness and other sequels. .Non-invasive measurements of blood glucose have been a long-standing research goal. Such a capability would immediately allow the development of a variety of devices for diabetic health care, including continuous painless glucose monitoring, control of an insulin pump, and warning systems for hyper and hypoglycemic conditions. The acute and chronic problems of diabetics and hypoglycemia can be ameliorated by continuous monitoring of blood glucose. At present the only reliable method to measure blood glucose is by a finger stick and subsequent glucose measurement, typically by glucose oxidase. This procedure is painful and even the most compliant individuals, with good understanding and motivation for glucose control, are not willing to stick themselves more than several times per day. The absence of a suitable non-invasive glucose measurement has resulted in decades of research, little of which has resulted in simpler and/or improved glucose monitoring.
In the present report we describe the use of a thermostable glucokinase for use as a reversible glucose sensor. We believe hexokinases have good potential for use as glucose sensors.
The structure of the hexokinase A from yeast has been determined by x-ray diffraction both in the absence and presence of glucose. In Figure 1 is showed the structure of glucokinase in the presence of glucose. The polypeptide chain of 485 amino acid residues in the yeast protein is folded into 2 distinct domains, a smaller N-terminal domain and a larger C-terminal domain. From the high-resolution crystal structures of the enzyme is evident that in the absence of ligand, the two domains are separated by a deep cleft. This cleft represents the enzyme active site. It is in this region that the enzyme binds the substrate. In particular, the binding of glucose causes the small lobe of the molecule to rotate by 12degrees relative to the large lobe, moving the polypeptide backbone as much as 8 degrees, closing the gap between the two domains. The domain rotation has two effects: the glucose molecule is buried into the interior of the protein and the side chains in the active site are rearranged[9].

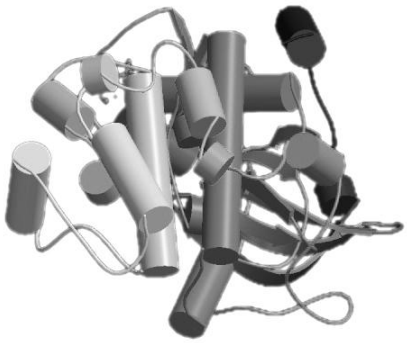

Fig. 1. Structure of glucokinase in the presence of glucose.

Resonance energy transfer (RET) reliably occurs whenever fluorescent donors and acceptors are in close proximity. We developed a method to use RET to develop a competitive glucose assay. To demonstrate the feasibility of a competitive glucose assay we used the unmodified protein and its intrinsic tryptophan emission as the donor. As the acceptor we used glucose containing the absorbing nitrophenyl group, ONPG shown in the upper part of Figure 2. Figure 2 shows also the intrinsic tryptophan emission of BSGK. Addition of ONPG (3 μM) results in an approximate 80% decrease in the tryptophan intensity. Addition of glucose results in recovery of the fluorescence intensity. At about 6 mM glucose concentration fluorescence intensity returns to its initial value before addition of ONPG. Further addition of glucose does not change the fluorescence signal. The fact that the intensity was sensitive to glucose demonstrates that the intensity changes are due to a binding event and not due to trivial inner filter effects from ONPG.

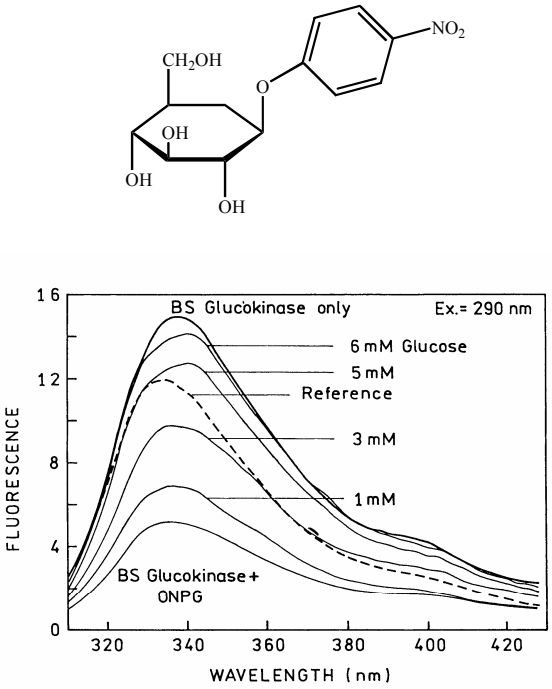

Fig. 2. Top: Structure of ONPG. Bottom: Effect of glucose on the ONPG-BSGK complex.

The results shown above demonstrate that a thermostable glucokinase can serve as a glucose sensor. Additional studies are needed to obtain a sensor that displays larger spectral changes. For example, we are hopeful that BSGK labeled with fluorophores other than IA-ANS will display larger intensity changes, spectral shifts or changes in lifetime. The results in the competitive RET are especially interesting because RET is a through-space interaction which occurs whenever the donor and acceptor are within the Forster distance (R_0), and does not require a conformational change and/or a change in the probe environment. For these reasons we are confident that BSGK can be used with longer wavelength donors and acceptors to develop practical glucose sensors for use in diabetes health care. Since the measurements through the skin can be easily performed by using a red laser diode or a light emitting diode (LED) as an excitation source, one may envision a polarization-based device with an external calibrated standard that will allow noninvasive glucose determinations. The main advantage of using this method is the obtainment of ratiometric polarization measurements that are not influenced by light instability and sample perturbation.

III. REFRACTIVE INDEX INTEGRATED SENSORS

Integrated optical sensors represent an important perspective for measuring physical and chemical quantities, via the monitoring of refractive index changes. In fact, these sensors offer unique advantages like immunity to electromagnetic

interference, high sensitivity, low price. In the last years, many types of integrated optical sensors have been developed like those based on Mach-Zehnder interferometers or waveguide bend loss[10-12].The most promising are the integrated Mach-Zehnder interferometers where the refractive index change of the substance placed on the sensor arm induces an optical path difference between the lightwaves propagating in the sensor and reference arms, respectively. This optical path difference gives rise, on its turn, to an easily detectable variation of the output intensity. However, Mach-Zehnder interferometers based devices often require a complex design geometry and large size.

III. ODOR BINDING PROTEINS

To reach their membrane receptors embedded in the membrane of the olfactory neurons, airborne odorant, which are commonly hydrophobic molecules, have to be conveyed through the aqueous nasal mucus. The odor-binding proteins, which are abundant low-molecular-weight soluble proteins (around 20 kDa) secreted by the olfactory epithelium in the nasal mucus of vertebrates, are candidates for playing a carrier role. These proteins reversibly bind odorants with dissociation constants in the micromolar range[13].

Although their functions are still unclear, odor-binding proteins are also suspected to participate in the deactivation of odorants. Vertebrate OBPs belong to the lipocalin super family. Although members of this family display low sequence similarity (usually less than 20% in amino acid content), all share a conserved folding pattern, an 8-stranded β-barrel flanked by an α-helix at the C-terminal end of the polypeptide chain. The β-barrel defines a central apolar cavity, called calyx, whose role is to bind and transport hydrophobic odorant molecules. Figure 3 shows the typical three dimensional structure of the odor binding protein. OBPs have been identified in a variety of species, including cow, pig, dog, rabbit, mouse and rat since the discovery of the first vertebrate OBP isolated from the bovine nasal mucus. Different OBP subtypes have been reported to simultaneously occur in the same animal species, three in pig, four in mouse, three in rat, three in rabbit and at least eight in porcupine. Their binding properties, investigated in rat, demonstrated that the three OBPs are specially tuned toward distinct chemical classes of odorants. Rat OBP-1 preferentially binds hetero-cyclic compounds such as pyrazine derivates and OBP-2 appears to be more specific for long-chain aliphatic aldeydes and carboxylic acids, whereas OBP-3 was described to interact strongly with odorants composed of saturated or unsaturated ring structure.

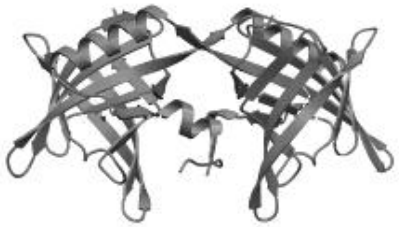

Fig. 3. Three dimensional structure of the odor binding protein

In order to assess the feasibility of the refractive index-based biosensor exploiting the odor binding protein as a biological interface, a set of experiments has been carried out by means of laboratory instrumentation. As a first measurement, the refractive index of an aqueous solution of OBP (0.75mg/ml), from dogs' nasal epithelium, has been determined by means of an Abbe refractometer, giving n=1.3595. The operation temperature was T=27.5°C. Subsequently, the protein solution has been mixed with a pyrazine solution (0.2mM 2-isobutyl-3-methoxypyrazine in 50mM TRIS, refractive index n=1.3970), keeping a constant volume and letting the pyrazine percentage range from 0% to 100%.

The results are shown in Figure 4. An inspection of the above figure reveals that the refractive index of the mixture is not simply given by the weighted average of the components' refractive indexes. The experimental points are, in fact, well fitted by a quadratic curve. The observed behavior suggests a strong interaction between the protein and the odor, ultimately leading to a possible conformational change in the protein itself. This change is likely to be induced by the binding of pyrazine molecules inside the OBP's calyx.

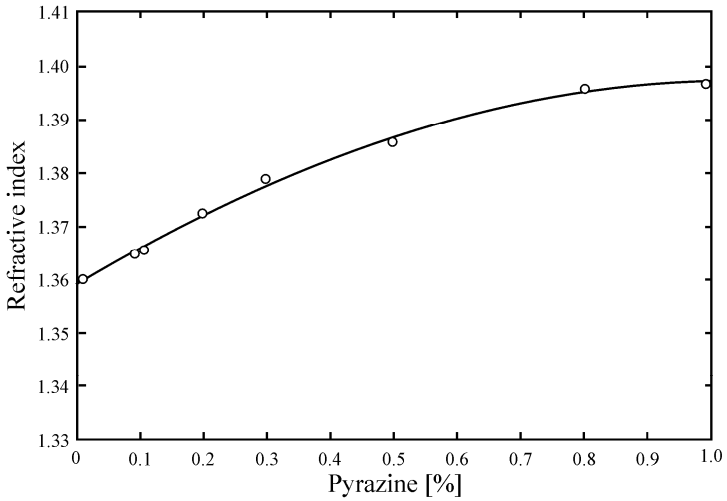

Fig. 4. Refractive index of the OBP-Pyrazine mixture.

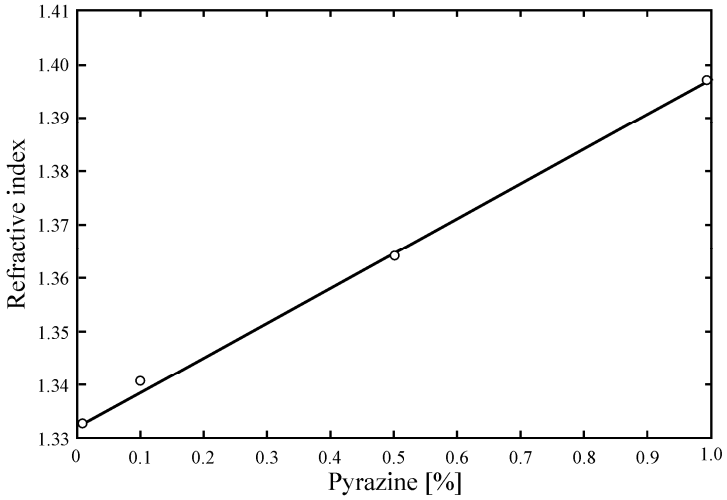

Fig. 5. Refractive index of the BSA-Pyrazine mixture.

For the sake of comparison, similar measurements have been performed using a standard Bovine Serum Albumin (BSA) aqueous solution (0.75mg/ml). The results are shown in Figure 5. In this case, the refractive index of the mixture follows the rule of the weighted average and the experimental points are well fitted by a straight line.
The non-linear behavior of the OBP-Pyrazine mixture refractive index indicates that OBP may represent a good candidate for refractive index-based biosensors.
To a better assessment of the OBP's behavior in presence of airborne odorant molecules, a second set of experiments has been carried out. In this case, an aqueous solution of odor binding protein, from pig's nasal epithelium, (2mg/ml) has been exposed to pyrazine vapors and constantly stirred for 3 minutes at a temperature of 27.5°C. The refractive index is, then, measured by means of the Abbe refractometer. The same procedure has been applied to BSA (0.75mg/ml), for comparison purposes. The results are summarized in Table 1.

Table 1. Refractive index of OBP and BSA.

Protein	**Refractive Index without pyrazine vapor**	**Refractive Index with pyrazine vapor**
Odor Binding Protein	1.3325±0.0001	1.3331±0.0001
Bovine Serum Albumin	1.3330±0.0001	1.3332±0.0001

It is evident, from the above table, that the OBP exhibits a refractive index change of $6 \cdot 10^{-4}$ when exposed to pyrazine vapor, while the variation of BSA refractive index falls within the experimental uncertainty. It is important to stress that the observed refractive index variation is greater than the minimum change detectable by means of the integrated refractometer based on antiresonant waveguide. These preliminary results seem to indicate the feasibility of a refractive index-based biosensor exploiting the odor-binding protein as the bio-probe. However, further investigations are needed to fully assess the capabilities of OBPs, also from other vertebrates, to bind different odorant molecules and the minimum detectable concentration.

IV. CONCLUSIONS

The possibility to exploit new enzymes and odor-binding proteins to realize non-consuming analyte biosensors has been devised.
Work is, now, in progress to characterize from a biophysical point of view these two proteins and immobilize them on a solid support for the realization of miniaturized biosensors.

ACKNOWLEDGEMENTS

This work was supported by the NATO project PST.NR.CLG 981025 (S.D., K.T.), CNR-NATO project 215.36S (O.S.), Program MCB RAS (K.T.), RFBR 06-04-48231 (O.S.), Program "Leading Scientific Schools of Russia" 9396.2006.4, Federal Agency of Science and Innovation (Contract# 02.512.11.2108 (K.T.), Russian Science Support Foundation (O.S.), INTAS YSF 06-1000014-5586 (O.P.), and it was partially supported at ISA-CNR by CNR-Bioinformatics Project (A.M.). This work was also supported by the CNR Commessa Diagnostica avanzata ed alimentazione (S.D.).

REFERENCES

1. O. S. Wolfbeis, "Fiber-optic chemical sensors and biosensors" *Anal. Chem.* 72, 81R-89R (2000).
2. J. R. Lakowicz, "Advances in fluorescence sensing technology", *II Proc. SPIE* 2388, 598pp (1995).
3. U. E. Spichiger-Keller, "Chemical sensors and biosensors for medical and biological applications" Wiley-VCH, New-York, 313 pp (1998).
4. A. S. Verkman, M. C. Sellers, A. C. Chao, T. Leung, R. Ketcham, "Synthesis and characterization of improved chloride-sensitive fluorescent indicators for biological applications", *Anal. Biochem.* 178, 355-361 (1989).
5. R. Y. Tsien, T. J. Rink, M. Poenie, "Measurements of cytosolic free Ca++ in individual small cells using fluorescence microscopy with dual excitation wavelengths", *Cell. Calcium.* 6, 145-157 (1985).
6. V. A. Romoser, P. M. Hinkle, Persechini A, "Detection of living cells of Ca++ dependent changes in the fluorescence emission of an indicator composed of two green fluorescent protein variants linked by a calmodulin-binding sequence", *J.Biol. Chem.* 272 (20), 13270-13274, (1997).
7. M. Staiano, M. Sapio, V. Scognamiglio, A. Marabotti, A. M. Facchiano, P. Bazzicalupo, M. Rossi, S. D'Auria, "A thermostable sugar-binding protein from the Archaeon *Pyrococcus horikoshii* as a probe for the development of a stable fluorescence biosensor for diabetic patients", *Biotechnol Prog*. 20(5), 1572-1577 (2004).
8. A. Marabotti, S. D'Auria, M. Rossi, A. M. Facchiano, "Theoretical model of the three-dimensional structure of a sugar-binding protein from *Pyrococcus horikoshii*: structural analysis and sugar-binding simulation", *Biochem. J*. 380 (Pt 3), 677-684 (2004).
9. S. D'Auria, N. Di Cesare, M. Staiano, Z. Gryczynski, M. Rossi and J. R. Lakowicz, "A novel fluorescence competitive assay for glucose determinations by using a thermostable glucokinase from the thermophilic microorganism *Bacillus stearothermophilus*", *Anal Biochem.* 303, 138-144 (2001).
10. J. Veldhuis, L. E. W. Van der Veen, P. V. Lambeck, "Integrated optical refractometer based on waveguide bend loss", *IEEE/OSA Journal of Ligthwave Technology*, 17, 857-864, (1999).
11. Maisenholder, H. P. Zappe, M. Moser, P. Riel, R. E. Kunz, J. Edlinger, "Monolithically integrated optical interferometer for refractometry", *Electronics letters*. 33, 986-988, (1997).
12. A. Cole, A. Kathman, A. McPherson, "Determination of Local Refractive Index for Protein and Virus Crystals in Solution by Mach-Zehnder Interferometry", *Analytical Biochemistry*, 231(1), 92-98 (1995).
13: O. V. Stepanenko, A. Marabotti, I. M. Kuznetsova, K. K. Turoverov, C. Fini, A. Varriale, M. Staiano, M. Rossi, S. D'Auria "Hydrophobic Interactions and Ionic Networks Play an Important Role in Thermal Stability and Denaturation Mechanism of the Porcine Odorant-Binding Protein", Proteins, In press (2007).

research articles Journal of proteome research

A Strategic Fluorescence Labeling of D-Galactose/D-Glucose-Binding Protein from *Escherichia coli* Helps to Shed Light on the Protein Structural Stability and Dynamics

Viviana Scognamiglio,[†,§] Andrea Scirè,[‡,§] Vincenzo Aurilia,[†] Maria Staiano,[†] Roberta Crescenzo,[†] Cristina Palmucci,[‡] Enrico Bertoli,[‡] Mosè Rossi,[†] Fabio Tanfani,[‡] and Sabato D'Auria*[,†]

Institute of Protein Biochemistry, National Research Council of Italy (CNR), Via P. Castellino, 111 80131, Naples, Italy, and Institute of Biochemistry, Università Politecnica delle Marche, Via Ranieri, 60131, Ancona, Italy

Received July 16, 2007

The D-glucose/D-galactose-binding protein (GGBP) of *Escherichia coli* serves as an initial component for both chemotaxis toward D-galactose and D-glucose and high-affinity active transport of the two sugars. GGBP is a monomer with a molecular weight of about 32 kDa that binds glucose with micromolar affinity. The sugar-binding site is located in the cleft between the two lobes of the bilobate protein. In this work, the local and global structural features of GGBP were investigated by a strategic fluorescence labeling procedure and spectroscopic methodologies. A mutant form of GGBP containing the amino acid substitution Met to Cys at position 182 was realized and fluorescently labeled to probe the effect of glucose binding on the local and overall structural organization of the protein. The labeling of the N-terminus with a fluorescence probe as well as the protein intrinsic fluorescence were also used to obtain a complete picture of the GGBP structure and dynamics. Our results showed that the binding of glucose to GGBP resulted in no stabilizing effect on the N-terminus portion of GGBP and in a moderate stabilization of the protein matrix in the vicinity of the ligand-binding site. On the contrary, it was observed that the binding of glucose has a strong stabilization effect on the C-terminal domain of the GGBP structure.

Keywords: galactose/glucose-binding protein; fluorescence; FT-IR; biosensor; glucose; protein structure

Introduction

In the proteomic and post-proteomic era, the study of the stability of proteins has gained interest because of a better understanding of the structure−function relationship in biomolecules that helps to shed light on the intra- and intermolecular interactions in which proteins are involved.[1] In fact, most globular proteins undergo conformational alterations when they interact with small molecules and other proteins.[1] Often these structural alterations result in changes of the functional features of proteins as well as in variations of their structural stability. It is obvious that the understanding of the full details of protein function requires both the knowledge of the molecular dynamics of the entire protein structure and the local protein motions.[2]

The periplasm of Gram-negative bacteria contains a large family of specific binding proteins that are essential primary receptors in transport and, in some cases, chemotaxis.[3−5] These proteins usually have a monomeric structure that folds in two main domains linked by three strands commonly referred to as the "hinge region". Conformational changes involving the hinge are thought to be necessary for sugars to enter and/or exit the protein binding site.[4,5] Differences in the structures of the ligand-bound and ligand-free proteins are essential for their proper recognition by the membrane components.[6] This property of binding proteins makes them good candidates for biological-recognition elements for the development of biosensors.[7]

The D-glucose/D-galactose-binding protein (GGBP) of *Escherichia coli* serves as an initial component for both chemotaxis toward D-galactose and D-glucose and high-affinity active transport of the two sugars. GGBP is a monomer with a molecular weight of about 32 kDa that binds glucose and galactose with micromolar affinity. Refined X-ray structures determined by Vyas et al.[8] for GGBP in the absence and in the presence of D-glucose provide a view of the sugar-binding site at the molecular level. The sugar-binding site is located in the cleft between the two lobes of the bilobate protein structure. The protein binding specificity and affinity are conferred primarily by the presence of polar planar side-chain residues that form an intricate network of cooperative and bidentate hydrogen bonds with the sugar substrate and, secondarily, by the presence of aromatic residues that sandwich the pyranose ring.

* Corresponding author. Address: Institute of Protein Biochemistry, National Research Council of Italy, Via Pietro Castellino, 111, 80131 Naples, Italy. Tel. +39-0816131250. Fax: +39-0816132277. E-mail: s.dauria@ibp.cnr.it.
† CNR.
‡ Università Politecnica delle Marche.
§ These authors contributed equally to this work.

10.1021/pr070439r CCC: $37.00

Frequent monitoring of the blood D-glucose level can prevent many long-term complications associated with diabetes, a medical condition affecting more than 20 million people in the United States alone. New noninvasive methods for real-time D-glucose-level monitoring include using interstitial fluids[9] and tears.[10] Since GGBP protein has a high affinity for D-glucose, it is suitable to use it as a probe for an implantable biosensor to monitor the low D-glucose concentrations known to be present in those fluids.[9,10]

Usually, biosensors for convenient optical measurements analytes should be designed planning the use of genetically engineering proteins. In fact, for practical purposes, biosensors should operate in the light visible region, and usually this is accomplished by labeling the cysteine residues of the proteins with visible-emitting fluorescence probes.

In the present study, the local and global structural features of GGBP were investigated by Fourier transform infrared (FT-IR) and fluorescence spectroscopy. In particular, a mutant form of GGBP containing the amino acid substitution Met to Cys at position 182 was realized and used to probe the effect of this mutation on the local and overall structural organization of GGBP. In fact, with respect to the three-dimensional organization of GGBP, the Cys 182 residue is located in the vicinity of the glucose-binding site of GGBP, thus it represents a strategic thiol-reactive position for labeling the protein with an extrinsic fluorescence probe.

Materials and Methods

Materials. Deuterium oxide (99.9% ^2H_2O), ^2HCl, and NaO^2H were purchased from Aldrich. Hepes, 5-dimethylamino-1-naphthalenesulfonyl chloride (dansyl chloride), and D-glucose were obtained from Sigma. 6-Acryloyl-2-dimethylaminonaphthalene (acrylodan) was obtained from Invitrogen. All other chemicals were commercial samples of the purest quality.

Preparation of Samples for FT-IR Measurements. Recombinant E. coli GGBP (GGBP-WT) or GGBP-M182C mutant (GGBP in which methionine 182 was changed into cysteine) concentrated solutions were prepared in ^2H_2O or ^1H_2O medium, in the absence and in the presence of D-glucose. The buffers used for infrared analysis were 25 mM Hepes/NaO^2H, p^{2}H 7.0 or pH 7.0 (buffer A), and 25 mM Hepes/NaO^2H, 10 mM D-glucose, p^{2}H 7.0 or pH 7.0 (buffer B). The p^{2}H corresponds to the pH meter reading +0.4.[11] About 1.5 mg of protein, dissolved in the buffer used for its purification, was concentrated to a volume of approximately 50 μL using a "10 K Centricon" micro concentrator Amicon at 3000*g* and 4 °C. Afterward, 250 μL of buffer A (pH or p^{2}H 7.0) or buffer B (pH or p^{2}H 7.0) was added, and the protein solution was concentrated again. This procedure was repeated several times, in order to completely replace the original buffer with buffer A (pH or p^{2}H 7.0) or buffer B (pH or p^{2}H 7.0). In the last washing, the protein solution was concentrated to a final volume of approximately 40 μL and used for FT-IR measurements.

Infrared Spectra. The concentrated protein samples were placed in a thermostated Graseby Specac 20500 cell (Graseby-Specac, Ltd., Orpington, Kent, U.K.) fitted with CaF_2 windows and a 25 μm Teflon spacer. FT-IR spectra were recorded by means of a Perkin-Elmer 1760-x FT-IR spectrometer using a deuterated triglycine sulfate detector and a normal Beer−Norton apodization function. At least 24 h before and during data acquisition, the spectrometer was continuously purged with dry air at a dew point of −70 °C, obtained by using a Parker Balston 75-62 FT-IR air dryer (Balston AGS, Haverhill, MA). Spectra of the buffers and samples were acquired at 2 cm^{-1} resolution under the same scanning and temperature conditions. In the thermal denaturation experiments, the temperature was raised in 5 °C steps from 20 to 95 °C using an external bath circulator (HAAKE F3). Temperature in the cell was controlled by a thermocouple placed directly onto the CaF_2 windows. Before spectrum acquisition, samples were maintained at the desired temperature for the time necessary for the stabilization of temperature inside the cell (6 min). Spectra were collected and processed using the SPECTRUM software from Perkin-Elmer. Correct subtraction of H_2O was judged to yield an approximately flat baseline at 1900−1400 cm^{-1}, and subtraction of ^2H_2O was adjusted to the removal of the ^2H_2O bending absorption close to 1220 cm^{-1}.[12] The deconvoluted parameters were set with a gamma value of 2.5 and a smoothing length of 60. Second-derivative spectra were calculated over a nine-data-point range (9 cm^{-1}). The percentage of $^1H/^2H$ exchange was obtained by monitoring the intensity of the amide II band at 1550 cm^{-1}.[13] In the spectrum of the protein recorded in H_2O, the intensity at 1550 cm^{-1} was considered corresponding to 100% of amide hydrogens (^1H). In the spectrum of the protein in ^2H_2O medium, full $^1H/^2H$ exchange was considered to occur at 98 °C, the temperature at which the protein was completely unfolded. In this spectrum, the intensity at 1550 cm^{-1} was taken as a reference for 0% of the amide hydrogens (^1H).[14]

Construction of the M182C Mutant of GGBP. The mglB gene that encodes for wild-type GGBP and its natural promoter were isolated from the *E. coli* K-12 genome by polymerase chain reaction (PCR). The gene-promoter DNA fragment was cloned into the *SacI*/*PstI* restriction sites of the plasmid pTz18U.[15] The resulting recombinant plasmid was used as template for the construction of the GGBP-M182C mutant. Site-directed mutagenesis was accomplished using overlap-extension PCR.[16] The forward primer mglB-FW 5′-AGGAATTC*GAGCTC*ACTTCATTAACTCTAC-3′, including the natural promoter of GGBP, was designed to introduce a *SacI* site (underlined). The reverse primer mglB-RV 5′-AA*CAGCTG*TTATTTCTTGCTGAATTCAAGC-3′, covering the stop codon of GGBP, was used to introduce a *PstI* site (underlined). Two internal primers were used for point mutation to replace the methionine at position 182 with a cysteine; the forward primer (mglB-M182C-forward) had the following sequence: 5′-TAGATACCGCA**TGT**TGGGACACCGCTCAGGCA-3′, and the reverse primer (mglB-M182C-reverse) had a sequence as follows: 5′-AGCGGTGTCCCA**ACA**TGCGGTATCTAACTGTAAC-3′; the mutated codon is indicated as boldfaced letters. The PCR cycle conditions were 95 °C for 5 min followed by 30 cycles of 95 °C for 1 min, 50 °C for 1 min, and 72 °C for 2 min. The amplified 1100 bp DNA fragment was ligated into the *SacI*/*PstI* site of the high copy number plasmid pTZ18U. The DNA sequencing data (PRIMM-SeqCore, Naples, Italy) verified that no mutation occurred except for of the desired point mutation. Transformation and subsequent expression of the resulting GGBP-M182C gene was performed in *E. coli* strain NM303.

Isolation of GGBP-M182C. The monocysteine mutant of GGBP was overproduced in *E. coli* NM303 (F1 *mgl* 503 *lacZ lacY*1 *recA*1), a mutant strain that does not produce GGBP. The cultures consisted of 0.5% inoculum, 50 μg/mL ampicillin in 2 L of Luria−Bertani medium (10 g/liter bacto-tryptone, 5 g/liter bacto-yeast extract, and 10 g/liter NaCl, pH 7.2), and 1.0 mM D-fucose incubated at 37 °C for 16−18 h. Cells were harvested, and GGBP-M182C was extracted by osmotic shock.[3] The crude

extract was dialyzed against 10 mM Tris-HCl pH 8.0 at 4 °C for 16−18 h. The GGBP-M182C was purified using a diethylaminoethyl anion-exchange column (Bio-Rad). GGBP-M182C was eluted with a 10 mM Tris-HCl, pH 8.0, gradient from 0 to 0.5 M NaCl. Fractions were analyzed for the presence of GGBP-M182C by SDS−PAGE, and fractions containing GGBP-M182C were pooled and dialyzed against 10 mM Tris-HCl pH 7.2 at 4 °C for 16−18 h.

Protein Assay. The protein concentration was determined by the method of Bradford[17] with bovine serum albumin as the standard by a double beam Cary 1E spectrophotometer (Varian, Mulgrade, Victoria, Australia).

Steady-State Fluorescence Spectroscopy. Fluorescence data were measured on samples of GGBP-WT and GGBP-M182C in 10 mM Tris-HCl, pH 7.2, with a protein concentration of 0.05 mg/mL and in the presence of a saturation amount of glucose (1.0 mM). Steady-state fluorescence measurements were performed on a K2 fluorometer (ISS, Champaign, IL) equipped with the two-cell temperature controlled sample holder. Tryptophan fluorescence was excited at 295 nm with the slit width of 1 nm, in order to avoid tyrosine contribution. The temperature of the samples was measured directly in the cuvette with an accuracy of ±0.2 °C. Before measurements, all samples were temperature equilibrated for 2 min.

Labeling of GGBP-M182C. In order to study locally the structure of GGBP-M182C, we labeled the cysteine 182 or the N-terminus of the engineered GGBP mutant with suitable fluorescence probes. Regarding the Cys labeling procedure, we used acrylodan. In particular, a 3-fold excess of acrylodan in dimethyl sulfoxide (DMSO) was added dropwise to a solution of 5.0 mg/mL of GGBP-M182C in 10 mM Tris-HCl pH 7.2, and then the solution was left to react for 3 h at room temperature. The resulting labeled protein was separated from the free dye by a Sephadex G-25 column.

A different procedure was carried out for the labeling of the N-terminus of the protein. In particular, a 3-fold excess of dansyl chloride in DMSO was added dropwise to a solution of 5.0 mg/mL of GGBP-M182C in 10 mM Tris-HCl pH 7.0, and then the solution was left to react for 2 h at 37 °C. The resulting labeled protein was separated from the free dye by a Sephadex G-25 column.

Results and Discussion

GGBP is a monomeric globular macromolecule with a 32 KDa molecular weight; the protein contains five tryptophan residues, four of which are located in the C-terminal domain of the protein, while one tryptophan residue is located at position 284 headed toward the N-terminal domain. The glucose-binding site of GGBP is located in the cleft between the two domains of the protein. The mutant protein GGBP-M182C contains a single cysteine residue at the 182 amino acid position in the proximity of the sugar-binding site (Figure 1).

Comparison of the Secondary Structures of GGBP-WT and GGBP-M182C. The most used band in structural studies of proteins by FT-IR spectroscopy is the amide I′ band, located between 1700 and 1600 cm^{-1}. The amide I′ band consist of a series of component bands that occur as the result of the secondary structural elements present in proteins. Resolution enhancement of absorbance spectra, as obtained in deconvoluted and second-derivative spectra, allows the identification of these secondary structures.[18,19]

Figure 2 shows the second derivatives spectra of GGBP-M182C (Figure 2A) and GGBP-WT (Figure 2B) in the absence (solid line) and in the presence (dashed line) of glucose at 20 °C. Figure 2C compares the second-derivative spectra of GGBP-WT (solid line) and GGBP-M182C (dashed line) in the absence of glucose. In the amide I′ region, the resolution-enhanced spectra show seven bands for both GGBP-M182C and GGBP-WT. The 1628, 1636.6, and 1697.0 cm^{-1} bands are characteristic of β-sheet structures. In particular, the 1628 cm^{-1} band could be assigned to the β-edge, that is, β-strands particularly exposed to the solvent.[20,21] The bands at 1650.9 and 1658 cm^{-1} are attributed to α-helix structures, which could

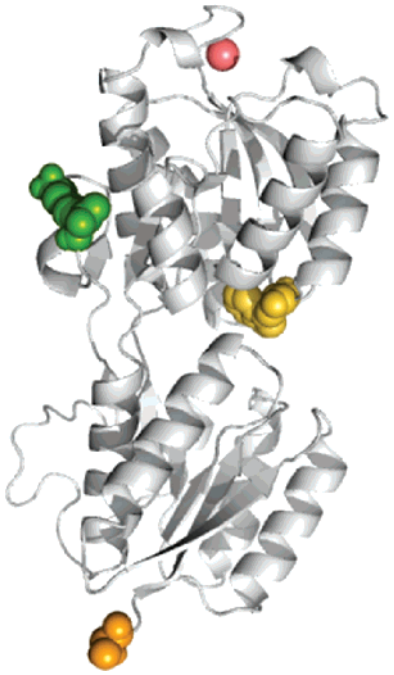

Figure 1. Three-dimensional structure of GGBP from *Salmonella typhimurium*. The Cys residue, introduced by site-direct mutagenesis and labeled with acrylodan, is represented in yellow; the Trp 284 is represented in green; the calcium atom, close to the binding site, is represented in red; the protein N-terminus is represented in orange.

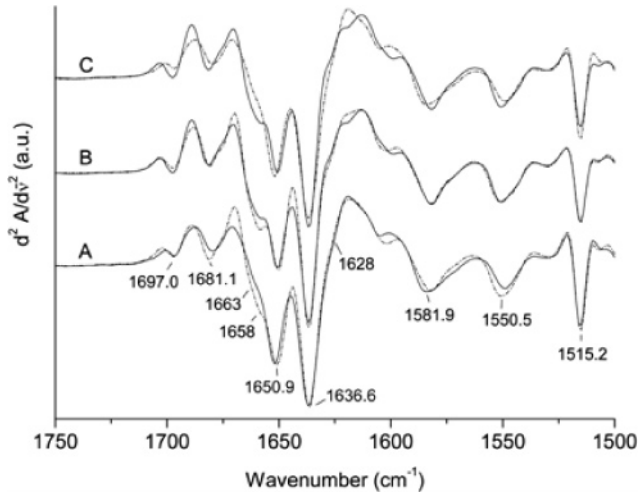

Figure 2. Second-derivative spectra of GGBP-M182C and GGBP-WT at 20.8 °C. (A) Spectra of GGBP-M182C in the absence (solid lines) and in the presence (dashed lines) of D-glucose. (B) Spectra of GGBP-WT in the absence (solid lines) and in the presence (dashed lines) of D-glucose. (C) Spectra of GGBP-WT (solid lines) and of GGBP-M182C in the absence of D-glucose.

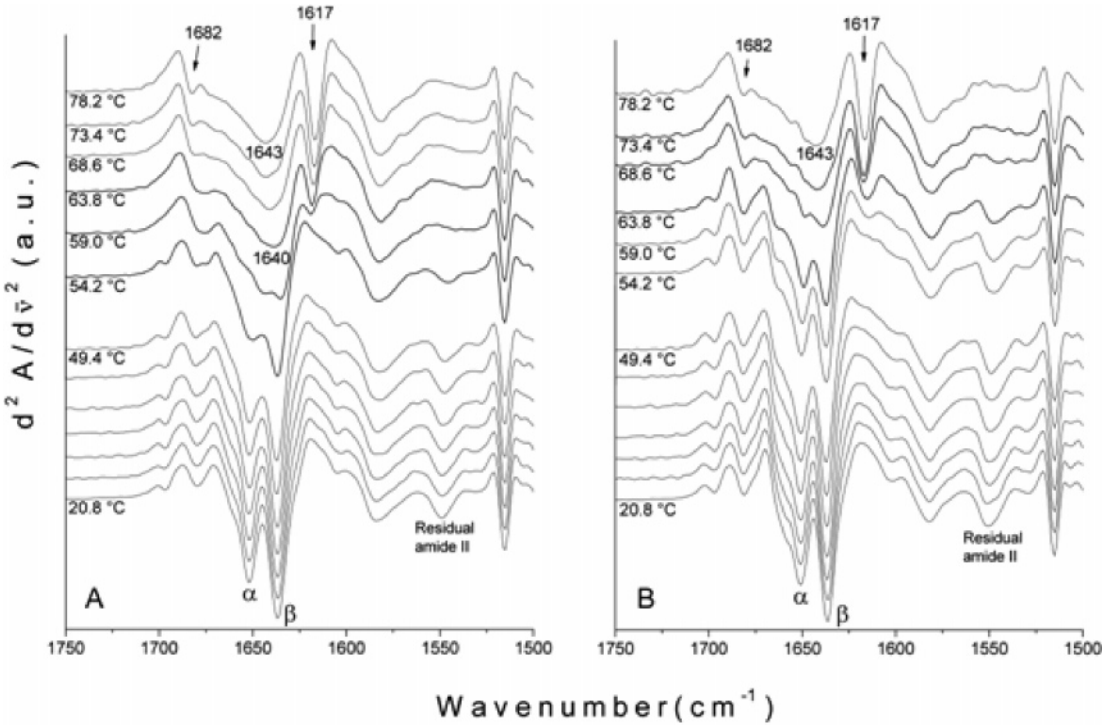

Figure 3. Temperature-dependent changes in the second-derivative spectra of GGBP-M182C in the absence (A) and in the presence (B) of D-glucose in the 20.8−78.2 °C temperature range.

represent two different populations of helices differing in exposition to the solvent (^2H_2O) or in the regularity of folding (distortion).[22] Since deuteration of proteins causes a downshift in the wavenumber of the α-helix and β-sheet bands,[23] the 1650.9 and 1658 cm^{-1} bands could be due to more and less solvent-exposed α-helices, respectively. The 1663 cm^{-1} band is due to turns, while the 1681.1 cm^{-1} band could be assigned to turns and/or β-sheets.[19,24] The bands below 1620 cm^{-1} are assigned to absorptions of amino acid side chains[25] except for the band at 1550.5 cm^{-1}, which is due to the residual amide II band.

Spectra 2C are very similar, indicating only small differences in the secondary structure of the proteins. In particular, in GGBB-M182C, the 1658 cm^{-1} band (less solvent-exposed α-helices) is present as a small shoulder as compared to that of GGBP-WT, suggesting that, in the mutant protein α-helices, the structures are more exposed to the solvent than those in GGBP-WT.

Derivatives spectra show that the binding of the sugar slightly affects the secondary structure of GGBP-WT and of GGBP-M182C. Indeed, in the presence of glucose, a small increase in the 1658 cm^{-1} band intensity is observed in both protein forms, and a previous study on GGBP-WT[3] showed that the binding of D-glucose results in a small increase in the population of α-helix structures of GGBP (1658 cm^{-1} band).

The amide II band (1600−1500 cm^{-1}, with a maximum close to 1550 cm^{-1}) is also an important absorption band for protein conformational studies. In fact, the spectrum of a protein in ^1H_2O usually is characterized by an amide II band intensity approximately equal to 2/3 of the intensity of the amide I band. When a protein is studied in ^2H_2O, the amide II band, which is very sensitive to $^1H/^2H$ exchange, shifts to lower wavenumbers (1450 cm^{-1}), and, as a consequence, we can register a decrease in the absorption band at 1550 cm^{-1}. The higher the $^1H/^2H$ exchange, the bigger is the decrease in amide II band intensity. The remainder absorption at 1550 cm^{-1} (residual amide II band) is due to polypeptide segments that do not have exchanged amide hydrogens with deuterium. Hence, the residual amide II band can provide information on the accessibility of solvent to the peptide backbone. The lower the residual amide II band intensity, the higher is the accessibility of the solvent (^2H_2O) to the protein. Since in the GGBP-M182C spectrum the residual amide II band is smaller than that in GGBP-WT (Figure 2C), this indicates that the GGBP-M182C structure is more exposed to the solvent as compared to wild-type proteins. This result is also in agreement with the lower content of α-helix structures poorly exposed to the solvent (1658 cm^{-1} band) found in GGBP-M182C.

The binding of glucose to GGBP-WT and to GGBP-M182C causes the increase in intensity of the 1658 cm^{-1} band in both cases, but this increase is accompanied by an increase in intensity of the residual amide II band in GGBP-M182C only. This result suggests that the compactness of GGBP-WT and GGBP-WT/Glc structures is similar, while the structure of GGBP-M182C is less compact than that of GGBP-M182C/Glc.

Thermal Stability. The temperature-induced conformational changes in proteins may be analyzed by monitoring the progress of the spectral bands recorded with the increasing temperature. Figure 3 shows the second-derivative spectra of GGBP-M182C in the absence (Figure 3A) and in the presence (Figure 3B) of D-glucose in the range of temperature between 20.8 and 78.2 °C.

In Figure 3A, the second-derivative spectra are almost identical up to 49.4 °C, suggesting that the protein in the temperature range between 20.8 and 49.4 °C does not undergo drastic conformational changes. At 54.2 °C, a decrease in the intensity of the bands due to α-helix and β-sheet structures starts to appear. This decrease is almost completed at 59.0 °C, while at 63.8 °C the α-helix and β-sheet bands are not visible anymore, and a broad band, centered at 1640 cm^{-1}, character-

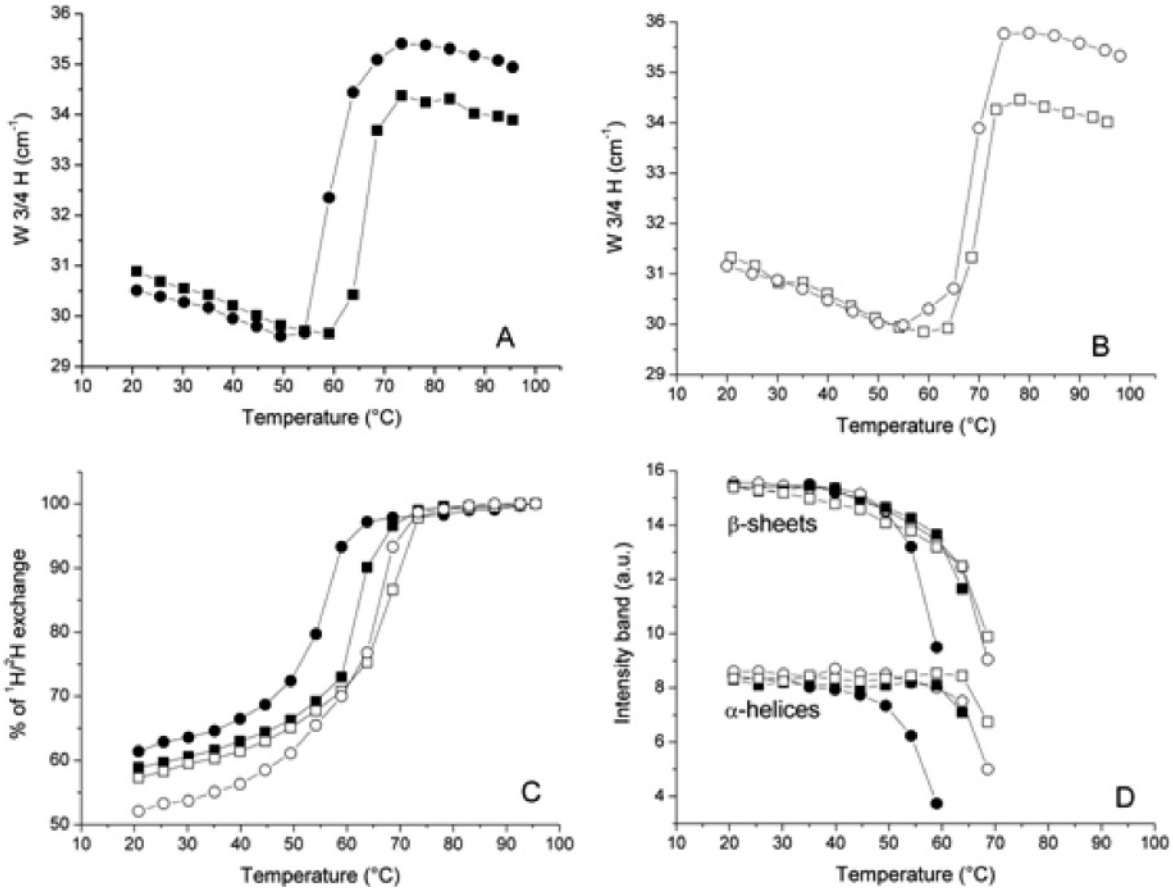

Figure 4. Temperature-dependent changes in amide I′ bandwidth (A,B), in the percentage of ^{1}H/^{2}H exchange (C), and in α-helix and β-sheet band intensity (D) for GGBP-WT and GGBP-M182C. In all graphs, the symbols (■), (□), (●), and (○) refer to GGBP-WT, GGBP-WT/Glc, GGBP-M182C, and GGBP-M182C/Glc, respectively. Thermal denaturation curves (A and B) were obtained by monitoring the amide I′ bandwidth, calculated at three-fourths of the amide I′ band height (W3/4H), as a function of the temperature. The percentage of ^{1}H/^{2}H exchange (C) was calculated as reported in the Materials and Methods section. The intensity of the main α-helix (1650.9 cm^{-1}) and β-sheet band (1636.6 cm^{-1}), in the second-derivative spectra of proteins (D), was multiplied by a factor of 10^4 and plotted as a function of the temperature.

izes the protein spectrum. At 78.2 °C, this broad band shifts to 1643 cm^{-1}, a frequency that is characteristic of protein unordered structures.[19,24] At 59.0 °C, a new band also appears at 1617 cm^{-1}. This band is a consequence of protein aggregation that is due to GGBP-M182C denaturation (loss of secondary structure). The intensity of this band usually increases with the extent of denaturation, as can be observed at high temperatures. The 1682 cm^{-1} band is also due to aggregation, and it is well seen only at high temperatures because of its low intensity.[26,27]

The progress of the spectral changes in Figure 3A shows that a large loss of secondary structure organization of GGBP-M182C takes place between 54.2 and 63.8 °C, suggesting that the temperature of protein melting (T_m) is within this range of temperature. The occurrence of protein denaturation is also suggested by the decrease in intensity of the residual amide II band at 54.2 °C. Indeed, a more relaxed or denatured protein structure could allow a deeper contact of the solvent (^2H_2O) with the polypeptide chain, causing a further ^{1}H/^{2}H exchange. At 59.0 °C and higher temperatures, this band is not visible, indicating a very large or total ^{1}H/^{2}H exchange.

When GGBP-M182C in the presence of D-glucose is exposed to the same thermal treatment, the temperature-dependent spectral changes described above are different, and they occur at higher temperatures (Figure 3B). In particular, at 63.8 °C, the temperature that precedes the dramatic loss of protein secondary structure (Figure 3B, 68.6 °C), the α-helix band intensity is higher as compared to the corresponding protein spectrum in the absence of D-glucose (Figure 3A, 54.2 °C). This suggests that, in the presence of D-glucose, the protein α-helices are more resistant to thermal denaturation. In synthesis, Figure 3B shows that a marked protein unfolding occurs between 63.8 and 73.4 °C and that the residual amide II band disappears at 68.6 °C, a temperature almost 10° higher with respect to that of GGBP-M182C in the absence of glucose.

A whole scenario of the temperature-dependent spectral changes of GGBP-WT and GGBP-M182C in the absence and in the presence of D-glucose is shown in Figure 4. In particular, Figure 4A displays the thermal denaturation curves of GGBP-WT and GGBP-M182C obtained by plotting the amide I′ bandwidth, calculated at three-fourths of the amide I′ band height (W3/4H), as a function of temperature.[28] The plot shows that GGBP-M182C is less thermostable than GGBP-WT, with T_m values of 59.0 and 64.5 °C, respectively. Figure 4B shows that glucose binding stabilizes the structure of both GGBP-M182C and GGBP-WT showing T_m values of 68.3 and 70.0 °C, respectively. It is noteworthy that the binding of glucose to GGBP-M182C has a higher stabilizing effect toward high temperatures than that observed for GGBP-WT. As a consequence, the difference in the thermal stability between

GGBP-WT and GGBP-M182C in the presence of glucose is only 1.7 °C (Figure 4B).

Figure 4C shows the percentage of $^1H/^2H$ exchange as a function of temperature (see Materials and Methods). The $^1H/^2H$ exchange depends on different factors. A temperature-dependent gradual increase could be attributed to the increase in molecular dynamics of the protein structure, while a marked increase at a specific temperature could be due to denaturation and/or relaxation of the protein tertiary structure.[23]

The graph shows that the rate of $^1H/^2H$ exchange increases dramatically at 56.1, 62.2, 66.1, and 68.0 °C for GGBP-M182C, GGBP-WT, GGBP-M182C/Glc, and GGBP-WT/Glc, respectively. These temperatures are about 2−3 °C lower than the T_m values registered for the corresponding proteins, suggesting that the dramatic increase in $^1H/^2H$ exchange is mainly due to protein denaturation. However, since the above-reported temperatures do not correspond exactly to the protein T_m values, one must consider that the increase in the rate of $^1H/^2H$ exchange could also be due to a relaxation of the tertiary structure that precedes protein denaturation.

Figure 4D shows the temperature-dependent intensity of the α-helices and β-sheet bands calculated in the second-derivative spectra of GGBP-M182C and GGBP-WT in the absence and in the presence of glucose. The binding of the sugar stabilizes to a small extent the α-helix and β-sheet structures of GGBP-WT, while, in GGBP-M182C, this stabilization occurs to a larger extent (about 10 °C). Moreover, Figure 4D shows that, in GGBP-WT, the intensity of the main β-sheet band (1636.6 cm^{-1}) decreases continuously and similarly up to 60 °C, and then it drops markedly, corresponding to the large protein unfolding. Conversely, the second-derivative signal related to the main α-helix band is almost constant up to 60 °C, indicating that α-helix structures are more stable than β-sheets within the range of temperature between 20 and 60 °C. A similar behavior is reported for GGBP-M182C/Glc, while, in GGBP-M182C, the main β-sheet band intensity decreases continuously with a similar slope up to 50 °C, and the intensity of the main α-helix band is almost constant up to 40−45 °C. In any case, with the exception of GGBP-M182C, Figure 4D indicates that the α-helices are more thermostable than β-sheets. In the GGBP-M182C mutant in the absence of glucose, the data suggest that α-helices are less stable than β-sheets (see also Figure 3B).

Fluorescence Spectroscopy. The tryptophan steady-state emission spectra of GGBP-WT and GGBP-M182C in the absence and in the presence of glucose are similar (data not shown) for both proteins with a maximum of emission at 340 nm. Binding of glucose results in a small fluorescence quenching for both proteins of about 5%. This quenching is probably due to the interaction between the pyranose ring of the bound sugar and the aromatic residue Phe 16 and Trp 183 of the protein.[29]

Figure 5 shows the effect of glucose on the thermal stability of GGBP-WT and GGBP-M182C in the range of temperature 20−95 °C. As for GGBP-WT, the progress curves of the intrinsic tryptophan fluorescence of GGBP-M182C, in the absence and in the presence of glucose, as a function of temperature, are well fitted to a two-state unfolding model, and the resulting melting temperatures are very similar to that registered for GGBP-WT. The calculated T_m values are reported in Table 1.

To estimate the extent of GGBP-M182C tryptophan shielding from the solvent, we examined the collision quenching by acrylamide. Acrylamide is a highly water-soluble and polar substance that does not penetrate the hydrophobic interior of proteins.[30] Figure 6 depicts the effect of acrylamide on the fluorescence emission of GGBP-WT (A) and GGBP-M182C (B) in the absence and in the presence of glucose at two different temperatures: 25 and 45 °C. While for GGBP-WT the presence of glucose affects the protein tryptophan shielding only at 45 °C, the Stern−Volmer plots of GGBP-M182C and GGBP-M182C/Glc are different both at 25 and 45 °C. The calculated Stern−Volmer quenching constants for GGBP-M182C and GGBP-M182C/Glc at 25 °C are 3.25 and 2.37 M^{-1}, respectively, while for GGBP-M182C and GGBP-M182C/Glc at 45 °C they are 6.7 and 3.14 M^{-1}, respectively (Table 2). These results show that the quencher's accessibility to the tryptophan residues of GGBP-M182C is higher in the absence of glucose, suggesting that the mutant protein in the presence of glucose assumes a more rigid conformation both at 25 °C and 45 °C. This behavior differs from GGBP-WT, which shows a different tryptophan shielding only at 45 °C. In addition, for GGBP-WT, the Stern−Volmer plots show a downward progress, indicating a dynamic quenching of the tryptophan from acrylamide during the tryptophan lifetime of the excited state. Conversely, for GGBP-M182C, the Stern−Volmer plots show an upward course, resulting in both dynamic and static quenching. In this case, the tryptophan fluorescence can be quenched both by collisions and by complex formation with the same quencher molecule, indicating the presence of different tryptophan populations. In Figure 6B we can also see that the static quenching happens at higher quencher concentrations, that is, when a fraction of the fluorophore is adjacent to the quencher at the moment of the excitation, and thus it is immediately deactivated.

In order to obtain structural information on a more restricted portion of the protein matrix, we labeled the introduced Cys residue in the GGBP-M182C with a thiol-reactive fluorescence probe. It is noteworthy that GGBP-WT does not possess any

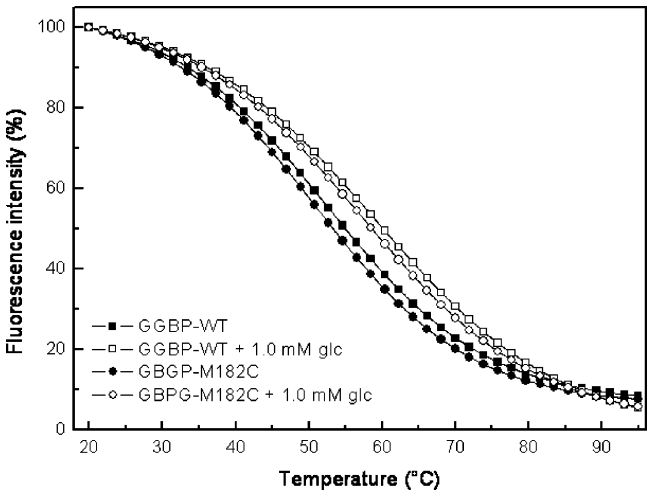

Figure 5. Temperature dependence of the emission spectra of GGBP-WT and GGBP-M182C in the absence and in the presence of 1.0 mM glucose, at a maximum emission intensity in the range of temperature 20−95 °C.

Table 1. Thermodynamic Fluorescence Parameters for Thermal Unfolding of GGBP-WT and GGBP-M182C in the Absence and in the Presence of 1.0 mM Glucose

	GGBP-WT	GGBP-WT glc	GGBP-M182C	GGBP-M182C glc
T_m (°C)	52.48	59.15	50.92	57.22

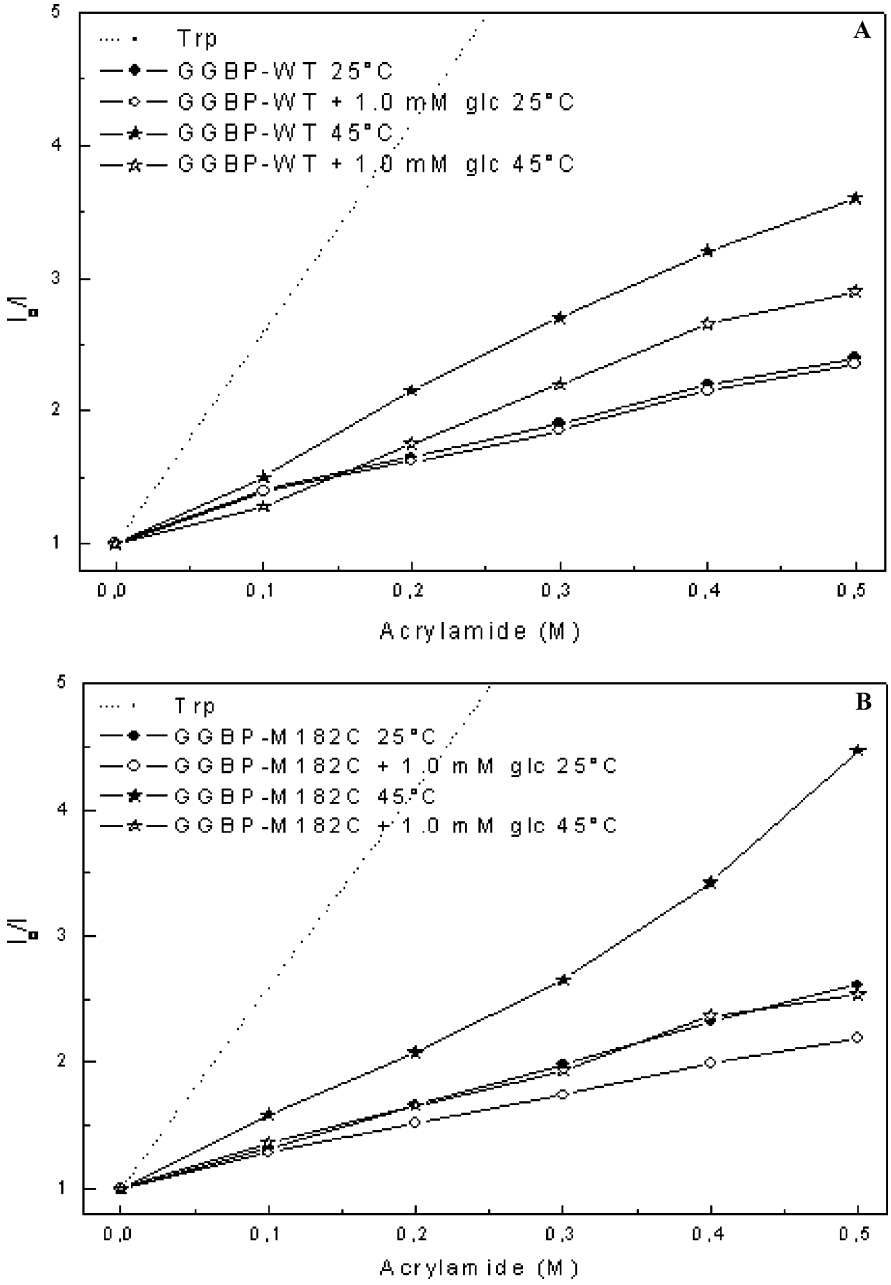

Figure 6. Effect of acrylamide on the fluorescence emission of GGBP-WT and GGBP-M182C in the absence and in the presence of 1.0 mM glucose, at 25 and 45 °C.

Table 2. Stern−Volmer Quenching Constants (K_{sv}) of GGBP-WT and GGBP-M182C in the Absence and in the Presence of 1.0 mM Glucose, at 25 and 45 °C

	25 °C	25 °C Glc	45 °C	45 °C Glc
GGBP-WT K_{sv}	2.75	2.64	5.32	4.02
GGBP-M182C K_{sv}	3.25	2.37	6.7	3.14

Cys, and this unique residue of Cys that we have introduced in the protein is located in the close proximity of the glucose-binding site of the protein, thus it could be considered as being associated with the protein structural variations resulting from the binding of the sugar. We labeled GGBP-M182C with acrylodan at Cys 182. Figure 7 shows the effect of glucose on the thermal stability of acrylodan-labeled GGBP-M182C in the absence and in the presence of glucose in the range of temperature between 20 and 95 °C. Binding of glucose to acrylodan-labeled GGBP-M182C results in a small stabilization of the protein structure portion, probably to refer to where the fluorescence probe is located. In fact, Figure 7 clearly shows that the difference in T_m between acrylodan-labeled GGBP-M182 and acrylodan-labeled GGBP-M182C/Glc is about 3 °C. On the contrary, the difference in T_m values in reference to the entire structure of protein, that is, unlabeled GGBP-M182 and unlabeled GGBP-M182C/Glc, is about 7 °C.

Figure 8 shows the effect of glucose on GGBP-M182C N-terminal domain thermal stability, where dansyl chloride was covalently attached at the N-terminal amino acid residue. The temperature dependence of GGBP-M182 is the same both in the absence and in the presence of glucose in the temperature range between 20 and 95 °C. This suggests that the binding of glucose does not affect the N-terminal portion of the protein.

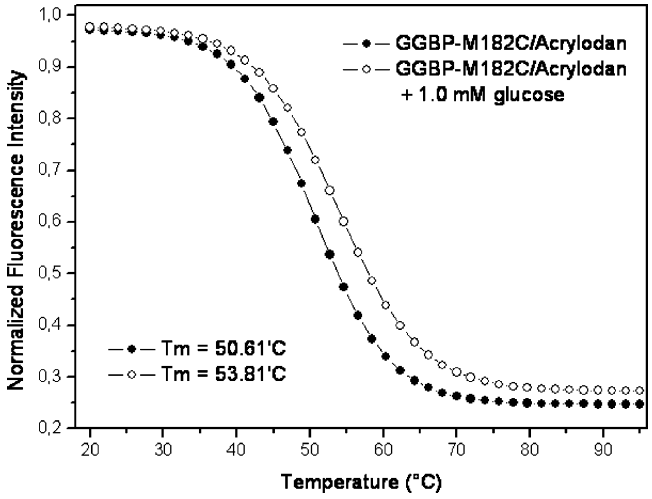

Figure 7. Thermal denaturation of GGBP-M182C/acrylodan in the absence and in the presence of 1.0 mM glucose.

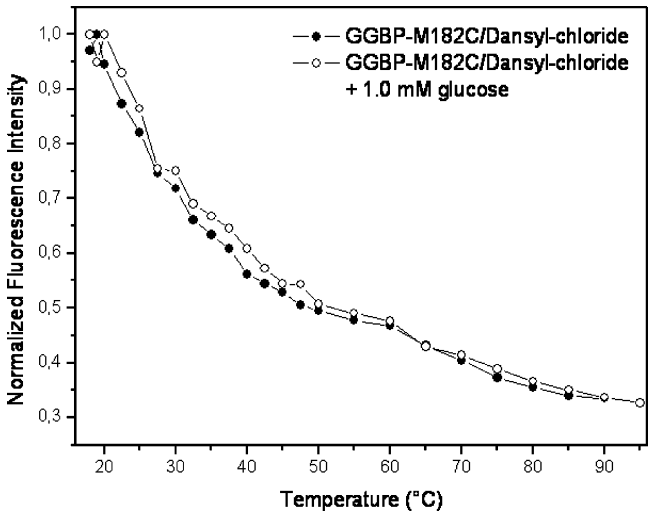

Figure 8. Thermal denaturation of GGBP-M182C/dansyl chloride in the absence and in the presence of 1.0 mM glucose.

In conclusion, in the present study, we have documented that the binding of glucose to GGBP results in no stabilizing effect on the N-terminus of GGBP and in a moderate stabilization of the protein matrix close to the sugar-binding site of GGBP. On the contrary, the binding of glucose has a strong stabilization effect on the C-terminal domain of the GGBP. In particular, infrared data showed that GGBP-WT and GGBP-M182C have a similar secondary structure content, with two populations of α-helices differently exposed to the solvent. In the mutant protein, the infrared data indicated a lower content of buried α-helices than in GGBP-WT. This finding is in agreement with the fact that GGBP-M182C also shows a higher $^1H/^2H$ exchange than GGBP-WT, and with the Stern−Volmer results. Taken together, these data suggest a less compact structure of the mutant protein with respect to GGBP-WT. The binding of glucose to GGBP-M182C leads to an increase in the content of buried α-helices and to a lower accessibility of the solvent to the protein.

Abbreviations: FT-IR, Fourier transform infrared; amide I′, amide I in ^2H_2O medium; GGBP-WT, recombinant *Escherichia coli* D-galactose/D-glucose binding protein; GGBP-M182C, mutant of GGBP-WT in which methionine 182 was changed into cysteine; GGBP-WT/Glc, GGBP-WT in the presence of D-glucose; GGBP-M182C/Glc, GGBP-M182C in the presence of D-glucose.

Acknowledgment. The authors thank Leandro Maria D'Auria for his help in the manuscript typewriting. This work was supported by the ASI project MoMa No. 1/014/06/0, by a grant from the Ministero degli Affari Esteri, Direzione Generale per la Promozione e la Cooperazione Culturale (S.D., M.S., M.R.), by CRdC-ATIBB POR UE-Campania Mis 3.13 activities (S.D., M.R.), and by the CNR Commessa Diagnostica avanzata ed alimentazione (S.D., M.S.).

References

(1) Carugo, O.; Patrick, A. *Protein Eng.* **1997**, *10* (7), 777−787.
(2) Nishimoto, E.; Yamashita, S.; Szabo, A. G.; Imoto, T. *Biochemistry* **1998**, *37* (16), 5599−5607.
(3) D'Auria, S.; Alfieri, F.; Staiano, M.; Palella, F.; Rossi, M.; Scire, A.; Tanfani, F.; Bertoli, E.; Gryczynyski, Z.; Lakowicz, J. R. *Biotechnol. Prog.* **2004**, *20* (1), 330−337.
(4) Quiocho, F. A. *Curr. Opin. Biol.* **1991**, *1*, 922−933.
(5) Vyas, N. K.; Vyas, M. N.; Quiocho, F. A. *J. Biol. Chem.* **1991**, *266*, 5226−5237.
(6) Flocco, M. M.; Mowbray, S. L. *J. Biol. Chem.* **1994**, *269*, 8931−8936.
(7) Tolosa, L.; Gryczynski, I.; Eichhorn, L. R.; Dattelbaum, J. D.; Castellano, F. N.; Rao, G.; Lakowicz, J. R. *Anal. Biochem.* **1999**, *267*, 114−120.
(8) Vyas, M. N.; Vyas, N. K.; Quiocho, F. A. *Science* **1988**, *242*, 1290−1295.
(9) Tamada, J. A.; Bohannon, N. J. V.; Potts, R. O. *Nat. Med.* **1995**, *1*, 1198−1201.
(10) Badugu, R.; Lakowicz, J. R.; Geddes, C. D. *J. Fluoresc.* **2003**, *13*, 371−374.
(11) Salomaa, P.; Schaleger, L. L.; Long, F. A. *J. Am. Chem. Soc.* **1964**, *86*, 1−7.
(12) Tanfani, F.; Galeazzi, T.; Curatola, G.; Bertoli, E.; Ferretti, G. *Biochem. J.* **1997**, *322*, 765−769.
(13) Osborne, H. B.; Nabedryk-Viala, E. *Methods Enzymol.* **1982**, *88*, 676−680.
(14) Capasso, C.; Abugo, O.; Tanfani, F.; Scire, A.; Carginale, V.; Scudiero, R.; Parisi, E.; D'Auria, S. *Proteins* **2002**, *46*, 259−267.
(15) Tolosa, L.; Gryczynski, I.; Eichhorn, L. R.; Dattelbaum, J. D.; Castellano, F. N.; Rao, G.; Lakowicz, J. R. *Anal. Biochem.* **1999**, *267* (1), 114−120.
(16) Urban, A.; Neukirchen, S.; Jaeger, K. E. *Nucleic Acids Res.* **1997**, *25* (11), 2227−2228.
(17) Bradford, M. M. *Anal. Biochem.* **1976**, *72*, 248−254.
(18) Byler, D. M.; Susi, H. *Biopolymers* **1986**, *25*, 469−487.
(19) Arrondo, J. L.; Muga, A.; Castresana, J.; Goni, F. M. *Prog. Biophys. Mol. Biol.* **1993**, *59*, 23−56.
(20) Casal, H. L.; Kohler, U.; Mantsch, H. H. *Biochim. Biophys. Acta* **1988**, *957*, 11−20.
(21) Surewicz, W. K.; Mantsch, H. H. *Biochim. Biophys. Acta* **1988**, *952*, 115−130.
(22) Tanfani, F.; Lapathitis, G.; Bertoli, E.; Kotyk, A. *Biochim. Biophys. Acta* **1998**, *1369*, 109−118.
(23) Pedone, E.; Bartolucci, S.; Rossi, M.; Pierfederici, F. M.; Scire, A.; Cacciamani, T.; Tanfani, F. *Biochem. J.* **2003**, *373*, 875−883.
(24) Krimm, S.; Bandekar, J. *Adv. Protein Chem.* **1986**, *38*, 181−364.
(25) Barth, A. *Prog. Biophys. Mol. Biol.* **2000**, *74*, 141−173.
(26) Jackson, M.; Mantsch, H. H. *Biochim. Biophys. Acta* **1991**, *1078*, 231−235.
(27) D'Auria, S.; Barone, R.; Rossi, M.; Nucci, R.; Barone, G.; Fessas, D.; Bertoli, E.; Tanfani, F. *Biochem. J.* **1997**, *323* (3), 833−840.
(28) Scirè, A.; Saccucci, F.; Bertoli, E.; Cambria, M. T.; Principato, G.; D'Auria, S.; Tanfani, F. *Proteins* **2002**, *48*, 126−133.
(29) Marabotti, A.; Ausili, A.; Staiano, M.; Scire, A.; Tanfani, F.; Parracino, A.; Varriale, A.; Rossi, M.; D'Auria, S. *Biochemistry* **2006**, *45* (39), 11885−11894.
(30) Eftink, M. R.; Ghiron, C. A. *Biochemistry* **1976**, *15* (3), 672−680.

PR070439R